DOCTOR OF PHILOSOPHY

Dynamics of sands and suspended particulate matter in the macrotidal Conwy estuary, North Wales, U.K.

Missias, Stefanos

Award date:
2007

Awarding institution:
Bangor University

DYNAMICS OF SANDS AND SUSPENDED PARTICULATE MATTER IN THE MACROTIDAL CONWY ESTUARY, NORTH WALES, U.K.

By

Stefanos Missias

A thesis submitted to the University of Wales (Bangor)

for the Degree of Doctor of Philosophy

School of Ocean Sciences, University of Wales, Bangor

Anglesey, LL59 5EY, U.K.

October 2007

ABSTRACT

Dynamics and properties of sands and suspended particulate matter (SPM) in the Conwy Estuary were investigated. SPM properties were measured at specific locations over tidal cycles. Floc formation was restricted by increased turbulence at 3 h before low water (LW). At LW, decreased velocities allowed floc formation and partial sedimentation of SPM. At peak velocities c.3h after LW, the mean suspended sediment concentration (SSC) at the surface reached a maximum of 47mgl^{-1}. Particle size increased and effective density decreased due to resuspension of low density, large particles. At high water slack (HW) when turbulence was a minimum, larger flocs formed. At the 5 anchor stations, the total cumulative flood flux (11kgm-1) was twice the total cumulative ebb flux (5 kgm^{-1}).

SPM properties (of surface waters) were measured along the longitudinal axis of the estuary at HW. In the upper estuary (mean salinity 0), large flocs (median size 119 μm) of low density (82 kgm^{-3}) were observed with average surface SSC of 22 mgl^{-1}. In the estuarine turbidity maximum (ETM) region (mean salinity 5), the median floc size was 98 μm, while floc density increased to 135 kgm^{-3}, with average surface SSC of 43 mgl^{-1}. In the lower estuary (mean salinity 27), the median floc size (114 μm) was similar to that in the upper estuary, but with twice the floc density (159 kgm^{-3}).

At HW, the ETM occurred between 8 and 19 km from the mouth. It was found that the controlling factor of ETM location changed with the season and its SPM properties followed a seasonal cyclic pattern. ETM location varied with the flow ratio (river discharge / tidal range^3); ETM location was predicted by: $\log(D)=0.997 - 0.103*\log(Q/T^3)$. Similarly, SSC in the ETM was predicted by: $\log(SSC_{ETM})= 1.48+0.201*(\log(Q/T^3))^2+0.21*\log(Q/T^3)$, where D (km) is the distance from the mouth, Q (m^3s^{-1}) is river discharge, and T (m) is tidal range. The relationship placed the predicted ETM between 10 and 16 km from the mouth. The estimated depth average SSC in the ETM, agreed well with observed values. After modifying these relationships for summer conditions only, they were compared with ones produced for the Taf estuary (Jago et al., 2006) using the Conwy flow ratios. The Taf relationship underestimated the ETM location by c. 4 km. At very low flow ratios; the Taf SSC relationship overestimated the concentration by 200 - 400 mgl^{-1}.

The estuarine sands, of modal grain size (180 μm), were made-up of 70 – 90% quartz particles. Mineralogical analysis showed that the provenance of the estuarine sands is Conwy Bay. Net transport paths of the estuarine sands were defined by analysis of the spatial variation of grain size characteristics; the overall sand transport was found to be in the up-estuary direction. Thresholds of motion and suspension for the estuarine sands were established for each of the 5 anchor stations, and sediment transport rates (bed and suspended loads) were calculated. The total flood transport was 0.4-6.0 kgm^{-1}/survey, whilst total ebb transport was 0.1-2.2 kgm^{-1}/survey.

DEDICATION

To my loving parents
Kostas and Trudy,
for their support and enduring patience.

"Little by little one travels far."

(J.R.R. Tolkien, author)

ACKNOWLEDGEMENTS

There are many people to whom I am indebted for their advice, assistance and support, which has enabled me to bring this thesis into reality.

My principal thanks go to my supervisor, Dr. Colin F. Jago; both for his major input to the work, and his support throughout my study period, especially during the last stages. His help, encouragement and critical assessment have been invaluable, and are reflected in both completion and content of this thesis. I also wish to acknowledge the help and support given by other members of my supervisory committee; Dr. Sarah E. Jones and Dr. Dei Huws.

My many thanks also go to all members of the technical staff who helped during this project, in particular Alan Nield, Ben Powell and Gwyn Parry Jones. I would especially like to thank Gwyn P. Jones for his superb assistance and advice throughout the sampling and data collecting period.

I would like to thank my colleagues who helped me at various stages of my PhD project, in particular Ben Moat and Guy Springett who helped in the field and provided invaluable support and advice when needed.

I am grateful to Dr. Jim Bennell for providing the Excel spread-sheet for the grain size analysis; Dr. Sarah E. Jones for providing the programming for analysing the LISST data; and the Environmental Agency for providing the river discharge data for the Conwy.

Finally I would like to thank David Webb and Joan Truss for their understanding, caring and supportive nature; my fiancée, Katerina, for keeping me sane and focused during the final stages of this thesis; and my parents for standing behind me throughout my education and for their financial support which enabled me to carry out this study.

CONTENTS

LIST OF FIGURES

CHAPTER 6

CHAPTER 7

LIST OF TABLES

NOTATIONS AND SYMBOLS

c	Beam attenuation coefficient
C_D	Drag coefficient
D	Particle diameter
d_w	Relative settling velocity
d_{50}	Median grain size
D	Distance
D_*	Dimensionless grain size
E_d	Turbulent energy dissipation rate
F_D	Drag force
g	Acceleration due to gravity
h	Total water depth
I	Immersed weight
J_B	Collision rate due to Brownian motion
J_D	Collision rate due to differential settling
J_I	Collision rate due to internal encounters
J_S	Collision rate due to fluid shear
K_G	Kurtosis
L	Transmissometer path length
M_d	Graphic median diameter
M_z	Graphic mean diameter
M	Slope of regression curve
No	Number concentration of particles
N	The intercept of regression curve
q_b	Volumetric bedload transport rate
Q	River discharge
Q_b	Mass bedload transport rate
Q_{bN}	Net mass bedload transport rate
Q_s	Mass suspended load transport rate
Q_{sN}	Net mass suspended load transported load
Q_{TN}	Total load net transport rate
Q/T^3	Flow ratio
Re	Reynolds number
s	Particle (or floc) density divided by water density
S_{KI}	Graphic skewness
SSC_{OBS}	Suspended sediment concentration from OBS
SSC_{ETM}	Suspended sediment concentration in the ETM
SSC_{Ltrn}	Suspended sediment concentration from the LISST transmissometer
SSC_{trn}	Suspended sediment concentration from the transmissometer
T	Tidal range
u_*	Shear velocity
$\overline{U}$	Depth averaged current velocity
$\overline{U_{cr}}$	Critical depth averaged current velocity
VC	Volume concentration

VDC	Volts direct current
w_s	Settling velocity
α_ϕ	First "degree" skewness
$\alpha_{2\phi}$	Second "degree" skewness
θ	Shields' parameter
θ_{cr}	Critical threshold Shields' parameter
θ_s	Threshold of suspension Shields parameter
κ	Boltzman's constant
μ	Molecular viscosity
ν	Kinematic viscosity
π	Pi
ρ	Water density
ρ_s	Particle density
σ_I	Inclusive standard deviation
σ_ϕ	Standard deviation
Σ_r	The sum of the radii of colliding particles
T	Temperature
τ_{cr}	Threshold shear-stress
τ_o	Bed shear-stress
ϕ	Phi unit
Φ	Dimensionless bedload transport rate
%T	Percent transmission

1 INTRODUCTION

1.1 Introduction

Estuaries are wetlands that form at margins of the land and the sea. The continual movement of the tide and the mixing of freshwater and saltwater, make estuaries complex and varying in nature. As a result of continual input, trapping and recycling of sediment and nutrients, the ecosystems supported by estuaries are amongst the most fertile and productive in the world (Davidson et al., 1991).

Estuaries are of great social and economic importance. For millennia people have settled on or around estuaries, taking advantage of the fertile farm lands and the productive waters. Ports were built enabling commercial fishing and shipping. Industries and towns flourished attracting more and more people.

The shallow sheltered areas of water in an estuary may cause tidal and river currents to slow, so that fine sediments settle out of suspension. Large quantities of these sediments are carried in suspension down rivers from often large catchment areas and into the sea. Sedimentation of fine particles carried down rivers is enhanced in estuaries by salt-related flocculation. This continual trapping and settling of sediments means that estuaries are generally depositional environments, composed chiefly of fine unconsolidated muds and sands (Davidson et al., 1991).

In order to understand how the ecosystems and sediments of an estuary respond to natural changes and/or human intervention, an understanding of sediment dynamics within this system is needed.

1.2 The Conwy Estuary

1.2.1 General Site Description

The Conwy Estuary is the largest and most westerly of the major estuaries of the North Wales coast, lying on a north-south axis (see Figure 1.1). It drains a predominantly upland area of about 660 km^2 from its source at Llyn Conwy in the mountains of Snowdonia (Hillier, 1985; Zhou et al., 2003). The main river channel covers a distance of about 56 km, flowing through Snowdonia National Park, falling rapidly towards the extensive flood plains of the lower Conwy, and the tidal limit, some 450 m below the source (National Rivers Authority, 1995). Several major tributaries join the upper Conwy, notably the Afon Crafnant, Ddu and Lludwy.

The Conwy Estuary is considered to be well-mixed and macrotidal in nature, with a flushing time of approximately 6 hours (Turrell et al., 1996; Humphreys, 1998; Clement, 1999; and Simpson et al., 2001). It has a tidal range at the mouth varying between 3.5m and 7m (Wallis, 1984; Nunes, 1985). The estuary is characterised by fast tidal currents which exceed 1 ms^{-1} in the lower estuary (Nunes, 1985), and a tidal asymmetry (short flood, long ebb) which becomes more pronounced with distance upstream (Knight, 1981). The tidal limit – landward limit of water level fluctuations due to the tide – on a large spring tide reaches Llanrwst, approximately 23 km from the mouth at Deganwy (Wallis, 1984; Nunes, 1985).

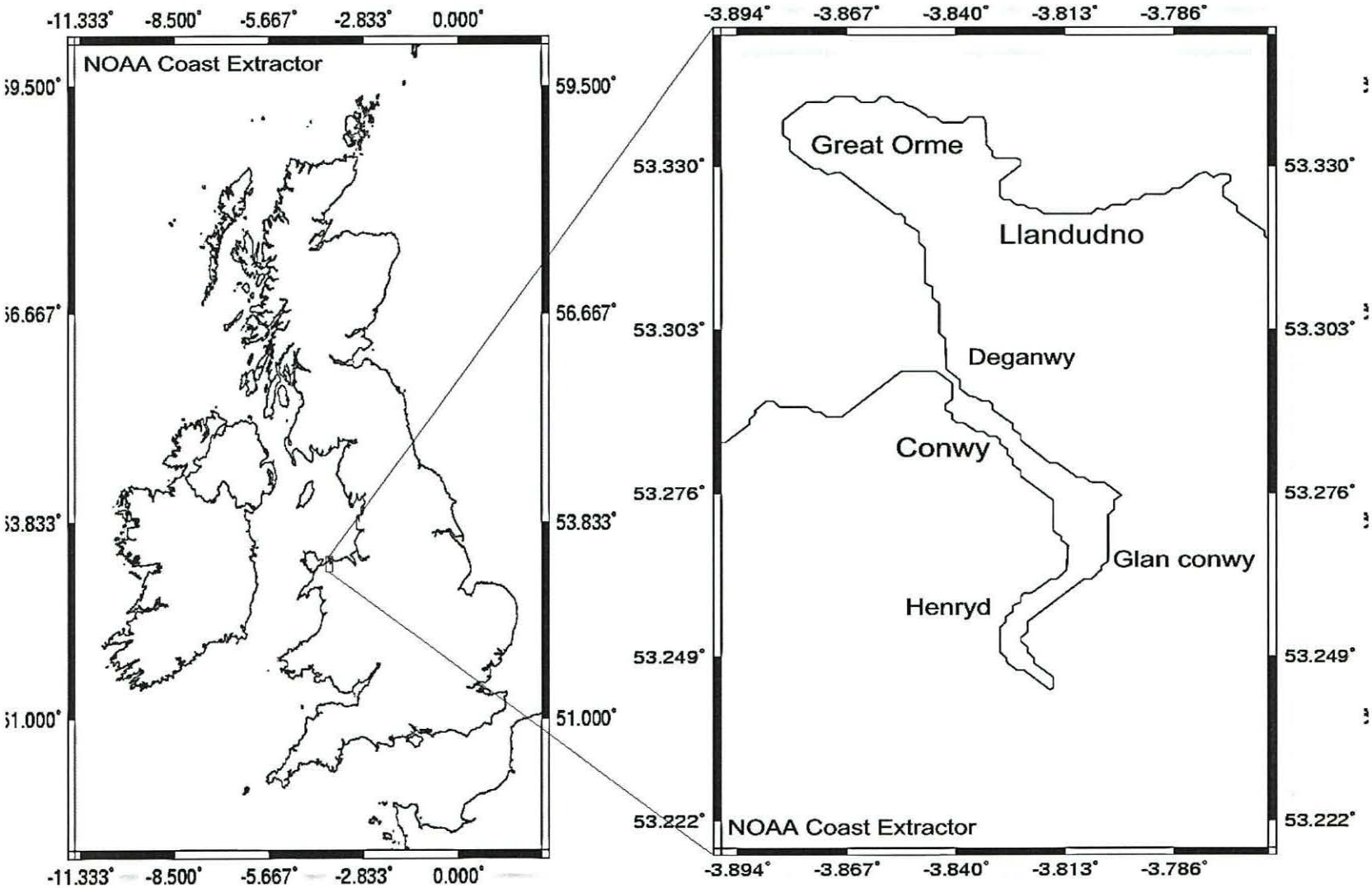

Figure 1.1: map of the study area obtained using the NOAA coastal extractor (Latitude and Longitude, in degrees).

1.2.2 Site Geology and Geomorphology

Initially the mountains of Snowdonia formed one vast dome. The drainage channels flowing from this found their ways along rock faults, and one such line developed into the 'then' Conwy valley, about 50ma (Senior, 1984). The river valley was over deepened by glacial action during the Pleistocene period. At the end of the last Ice Age, a general rise in sea level occurred, flooding lowland areas including the Conwy river valley. The inlet, created by fluvial and glacial action, was largely filled by fluvial and marine deposits, leaving an extensive flat plain, especially in the lower reaches, and an estuary that mostly drains with the tide (Senior, 1984; Maynard, 1985; and Hillier, 1985).

The Conwy estuary is a typical drowned river valley situated along the faulted boundary between Ordovician and Silurian rocks. On the eastern side, the bed rock consists of Silurian deposits: shales; mudstones, greywacke; and some limestone. On the west side the bed rock consists of Ordovician sedimentary (mainly shales and mudstones), and volcanic (mainly basalt, rhyolite, andesite and tuffs) deposits. These rocks in this area are characterised by a conformable geosyncline (Dunning, 1978; Maynard, 1985).

The nature of the underlying geology is such that groundwater plays an insignificant role in the general hydrology of the Conwy catchment, except locally where water discharging from old mine workings can be significant (National Rivers Authority, 1995).

1.3 Survey Area

The survey area occupies the entire Conwy estuary extending from the Deganwy beacon at the mouth (3°50.9'W, 53°18.1'N) to Llanrwst (3°47.9'W, 53°8.2'N). The beacon is set as the bench mark from which all distances during the survey are measured. The distances are measured from the bench mark landward following

the main channel. The total distance between the seaward and landward extent of the survey area is approximately 23 km (see Figure 1.2).

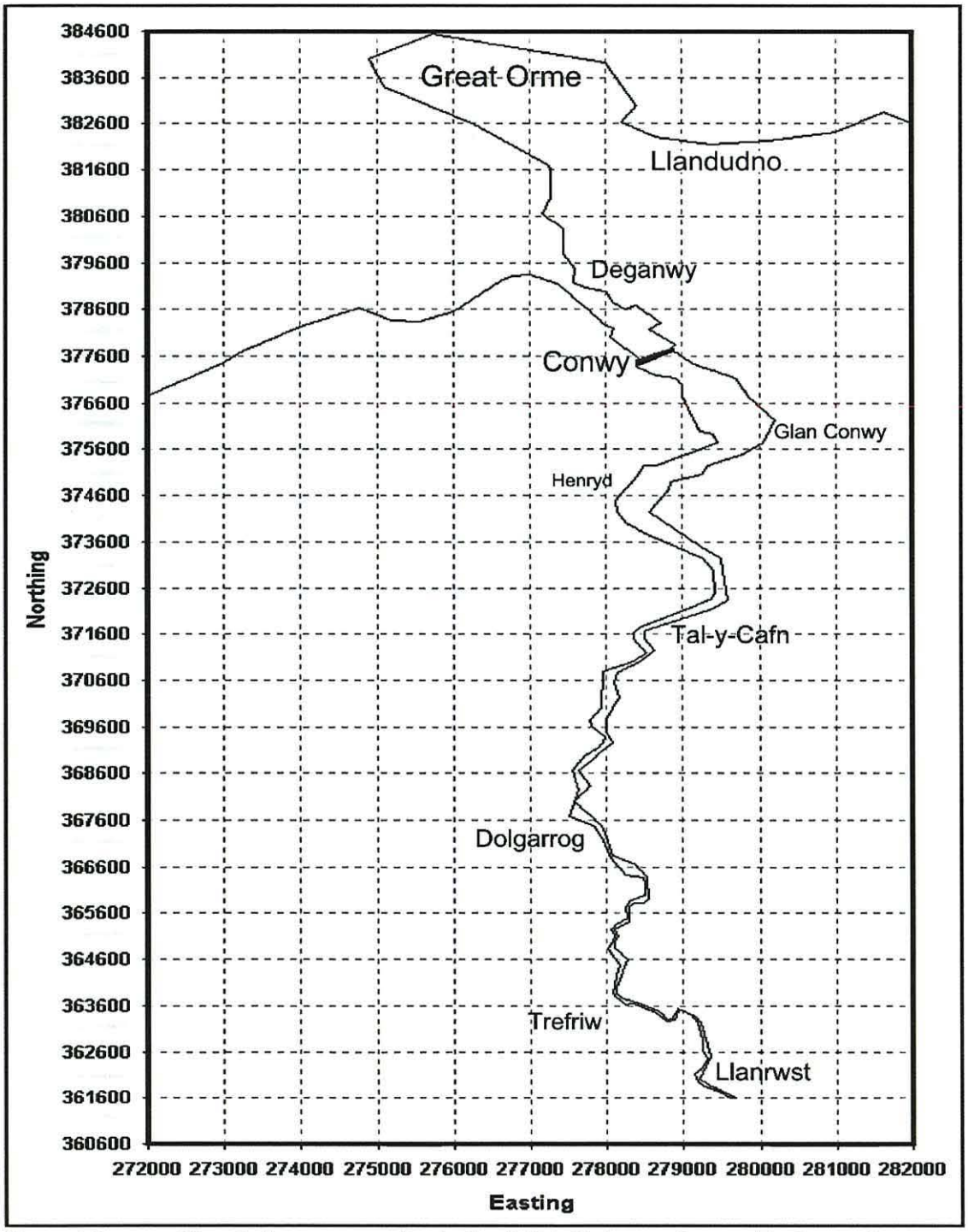

Figure 1.2: map of the study area according to the British Ordnance Survey (Easting and Northing, in m). Note that the north-south and west-east scales are not the same; this is done for practical reasons.

For the purpose of this project the Ordnance Survey coordinates are used. This is done for practical reasons, making field work easier. From this point onwards when referring to a location, the coordinates are in Eastings and Northings (in metres). Note that the north-south and west-east scales, on the maps used, are not the same, this is done for practical reasons.

1.4 The Objectives and Hypotheses of the Study

A thorough understanding of the behaviour and transport of suspended particulate matter in estuaries is crucial to the management of various engineering and environmental issues, such as commercial fisheries, contaminant transport, harbour maintenance and others (Bale, 1996; Fugate, 2002).

1.4.1 Specific Objectives of the Study

The main objectives of the study were two-fold:

1) To determine the characteristics of suspended particulate matter (SPM) in the estuary and, in particular, of the estuarine turbidity maximum (ETM) that, according to Hillier (1985), exists in the upper reaches of the Conwy estuary.

2) To investigate the bed sediment transport regime within the Conwy estuary.

More specifically, the aims were:

a) To determine spatial and temporal variations of SPM in the estuary.

b) To determine the factors controlling the location of, and concentration of SPM in the ETM.

c) To establish the provenance of the estuarine sands.

d) To identify the thresholds of motion and suspension for the estuarine sands.

e) To determine the net bedload and suspended load transport directions and rates, over a tidal cycle at specified locations.

f) To establish the net transport paths of estuarine sands.

1.4.2 Proposed Hypotheses of the Study

From the objectives it was anticipated that the following hypotheses could be tested:

- Hypothesis 1 – The ETM is located near the limit of salt water intrusion, with river discharge and tidal range being the primary controls of its location and strength.

- Hypothesis 2 – The properties (concentration, density and settling velocity rates) of SPM in the estuary are seasonally variable.

- Hypothesis 3 – The net sediment transport of sand is in the up-estuary direction.

- Hypothesis 4 – The estuarine sands are of marine origin (i.e. from Conwy Bay).

2 Estuaries and Sediment Dynamics

2.1 The Estuary

2.1.1 The Nature, Origin and Definition of Estuaries

Geomorphological features, such as rivers and coastlines, are ephemeral in geological time. When a river breaches a coastline and meets the sea, a region is formed that is also ephemeral and is commonly known as the "river mouth". This region is extensive, with high productivity and biodiversity, making it an important ecosystem in flux. The physical and biogeochemical processes of this region are of great importance. It is generally agreed that the river mouth can be broken down into two major types: estuaries and deltas, each of which can be subdivided into further types.

Before considering the different definitions found in scientific papers, it is imperative to consider the term "estuary". Where does this term come from and what does it mean? According to the Oxford English dictionary, the term estuary comes from the Latin substance *aestus* meaning heat, boiling and tide: and specifically the adjective *aestuarium* meaning tidal.

How does one define an estuary? The answer to that depends greatly on the field of science in which one works. Neutral parties, such as the Oxford English dictionary, give vague definitions such as:

a) An estuary is a tidal opening, an inlet or creek through which the tide enters; an arm of the sea indenting the land.

b) The estuary is the tidal mouth of a great river, where the tide meets the current of fresh water.

These definitions of the "estuary" are echoed, with slight variations, in all dictionaries and encyclopaedias.

When referring to estuaries in general, a universal standard for the definition must exist so that every one knows what is meant. The task of setting such standards belongs to the United Nations Educational, Scientific and Cultural Organization (UNESCO). UNESCO has an extensive list of definitions for a variety of terms and concepts, posted on its official Internet web-page, under "glossary". In this glossary: "the estuary is a partially enclosed coastal area at the mouth of the river where its fresh water, carrying fertile silt and runoff from the land mixes with salty seawater". Although this definition is overall accommodating towards all fields of science, it is vague.

A biologist, a geomorphologist and an oceanographer will give slightly different definitions, which will inevitably reflect their fields of expertise. An example of a biologically influenced definition is that of Garrison (1999), which states that the estuary is a body of water partially surrounded by land where fresh water from a river mixes with ocean water, creating an area of remarkable biological productivity and diversity.

More on the physical side of estuarine studies we have the following three definitions:

i) Pritchard (1967): "An estuary is a semi-enclosed body of water having a free connection with the open sea and within which the sea-water is measurably diluted with fresh water deriving from land drainage."

ii) Hansen and Rattray (1966): "Estuaries, in the traditional sense, are regions of transition from river to ocean. They are characterized by the possibility of tidal motions communicated from the sea, and by

gradients of salinity and density associated with the progressive admixture of river water and seawater."

iii) Fairbridge (1980): "An estuary is an inlet of the sea reaching into a river valley as far as the upper limit of tidal rise."

For the purpose of this thesis the definition of an estuary by Hansen and Rattray will be adopted, at the same time Fairbridge's definition will be, also, taken into account.

2.1.2 Classification of Estuaries

Estuaries are categorised into classes according to the similarities and differences between their governing factors; such as topography, river flow and tidal action. These factors are dependent on the geology and the latitude of the estuary itself, as well as the climate at the source of the fresh water input to the system, and the nature of the tidal regime which is largely determined by the morphology of the adjacent continental shelf. In general, classification criteria are based on the geomorphology and the tidal range of the estuary.

2.1.3 Classification of Estuaries Based on the Geomorphology

Pritchard (1967) divides estuaries into four basic types based on their geomorphology. These are: (1) drowned river valleys, (2) fjords, (3) bar built estuaries, and (4) estuaries produced by tectonic processes.

2.1.3.1 Drowned River Valleys

This type of estuary is generally confined to a region with a relatively wide coastal plain. Acknowledging this fact, Pritchard (1967) named these waterways

coastal plain estuaries (Dyer, 1973). This type of estuary was formed during the Flandrian transgression and is generally restricted to temperate latitudes.

Fairbridge (1980) explains that during the last glacial period the global sea level was about 120 m lower than present, with coastlines further out on the continental shelves. This meant that the melt-waters, from the glaciers, incised "V" shaped valleys into coastal plains. After the glaciers melted, and the world sea level rose, these river valleys were drowned forming today's coastal plain estuaries.

These estuaries retained their typical "V" shape, with their width-depth ratio usually being large, dependent on the local geology. Dyer (1973) describes them as being typically wider and deeper at the mouth, with overall depth seldom reaching 30 m and a central channel that is often sinuous and floored by mud in the upper reaches, but becoming increasingly sandy towards the mouth. River discharge is generally small compared with the volume of the tidal prism. Hence the sediment discharged by the river is typically small. According to Pritchard (1967), in most coastal plain estuaries the river bottom does not rise above mean sea level for a considerable distance landward from the point at which the last vestiges of sea-derived salt can be measured. Another important fact is that the duration of the flood tide will decrease toward the upper reaches.

Fairbridge (1980), points out that for the drowned river valley type there is a sub-type called a "ria". Rias are drowned river valleys, but that could either be caused by sea level rise or by tectonic subsidence. They are relatively deep, narrow, well defined, and are floored usually by bedrock.

2.1.3.2 Fjords

According to Davidson et al. (1991) and Dyer (1973), fjords are essentially drowned glacial troughs, often associated with major lines of geological

weakness. They were formed in areas covered by Pleistocene ice sheets. The pressure of the ice over-deepened and widened pre-existing river valleys, but left rock bars or sills particularly at the fjord mouth. These sills can be very shallow. Fjords are "U" shaped and have a small width-depth ratio, steep sides and an almost rectangular cross-section. Their outline in plain is also typically rectangular. Fjords generally have rocky floors, or very thin veneers of sediment, and deposition is generally restricted to the head of the fjord where the main rivers enter. The river discharge is relatively small in comparison with the total volume of the fjord, and river flow is often larger than the tidal prism. Finally their occurrence is restricted to high latitudes in mountainous areas, where there has been extensive glaciation.

2.1.3.3 Bar Built Estuaries

These estuaries are also in part drowned river valleys which have been incised during the ice ages and subsequently inundated. However, Davidson et al. (1991) point out that these estuaries are distinguished by recent sedimentation which has kept pace with the inundation, and they have a characteristic bar across their mouths. The bar is normally formed where the waves break on the beach, and for it to develop the tidal range must be restricted and large volumes of sediment must be available. Consequently, bar-built estuaries are generally associated with depositional coasts. These estuaries are only a few metres deep and often have extensive lagoons and shallow waterways just inside the mouth. Dyer (1973) stated that the restricted cross-sectional area at the mouth can cause currents with high velocities, but as the estuary widens further inland the current velocities rapidly diminish. Bar built estuaries are generally found in tropical areas or in areas with active coastal deposition of sediments.

2.1.3.4 Estuaries Produced by Tectonic Processes

Pritchard (1967) calls this type a catch-all classification for estuaries not clearly included in the other three divisions. Coastal indentures formed by faulting or by local subsidence, and having an excess supply of freshwater inflow, are covered by this category. Davidson et al. (1991 point out that estuaries in this group are of complex origin and so do not easily fit into other types. Such estuaries usually result from the influence of a mixture of geological constraints such as hard rock outcrops, glaciation, river erosion and sea-level change.

2.1.4 Classification of Estuaries Based on the Tidal Range

According to Davidson et al. (1991), the most important control on estuarine processes is tidal range. This determines the tidal current and residual current velocities and therefore the rates and amounts of sediment movement.

Many authors, (e.g. Davidson et al., 1991; Davies, 1973; and Hayes, 1975), have classified estuaries and coastal environments according to average spring tidal range: microtidal where the range is less than 2 m; mesotidal where it is between 2 m and 4 m; macrotidal where it is more than 4 m.

2.1.4.1 Microtidal Estuaries

In microtidal estuaries, processes are dominated by freshwater discharge upstream of the estuary mouth and by wind-driven waves from outside the mouth. Wind-driven waves tend to produce spits and barrier islands which enclose bar-built estuaries. Microtidal estuaries tend to be wide and shallow (Davidson et al., 1991).

2.1.4.2 Mesotidal Estuaries

Mesotidal estuaries are dominated by strong tidal currents, rather than the fresh water influence. The fairly limited tidal range, however, means that the tidal flow does not extend far upstream, and therefore most mesotidal estuaries are rather short and wide (Davidson et al., 1991).

2.1.4.3 Macrotidal Estuaries

In macrotidal estuaries, strong tidal and residual currents may extend far inland. Instead the central channel near the estuary mouth is occupied by long linear sand bars parallel with the tidal flow. The estuarine shape is the distinctive trumpet-shaped flare typical of coastal plain estuaries (Davidson et al., 1991).

2.2 Estuarine Circulation

In estuaries, the transport and deposition of sediments is predominantly controlled by the main channels. This is the result of the main channels being the principal conduits for both tidal and river flow. The magnitudes of tidal range and river discharge, combined with the morphology of these main channels determine the internal circulation dynamics of an estuary. There are three key types of estuarine circulation: highly stratified estuaries, partially mixed estuaries, and well mixed estuaries. Combinations of the above may exist.

2.2.1 Salt Wedge (highly/strongly stratified) Estuaries

Highly stratified estuaries develop where river discharge is large compared to the tidal prism (Dyer, 1972). The less dense river water flows over the surface of the underlying denser seawater which forms a salt wedge that penetrates and thins up-river (see Figure 2.1). The extent of the salt wedge varies with the river flow. When the discharge is low, the salt wedge penetrates further up the estuary than

when the discharge is high. According to Ketchum (1983), strongly stratified estuaries are commonly found among drowned river valleys.

There are very sharp salinity and density gradients between the overlying freshwater and underlying saltwater: a stable halocline develops. According to Dyer (1972), the upper surface of the wedge has a sharp halocline that can reach 20 PSU, in less than 0.5 m. The resulting strong density gradient (pycnocline) inhibits mixing between the two water masses. However, shear stresses at the interface between the flowing river water and the salt wedge generate internal waves. Where these waves break, small quantities of salt water from below are entrained into the freshwater – in other words, salt water from below is entrained into the freshwater above, making it brackish. Dyer (1972), states that in order to compensate for this loss of salt water there is a slow landward movement within the salt wedge. The slow landward flow within the salt wedge and the augmented seaward flow in the freshwater layer, due to entrainment, are known as residual flows. These are basic features of salt wedge estuaries, which develop only where the tidal range is small.

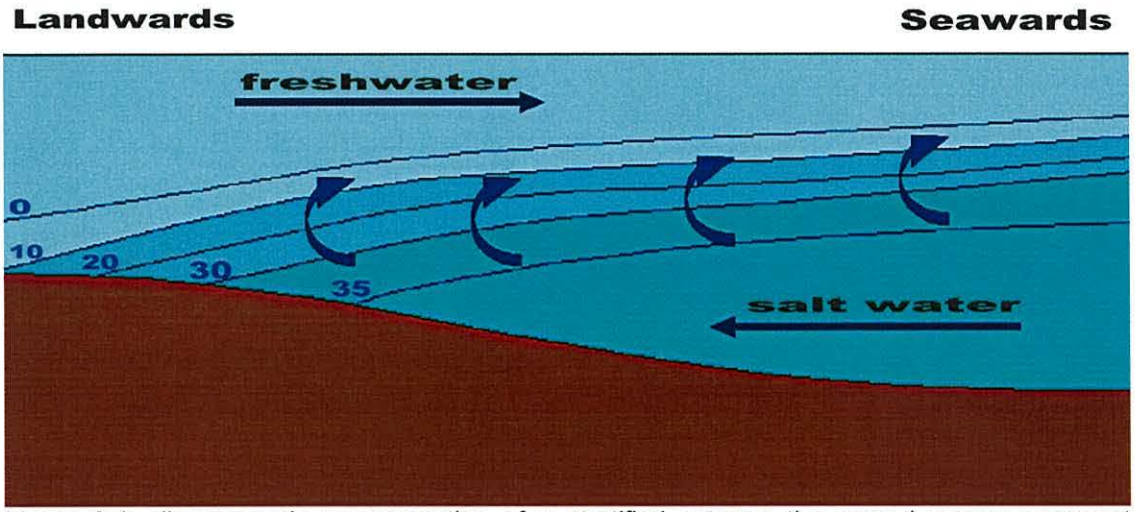

Figure 2.1: diagrammatic representation of a stratified estuary: the curved arrows represent mixing; the numbers represent salinity values (PSU).

2.2.2 Partially Mixed (weakly stratified) Estuaries

According to Dyer (1997), partially mixed estuaries develop where the tidal flow becomes equal or greater than river discharge, and the whole volume of the water oscillates up and down the estuary with the flood and ebb tides. Friction between the water and the estuary bed causes turbulence (Dyer, 1986).The turbulence causes more effective mixing than does simple entrainment at the freshwater/saltwater interface (see Figure 2.2). Saltwater is mixed upwards, and freshwater is mixed downwards, so the isohalines are more steeply inclined, with salinity in both layers increasing towards the mouth (Dyer, 1972).

In partially mixed estuaries, the freshwater flowing seawards mixes with a large amount of salt water, so the total discharge of water via the surface layer can be an order of magnitude greater than the river discharge. For example Bowden (1967) suggests that the seaward transport in the upper layer might be 20 times the river flow. Continuity requires that the salt water mixed into the surface layer be replaced, and so the landward flow within the bottom salt water layer is significantly stronger, 19 times the river flow in the example given by Bowden (1967). Thus, in partially mixed estuaries, the vertical mixing between the upper and lower layers produces larger landward residual flow. This enhanced residual flow, caused by the density differences and mixing, is termed the vertical gravitational circulation (Dyer, 1997).

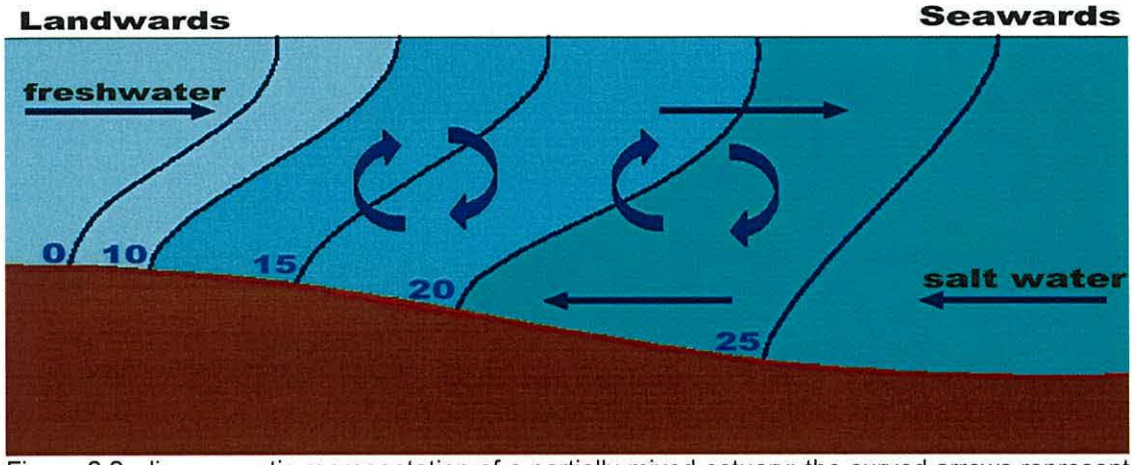

Figure 2.2: diagrammatic representation of a partially mixed estuary: the curved arrows represent mixing; the numbers represent salinity values (PSU).

2.2.3 Well Mixed Estuaries

According to Dyer (1997), well-mixed estuaries develop where tidal range is large compared with the depth of the estuary. In this regime tidal currents are strong relative to the river flow and the whole water column is mixed, so that salinity hardly varies with depth at all (Ketchum, 1983). Although the entire well-mixed water mass oscillates landwards and seawards with the tides, the average salinity decreases towards the upstream limit of the tidal influence (see Figure 2.3).

In well-mixed estuaries a horizontal circulation can develop. This happens when the ratio of width to depth is sufficiently large so that the Coriolis force can laterally separate both the incoming tidal flow and the outgoing river water (Dyer, 1997). According to Bowden (1967), and Dyer (1972), in the northern hemisphere the residual flow is seaward at all depths on the right side of the estuary (looking seawards), and landwards at all depths on the left.

If though, the width to depth ratio is relatively small, then the horizontal effects are suppressed. In this regime there is an overall seaward flow throughout the cross-section and the landward transport is by diffusive processes (Dyer, 1972; Bowden, 1967).

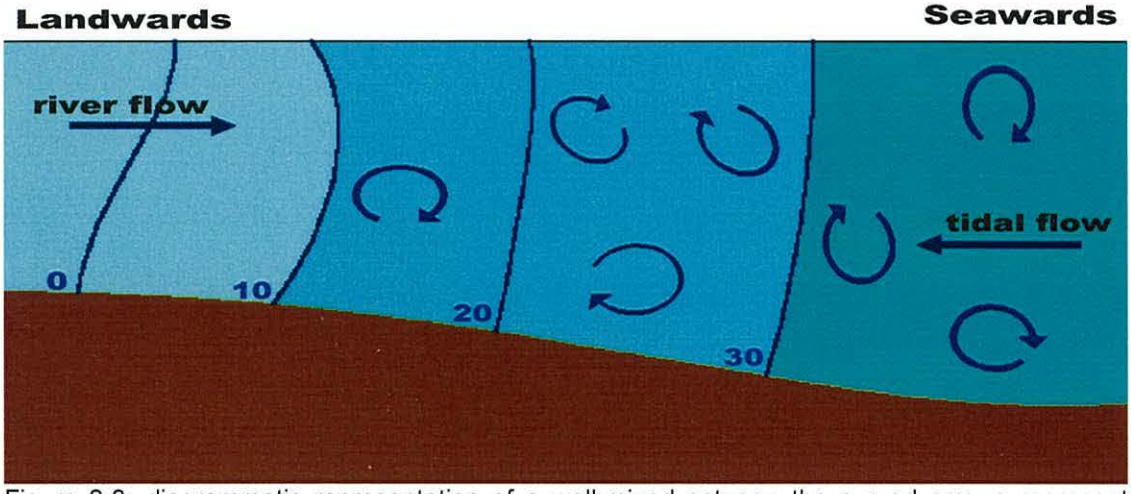

Figure 2.3: diagrammatic representation of a well-mixed estuary: the curved arrows represent mixing; the numbers represent salinity values (PSU).

2.2.4 The "Null Point"

According to Dyer (1997), in all estuarine circulation regimes the net salt-water flow is always landwards with the net fresh-water flow seawards. Since the water masses are moving in opposite directions there must be a level in the water column where the mean flow is zero. According to measurements by Dyer (1986), the landward bottom flow diminishes, and the seaward surface flow increases towards the head of the estuary, and the level of no mean motion gets progressively deeper (see Figure 2.4). Near the head of the salt intrusion, the level of no motion coincides with the bed of the channel. At this point on the bed there is no net movement of water in either direction, and is known as the null point. Landward of this null point, although the water mass is oscillating back and

forth with the tides, the net flow throughout the water column is towards the sea (Dyer, 1986; Dyer, 1997).

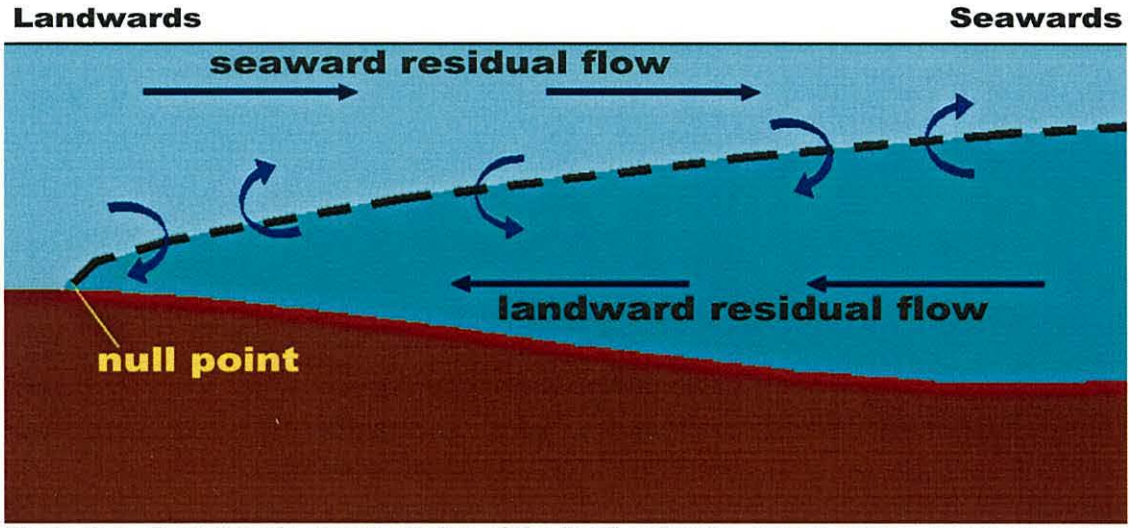

Figure 2.4: diagrammatic representation of the "null" point: the curved arrows represent mixing; the dashed line shows the depth at which there is no residual horizontal flow.

2.3 Sediment Distributions in Temperate Estuaries

Estuaries consist of three complex sections: the mouth of the estuary (or lower estuary), the body of the estuary (or middle estuary), and the head of the estuary (or upper estuary). These three sections are sub-divided vertically, into three zones, which are defined by the tide, and are:

1) The area that extends inland from the mean high water line (MHW) is termed the "supratidal" zone. This area may be inundated as a result of exceptionally high tides. Around the main estuary, the supratidal zone is usually characterised by salt marshes. At the mouth of the estuary, the supratidal zone is usually characterised by sand dunes, shingle, or hard geology.

2) The area of tidal influence occurring between the mean low water line (MLW), and mean high water line (MHW) is termed the "intertidal" zone. This zone is further divided into: 2a) higher and 2b) lower intertidal zone. The higher intertidal zone, within the body of the estuary, is usually characterised by mudflats, whilst the lower intertidal zone is characterised by sandflats.

3) The area below mean low water (MLW) is termed the "subtidal" zone. In this zone the sediments are coarser as the flow of water is continuous. Sediments may be: alluvial in character at the head of the estuary; a mixture of sands and gravels in the body; and more marine in character at the mouth of the estuary.

2.4 Sediment Transport

2.4.1 Modes of Particle Transport

The effects of currents on sediment dynamics are expressed in terms of the bed shear-stress, τ_0, which is defined as the frictional force exerted by the flow per unit area of the bed (Soulsby, 1997).

The bed shear-stress is associated with a shear velocity, through Equations 2.1 and 2.2:

$$\tau_0 = \rho u_*^2 \qquad [2.1],$$

$$u_* = (\tau_0 / \rho)^{1/2} \qquad [2.2],$$

where: τ_0 is the bed shear stress, in Nm^{-2}; ρ is the water density, in kgm^{-3}; and u_* is the shear velocity, in ms^{-1}.

The total bed shear-stress, τ_0, acting on the bed is the sum of: a) the skin friction, τ_{0s}, produced by (and acting on) the sediment grains; b) the form drag, τ_{0f}, produced by the pressure field associated with the flow over ripples and/or large features on the bed; and c) a sediment transport contribution, τ_{0t}, caused by momentum transfer to mobilise the grains (Dyer, 1986; Soulsby, 1997).

According to Soulsby (1997), only the skin-friction contribution acts directly on the sediment grains. Hence, the skin friction is used in calculating the threshold of motion.

Once the grains start moving (i.e. the threshold of motion has been reached), they do so in three different ways, (Dyer, 1986):

i) Rolling: At stresses very close to the threshold the exposed grains will be forced to roll out of positions and roll downstream until they find a new stable position.

ii) Saltation: Momentary initial impulses of fluid drag and lift cause particles to jump into the flow at an angle of about 50 degrees. They perform a ballistic trajectory which is continuously concave downwards. The maximum height of rise is about two to four grain diameters. On landing the grain may bounce, but normally there is insufficient inertia in the grain to cause other grains to saltate after the impact.

iii) Suspension: When the vertical components of the turbulent velocity are approximately equal to the settling velocity of the grain, the form of the grain trajectory changes. They become wavy in their upper part, with convex downwards sections, and the jumps become much longer. These jumps are also higher, the grains seldom approaching less than

two to three diameters from the bed. If they do, they normally return to the bed, where they can saltate or be taken again into suspension. It is commonly assumed that suspension occurs when the upward directed components of the turbulent velocity fluctuations w'_{up} exceeds the settling velocity of the grains.

The total sediment load that moves by rolling, or saltation, is termed "bedload", and is mainly made up of non-cohesive sediment. On the other hand, the total sediment load in suspension is termed "suspended load" and although it can contain fine non-cohesive particles, it mainly consists of cohesive sediment.

2.4.2 Non-Cohesive Sediment

Non-cohesive sediment deposits are composed of individual grains of minerals. The precise composition depends on the geology of the estuary and its surroundings. Many deposits contain large portions of quartz and feldspar, which have similar densities (about 2.65 times that of water). However, deposits also contain calcium carbonate shell fragments and small amounts (usually < 2% of the total) of heavy minerals such as zircon and magnetite (with a density of about 4 to 5 times that of water). The presence of particular heavy minerals can be very useful in establishing the source of particular sediments (McDowell and O'Connor, 1977).

The mineral composition of individual sediment grains is also largely responsible for the wide variety of particle shapes found in natural deposits. Igneous materials, such as feldspar, produces spheroidal-shaped grains, while the metamorphic slates and shales produce flat disc-like particles. All particles moving on the estuary bed are smoothed and rounded by the abrasive action of other grains during sediment motion. A particular estuarine deposit thus usually contains a large number of particles of widely different density, shape and form, with the harder materials, such as quartz, forming the bulk of the deposit. Particle

shape, size and density are of fundamental importance from a sediment transport view point since they influence both the erosion and deposition of material (McDowell and O'Connor, 1977).

The size and distribution of particles in a particular estuarine deposit are largely controlled by the ability of the tidal streams to move and transport individual sediment grains. Thus, silt and fine sand deposits are found along estuary margins while medium to coarse sand is found in the main channel(s). Gravel may appear locally in areas of high velocity and turbulence, such as occur on the outside of channel bends. However, the presence of grains of widely different density or size can produce a protective layer on the surface of a deposit which prevents the erosion of any underlying fine material (McDowell and O'Connor, 1977).

As sediment grains become mobile, an initially flat bed deforms into a series of undulations which in turn affect sediment transport rates and cause an increase in resistance to flow. A progressive increase in velocity results in development of bed forms similar to those found in steady state flow. If bed material is less than 600 μm diameter, ripples form on the bed. At higher flow speeds, ripples give way to dunes which are much larger (McDowell and O'Connor, 1977).

Many estuary deposits contain large proportions of fine-medium sized material (60-200 μm) which is readily set in motion by tidal currents. Such particles have a relatively small submerged weight and therefore are easily entrained within the flow by turbulent eddy motions, particularly from the crest of bed forms. The primary transport mode of such sediment in a high energy flow is as suspended load and such sediment may amount to some 75-95 % of the total load (McDowell and O'Connor, 1977).

2.4.3 Cohesive Sediment

Cohesion is the attractive force between particles of the same kind, whereas adhesion refers to the attractive force between materials of different kinds (Press and Siever, 1998).

Particles in suspension are usually composed of individual particles of clays, whose size is in the range 1 - 10 μm. However these may be aggregated with organic matter and water to form much larger, low density flocs (Postma, 1980).

Clay particles are plate-like with a length dimension of typically less than 2 μm, which is typically of the order of 10 times the thickness (Dyer, 1986). These clay particles are mainly minerals such as illite, kaolinite, montmorillonite, and chlorite which are derived principally from the weathering of rocks and by the reduction of one clay mineral to another. The clay minerals themselves are composed of hydrated silicates of iron, aluminium and magnesium and may also be mixed with electrochemically charged organic matter from chemical plants and sewage works (McDowell and O'Connor, 1977). Their surfaces have ionic charges creating forces comparable to or exceeding the gravitation force, and these cause individual particles to interact electrostatically. Consequently they do not act as separate individual particles but stick together. The degree of 'stickiness' – cohesion – rises with the proportion of clay minerals in the sediment and starts becoming significant when the sediment contains more than 5-10 % of clay by weight. Cohesive sediments have different threshold characteristics, packing structure and physical and hydraulic properties from cohesionless sands (Dyer, 1986).

The clay particles carry a negative surface charge arising from lattice discontinuities. This total negative charge is balanced by a double layer of hydrated cations. The stability of the charge balance is directly depended on the ionic concentrations in the bulk water, and as ionic strength increases there is a

tendency for the particles to flocculate as the charge equilibrium is disturbed (Aston and Chester, 1976), see section 2.4.4 for more details on flocculation.

The erosion of flocculated deposits is a much more complicated process than that of non-cohesive particles. The erosion resistance of a deposit depends largely on the cementation action of chemicals on surface particles, the ionic bond strength of surface flocs and the degree of consolidation of the deposit. This latter facet depends, in turn on the mineral composition of the sediment, the shape and packing of individual flocs and floc groups, the presence of easily compressible organic material and sand drainage paths, the physical and chemical properties of fluid environment and time (McDowell and O'Connor, 1997).

Clay material deposited in saline water may exhibit a total loss in shear strength if exposed to a freshwater environment for sufficient time, so that the saline pore water is replaced by freshwater. A slight disturbance may then be sufficient to set the bed in motion. Clay deposits sometimes exhibit thixotrophic behaviour and show an increase in shear strength (and thus in resistance to erosion) during slack water periods. In this way sediment deposits may accumulate on the bed during neap tide periods only to be eroded again during the next spring tide cycle (McDowell and O'Connor, 1997).

2.4.4 Flocculation

Inorganic flocculates form because of short-range attractive forces between grains. In seawater, which is a strong electrolyte, swarms of ions leave the clay particles. Left "unprotected", the particles may coalesce into chains and large clumps.

Organic flocculates form when small grains coalesce with others due to mucous binding (by bacteria and other micro-organisms).

In more detail, the Van Der Waals forces cause attraction whilst the electrostatic forces cause repulsion, where:

1) Van Der Waals force is a molecular attractive force, V_A. For spheres $V_A \propto d^{-7}$ and for plates $V_A \propto d^{-3}$ (where d is the diameter).

2) Electrostatic force V_R is due to: a) broken bonds (-ve on face and +ve on edge); b) unbalanced ionic substitution (-ve). For clays, V_R is –ve overall.

In saline waters the negative charge of clay particles is reduced, $V_A > V_R$, causing particles to flocculate. The negative charge decreases exponentially with increasing salinity, so flocculation occurs rapidly at low salinities. Mucous films (from bacterial activity) having positive charge, enhance the flocculation by decreasing V_R.

The biogeochemical/ecological impact of suspended particulate matter (SPM) is determined primarily by the size of the particles (Jago and Jones, 2002). Light scattering, absorptive capacity, and settling flux are controlled by particle size. There are two modes that contribute to the distribution of aggregate size: macroflocs that reach a size of the order of millimetres and microflocs of the order of 10 to 20 microns (Mehta and Dyer, 1990). Macroflocs can be readily broken down in stages by turbulent shear to eventually form microflocs, which are more resistant to turbulence.

Flocs can grow to a large size, but have relatively low density, because of high water content (Dyer, 1986). Though the individual particles may have densities of about 2600 kgm^{-3}, the flocs range in density are between 1060 - 1800 kgm^{-3}. A floc with density of ~1150 kgm^{-3} would have porosity 91% water by volume. Consequently the floc size and surface area will be much larger than that of a quartz grain having the same settling velocity. They are also fragile and easily

broken, e.g. by conventional sampling methods, into components an order of magnitude smaller than the flocs themselves (Jago and Jones, 2002).

For flocculation to occur the particles must be in close proximity. So collisions are essential (Dyer, 1986). Several mechanisms are thought to contribute:

1. Brownian motion. This is caused by bombardment of particles by thermally agitated water molecules. If particles are of uniform size, then the collision rate is:

   $J_B = (4 \kappa T No) / (3 \mu)$ [2.3],

   where κ is Boltzmann's constant, T is temperature, No is number concentration of particles, μ is the molecular viscosity of water. This mechanism is only effective at high particle concentrations and for particle diameters < 1μm.

2. Fluid shear. In zones of fluid shear, collisions will occur if the distance between shearing layers is less than the sum of the particle radii. The collision rate will be:

   $J_S = (4/3) No \Sigma r^3 (du/dz)$ [2.4],

   where Σr is the sum of the radii of colliding particles, du/dz is the local shear. If Σr is large and du/dz is small, then $J_S > J_B$. If Σr is small and du/dz is large, then $J_S < J_B$. If du/dz though is very large, particles will break up.

3. Internal encounters. Larger particles exhibit greater inertia and respond more slowly to fluid accelerations than do smaller particles. So smaller particles overtake larger ones and collisions occur. The collision rate is:

$$J_I = 1.294\ \Sigma r^3\ (E_d/\nu)^{1/2}\ N_1\ N_2 \qquad [2.5]$$

where E_d is turbulent energy dissipation rate, ν is kinetic viscosity; N_1 and N_2 are number concentrations of particles of two different sizes. Important when there are a few large particles in a suspension of mostly fine particles and when particles differ in size by more than 4 times the turbulent microscale length (which is c. 100μm).

4. Differential settling. In this case, collisions will occur, since large particles settle faster than smaller ones. The collision rate is:

$$J_D = \pi\ \Sigma r\ dw\ No \qquad [2.6],$$

where dw is relative settling velocity. Important when there is little fluid shear (e.g. slack water) but produces weak flocs.

Since flocculation depends on the particle number concentration and on the velocity shear, it can be expected that the floc strength, and settling velocity will vary with these parameters, hence be time variable (Dyer, 1986).

2.4.5 Settling

According to Dyer, (1986), when a spherical particle with density greater than the density of water is released within a column of water, then the particle will start to fall. After a distance of a few particle diameters its velocity becomes constant. This velocity is termed the terminal fall velocity, and it is achieved when the drag forces equal the immersed weight of the spherical particle.

From Dyer, (1986), the drag force on the particle can be written in terms of a drag coefficient and thus:

$$F_D = C_D \pi (d^2/4) \rho (w_s^2/2) \quad [2.7],$$

where F_D is the drag force, C_D is the drag coefficient, d is particle diameter, ρ is water density, and w_s the settling velocity.

The difference between the force of gravity acting downwards and the buoyancy force acting upwards, is called immersed weight, I.

$$I = (4/3) \pi (d^3/8) (\rho_s - \rho) g \quad [2.8],$$

where ρ_s is the density of the particle and g is the acceleration due to gravity.

The flow around a spherical particle, according to Dyer (1986), will differ depending on whether it falls slowly, when viscosity will be important, or fast, when the grain inertia dominates. A Reynolds number can be formed from the fall velocity and the particle diameter as a measure of these effects:

$$Re = (w_s d) / \nu \quad [2.9],$$

where Re is the Reynolds number and ν is the kinematic viscosity.

At Reynolds number <1 laminar flow conditions exist, and the drag force can be calculated as:

$$F_D = 3 \pi \mu d w_s \quad [2.10],$$

where μ is the molecular viscosity, $\mu = \nu \rho$.

From Equations 2.8 and 2.10 we have:

$$w_s = g (d^2/18) [(\rho_s - \rho) / \mu] \quad [2.11],$$

This is Stokes Law and it demonstrates that $w_s \propto d^2$.

From Equations 2.7 and 2.10 we have:

$$C_D = 24/Re \qquad [2.12]$$

For non-laminar flow, equation 2.12 no longer applies when Re >1, and when Re $>10^3$, C_D becomes constant. Then C_D is independent of the d in equation 2.7, so $w_s \propto d^{1/2}$. This is generally known as the Impact Law.

2.5 The Estuarine Turbidity Maximum

2.5.1 The Formation and Maintenance of the Estuarine Turbidity Maximum

For the middle to lower reaches of a well-mixed or stratified estuary, the longitudinal density-gradient will usually be dominant; and the net bottom current will be in an up-estuary direction (Officer, 1983). This landward bottom flow is sufficiently strong to move suspended sediment up the estuary to the head of the salt intrusion (Postma, 1980).

For the uppermost reaches of an estuary and its associated tributary river, the longitudinal salinity gradient will be negligible, and the flow will be riverine in character and down-estuary at all depths. In addition materials, or their derived products, which are carried seaward by the surface waters may sink during their down-estuary transport to the bottom waters, and can be carried back up-estuary (Officer, 1983). Vertical mixing may eventually bring the particles back into the upper water layer, so that they are again carried seaward. The process may be repeated, or the particles may be carried to the sea.

Theoretically, particles may be carried back and forth a number of times before they finally escape (Guilcher, 1967). This back and forth cycling of material produces a significant accumulation of suspended particulate matter, at and near the null point, which acts as a "nutrient and sediment trap" (Postma, 1980; Schubel, 1969; and Officer, 1983). The concentrations of suspended particulate matter within this region can be 10 to 100 times greater than those landward or seaward (Orton and Kineke, 2001).

This phenomenon of accumulated SPM within a specific region of the estuarine channel is referred to as the "estuarine turbidity maximum", or ETM (Orton and Kineke, 2001; Schubel, 1969; Officer, 1983; Postma, 1980; Guilcher, 1967; Brenon and Hir, 1999). Therefore the presence of a turbidity maximum is one of the most distinctive features of sediment transport in meso- or macrotidal estuaries (Dyer, 1986).

According to Dyer (1986), there are two dominant mechanisms which contribute to the maintenance of the turbidity maximum. For mesotidal estuaries the residual circulation of water, as described above, is the most commonly cited cause. For macrotidal estuaries the tidal asymmetry produces a net landward movement of sediment.

Tidal asymmetry is caused by the deformation of the tidal wave as it propagates upstream. Friction causes the crest of the tidal wave to travel faster than the trough (Dyer, 1986). That means that the time lag of high water between the mouth and the head of the estuary is smaller than the time lag of the low water. This causes the ebb period to become longer and the flood duration shorter, resulting in an asymmetrical tidal curve (Brenon and Hir, 1999). The flood currents are thus of higher velocity than the ebb currents. The asymmetry becomes more marked towards the head of the estuary.

Consequently there is a preferential movement of sediment landwards towards the head of the estuary, until the point where the seaward current due to river flow becomes dominant in transporting sediment. In addition the slack water period at high water is longer than that at low water, enabling a greater proportion of material to settle to the bed. The combination of the greater velocity on the flood tide, and the settling at high water is responsible for the turbidity maximum being more pronounced on the flood than on the ebb. The landward flux over the flood tide is then balanced by a seaward flux during the ebb tide, which, though it has a lower concentration and a lower velocity, persists far longer (Dyer, 1986).

An example of tidal asymmetry can be found at the Tamar estuary, where it has been long known that tidally-induced resuspension of particulate matter is an essential mechanism for generating and maintaining the turbidity maximum (Uncles and Stephens, 1993).

The balance between residual circulation and tidal asymmetry changes along the estuary, and since the degree of stratification changes during the spring-neap cycle, both processes may be active in the same estuary at different positions and at different times. In macrotidal estuaries, residual circulation should be important at neaps with high river flow, but may not be significant at spring tides (Dyer, 1986). Also in macrotidal estuaries the turbidity maximum is maintained mainly by tidal asymmetry on short time-scales, but is influenced by the gravitational circulation at larger time-scales (Uncles et al., 2002).

The freshwater-seawater interface (FSI) is strongly associated with flocculation of fine grained SPM. Since the peak of the estuarine turbidity maximum is often situated at or near the FSI, it has been assumed to be caused by flocculation (Guilcher, 1967). The increase in settling rate due to flocculation at the limit of salt intrusion could produce a turbidity maximum. Dyer (1986), states that although the ETM has been linked to the flocculation-deflocculation process, this

has not been proved due to the inability, at that time, to measure the size of flocs in situ. He also states that even if it is proved it will most likely be a process of minor importance.

In the case of the Humber-Ouse estuary, tidal processes appeared to dominate ETM generation, and flocculation and rapid settling velocity over high water slack enhanced the ETM formation process (Uncles et al., 1994).

2.5.2 The Location and Magnitude of the Estuarine Turbidity Maximum

The peak of the turbidity maximum is often located near the salt boundary (Guilcher, 1967). Uncles et al. (1994) and Grabemann et al. (1997), for example, present a strong ETM associated with the lower salinity reaches of the Tamar and Weser estuaries. Since the freshwater-saltwater interface moves up and down the estuary in accordance to the tides, the ETM should also follow the same pattern.

2.5.2.1 Estuarine Turbidity Maximum in a Simplified Estuary

In order to understand the continuous change in location and magnitude of the ETM, a simplified estuary will be considered. To be exact, this estuary will have a constant river discharge; a constant tidal cycle, meaning there are no spring-neap cycles or any changes in tidal range; and it will also be of average dimensions, with a funnel-like shape; finally it will have a sufficient sediment stock, throughout, for the formation of the ETM.

The turbidity maximum forms at low-water slack by the density circulation, as described previously, within the estuary near the mouth. As the flood tide forces seawater into the estuary, the ETM moves with the intruding tide, following the FSI. The strong flood currents encourage erosion and resuspension of sediment that had been deposited either during the weaker ebb tide, or during the low-

water slack. This means that there is more mobile SPM in the water column to feed the ETM, which gradually intensifies as it moves up-estuary. The turbidity maximum reaches its upper limit at high-water. There, the particulate matter that needs the fast moving currents of the flood to stay in suspension start to settle, and some of them are deposited in situ during the high-water slack. When the tide starts ebbing the currents at the bed are not strong enough to resuspend settled sediment. Eventually the ebb currents pick up, but the amount of sediment resuspended is generally less than that resuspended on the flood. During the ebb, both the FSI and the ETM are pushed gradually down-estuary. At low-water the ETM has reached its lower limit, and at slack water it has lost the ability to maintain the particulate matter in suspension. So the turbidity maximum weakens and a considerable amount of sediment settles and is deposited. Finally the cycle starts over again when the tide turns.

In this simplified estuary it is clear that the ETM is formed by the density circulation caused by the FSI. It is also clear that the tidal dynamics control its location and magnitude. In actual estuaries, though, it is more complex. Specifically the controls for the formation, maintenance, location and magnitude of the turbidity maximum are complex. For example, the magnitude depends on a number of factors, and the *amount* of suspended matter supplied to the river or the sea is most important. The strength of the estuarine circulation is a second important factor. The settling velocity of the available material also exerts a strong influence (Guilcher, 1967). And according to Festa and Hansen (1978) the magnitude of the ETM, relative to the total source concentration, depends upon the settling velocity and circulation patterns alone, except at the smallest settling velocities for which the phenomenon is poorly developed.

2.5.2.2 Estuarine Turbidity Maximum in Actual Estuaries

The complex controls of the ETM characteristics are due to a number of factors. The most straightforward way of understanding this complex system of controls

is to consider each influencing factor on its own. These major factors are: tide dynamics; river discharge; geomorphology of the estuary; availability of sediment from within the estuary and the surrounding areas; time of year; and human intervention.

2.5.2.2.1 Tidal Dynamics

In estuaries such as the Gironde, where tidal action is strong and there is a relatively large influx of suspended sediment, the ETM is a permanent feature, and its density and size vary with tidal conditions (Allen, 1975). Tidal conditions are the range of the tide, the spring-neap cycle and any specific tidal characteristics due to the geographical location of the estuary.

In steady river discharge conditions the tidal range is the main control of the degree of mixing within the estuary, i.e. is the estuary going to be stratified or well mixed? This means that the physics of the estuary, such as density circulation, will be dependent on the tidal range. Uncles et al. (2002), after measurements, highlight the fact that the tidal range is a major control of the magnitude of the ETM.

The neap-spring cycle, though, controls the actual sedimentation processes, especially SPM levels (Allen, 1975). According to Grabemann et al. (1997), there is a hysteresis in SPM concentrations, in which concentrations are higher on the falling spring-neap cycle than on the rising cycle. This appears to be due to some degree of consolidation of depositional sediment during the neap tides, when resuspension is relatively small or absent.

Dyer (1986) explains how both the tidal range and the spring-neap cycle interact, and in doing so they influence the physical characteristics of the ETM. He does this by considering the large variation in energy between spring and neap tides in macrotidal estuaries. During the neap-spring cycle the tidal prism varies

significantly, changing the ratio of river flow to tidal volume. Consequently, though the estuary may be well mixed at spring tide, at neap tides it can be partially mixed, or even well stratified. At spring tide the turbidity maximum will have its highest concentration, the currents being able to erode and sustain more sediment in suspension, and it will be further up the estuary. This is due to the fact that there is a higher mean sea level in the upper estuary at springs than at neap tides, arising because the increased range at spring tides involves a large extra volume of water at high tide, but only a slight volume difference at low tide, relative to the neaps. During decreasing tidal amplitude towards neaps, the peak currents decrease, and less and less material is capable of being re-eroded and suspended. Additionally the durations of slack water increase, enhancing deposition.

2.5.2.2.2 River Discharge

A strong river flow can push the ETM out of the estuary and at the same time decreases its magnitude (Guilcher, 1967; Postma, 1980; Uncles and Stephens, 1993; and Grabemann et al., 1997). An example of this can be seen in the Tamar and Gironde Estuaries, where the ETM migrates up-estuary during low river runoff and is located down-estuary during high runoff (Uncles et al., 1994).

The depression in the magnitude of the ETM may be explained as follows: assuming that the tidal forces remain the same, an increase of the river discharge will cause better stratification and less vertical mixing. This will decrease upstream water transport in the salt-wedge. The flow of the river water to the sea will be accelerated. As a result, the opportunity for entrapment of particles is reduced, and concentrations of suspended matter must decrease. It should be added that very low river discharges must also be detrimental to the development of an ETM, since the estuarine circulation may practically disappear. Hence, in a constant tidal regime, a certain volume of river discharge will be optimal for the formation of the turbid zone (Guilcher, 1967).

Gibbs (1977) shows that data from representative estuaries suggest a good correlation between the flushing velocity and the position of the turbidity maximum. The flushing velocity may be obtained by dividing the river discharge, Q, by the cross-sectional area, A, of that part of the estuary: $f_v = Q/A$. In the case of an estuary having a low flushing velocity, the ETM will develop in the upper part of the estuary and never be exposed to the oceanic transport agents.

2.5.2.2.3 Sediment Availability

Mobile sediment is a large source of material for resuspension and its location is crucial to the magnitude and location of the ETM. Clearly, areas devoid of erodible sediment are unable to contribute to the ETM (Uncles et al., 1994).

Grabemann et al. (1997), indicate the importance of a mobile sediment source with the following example. In the Tamar estuary there is a pronounced ETM, which occurs up-estuary of the freshwater-saltwater interface, under low runoff, spring tide conditions and is due to resuspension from a large source of bed sediment there. Such an up-estuary ETM is not observed in the Weser, because of the absence of a corresponding large bed-source of sediment.

Mitchell at al. (2003), conclude that the suspended sediment concentrations on any given tide is related to the tidal range, the freshwater flow, the proximity of the mobile mud-reach (non-consolidated sediment), and the availability of sediment within the mud reach.

2.5.2.2.4 Seasonal Effects

Seasonal variations in river discharge control the position of the ETM and hence the locus of accumulation of suspended sediment (Uncles and Stephens, 1993; and Allen, 1975).

In the Gironde the ETM migrates longitudinal according to the river flow, as seen above. There is an accompanying shift in the sediment shoaling pattern, which consists of sediment accumulation in the upper estuary in summer and autumn and in the lower estuary in winter and spring. A similar seasonal pattern of sediment movement has been observed in the Tamar estuary (Uncles et al., 1994).

2.5.2.2.5 Geomorphology and Human Intervention

The bathymetry can affect the location and concentration of the sediment (Brenon and Hir, 1999). Also the alteration of the estuarine topography can have an effect on turbidity maximum characteristics. In the Seine estuary there has been progressive marsh reclamation and landfill, coupled with dredging of the channel, over the last 130 years. This has caused a progressive migration of the turbidity maximum about 50 km down the estuary. Consequently the area of maximum deposition now occurs in harbour areas at the mouth (Dyer, 1986).

From all of the above it is obvious that the formation and the physical characteristics of the estuarine turbidity maximum are dependent on a variety of controlling factors. This causes problems when coming to study and understand the ETM, because not only is there a combination of controls, there is also a wide variety of combinations, changing from estuary to estuary.

2.5.3 Sediment Within the Estuarine Turbidity Maximum

According to Schubel (1969), for a given circulation regime the population of particles suspended within an ETM might be expected to have a narrow size distribution – at least in terms of Stoke's diameter or settling velocities. Particles with settling velocities much greater than the mean vertical mixing velocity would be deposited, and once deposited these particles whose threshold erosion

velocities exceed the maximum current velocity would not be resuspended; others would be alternately suspended and deposited. On the other hand, particles with settling velocities much less than the mean vertical mixing velocities would eventually be carried far downstream or out to sea by the net non-tidal seaward flow of the upper layer. Between these two "critical" settling velocities, there would be a subset of particles which would be repeatedly exchanged between, the upper and lower layers and which would be effectively trapped within the zone of the turbidity maximum. Some of these particles would be alternately resuspended and deposited on time scales of a few hours with the waxing and waning of the tidal currents, while others would remain in suspension over much longer time scales.

In a number of estuaries, very high concentrations of suspended material occur near the bed, beneath the turbidity maximum. These concentrations are called fluid mud, which is a dense mud (fine particle) layer. According to Normant et al. (1998) the fluid mud is formed during low energy conditions, when the mud flocs settle and concentrate near the bed. This layer of 0.5 – 2 m thick and with concentrations between 50 gl^{-1} and 200 gl^{-1} is able to flow horizontally under the influence of gravity, hydrostatic forces or the overlying water currents. The fluid mud plays an important role in the total fine sediment transport in many macrotidal estuaries. This dense suspension contains a concentration of mud flocs which is high enough to cause a significant change in the physical properties of the mud water mixture compared to those of clear water. Fluid mud in different sites can have different rheological behaviours.

3 METHODOLOGY

This research encompasses a two part study of the Conwy estuary. The first part focuses on the dynamics of suspended particulate matter (SPM): total SPM loads, net SPM flux, turbidity maximum etc. The second part focuses on the properties, distribution and provenance of the estuarine sands.

3.1 Suspended Particulate Matter dynamics

3.1.1 Instruments

In order to obtain the measurements needed for this part of the project a Conductivity Temperature Depth (CTD) profiler, an Optical Backscatter Sensor (OBS), a Transmissometer, and a Laser In-Situ Scattering and Transmissometry (LISST) profiler were deployed in both moored and spatial surveys. During the moored surveys, a current meter was also used for obtaining flow velocities.

3.1.1.1 Conductivity Temperature Depth Profiler

The CTD used was a SBE 19plus SEACAT Profiler (see Figure 3.1). This type of oceanographic instrument is designed to make in-situ measurements of conductivity, temperature and depth in both marine and fresh water environments. The 19plus is self-powered, self-contained and runs continuously, sampling at four scans per second (4Hz), it can be set to average up to 32,767 samples, whilst internally storing only the averaged data.

The three basic parameters are obtained as follows:

- Conductivity is acquired using an ultra-precision Wein-Bridge oscillator to generate a frequency output in response to changes in conductivity.
- Temperature is acquired by applying AC excitation to a bridge circuit containing an ultra-stable aged thermistor.

- Depth is measured with a pressure sensor. Strain gauge pressure is acquired by applying an AC excitation to the high performance strain gauge bridge.

Figure 3.1 Photograph provided by Ben Powell and it shows the CTD, OBS and the transmissometer units on the frame, during a survey.

3.1.1.2 Optical Backscatter Sensor

The optical backscatter sensor used was a D & A Instruments OBS-3 (see Figure 3.1). An OBS is an optical sensor for measuring turbidity and suspended solids concentrations by detecting and integrating infrared (IR) radiation scattered (at angles between 140° and 160°) from suspended matter.

This instrument consists of a high intensity infrared emitting diode (IRED), a detector (four photodiodes), and a linear, solid state temperature transducer. It is powered from the CTD unit on which it is mounted. The IRED produces a beam with half-power points at 50° in the axial plane of the sensor and 30° in the radial plane (Downing et al., 1981; OBS-3 manual).

3.1.1.3 Transmissometer

The transmissometer used was a 25 cm path length Sea Tech Transmissometer (see Figure 3.1). The instrument contains a light emitting diode (LED), and a synchronous detector separated by a fixed path length. The LED transmits a collimated laser beam, which has a wavelength of 670 nm and is 15 mm in diameter. The instrument uses the fact that suspended particles absorb and scatter light. So the detector, at a distance of 25 cm, measures the intensity of the transmission reaching it, with an accuracy of ± 0.5% (Bunt et al., 1999; Transmissometer manual).

Measuring in the red spectral band ensures that sunlight does not contaminate the received signal, and eliminates attenuation due to "gelbstoff" (i.e. coloured dissolved organic matter). The instrument is temperature compensated, has excellent long term stability, low power requirements and is usually mounted on a CTD frame.

3.1.1.4 Laser In-Situ Scattering and Transmissometry Profiler

The LISST-100 (see Figure 3.2) instrument is a multi-parameter system for in-situ observations of particle size distribution (PSD). It is self-contained and consists of a solid state laser operating at 670 nm wavelength and fibre-optically connected to a laser beam collimating system, a beam manipulation and orienting system, a scattered-light receiving lens, a specially constructed 32-ring detector, electronics for signal pre-amplification and processing, a data logger and a battery system.

The LISST-100 records the scattering intensity over a range of small angles using the 32-ring detector. The amplified outputs of this 32-ring detector, are stored in memory. This primary measurement is then mathematically inverted to get the particle size distribution. The particle size distribution is presented as volume concentration (ml/l) in each of the 32 log-spaced size bins. Optical transmission (5 cm optical path length), water depth and temperature are also recorded as supporting measurements (Agrawal and Pottsmith, 2000; LISST manual).

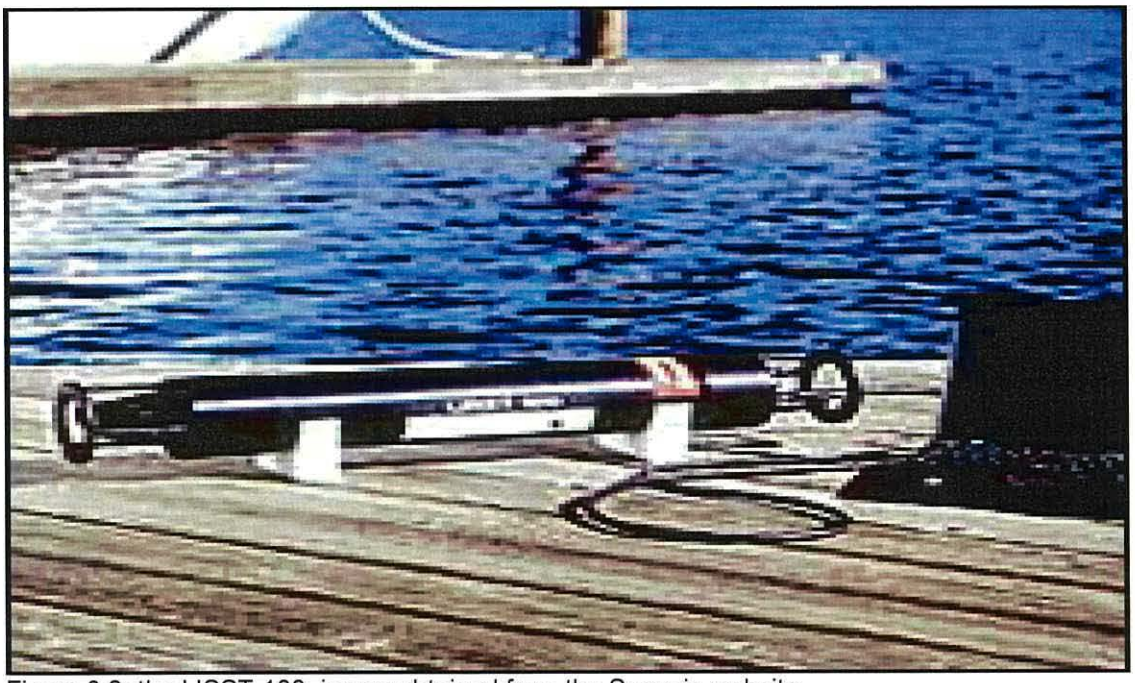

Figure 3.2: the LISST-100, image obtained from the Sequoia website.

3.1.1.5 Current Meter

The current meter used was a Valeport 108 Mk III (see Figure 3.3). This is a vector averaging, impeller current meter with temperature, conductivity and depth sensors. The vector average is based on a 5 second period during which impeller counts are measured (with an accuracy of ±1.5% of the reading for currents up to 5 m/s) and a single flux-gate compass reading is made (with an accuracy of ±0.25°), and the vector average is built up over the averaging period set.

Real time display is updated at the end of each averaging period. The control/display unit used was a Valeport CDU, model 8008. This unit features an LCD graphics display of all parameters and allows full sampling set up of the instrument. Both the current meter and the CDU were powered by a car battery.

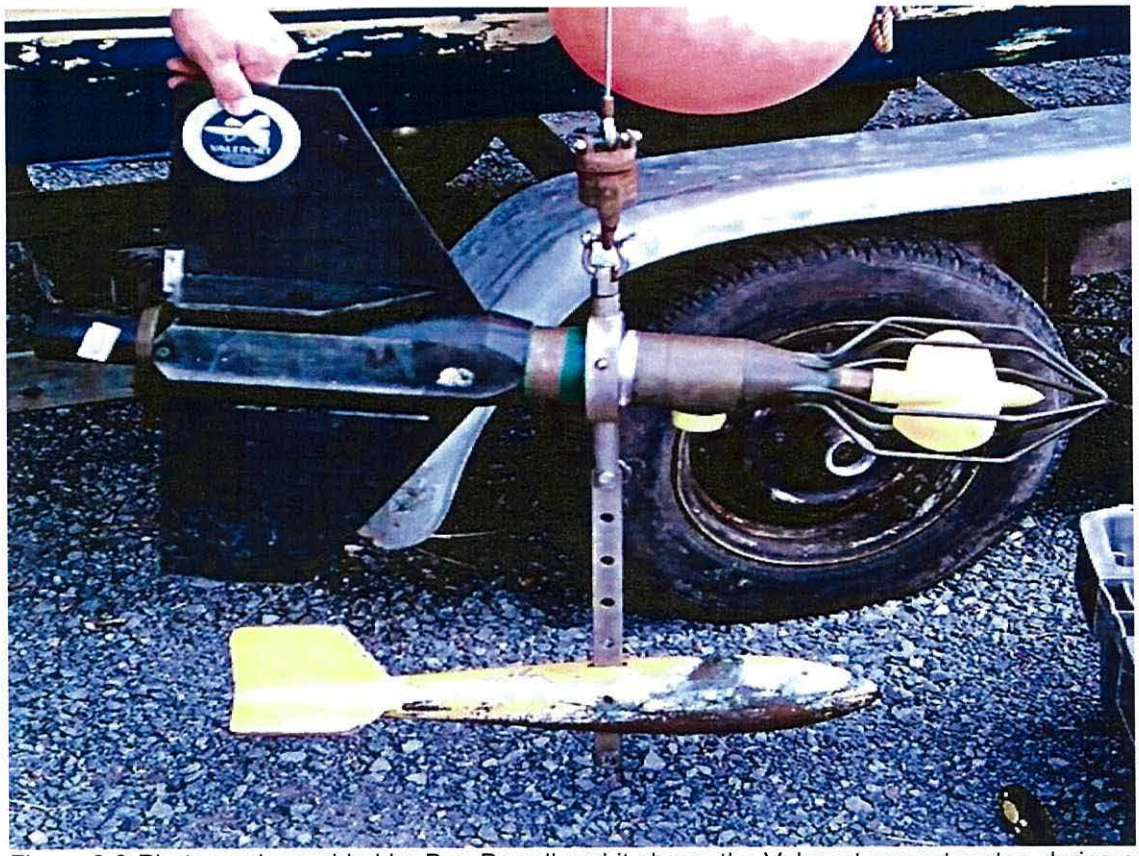

Figure 3.3 Photograph provided by Ben Powell and it shows the Valeport current meter, during a survey.

3.1.2 Strategies

In an attempt to understand the dynamics of SPM in the Conwy estuary, two surveying strategies were used. The first strategy was to obtain measurements of flow velocity and water column properties including SPM properties at discrete depths over a tidal cycle. This was done by using anchor stations (moored surveys) at predetermined positions in the estuary. The second strategy was to carry out spatial surveys to obtain quasi-synoptic measurements of water column and suspended sediment properties over the length of the estuary at high water.

3.1.2.1 Anchor Stations

Moored surveys were carried out at five different locations within the main body of the estuary (see Table 3.1 and Figure 3.4). An anchored, Leeward 18, MCA category C boat, named Mya was used as an operating platform.

The Mya was moored into position, and the surveys started as soon as the instruments were up and running. In total there were about 25 deployments at each location. Deployments took place every 30 minutes over a period of about 12.5 hours.

The current meter assembly was lowered by hand winch. Once it reached the bed, it was raised about 15 centimetres to avoid damage to the instrument by wave action or sudden movement of the boat. The current meter was left to measure and average the speed and direction of the current over a minute. The data output was read off the display unit, and was logged on waterproof paper. Then the instrument was raised to a new depth and the process repeated itself until it reached the surface, where the last reading was taken. In shallow waters the current meter was raised in 0.3 to 0.5 m intervals, whilst in deeper waters it was raised at 1.0 m intervals.

The LISST instrument was turned on before each cast and then lowered by hand, over the right-side of the boat. It was slowly lowered until it reached the bed, and then raised at the same rate. Once back on board the instrument was turned off.

The OBS and transmissometer were fitted onto the CTD frame. The frame assembly was lowered and raised by hand. Before lowering, the frame was held just beneath the water surface to allow the instruments to settle and start taking readings. Data from all three instruments were stored internally within the CTD unit. The instruments were turned on just before the cast and turned off once back on board.

Finally at the end of each deployment, water samples for gravimetric analysis were collected. These samples were taken by hand from just below the water surface, using 1 litre, plastic sampling bottles.

Station No	Site name	Date	Distance from mouth	Easting	Northing
MS1	Conwy	21/09/2004	~ 3.00 km	278700	377250
MS2	Tal-y-cafn	23/09/2004	~ 10.00 km	278750	371835
MS3	Deganwy	3/07/2006	~ 0.90 km	277600	379000
MS4	Henryd	4/07/2006	~ 6.65 km	278329	374736
MS5	Glan-Conwy	6/07/2006	~ 5.35 km	279271	375347

Table 3.1. The locations of the anchor stations according to British Ordnance Survey.

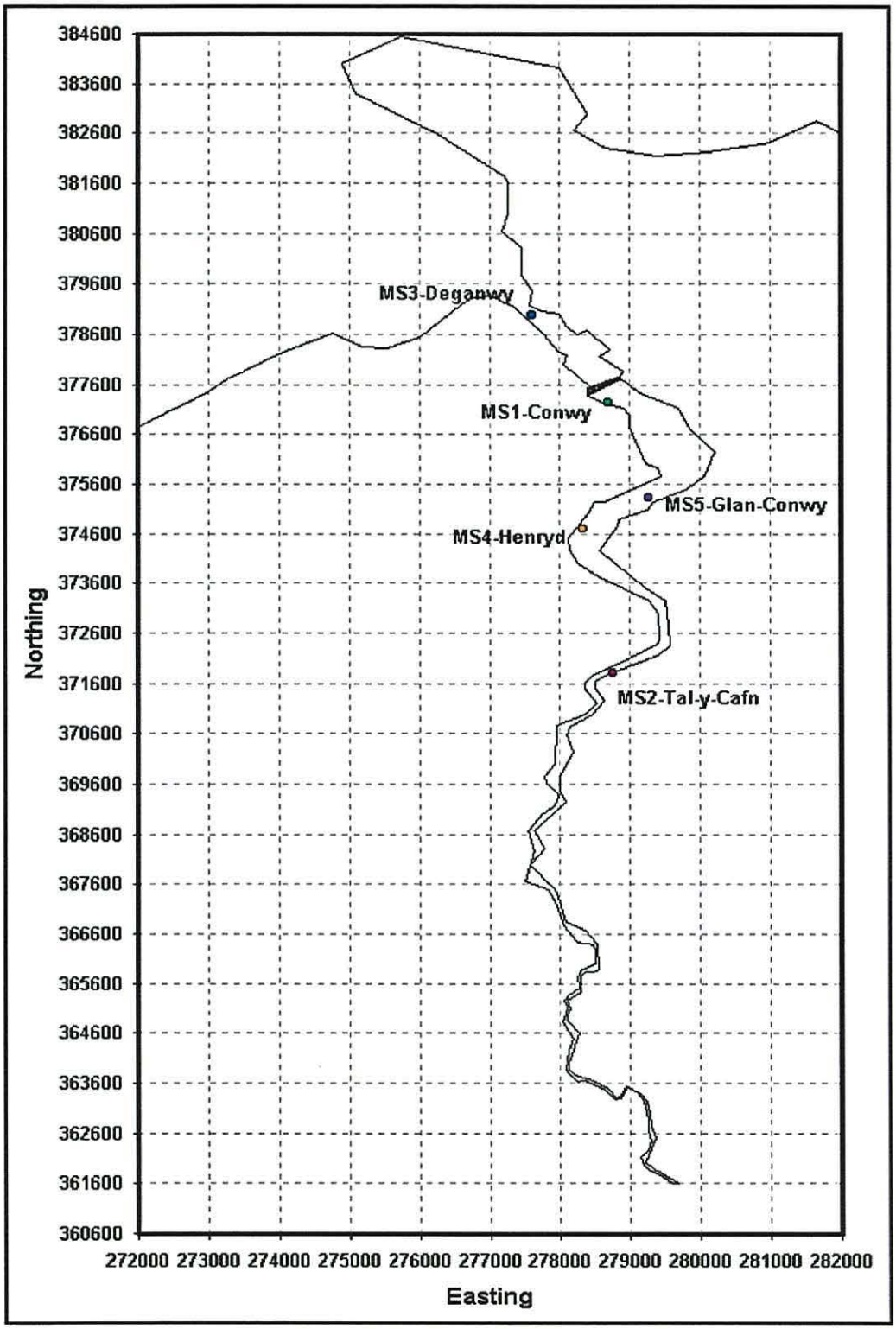

Figure 3.4 Map showing the locations of the anchor stations. The coordinates are in Easting and Northing, according to British Ordnance Survey.

3.1.2.2 Spatial Surveys

A Quintex 4.2, MCA category D, aluminium boat named Alwen Môn was used for the spatial surveys. This small boat was chosen for its good manoeuvrability, durability and its shallow draft, which allowed it to reach beyond the ETM of this relatively shallow estuary.

In total, 26 spatial surveys were carried out (see Table 3.2 for survey No and dates). The surveys started as far up estuary as it was physically possible to go on each day. The starting points themselves were determined by the on-day tidal range, but were almost always in the fresh water region beyond the estuarine turbidity maximum. Surveys commenced as close as possible to high water slack. The course of the surveys followed as closely as possible the main channel and finished down estuary at approximately 0.9 km from the mouth (see an example of sampling locations in Figure 3.5).

Each axial survey consisted of about 25 profiling stations spread out over its range, which was typically between 14 and 20 km. Profiling started just before high water slack at Conwy and ended just after the ebb tide had begun. At each station four instruments were deployed and the position was fixed by using the boat's GPS. The location and time of sampling were logged on a waterproof log sheet.

The OBS and the transmissometer were mounted on to the CTD frame. The assembly was switched on and then deployed, as with the anchor stations, over the side of the boat by hand. After the instruments were allowed to settle, the frame was lowered and raised slowly through the water column. The LISST-100 was lowered immediately after the CTD frame. In order for all instruments to sample the same water mass, the boat was allowed to drift with the current, if any.

As with the anchor stations at the end of each deployment, water samples for gravimetric analysis were collected. These samples were taken by hand from just below the water surface, using 1 litre sampling bottles. The bottle number was also noted on the log sheet.

Spatial Survey No	Date	Spatial Survey No	Date	Spatial Survey No	Date
SS1	23/11/2004	SS10	13/02/2006	SS19	25/05/2006
SS2	24/11/2004	SS11	14/02/2006	SS20	26/05/2006
SS3	26/11/2004	SS12	16/02/2006	SS21	27/05/2006
SS4	28/06/2005	SS13	17/02/2006	SS22	28/05/2006
SS5	29/06/2005	SS14	13/03/2006	SS23	25/07/2006
SS6	30/06/2004	SS15	14/03/2006	SS24	26/07/2006
SS7	12/12/2005	SS16	16/03/2006	SS25	27/07/2006
SS8	13/12/2005	SS17	23/05/2006	SS26	28/07/2006
SS9	15/12/2005	SS18	24/05/2006		

Table 3.2. Table showing the dates of the spatial surveys carried out in the Conwy estuary.

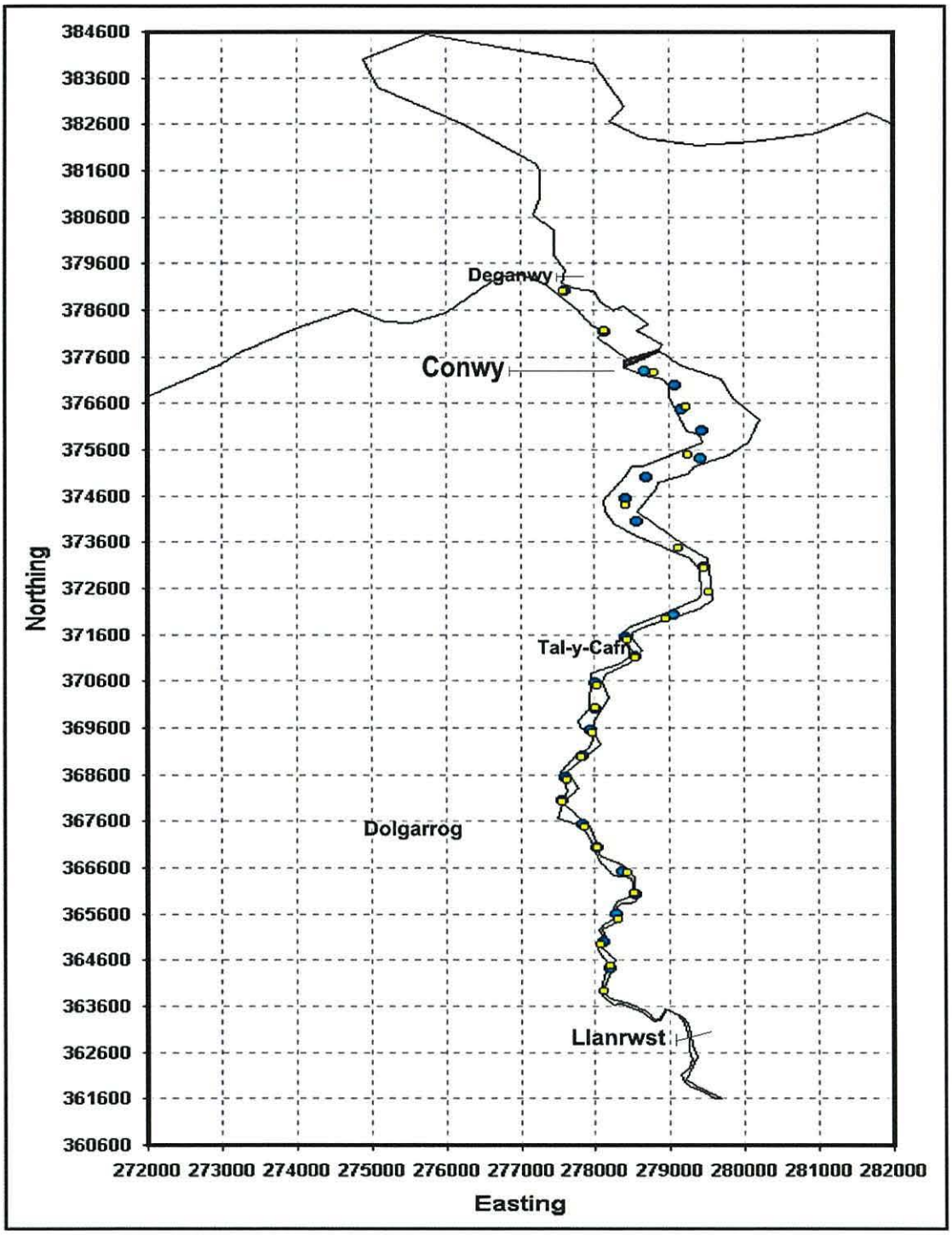

Figure 3.5 Map showing two examples of sampling locations. Yellow points indicate sampling locations for the survey carried out on the 14/3/2006, whilst the blue points indicate sampling locations for the survey carried out on the 26/7/2006. The coordinates are in Easting and Northing, according to British Ordnance Survey.

3.1.3 Instrument Calibration and Data Processing

3.1.3.1 Gravimetric Analysis

On each surveying day, surface water samples were collected as described previously. Back at the laboratory, a known volume of water from each sample was filtered onto a Whatman® GF/F glass microfibre filter (47 mm pore size), in order to obtain the total SPM concentration for that sample.

All filters were prepared at an earlier date. During their preparation they were pre-washed under suction, with 100 ml distilled water; dried in an oven, at 80 °C, over night; then placed in a desiccator to reach room temperature; and finally they were pre-weighed on a five decimal place electronic balance.

3.1.3.1.1 Procedure

The samples, in all 713, were filtered one at a time. Each sample was vigorously shaken and a known volume of water (between 250 - 500 ml, depending on the amount of solids in the sample) was then placed into the filtering unit. The unit was under negative pressure caused by a small electric pump. When all the water had passed through the filter, the filtering unit was rinsed with 100 ml distilled water to remove any residual salt. The filter with the sediment was then placed on an aluminium dish, which in turn was placed in the oven, at 80 °C, and left there over night. The next day, the filters where removed from the oven and placed in a desiccator, so that they could reach room temperature without absorbing moisture from the air. Thirty minutes later, the filters were re-weighed allowing the gravimetric determination of the total SPM concentration.

3.1.3.1.2 Accuracy of the Procedure

Ten pre-weighed filters were used to determine the overall accuracy of the above procedure. 250 ml of distilled water was passed through the blank filters, which were then dried and re-weighed. After comparing the new weights with their old ones, a loss in weight was observed. This loss was on average 0.02870 % of the initial weight. For the purpose of this project, a loss of that amount is deemed insignificant.

3.1.3.1.3 Removing the Salt

Although the filters used in the filtering, were rinsed with distilled water, not all of the salt was removed. This produced overestimated total SPM concentrations. In order to correct the measurements another pre-weighed filter was placed under every fourth (on average) filter. These blank filters were dried and re-weighed as the rest of the filters. After obtaining the weights of the blanks, the concentration due to salt could be estimated, and hence, the SPM concentrations corrected.

3.1.3.2 Calibration of the Instruments

3.1.3.2.1 OBS

The OBS is a miniature nephelometer that measures backscattering of infrared radiation by suspended particles. The strength of the backscattered signal is dependent upon the concentration and optical properties of the suspended material. Therefore, the OBS must be calibrated with a representative suspension collected in situ (Kineke and Sternberg, 1992; Schoellhamer, 1993; Green and Boon, 1993). However, potential errors exist where environmental variability causes mismatch between the target volume of suspended particles and the sample used for calibration (Hatcher, 2000).

Kineke and Sternberg (1993) compared the OBS response with mass concentration from filtered water samples. They found that the OBS response increased in the low range, reaching a maximum at a concentration of about 20,000 mgl^{-1}, and then decreased in the high range (>20,000 mgl^{-1}). Overall the OBS output was observed to increase approximately linearly for concentrations up to 10,000 mgl^{-1}.

Since total SPM concentrations from the filtered water samples did not exceed 230 mgl^{-1}, the linear part of the OBS response curve was used. This enabled the conversion of the OBS output voltage into suspended sediment concentration (SSC) data, using a simple linear regression calibration. A separate SSC data set was produced for each surveying day.

For each day the OBS voltage output, V was plotted against concentration derived from the water samples. After linear regression a calibration equation was produced:

$$SSC_{OBS} = (M * V) + N \qquad [3.1]$$

where SSC_{OBS} is the SSC derived from the OBS, M is the slope of the line and N is the y-intercept. According to Conner (1992), M is the reciprocal of the OBS gain, whilst N represents a bias in the calibration procedure resulting from the OBS output voltage not being equal to zero for measurements in distilled water.

Although the data conversion was done separately for each day using day-specific calibration curves, the regression coefficients did not vary significantly, so all the data (from 659 casts) were pooled in order to demonstrate the linear response of the instrument (see Figure 3.6).

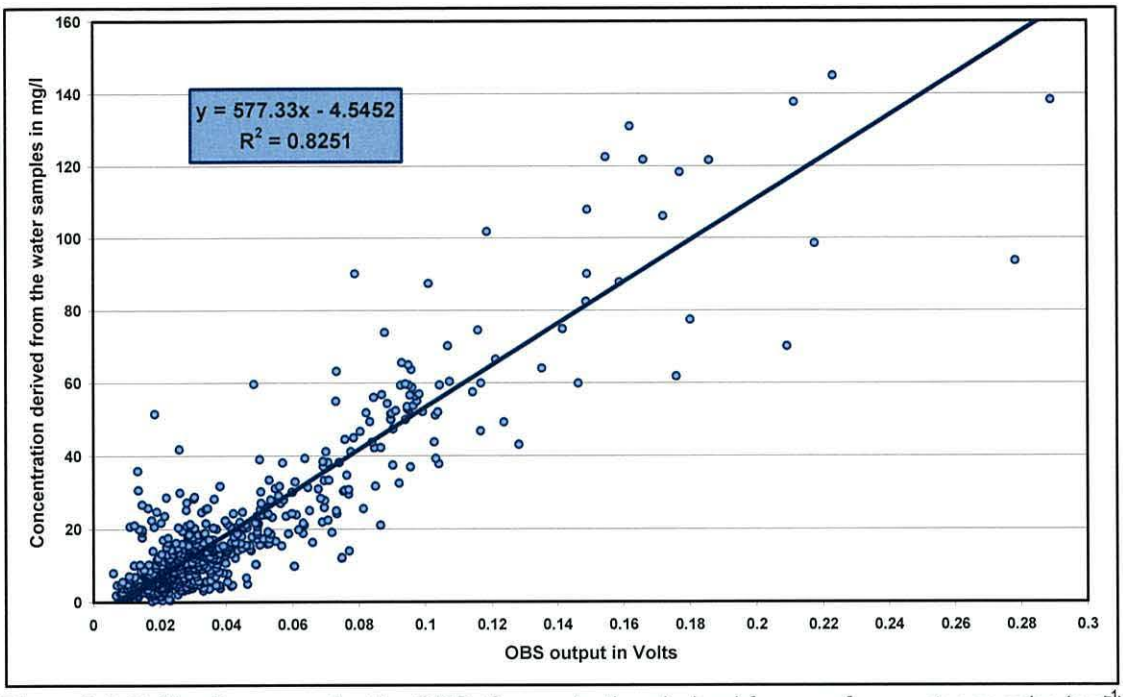

Figure 3.6 Calibration curve for the OBS. Concentration derived from surface water samples (mgl^{-1}) plotted against OBS output (volts).

The scatter around the above calibration was probably due to a combination of indeterminate error in gravimetric technique, and localised or temporal variations in particle population characteristics such as size, shape and refractive index (Campbell, 1996; Jago, 1998). The standard error derived from the above regression curve (Figure 3.6) was found to be about ± 10 mgl^{-1}.

3.1.3.2.2 Transmissometer

According to the Sea Tech transmissometer manual, the conversion of the instrument's output into beam attenuation is in two stages. The first stage is the conversion of volts direct current (VDC) to percent transmission (%T). This was done by using Equation 3.2:

$$\%T = 20 * VDC \qquad [3.2]$$

The second stage is the conversion of percent transmission (%T) to beam attenuation coefficient (c), by using Equation 3.3:

$$c = - (1/L) * \ln(\%T/100) \quad [3.3]$$

where L is the path length of the beam (in metres) and ln() is the natural logarithm.

Hence, all raw data from the 25 cm transmissometer were converted to beam attenuation data by combining Equations 3.2 and 3.3:

$$c = - (1/0.25) * \ln((20*VDC)/100)$$
$$= - 4 * \ln(VDC/5) \quad [3.4]$$

Beam attenuation (m^{-1}) was calibrated against concentration (mgl^{-1}) derived from gravimetric analysis (e.g. Campbell and Spinrad, 1987; Ishak, 1997; Jago, 1998; and Bunt et al., 1999). Therefore, the relationship, given by the linear regression, between c and SSC is:

$$SSC_{trn} = (M * c) + N \quad [3.5]$$

Where SSC_{trn} is the transmissometer derived SSC, *M* is the slope of the line and *N* is the y-intercept.

Similar to the OBS, the regression coefficients did not vary significantly, so the data were pooled in order to demonstrate the linear response of the instrument (see Figure 3.7).

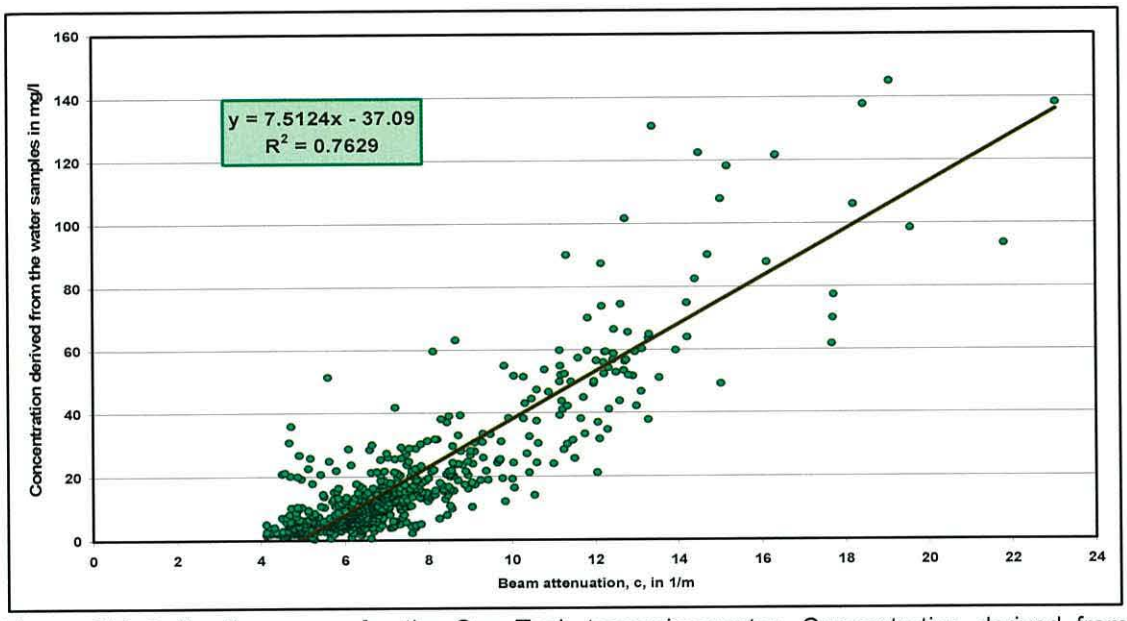

Figure 3.7 Calibration curve for the Sea Tech transmissometer. Concentration derived from surface water samples (mgl^{-1}) plotted against beam attenuation coefficient, c (m^{-1}) – data from 659 casts.

Scatter was probably due to a combination of indeterminate error in gravimetric technique, and localised or temporal variations in particle population characteristics. The standard error derived from the above regression curve (Figure 3.7) was found to be about ± 11 mgl^{-1}.

3.1.3.2.3 CTD

The data from the CTD, OBS and transmissometer were all stored within the CTD's memory. The data were stored in binary format for efficiency. A simple suite of programs (SBE data processing software) was provided by the CTD manufacturers for converting and manipulating the data.

The software converted the binary files into text, and then split the data, for upcasts and downcasts separately, into depth bins (0.3m each). The final output variables chosen were: depth in m; density in kgm^{-3}; salinity in PSU; temperature in °C; and OBS and transmissometer output voltages.

3.1.3.2.4 LISST-100β

The LISST data was stored, as with the CTD, in binary format. The data were downloaded using the LISST processing software, provided by the manufactures. The software converted the data into an ASCII particle size file, which is a spaced delimited file containing all the processed data (one file per surveying day).

The ASCII files were processed in Matlab, using Matlab scripts provided by Dr S.E. Jones. Using these scripts the data were despiked, depth bin averaged (0.3m), and split into two main groups, upcasts and downcasts.

The final data file contained the following: volume concentration ($\mu l\ l^{-1}$) for each of the 32 size classes; (the LISST also measured transmittance) computed beam attenuation coefficient, c, in m^{-1}; cast number; total volume ($\mu l\ l^{-1}$); mean diameter in μm; median diameter in μm; and depth.

The LISST transmissometer data were converted into SSC in the same way as the Sea Tech transmissometer. After calibrating the LISST transmissometer data against the total sediment concentrations (from the water samples), the following relationship was found:

$$SSC_{Ltrn} = (M^* c) + N \qquad [3.6]$$

Where SSC_{Ltrn} is the LISST transmissometer derived SSC, M is the slope of the line and N is the y-intercept.

Similar to the OBS and Sea Tech Transmissometer, the regression coefficients did not vary significantly, so the data was pooled in order to demonstrate the linear response of the instrument (see Figure 3.8).

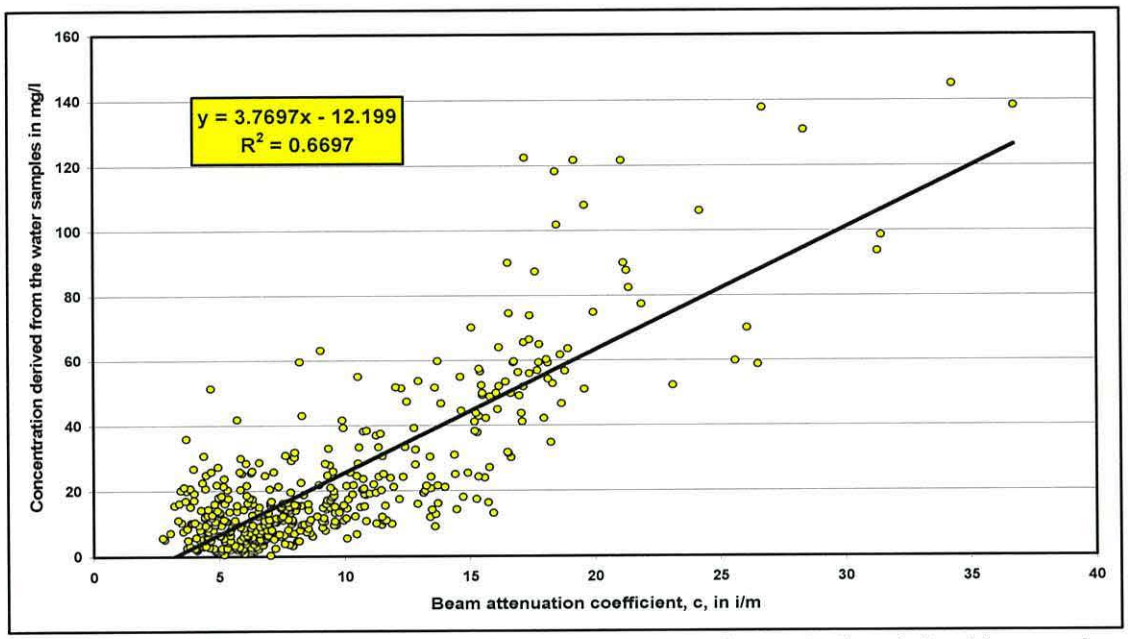

Figure 3.8 Calibration curve for the LISST transmissometer. Concentration derived from surface water samples (mgl^{-1}) plotted against beam attenuation coefficient, c (m^{-1}) – data from 436 casts.

NOTE: For technical reasons there is no LISST data for the spatial surveys carried out in February and May 2006.

3.2 Estuarine Bed Sediments – Sands

This research encompasses a two part study of the Conwy estuary: study of the SPM dynamics and study of bed sediments. This part focuses on the distribution of estuarine sands and on some of their properties.

3.2.1 Collection of Sand Samples

There were two sampling strategies employed. The first strategy involved sampling within the estuary on a grid, enabling statistical comparison between samples (grid samples). The second strategy involved collecting samples from around the estuary in order to determine the provenance of the estuarine sands (provenance samples).

3.2.1.1 Grid Samples

Samples from the mouth, body, and head of the estuary were collected using a grab sampler, deployed from a Zodiac inflatable. Sampling was done on a 0.25 x 0.25 km grid, which extended from the Deganwy beacon to Tal-y-Cafn (distance of about 10 km), see Figure 3.9. The location of each sample was entered into a GPS hand set the previous day, enabling quick and precise on-day sampling.

The use of the grid was only limited by the geomorphology of the estuary itself. Towards the head of the estuary (the last 2 km) geomorphology restrained sampling to the main channel.

In total there were 72 sampling locations visited over 3 days (21-23/11/2004), yielding 60 sand samples. The samples were, as mentioned earlier, collected using a grab sampler. A handful of sand from each sample was placed in pre-numbered plastic food bags for transportation back to the laboratory.

3.2.1.2 Provenance Samples

Provenance samples were collected in 2 phases. The first phase included sampling from the tributaries, whilst the second phase included sampling from the river and the bay.

3.2.1.2.1 Samples from the Tributaries

On the 17th of July 2006 sampling was done using a private car. The car, starting from Conwy, followed the road down the western side of the estuary all the way to Betws-y-Coed were it turned and followed the road up the eastern side of the estuary ending back in Conwy. Where access was possible, sampling was attempted. In most tributaries the sediment was of gravel size and coarser. In total seven samples were collected. The sampling locations were fixed using a handheld GPS, see Figure 3.9.

3.2.1.2.2 Samples from the River and Bay

The river and bay samples were collected on two separate days with two different sampling strategies.

3.2.1.2.2.1 River Samples

The river samples were collected on the 24th of November 2006 using a grab sampler deployed from RV Alwen Môn. Sampling started at Llanrwst and ended at Tal-y-Cafn, see Figure 3.9. Samples were mainly taken from the main channel. The sampling locations were fixed using a handheld GPS.

In total there were 17 sampling locations visited yielding 13 sand samples and 4 gravel samples. A handful of sand from each sample was placed in pre-numbered plastic food bags for transportation back to the laboratory. A handful of gravel from the gravel samples was also bagged.

3.2.1.2.2.2 Bay Samples

The bay samples were collected on the 18th of December 2006 using a grab sampler deployed from RV Alwen Môn. Sampling was done on a 1 x 1 km grid, which covered an area of 4 km^2, see Figure 3.9. The location of each sample was entered into a GPS hand set the previous day, enabling quick and precise on-day sampling.

In total there were 13 sampling locations visited yielding 9 sand samples and 4 gravel samples. A handful of sand from each sample was placed in pre-numbered plastic food bags for transportation back to the laboratory; the gravel samples were not bagged.

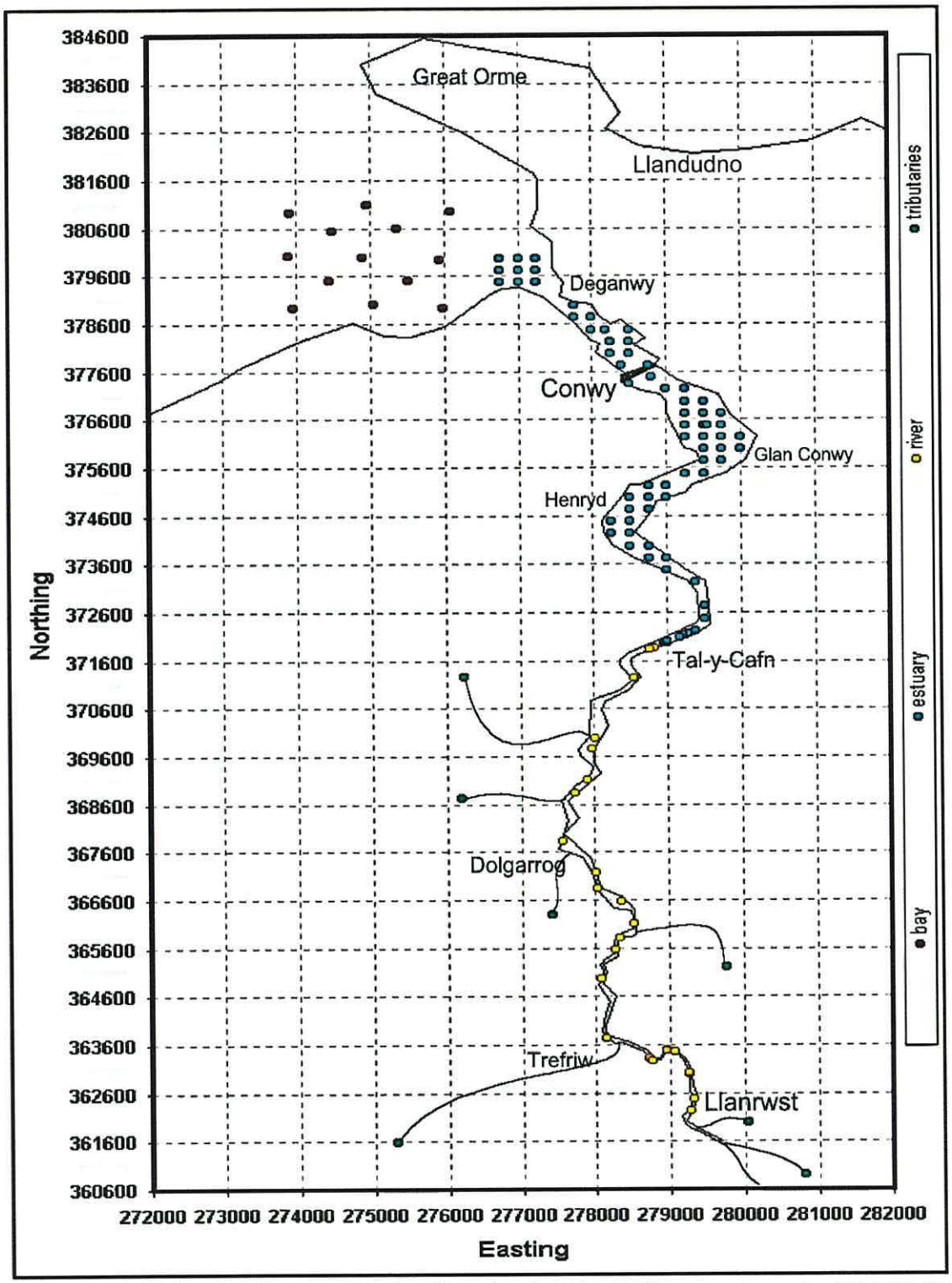

Figure 3.9 Map showing the sampling locations. Red points are the samples collected from the bay. Blue points are the samples collected from the estuary mouth and body. Yellow points are the samples collected from the river and the head of the estuary. Green points are the samples collected from the tributaries. The coordinates are in Easting and Northing, according to British Ordnance Survey.

3.2.2 Sample Processing

Back at the laboratories the sand samples were wet-sieved to remove anything with diameter less than 63 μm, then dry-sieved for determination of particle size properties. In order to determine the sand provenance, selected samples were compared under the microscope (microscopy).

In total 109 samples were collected, out of which 22 contained more than 80%, of their volume, either mud or gravel. These 22 samples were noted and were not processed further.

3.2.2.1 Wet-Sieving

The 87 remaining sand samples were wet sieved. Each sample was placed on a 63μm aperture sieve, where it was sieved under running, warm, water. After the majority of the mud/silt and salt were removed, the remaining sample was placed on a heat resistant plate. After all samples were sieved and placed on plates, they were all placed in the oven, at 60°C, and left there to dry thoroughly.

3.2.2.2 Dry-Sieving

Each sample after it was thoroughly dried was dry sieved as follows:

i. The sample was split into sixths using a School of Ocean Sciences made sand sample splitter. Three sixths (on average 100 -150 g), of the sample, were weighed to 0.01 g and then used for sieving.

ii. 25 sieves at 0.25ϕ intervals were used. The first sieve had an aperture of -2ϕ (4mm).

iii. Once the sample was placed on the sieves, the sieves where shaken for 10 minutes, using a mechanical shaker.

iv. After the sieves were shaken, one by one their content was emptied into an evaporating dish. The dish was sitting on an electrical balance. By emptying the sieves in such a way the cumulative weight was recorded (also recorded were the initial and final weight) using a purpose made table.

v. Finally the table was digitized. And by using an Excel spreadsheet (provided by Dr. J. Bennell) the grain size properties were determined. The spreadsheet plotted the cumulative coarser than, values against the 'phi' diameter on a probability graph (see Appendix A). It then calculated the Inman (1952), parameters (e.g. graphic mean size, sorting etc.).

3.2.2.3 Microscopy

In order to determine the sand provenance, 42 samples were selected for microscopy analysis (13 from the bay, 15 from the estuary, and 14 from the river and tributaries). The weight of the sand on the each sieve was plotted against the aperture of that sieve, see Figure 3.10. From the plot it was determined that the modal diameter of the estuarine sand samples was 0.18 mm.

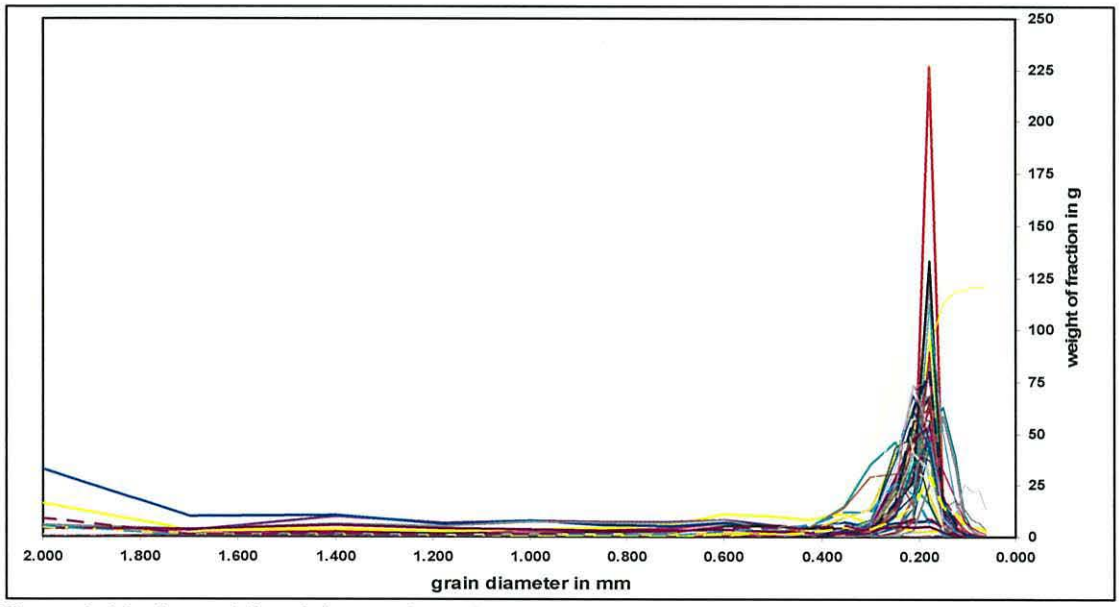

Figure 3.10: the weight of the sand on the each sieve plotted against the aperture diameter (in mm) of that sieve. The modal diameter was 0.18mm.

All of the samples were sieved again to obtain the 0.18 mm fraction (modal fraction). Using a microscope, 126 grains from each sample were split into 7 categories based on the characterisation of the grain. The categories were: clear quartz/feldspar; milky quartz/feldspar; iron stained quartz/feldspar; lithic; dark coloured; shell fragments; and other.

3.3 Complementary Data Sets

As well as the water column SPM data and the bed sediment data, four other data sets were considered. These were: river discharge data; tidal data; meteorological data; and bathymetry data.

3.3.1 River Discharge and Tidal Data

River discharge and tide data were the most important secondary data sets for this project. These two data sets were paramount for the interpretation of the observations.

River discharge was provided by the North Wales Environmental Agency from the Betws-y-Coed gauging station. The data is presented in chapter four, see Figures 4.1, 4.2, and 4.3.

Tidal data was provided by the Centre of Applied Marine Sciences. CAMS produce a tide table booklet on a yearly basis. The tidal data are presented in chapter four, see Figures 4.4, 4.5, and 4.6.

3.3.2 Meteorological Data

Meteorological data, for the survey area, were needed mainly for the planning of the surveys. The data was obtained from two weather websites: the

www.bbc.co.uk/weather; and www.weather.co.uk. Unfortunately the data were not always recorded. In the second half of the survey period, on-site weather conditions were recorded on each survey day (see Tables 4.1, 4.3, 4.4, 4.5, and 4.6).

3.3.3 Bathymetry Data

Bathymetry data is the data related to the water depth. The data used in this project was collected using an echo-sounder connected to a GPS set. The echo-sounder was mounted on the end of a fixed pole on the side of an inflatable Zodiac (the echo-sounder was submerged at a known depth). Two tidal gauges were deployed over the bathymetric survey period, to help relate the water depths to the Ordnance Datum. Unfortunately no workable data were recovered from the tidal gauges, as one of them was vandalised and no meaningful outcomes could be produced. This meant that the bathymetry data could only be viewed as a guide in finding the location of the main channel within the estuary, see Figure 3.11.

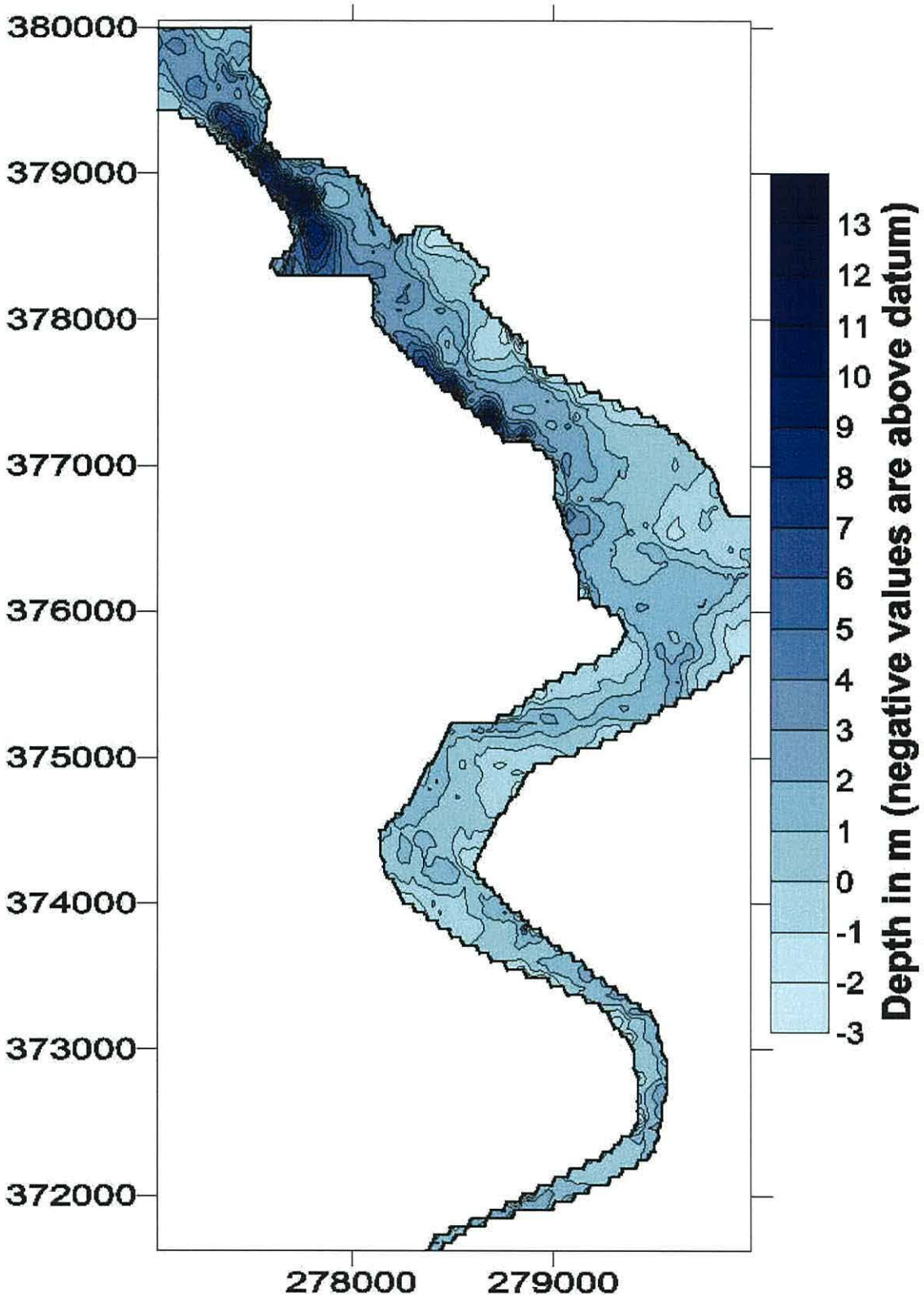

Figure 3.11: shows the bathymetry of the estuary relative to the tidal measurements at Conwy in 2003, (depth in metres ODN). To be used as a guide to the main channel only.

4 ESTUARINE HYDRODYNAMICS

4.1 Introduction

In this chapter, river discharge and tidal range data are presented. By combining these two data sets, flow ratios (see section 4.4) were produced. Each section of this chapter is divided into three surveying periods:

- Period one – 2004 – included 2 anchor stations (MS1 and MS2) in September and 3 spatial surveys in November.

- Period two – 2005 – included 6 spatial surveys, 3 in June and 3 in December.

- Period three – 2006 – included 3 anchor stations (MS3, MS4 and MS5) in July and 17 spatial surveys: 4 in February, 3 in March, 6 in May, and 4 in July.

Presentation of the data is done for the individual periods with the use of plots. Daily averages are plotted against date. The vertical solid, grey, lines represent surveying days.

4.2 River Discharge

4.2.1 Period One

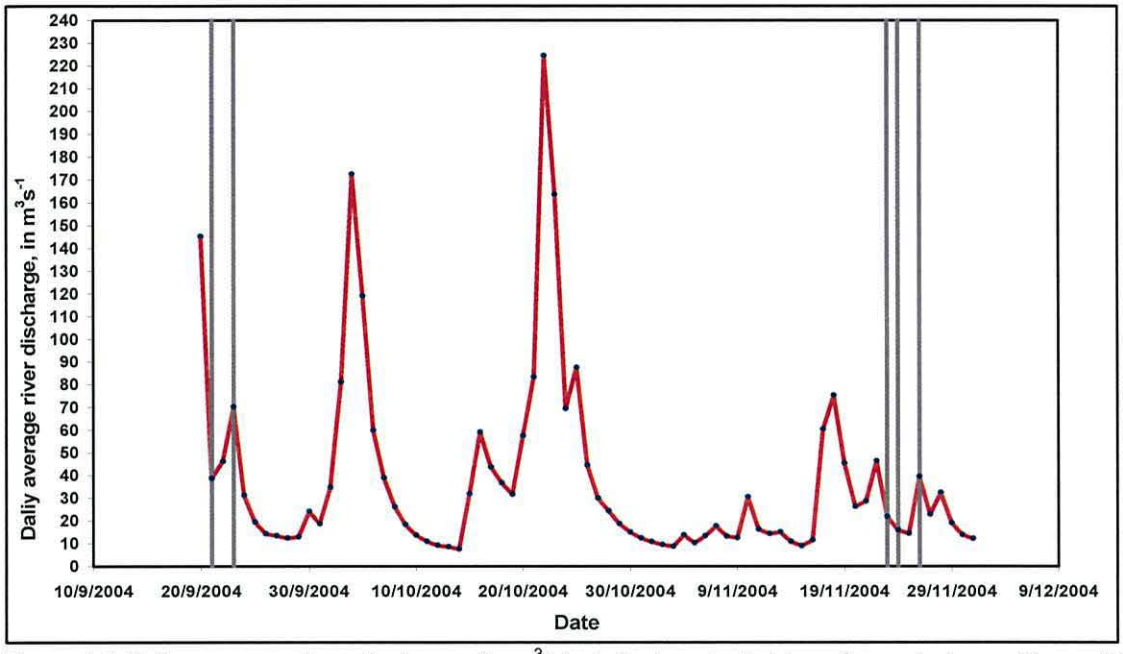

Figure 4.1 Daily average river discharge (in m^3/s) plotted against date – for period one. The solid vertical lines represent surveying days.

4.2.2 Period Two

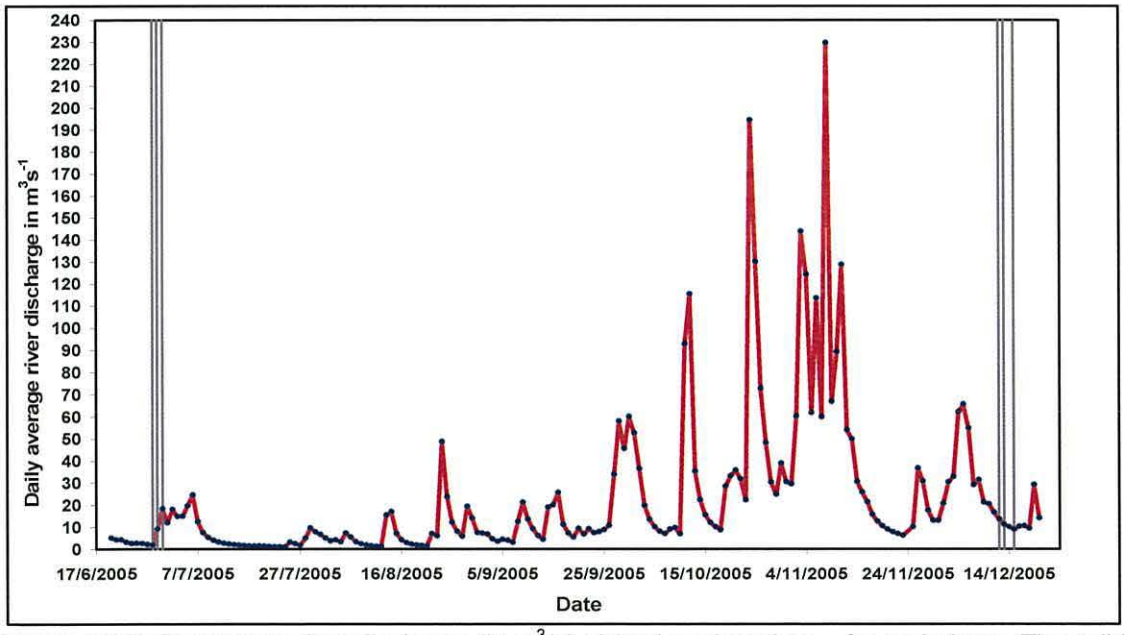

Figure 4.2 Daily average river discharge (in m^3/s) plotted against date – for period two. The solid vertical lines represent surveying days.

4.2.3 Period Three

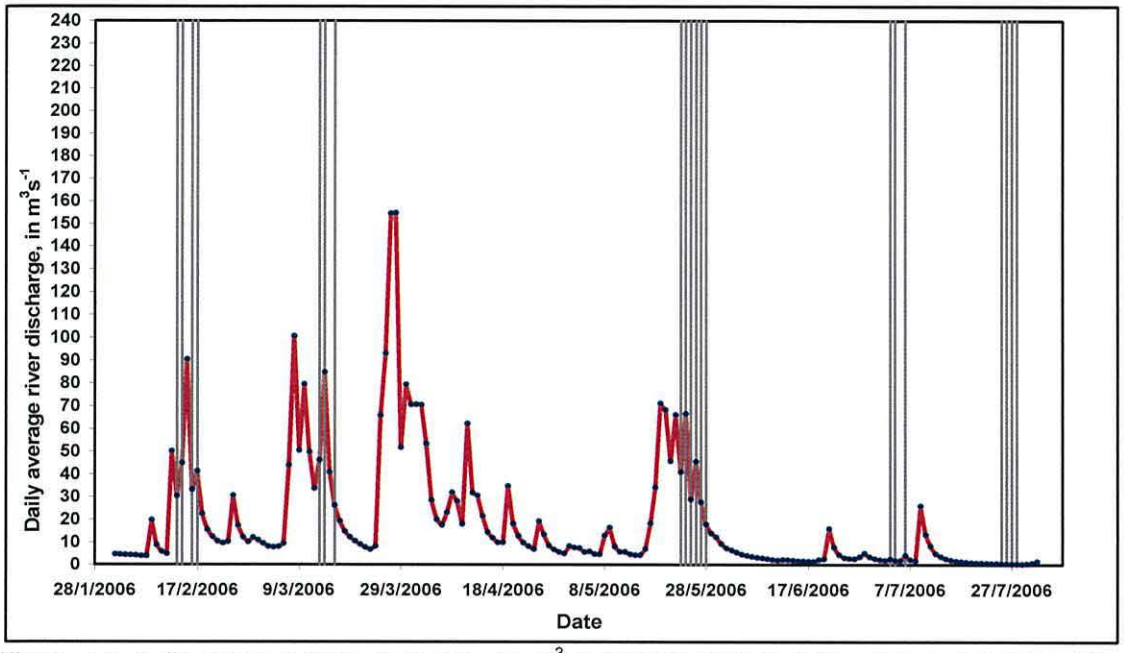

Figure 4.3 Daily average river discharge (in m^3/s) plotted against date – for period three. The solid vertical lines represent surveying days.

4.3 Tidal Range

4.3.1 Period One

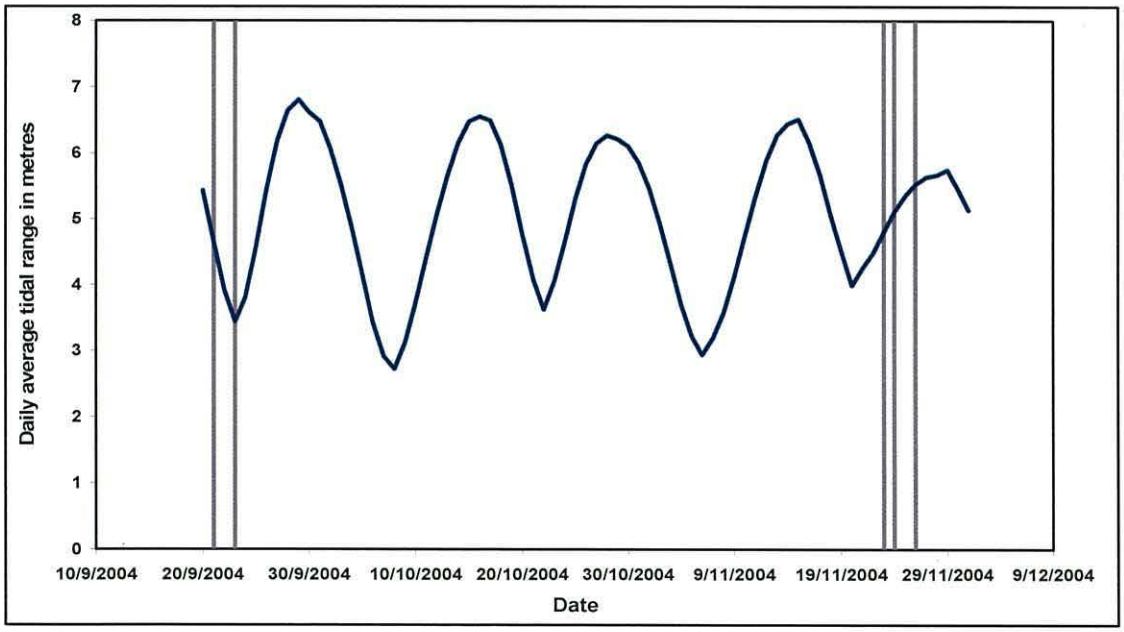

Figure 4.4 Daily average tidal range (in m) plotted against date – for period one. The solid vertical lines represent surveying days.

4.3.2 Period Two

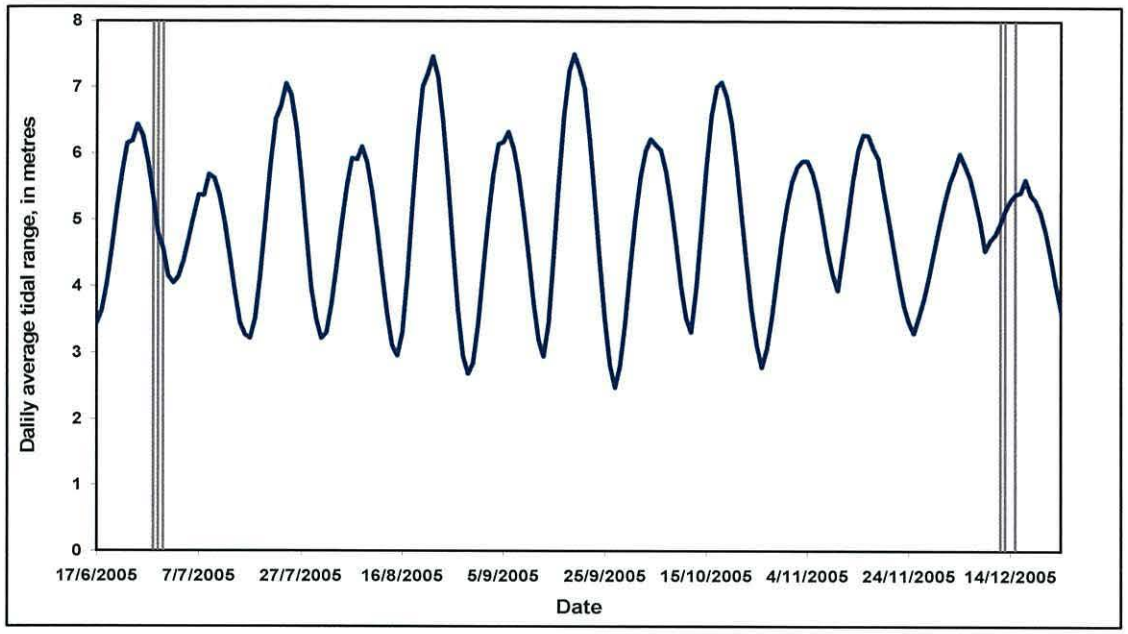

Figure 4.5 Daily average tidal range (in m) plotted against date – for period two. The solid vertical lines represent surveying days.

4.3.3 Period Three

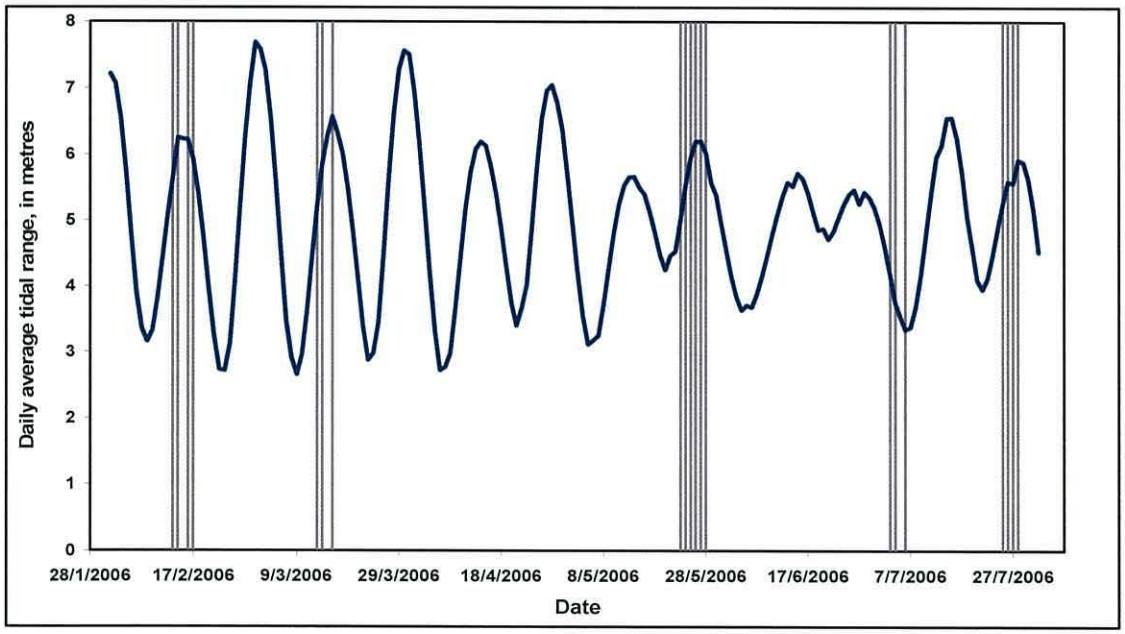

Figure 4.6 Daily average tidal range (in m) plotted against date – for period three. The solid vertical lines represent surveying days.

4.4 Flow Ratio: Q/T^3

As seen in section 2.5, the ETM should be closely related to the landward limit of salt intrusion. Jago et al. (2006) explain that the landward limit of salt intrusion is dependent on the contest between up-estuary and down-estuary transports by the tide and the river, respectively. This contest can be quantified by the flow ratio, which is the ratio of the volumes of freshwater and salt water per tidal inundation.

Jago et al. (2006) assume a simple triangular cross section for the estuary, the saltwater prism scales on Q/T^3, where Q is the river discharge (in m^3s^{-1}) and T is the tidal range (in m).

4.4.1 Period One

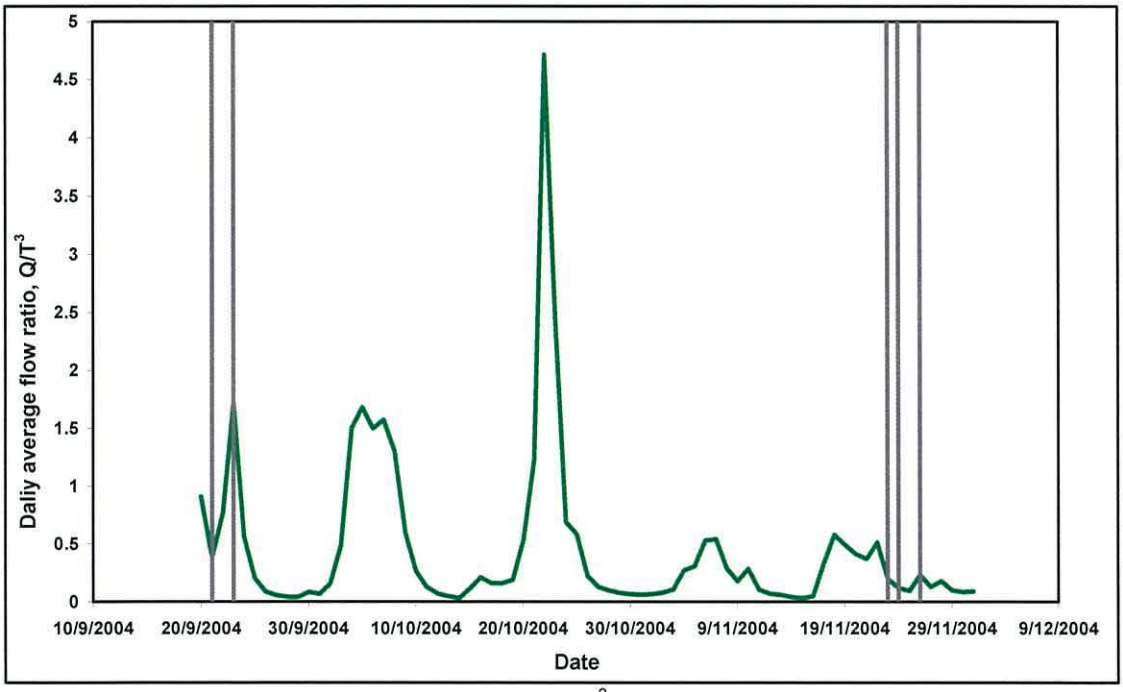

Figure 4.7 Diagram of daily average flow ratio, Q/T^3, for period one. The vertical solid grey lines represent survey days.

4.4.2 Period Two

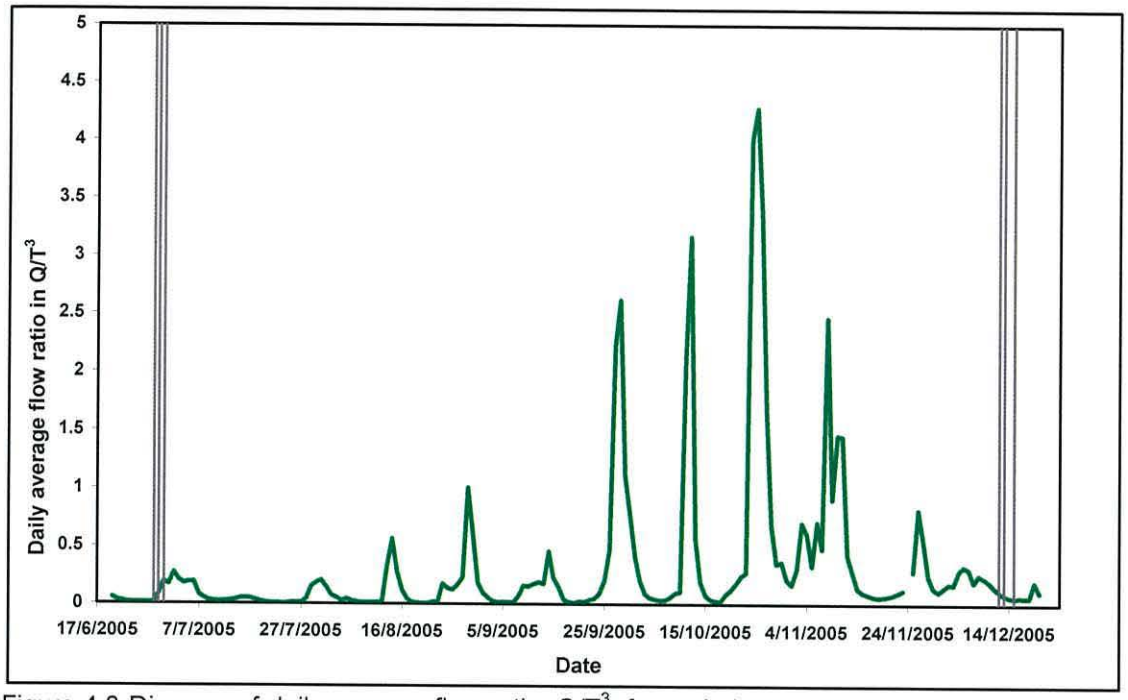

Figure 4.8 Diagram of daily average flow ratio, Q/T^3, for period two. The vertical solid grey lines represent survey days.

4.4.3 Period Three

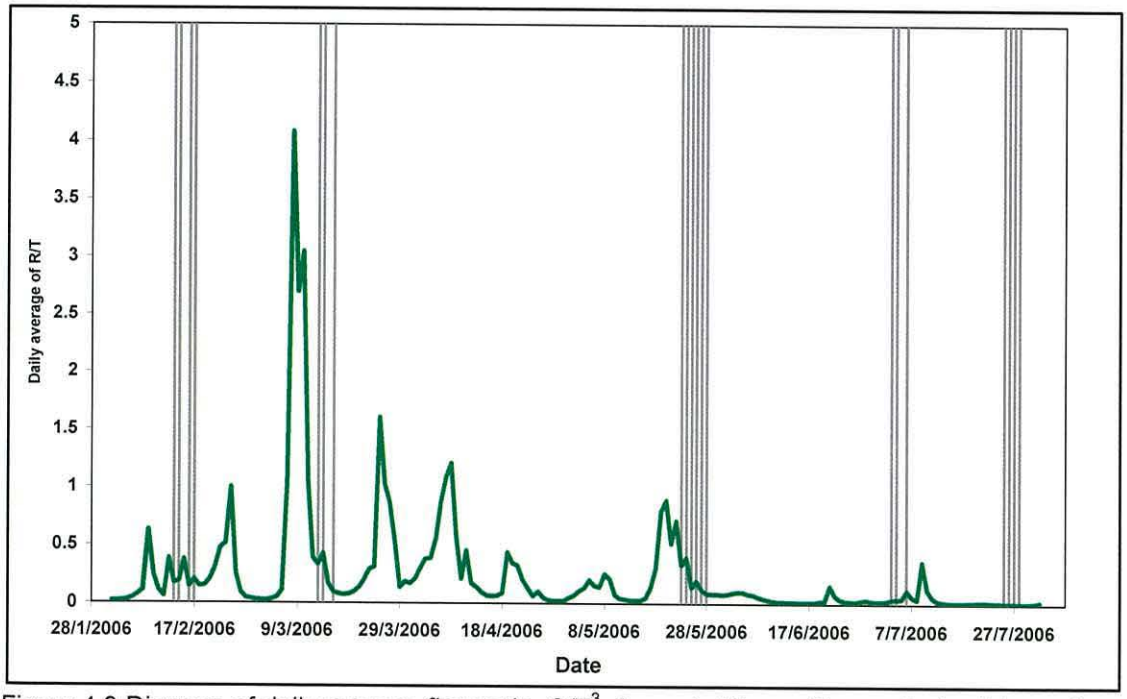

Figure 4.9 Diagram of daily average flow ratio, Q/T^3, for period three. The vertical solid grey lines represent survey days.

4.5 Discussion and Conclusions

According to the National River Authority (1993), the considerable variability in catchment rainfall both temporally and spatially, coupled with the geology and topography results in a rapidly changing and wide ranging flow regime (see Table 4.1) in the Conwy.

		River discharge in m^3s^{-1}		
Period	**Source**	**Minimum**	**Maximum**	**Average**
1982 – 1992	National River Authority	0.3	486.6	24
Period one, 2004	North Wales Environmental Agency	7.5	224.5	38
Period two, 2005		1.2	229.8	23
Period three, 2006		0.4	154.8	20

Table 4.1 presenting river discharge extremes and averages, in m^3s^{-1}.

Hillier (1985) found a monthly average river discharge of 0.7 m^3s^{-1} for July 1984, and states that a typical July value would be around 8 m^3s^{-1}. He also mentions that in July 1976, a drought year, the flow was about 3 m^3s^{-1}. These values agree with the ones observed during this project. The monthly river discharge for July 2005 was 6.4 m^3s^{-1}, whilst 3.1 m^3s^{-1} in July 2006.

According to Hillier (1985), the tidal ranges of the Conwy estuary vary between 3 and 7 metres over the neap-spring cycle. The minimum tidal range for the three survey periods was 2.7 m, whilst the maximum range was 7.7 m. The average tidal range for all three periods was about 5 m; placing the Conwy within the macrotidal estuaries (see section 2.1.4).

From Figures 4.1 through to 4.9, it can be deduced that the flow ratio is very sensitive to the variable river discharge rather than to the less variable tidal range.

5 SPATIAL SURVEYS

This chapter is divided into five main parts: the results from the spatial surveys; the analysis of SPM particle size; the surface SPM density; the location of the ETM; and the strength of the ETM.

5.1 Results

5.1.1 Main Results

The 26 spatial surveys were spread out over a period of two years. In this section the surveys are divided into seasons. The main results of autumn (November 2004), winter (December 2005 and February 2006), spring (March and May 2006), and summer (June 2005 and July 2006) surveys are presented in Table 5.1, 5.2, 5.3, and 5.4 respectively.

Note: The salinities, SPM concentrations, and median diameters are all depth averages.

Autumn: November 2004			
Spatial Survey No	**SS1**	**SS2**	**SS3**
Time of high water at Conwy, GMT	08:15	08:59	10:16
Day averaged tidal range, in m	4.81	5.1	5.5
Day averaged river discharge, m^3s^{-1}	21.8	15.9	39.5
River discharge to (tidal range)^3 ratio	0.196	0.120	0.237
Wind Conditions (mph and direction)			
Weather (Raining or dry?)	Drizzle	Drizzle	Drizzle
Time of first cast, GMT	07:52	08:24	09:42
Time of ETM cast, GMT	08:03	08:48	10:21
Time of last cast, GMT	09:08	09:52	11:01
First cast – distance from mouth, km	12.0	14.2	19.4
ETM cast – distance from mouth, km	10.0	10.0	10.0
Last cast – distance from mouth, km	0.0	0.8	0.9
First cast – SPM concentration, mgl^{-1}	25.13	27.07	3.85
ETM cast – SPM concentration, mgl^{-1}	38.10	44.70	50.70
Last cast – SPM concentration, mgl^{-1}	5.43	3.40	8.30
First cast – salinity	0.12	0.06	0.04
ETM cast – salinity	2.5	5.7	11.1
Last cast – salinity	31.11	30.9	31.56
First cast – median diameter, in μm	81.12	97.98	130.13
ETM cast – median diameter, in μm	104.00	104.00	103.00
Last cast – median diameter, in μm	105.37	137.09	101.00

Table 5.1 summarises the results for the autumn spatial surveys November 2004.

Winter: December 2005 and February 2006							
Spatial Survey No	**SS7**	**SS8**	**SS9**	**SS10**	**SS11**	**SS12**	**SS13**
Time of high water at Conwy, GMT	08:04	08:53	09:38	11:02	11:39	12.52	13.28
Day averaged tidal range, in m	5.0	5.1	5.4	5.7	6.3	6.2	5.9
Day averaged river discharge, m^3s^{-1}	13.8	11.3	9.0	30.4	44.9	33.2	41.3
River discharge to (tidal range)^3 ratio	0.110	0.085	0.057	0.164	0.180	0.139	0.201
Wind Conditions (mph and direction)			10 SW				
Weather (Raining or dry?)	Dry	Dry	Dry	Drizzle	Rain	Drizzle	Drizzle
Time of first cast, GMT	08:40	09:03	10:26	11:13	11:27	12:13	13:06
Time of ETM cast, GMT	09:19	09:30	11:05	12:15	12:02	13:09	14:03
Time of last cast, GMT	09:58	10:34	12:00	12:56	13:03	14:00	14:39
First cast – distance from mouth, km	16.6	18.9	19.675	20.125	19.4	19.4	20.125
ETM cast – distance from mouth, km	10	13.65	15.35	10.625	13.65	12.025	10.625
Last cast – distance from mouth, km	0.9	0.9	1	0.9	0.9	0.9	0.6
First cast – SPM concentration, mgl^{-1}	7.3	3.36	2.25	1.4	2.44	1.14	1.35
ETM cast – SPM concentration, mgl^{-1}	30.36	27.1	37.7	18.2	6.5	19.6	20.8
Last cast – SPM concentration, mgl^{-1}	29.24	14.19	34.02	6.8	3.27	6.04	7.02
First cast – salinity	0.05	0.04	0.05	0.03	0.03	0.03	0.03
ETM cast – salinity	4.7	0.8	0.2	4.3	3.1	4.5	3.3
Last cast – salinity	29.70	30.56	30.49	31.00	31.97	31.88	30.89
First cast – median diameter, in μm	81.51	98.50	182.36	---	---	---	---
ETM cast – median diameter, in μm	82.18	63.98	61.1	---	---	---	---
Last cast – median diameter, in μm	64.14	73.09	56.35	---	---	---	---

Table 5.2 summarises the results for the winter spatial surveys December 2005 and February 2006.

Spring: March and May 2006									
Spatial Survey No	**SS14**	**SS15**	**SS16**	**SS17**	**SS18**	**SS19**	**SS20**	**SS21**	**SS22**
Time of high water at Conwy, GMT	09:59	10:37	11:47	07:23	08:20	09:10	09:57	10:41	11:24
Day averaged tidal range, in m	5.2	5.9	6.6	5	5.5	5.9	6.2	6.2	6
Day averaged river discharge, m^3s^{-1}	46.2	84.6	26.2	41	66.6	28.9	45.6	27.6	17.9
River discharge to (tidal range)^3 ratio	0.329	0.412	0.091	0.328	0.400	0.141	0.191	0.116	0.083
Wind Conditions (mph and direction)	25 SW	S-SW	S-SW	13 SW	17 W	17 W	17 W	18 W	14 W
Weather (Raining or dry?)	rain	dry	dry	rain	rain	dry	showers	rain	dry
Time of first cast, GMT	09:41	10:12	11:15	07:04	08:17	09:08	10:02	10:41	11:18
Time of ETM cast, GMT	10:34	10:45	12:12	08:05	09:14	10:16	10:11	10:55	11:33
Time of last cast, GMT	11:20	11:44	13:02	08:44	09:56	10:54	11:27	12:10	12:18
First cast – distance from mouth, km	19.4	19.4	19.4	16.6	18.9	19.4	16.6	16.6	17.125
ETM cast – distance from mouth, km	10.625	13.65	11	8.6	9.85	8.6	14.725	14.2	14.2
Last cast – distance from mouth, km	0.9	0.9	0.9	0.9	0.9	0.9	0.9	0.9	3.2
First cast – SPM concentration, mgl^{-1}	1.2	13.3	1.6	3.1	6.5	1.9	10.3	6.9	9.9
ETM cast – SPM concentration, mgl^{-1}	28.8	35.4	21.5	17.6	37.7	44.2	20.4	19.3	38
Last cast – SPM concentration, mgl^{-1}	9.9	9.1	9.6	13.7	32.7	23.1	10.7	13.5	37.94
First cast – salinity	0.04	0.03	0.04	0.03	0.03	0.04	0.06	0.04	0.04
ETM cast – salinity	2.7	0.02	3.8	0.9	0.09	4.4	0.6	0.3	0.5
Last cast – salinity	31.46	31.02	31.81	27.59	28.22	30.2	31.58	30.73	30.13
First cast – median diameter, in μm	158.44	166.14	166.69	---	---	---	---	---	---
ETM cast – median diameter, in μm	89.7	108.2	112.9	---	---	---	---	---	---
Last cast – median diameter, in μm	70.99	124.93	100.82	---	---	---	---	---	---

Table 5.3 summarises the results for the spring spatial surveys March and May 2006.

Summer: June 2005 and July 2006							
Spatial Survey No	**SS4**	**SS5**	**SS6**	**SS23**	**SS24**	**SS25**	**SS26**
Time of high water at Conwy, GMT	15:49	16:56	18:04	10:53	11:32	12:10	12:47
Day averaged tidal range, in m	5.4	4.8	4.6	5.3	5.6	5.6	6
Day averaged river discharge, m^3s^{-1}	2	9.3	18.6	0.59	0.52	0.46	0.42
River discharge to (tidal range)^3 ratio	0.013	0.084	0.191	0.004	0.003	0.003	0.002
Wind Conditions (mph and direction)	calm	calm	calm	5 SW	10 SW	15 SW	17 SW
Weather (Raining or dry?)	dry	dry	dry	dry	dry	dry	dry
Time of first cast, GMT	15:07	16:16	17:31	10:58	11:31	12:15	12:47
Time of ETM cast, GMT	15:17	16:16	17:38	10:58	11:39	12:19	12:52
Time of last cast, GMT	17:10	17:59	18:51	12:36	13:14	13:45	14:19
First cast – distance from mouth, km	13.93	13.65	12.525	17.5	18.9	19.6	19.675
ETM cast – distance from mouth, km	13.65	13.65	12.025	17.5	17.75	18.9	18.9
Last cast – distance from mouth, km	0.275	0.275	0.9	0.9	0.9	0.9	0.9
First cast – SPM concentration, mgl^{-1}	35.0	67.0	34.3	166.0	160.4	95.5	---
ETM cast – SPM concentration, mgl^{-1}	59.4	67.0	37.9	166.0	206.1	170.9	201.5
Last cast – SPM concentration, mgl^{-1}	16.5	19.5	9.4	6.4	3.7	7.2	2.9
First cast – salinity	0.18	0.55	0.20	0.38	0.11	0.09	---
ETM cast – salinity	0.80	0.55	0.85	0.38	0.9	0.2	0.26
Last cast – salinity	32.69	32.61	31.77	33.14	33.12	33.19	33.26
First cast – median diameter, in μm	126.98	79.26	97.34	88.72	84.15	90.53	100.66
ETM cast – median diameter, in μm	83.2	79.26	103.9	88.72	81.3	76.7	75.8
Last cast – median diameter, in μm	106.33	101.64	97.09	114.88	112.50	108.85	103.32

Table 5.4 summarises the results for the summer spatial surveys June 2005 and July 2006.

5.1.2 The Spatial Surveys in Detail

From the seven sets of spatial surveys, one survey day per month was chosen to represent the conditions observed that month. For each survey, three time series are presented: salinity; total SPM concentration; and median diameter of the SPM.

5.1.2.1 Autumn – Survey SS3

Survey SS3 (November 2004)

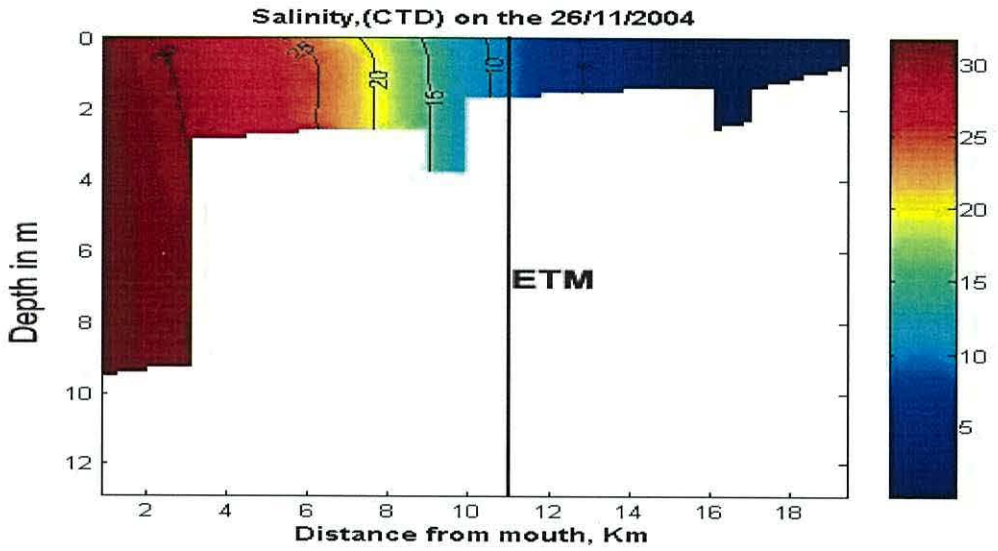

Figure 5.1: salinity distribution for SS3.

Figure 5.1 shows the salinity measured by the CTD. The estuary was well mixed, with salinity of 5 found around 13 km from the mouth.

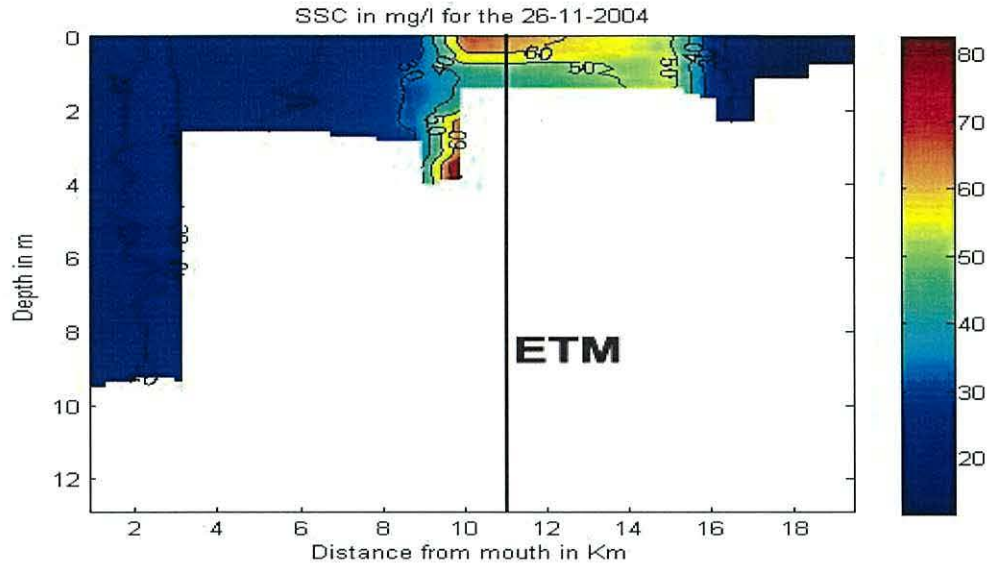

Figure 5.2: SSC distribution for SS3.

Figure 5.2 shows total SPM concentration, in mgl^{-1}, derived from the OBS. The concentration reached a maximum, i.e. in the ETM (> 70 mgl^{-1}) at about 10 -11 km upriver from the mouth.

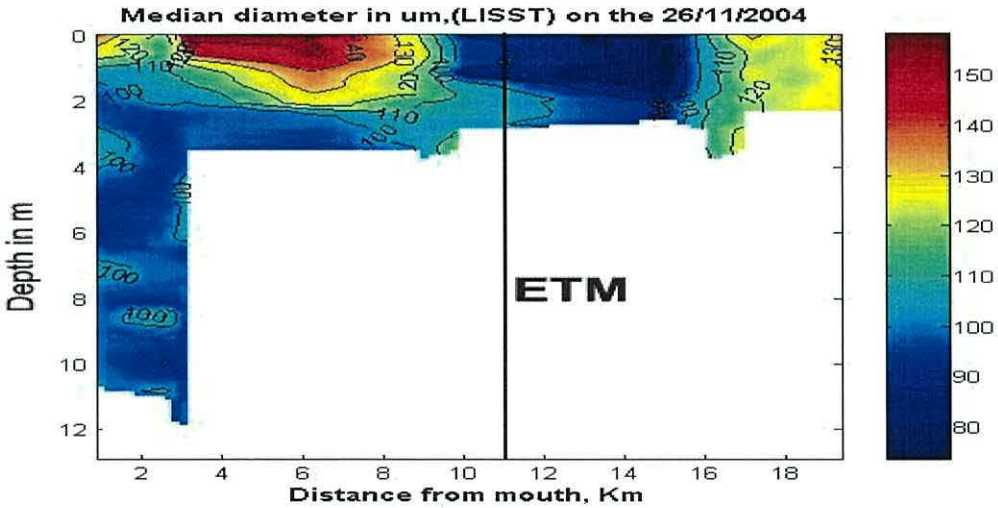

Figure 5.3: median diameter distribution for SS3.

Figure 5.3 shows the SPM median diameter, in μm, derived from the LISST-100β. The median diameter reached a minimum (~ 80 μm) around 14 km from the mouth (salinity of < 5), whilst reaching a maximum of (~ 150 μm) in the surface water around 4 - 5 km from the mouth (salinity of 25 – 30).

5.1.2.2 Winter – Surveys SS8 and SS12

Survey SS8 (December 2005)

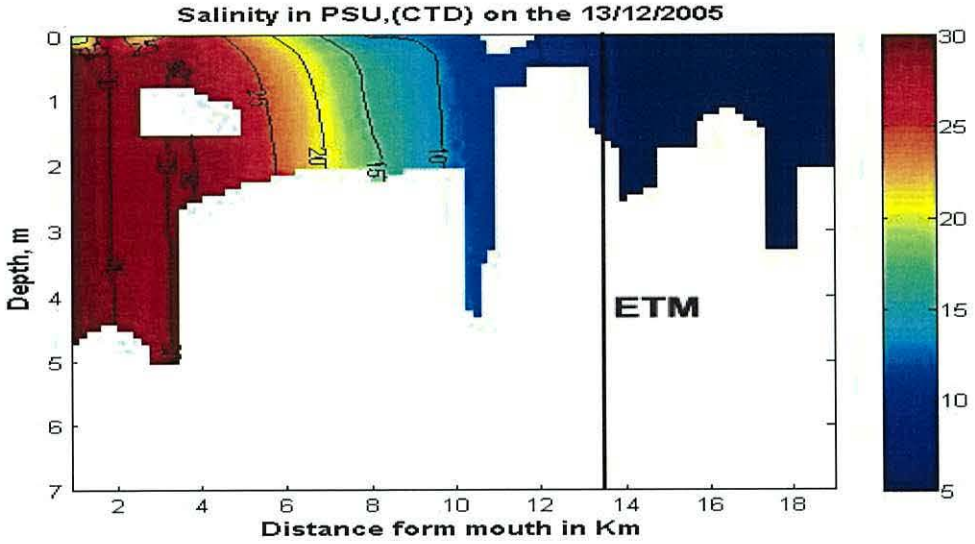

Figure 5.4: salinity distribution for SS8.

Figure 5.4 shows the salinity measured by the CTD. The estuary was mixed, with slight stratification occurring in the surface waters. Salinity of 5 was found around 13 km from the mouth.

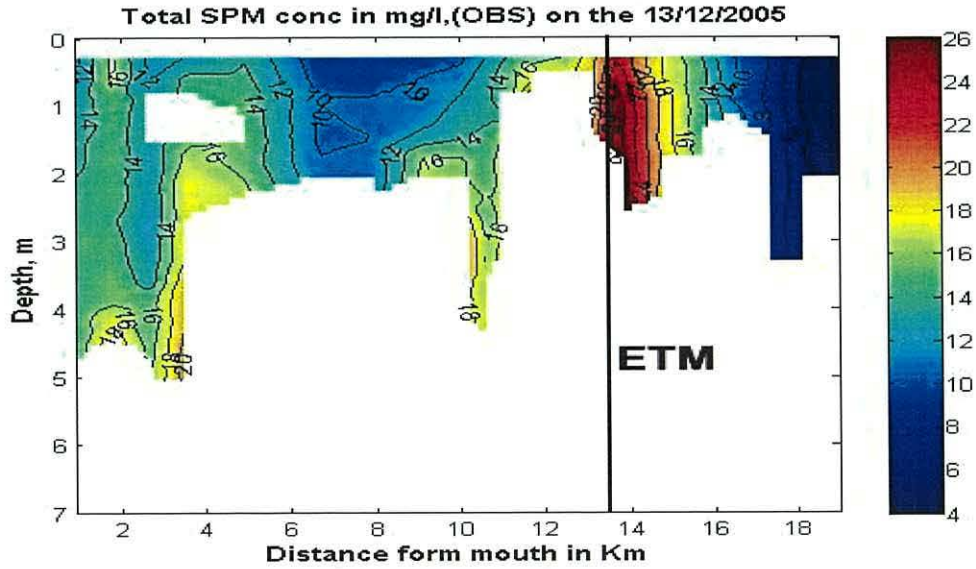

Figure 5.5: SSC distribution for SS8.

Figure 5.5 shows total SPM concentration, in mgl^{-1}, derived from the OBS. The concentration reached a maximum, i.e. in the ETM (~ 26 mgl^{-1}) at about 13.5 km from the mouth.

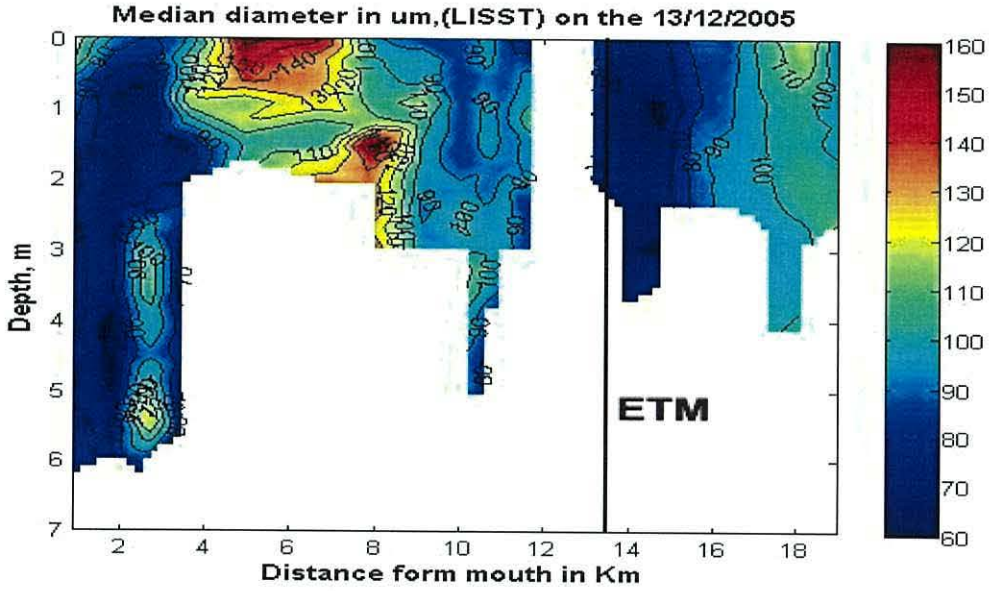

Figure 5.6: median diameter distribution for SS8.

Figure 5.6 shows the SPM median diameter, in μm, derived from the LISST-100β. The median diameter reached a minimum (~ 60 μm) around 2 km from the mouth (salinity of ~ 30 PSU), and around 14 km from the mouth (salinity of < 5). The median reached a maximum of (> 150 μm) in the surface water around 5 km from the mouth (salinity of 25 – 30), and in the bottom water around 8 km from the mouth (salinity of 15).

Survey SS12 (February 2006)

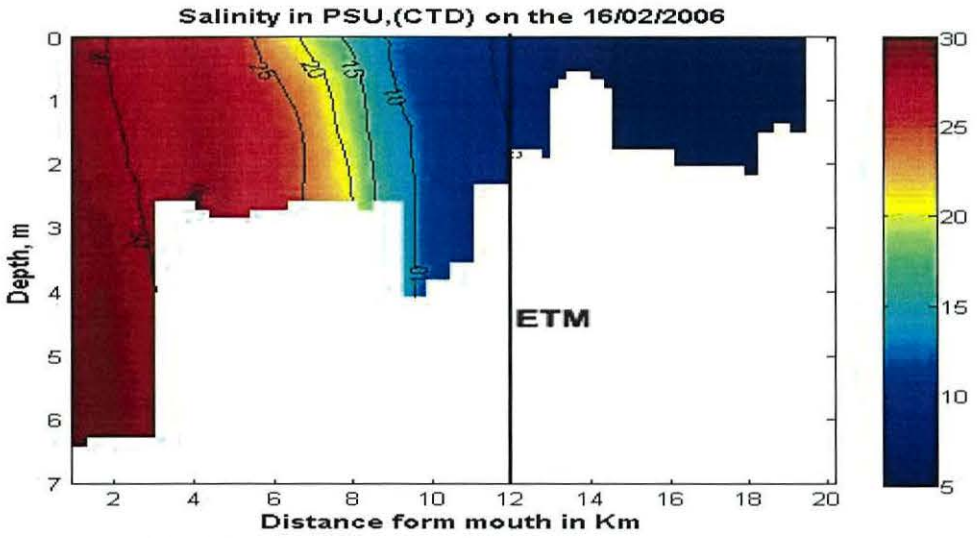

Figure 5.7: salinity distribution for SS12.

Figure 5.7 shows the salinity measured by the CTD. The estuary was well mixed, with salinity of 5 found around 12 km from the mouth.

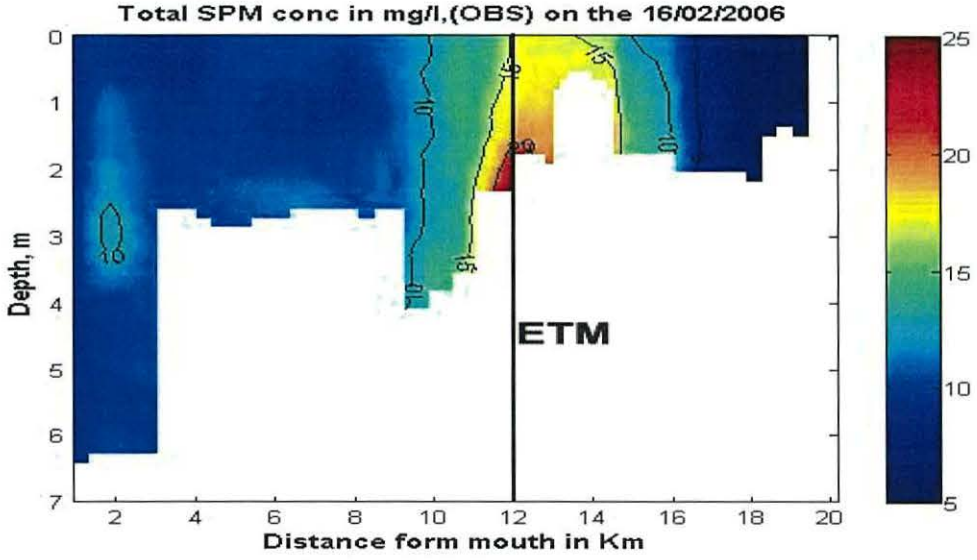

Figure 5.8: SSC distribution for SS12.

Figure 5.8 shows total SPM concentration, in mgl^{-1}, derived from the OBS. The concentration reached a maximum, i.e. in the ETM (~ 25 mgl^{-1}) at about 12 km

from the mouth. There was no LISST data for this survey, as the instrument malfunctioned.

5.1.2.3 Spring – Surveys SS15 and SS22

Survey SS15 (March 2006)

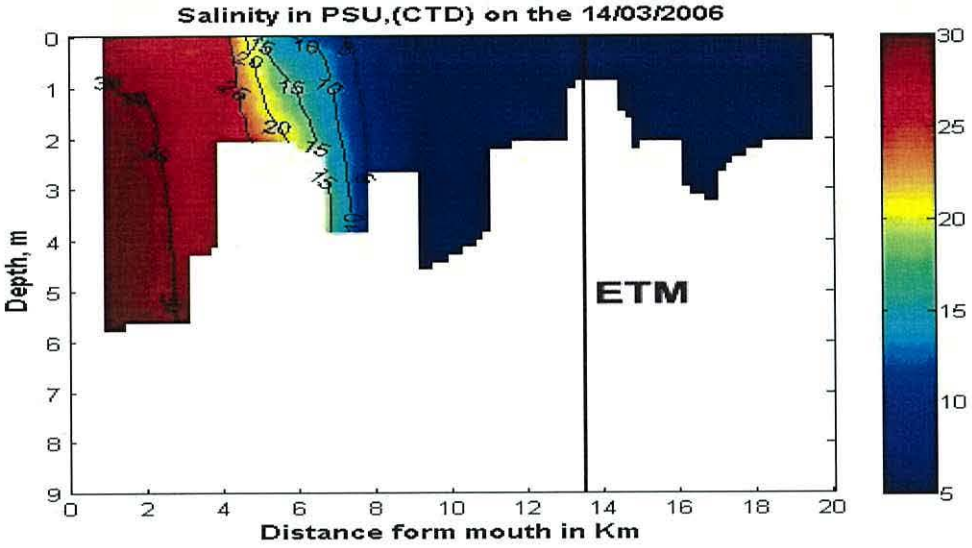

Figure 5.9: salinity distribution for SS15.

Figure 5.9 shows the salinity measured by the CTD. The estuary was mixed, with slight stratification occurring in the lower estuary. Salinity of 5 was found around 8 km from the mouth.

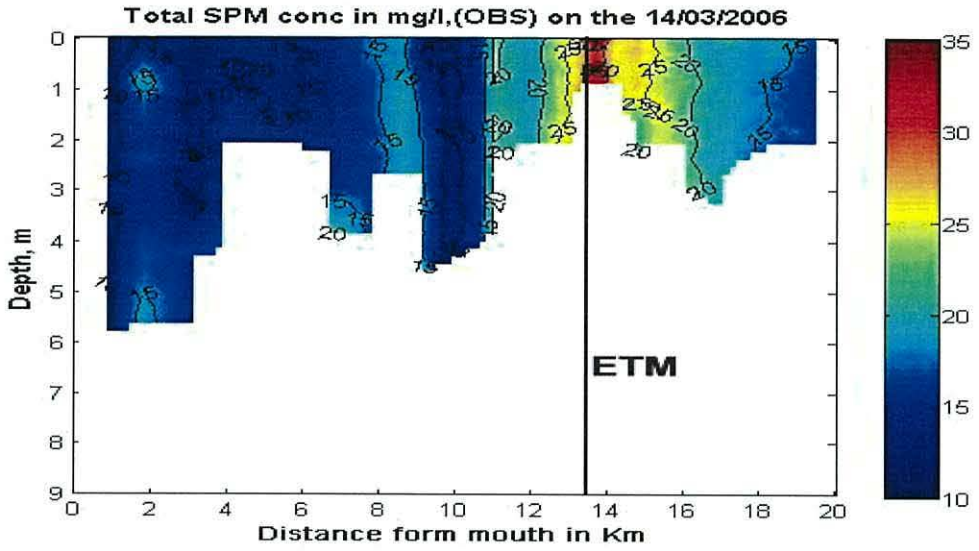

Figure 5.10: SSC distribution for SS15.

Figure 5.10 shows total SPM concentration, in mgl^{-1}, derived from the OBS. The concentration reached a maximum, i.e. in the ETM (~ 35 mgl^{-1}) at about 13.5 km from the mouth.

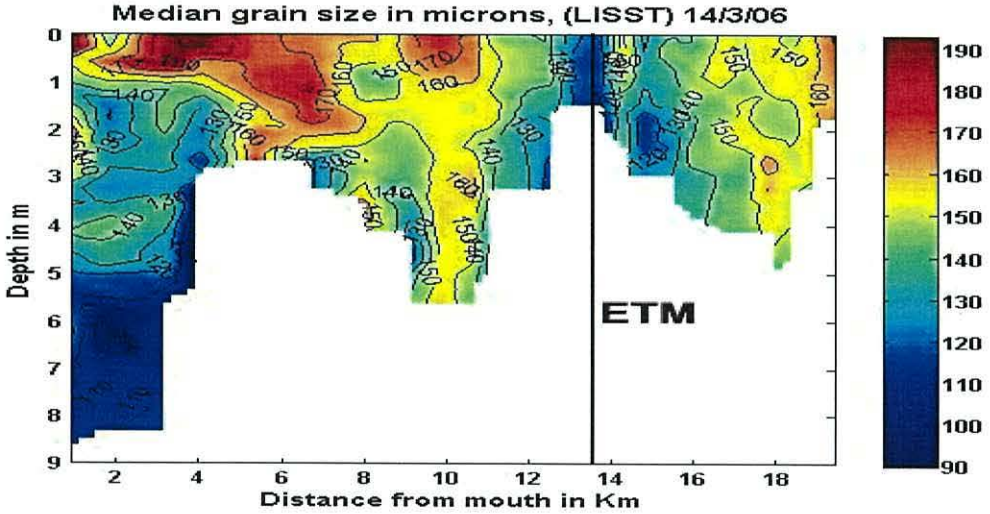

Figure 5.11: median diameter distribution for SS15.

Figure 5.11 shows the SPM median diameter, in μm, derived from the LISST-100β. The median diameter reached a minimum (< 100 μm) in bottom waters around 2 km from the mouth (salinity of > 30), and within the ETM, around 13.5 km from the mouth (salinity of <5). The median reached a maximum of (~ 190 μm) in the surface water around 4 km from the mouth (salinity of ~ 25).

Survey SS22 (May 2006)

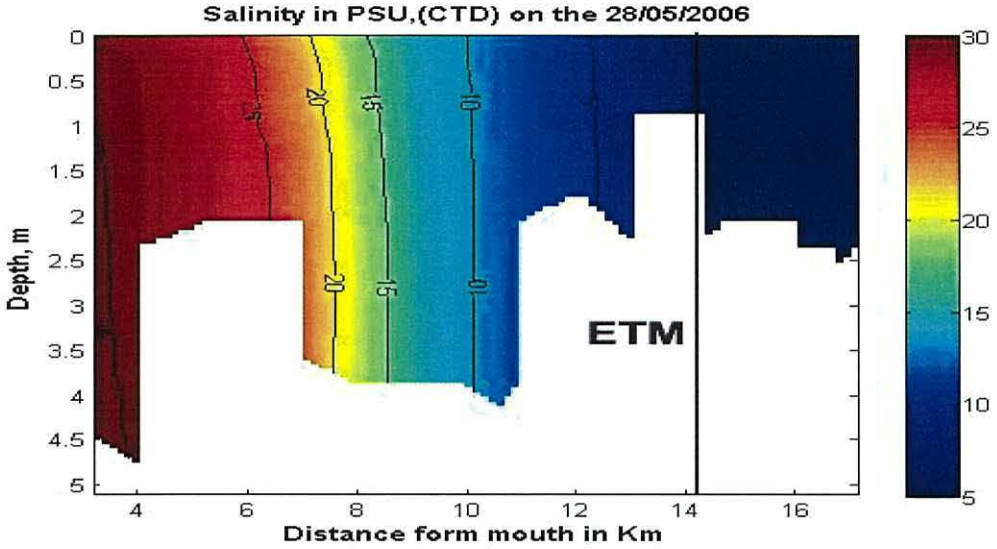

Figure 5.12: salinity distribution for SS22.

Figure 5.12 shows the salinity measured by the CTD. The estuary was well mixed, with salinity of 5 found around 12.5 km from the mouth.

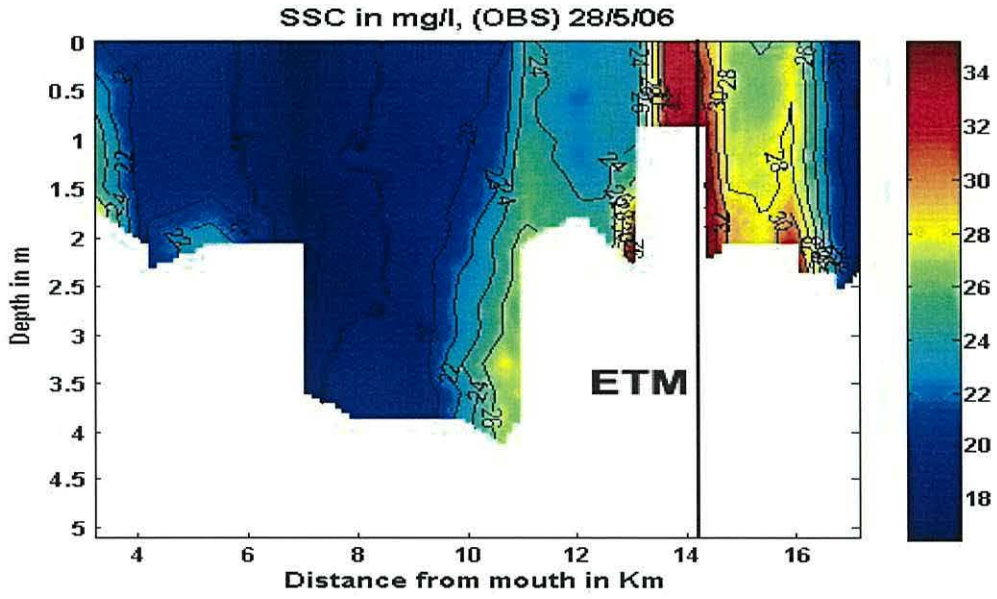

Figure 5.13: SSC distribution for SS22.

Figure 5.13 shows total SPM concentration, in mgl^{-1}, derived from the OBS. The concentration reached a maximum, i.e. in the ETM (~ 34 mgl^{-1}) at about 14 km from the mouth.

There was no LISST data for this survey, as the instrument malfunctioned.

5.1.2.4 Summer – Surveys SS5 and SS24

Survey SS5 (June 2005)

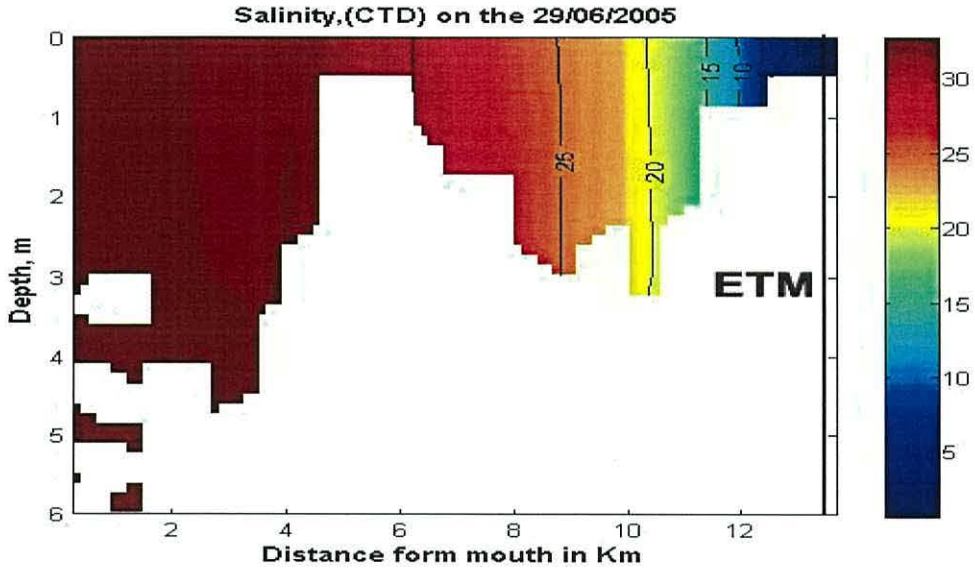

Figure 5.14: salinity distribution for SS5.

Figure 5.14 shows the salinity measured by the CTD. The estuary was well mixed, with salinity of 5 found around 12.5 km from the mouth.

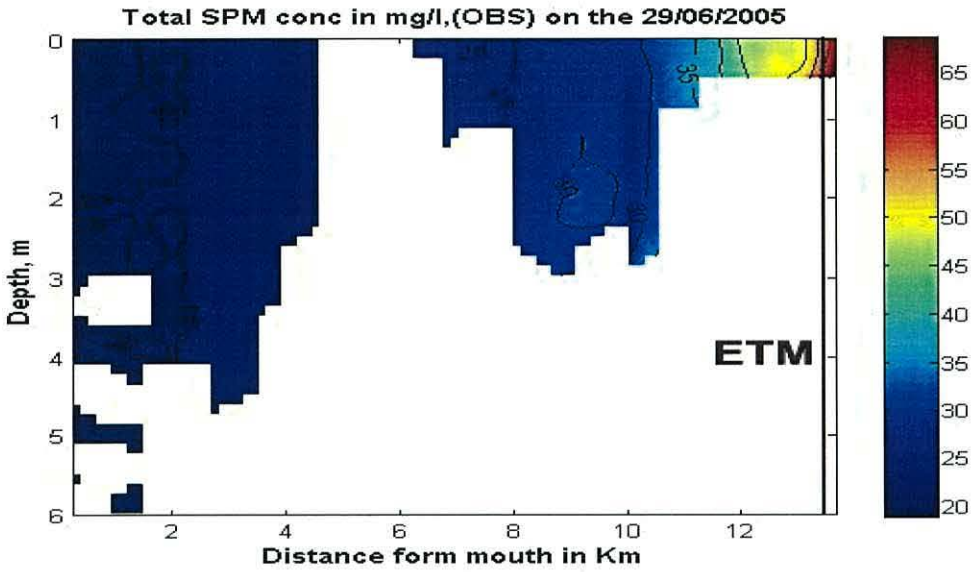

Figure 5.15: SSC distribution for SS5.

Figure 5.15 shows total SPM concentration, in mgl^{-1}, derived from the OBS. The concentration reached a maximum, i.e. in the ETM (> 65 mgl^{-1}) at about 13.5 km from the mouth.

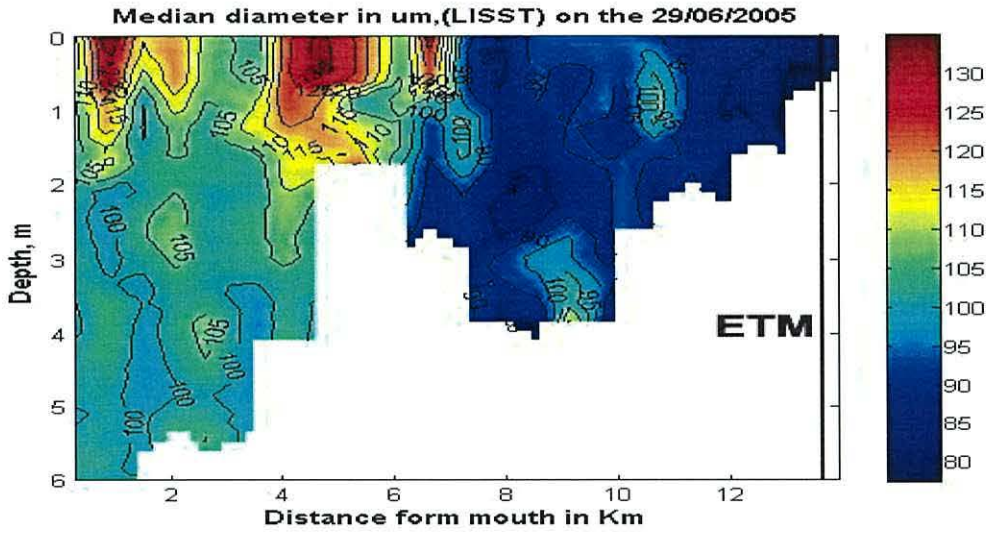

Figure 5.16: median diameter distribution for SS5.

Figure 5.16 shows the SPM median diameter, in μm, derived from the LISST-100β. The median diameter reached a minimum (~ 80 μm) within the ETM, around 13.5 km from the mouth (salinity of <5). The median reached a maximum

of (> 1300 μm) in the surface water around 1, 5, and 7 km from the mouth (salinity of ~ 30).

Survey SS24 (July 2006)

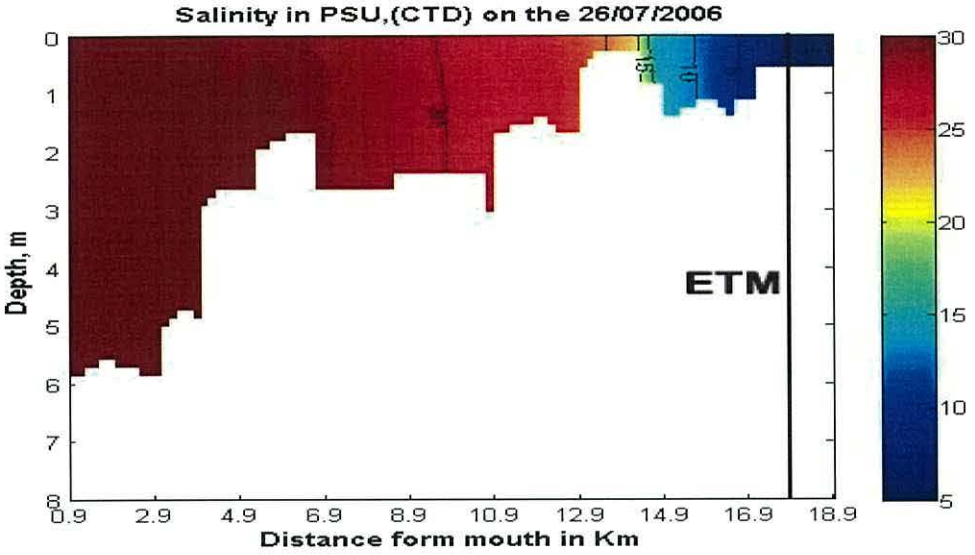

Figure 5.17: salinity distribution for SS24.

Figure 5.17 shows the salinity measured by the CTD. The estuary was well mixed, with salinity of 5 found around 17 km from the mouth.

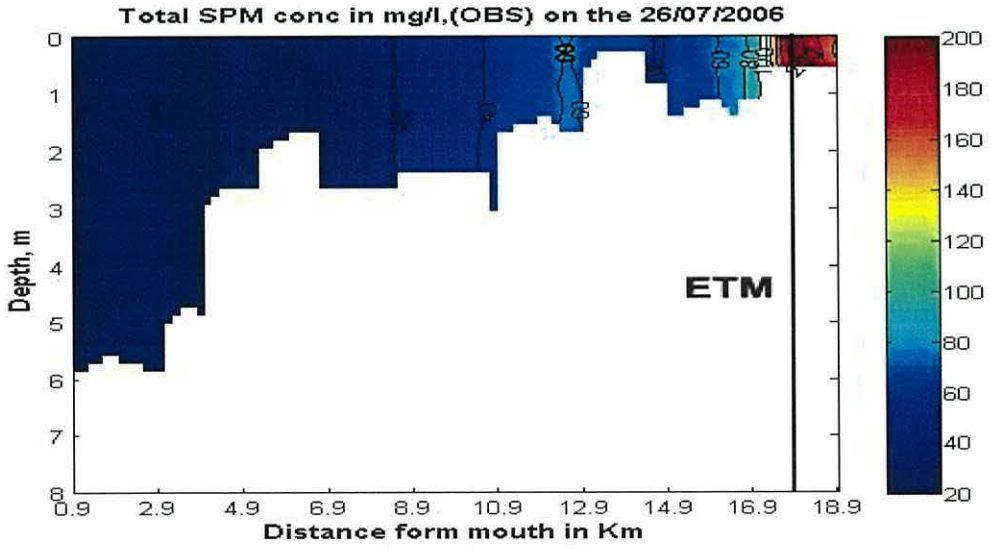

Figure 5.18: SSC distribution for SS24.

Figure 5.18 shows total SPM concentration, in mgl^{-1}, derived from the OBS. The concentration reached a maximum, i.e. in the ETM (~ 200 mgl^{-1}) at about 18 km from the mouth.

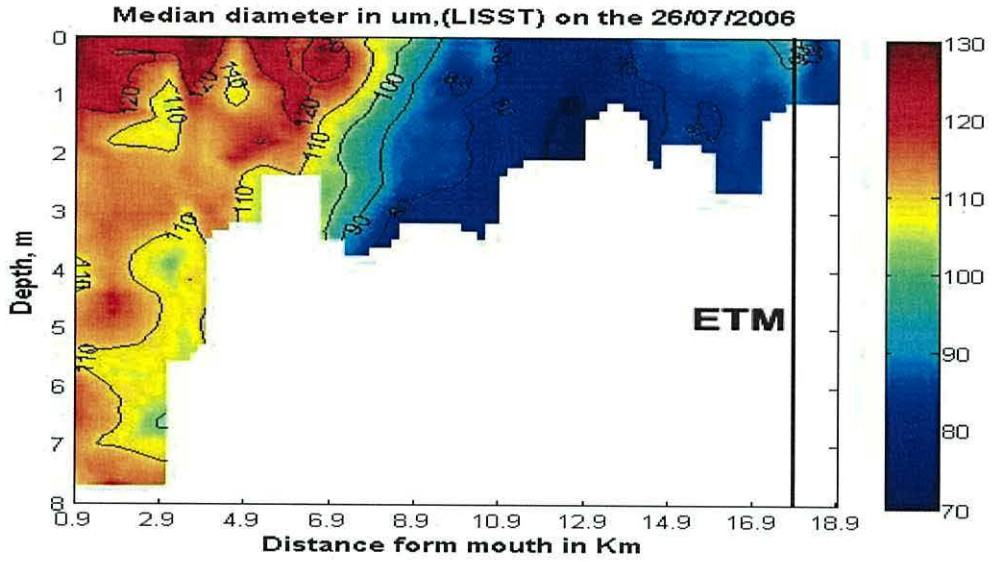

Figure 5.19: median diameter distribution for SS24.

Figure 5.19 shows the SPM median diameter, in μm, derived from the LISST-100β. The median diameter reached a minimum (~ 70 μm) in bottom waters around 12.5 km from the mouth (salinity of > 25). The median reached a maximum of (~ 130 μm) in the surface water of the first 6 km of the estuary (salinity of ~ 30).

5.2 Particle Size Analysis of SPM

The size of the suspended particulate matter was determined using a LISST instrument (see chapter three). The LISST-100β measures the size distribution over 32 size ranges. These 32 size ranges are logarithmically placed from 1.25 – 250 μm in diameter. Size classes 1 to 7; correspond to Wentworth's grain size range of clays (i.e. < 3.9 μm). Size classes 8 to 24; correspond to the silts range

(i.e. 3.9 – 62.5 μm). Finally, size classes 25 to 32; correspond to the fine sands range (i.e. 62.5 – 250 μm).

At any one time, the SPM was made up of particles from the three "grain" size ranges; clays, silts, and sands. Each size range was present at different volume concentrations. By acquiring the volume concentration of each range, and dividing it with the total volume concentration, the percentage of the total volume representing the size range was found (e.g. total volume concentration is made up of 3% clays, 37% silts and 60% sands).

This was done for all surface water readings, collected during the spatial surveys presented in section 5.1.2. Surface values were chosen, so that a comparison between the results and the effective density could be made.

Note: the LISST malfunctioned on the February-05 and May-06 surveys, so no particle size data were obtained for those surveys.

5.2.1 Autumn – Survey SS3

Survey SS3 (November 2004)

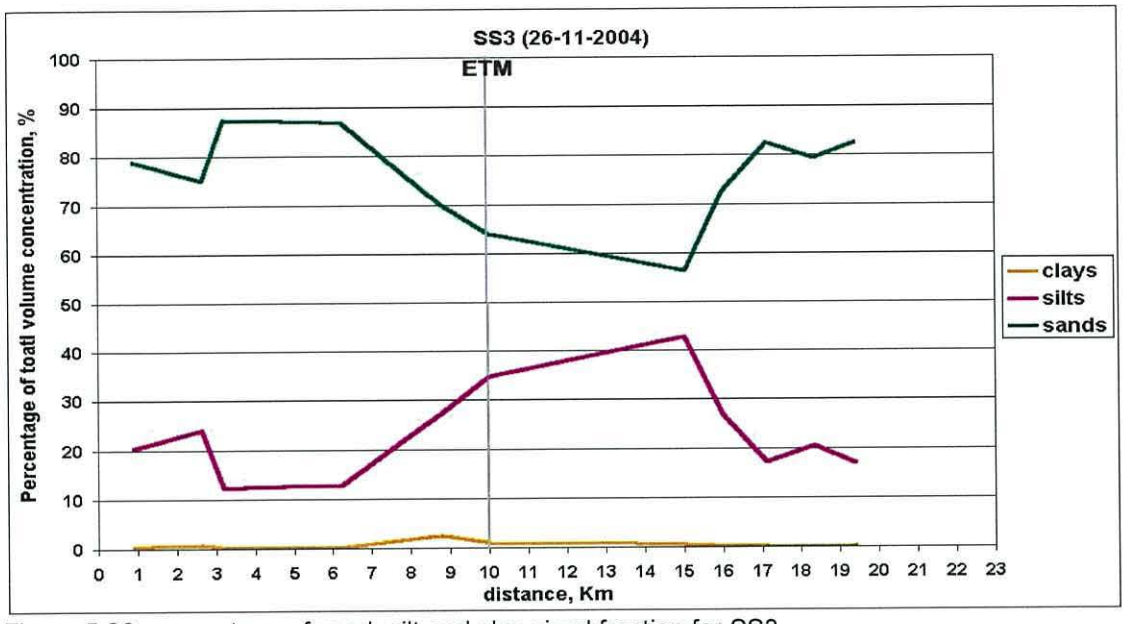

Figure 5.20: percentage of sand, silt and clay sized fraction for SS3.

5.2.2 Winter – Surveys SS8

Survey SS8 (December 2005)

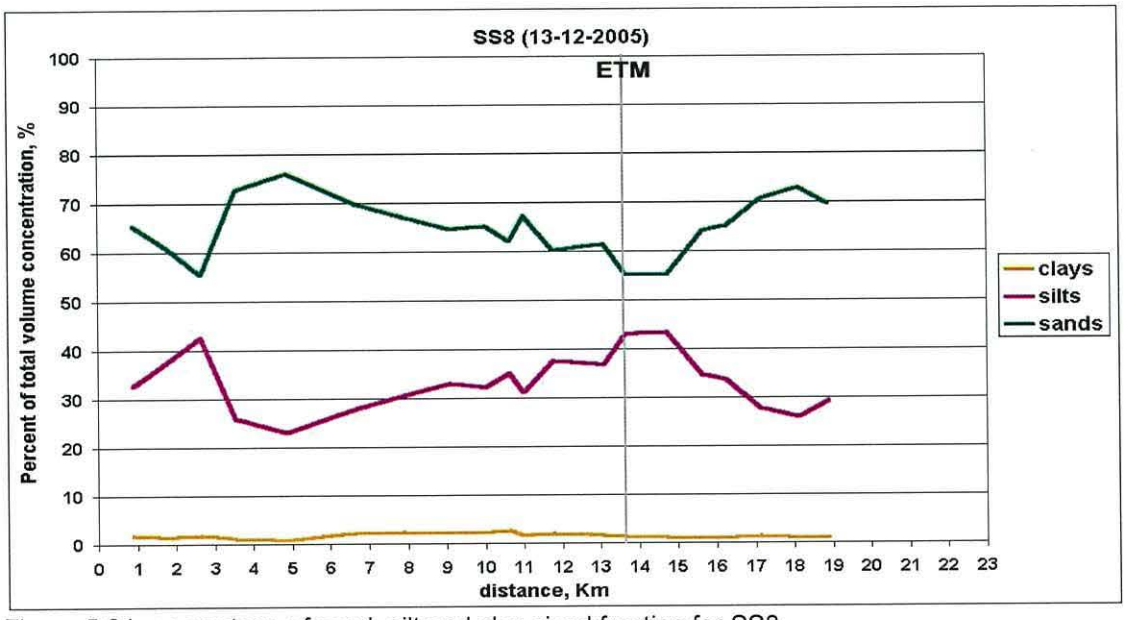

Figure 5.21: percentage of sand, silt and clay sized fraction for SS8.

5.2.3 Spring – Surveys SS15

Survey SS15 (March 2006)

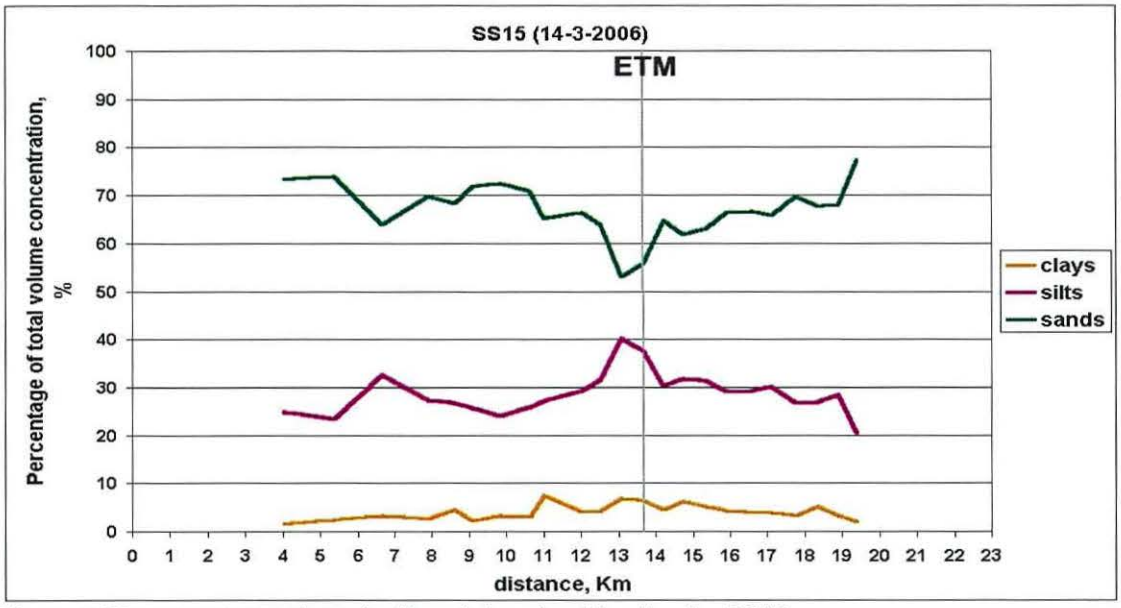

Figure 5.22: percentage of sand, silt and clay sized fraction for SS15.

5.2.4 Summer – Surveys SS5 and SS24

Survey SS5 (June 2005)

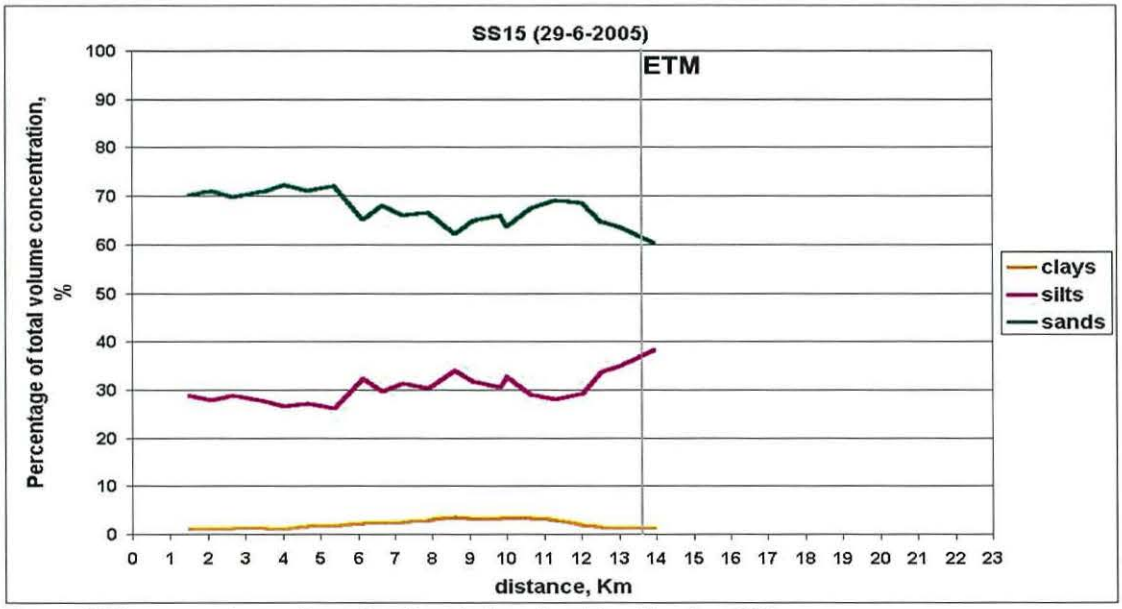

Figure 5.23: percentage of sand, silt and clay sized fraction for SS5.

Survey SS24 (July 2006)

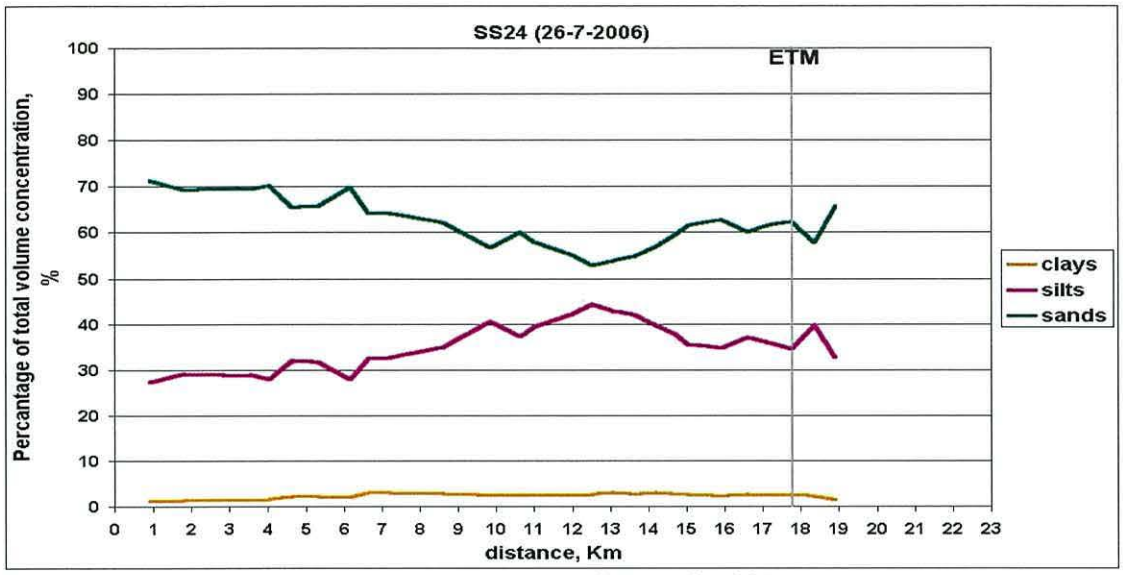

Figure 5.24: percentage of sand, silt and clay sized fraction for SS24.

5.2.5 Discussion

Figures 5.20 through to 5.24 indicate a seasonally constant analogy between the three size fractions: "clays" about 2.6%; "silts" about 38%; and "sands" about 59.4% (see Table 5.5).

	Clay-sized	Silt-sized	Sand-sized
November 2004	1%	37%	62%
December 2005	2%	43%	55%
March 2006	6%	38%	56%
June 2005	1%	37%	62%
July 2006	3%	35%	62%

Table 5.5 presents the percentage of total volume concentration in each size fraction within the ETM.

The percentage, of clay-sized particles remained constantly below 4%, except in March 2006, where it reached about 8%. This difference can be attributed to the increased flow ratio (0.4) in March.

It was observed that where the percentage, of the sand-sized particles, increased the percentage of silt-sized particles decreased. This could be caused by flocculation. Silt-sized particles could be flocculating to form particles of larger diameters and lower densities.

Where the percentage of sand-sized particles decreased the percentage of silt-sized particles increased. This is especially true in or around the estuarine turbidity maximum, where the region is wide and shallow, with salinity observed to be < 5. The only exception was observed during July 2006 (~ 25 PSU), where the flow ratio was very low (0.003).

5.3 SPM Density

5.3.1 Effective Density

According to Mikkelsen and Pejrup (2000), the effective density (ED) of suspended matter can be calculated using mass concentration (SSC) from water samples and volume concentration (VC) measured by the LISST-100. The ED is defined as $(\rho_f - \rho_w)$, where ρ_f is the floc bulk density and ρ_w is the density of the water.

$$ED = (SSC / VC) * 1000 \qquad [5.1]$$

SSC is in mgl^{-1}, VC in $\mu l/l$, and ED in mg/ml (= kgm^{-3}).

The effective densities of the surface suspended particulate matter were calculated for all spatial surveys. In the following table (Table 5.6) the values of SSC, VC and ED are presented for three different locations: LL = landward limit of survey; ETM = estuarine turbidity maximum; and SL = seaward limit of survey. See figures 5.25, 5.26, 5.27, 5.28, and 5.29 for plots of ED against time (in seasonal order).

Date	Location	Distance from mouth, km	SSC, mgl^{-1}	VC, µl/l	ED, kgm^{-3}
23/11/04	LL	12.000	33.26	231.52	143.66
	ETM	11.000	25.88	221.58	116.80
	SL	0.900	24.62	205.58	119.76
24/11/04	LL	14.200	25.96	155.33	167.13
	ETM	12.275	50.36	311.98	161.42
	SL	0.900	36.22	109.07	332.08
26/11/04	LL	19.400	7.14	74.54	95.79
	ETM	11.000	66.76	422.35	158.07
	SL	0.900	33.64	95.60	351.87
28/06/05	LL	13.930	32.90	265.12	124.09
	ETM	13.650	70.13	387.97	180.77
	SL	0.900	11.00	84.37	130.38
29/06/05	LL	14.200	32.23	---	---
	ETM	12.025	41.60	203.89	204.03
	SL	0.900	20.73	93.79	221.07
30/06/05	LL	14.200	24.53	181.61	135.09
	ETM	12.025	46.73	334.82	139.58
	SL	0.900	21.37	80.85	264.28
12/12/05	LL	16.275	5.72	61.98	92.29
	ETM	10.000	29.76	156.18	190.55
	SL	0.900	22.72	182.61	124.42
13/12/05	LL	18.900	4.90	58.22	84.17
	ETM	13.650	25.08	218.22	114.93
	SL	0.900	18.20	142.99	127.28
15/12/05	LL	19.675	2.04	123.32	16.54
	ETM	15.35	37.78	276.41	136.68
	SL	0.900	34.06	231.59	147.07
13/03/06	LL	19.400	1.90	104.91	18.11
	ETM	11.000	26.18	330.48	79.22
	SL	0.900	22.18	120.47	184.11
14/03/06	LL	19.400	13.10	308.01	42.53
	ETM	13.650	31.70	255.69	123.98
	SL	0.900	19.42	197.49	98.34
16/03/06	LL	19.400	2.44	192.44	12.68
	ETM	11.00	17.68	171.18	103.28
	SL	0.900	19.10	126.95	150.46
25/07/06	LL	17.500	145.03	1024.55	141.56
	ETM	17.500	145.03	1024.55	141.56
	SL	0.900	32.60	206.60	157.79
26/07/06	LL	18.900	137.77	835.03	164.98
	ETM	17.500	223.30	642.63	347.48
	SL	0.900	22.7	161.70	140.39

Table 5.6, is continued on next page.

27/07/06	**LL**	19.600	59.80	792.97	75.41
	ETM	18.900	98.57	964.18	102.23
	SL	0.900	24.10	148.48	162.31
28/07/06	**LL**	19.675	---	367.95	---
	ETM	18.900	93.67	917.13	102.13
	SL	0.900	25.13	153.87	163.35

Table 5.6 presents the surface values of the 16 surveys, at 3 locations: LL = landward limit of survey; ETM; and SL = seaward limit of survey.

27/07/06	**LL**	19.600	59.80	792.97	75.41
	ETM	18.900	98.57	964.18	102.23
	SL	0.900	24.10	148.48	162.31
28/07/06	**LL**	19.675	---	367.95	---
	ETM	18.900	93.67	917.13	102.13
	SL	0.900	25.13	153.87	163.35

Table 5.6 presents the surface values of the 16 surveys, at 3 locations: LL = landward limit of survey; ETM; and SL = seaward limit of survey.

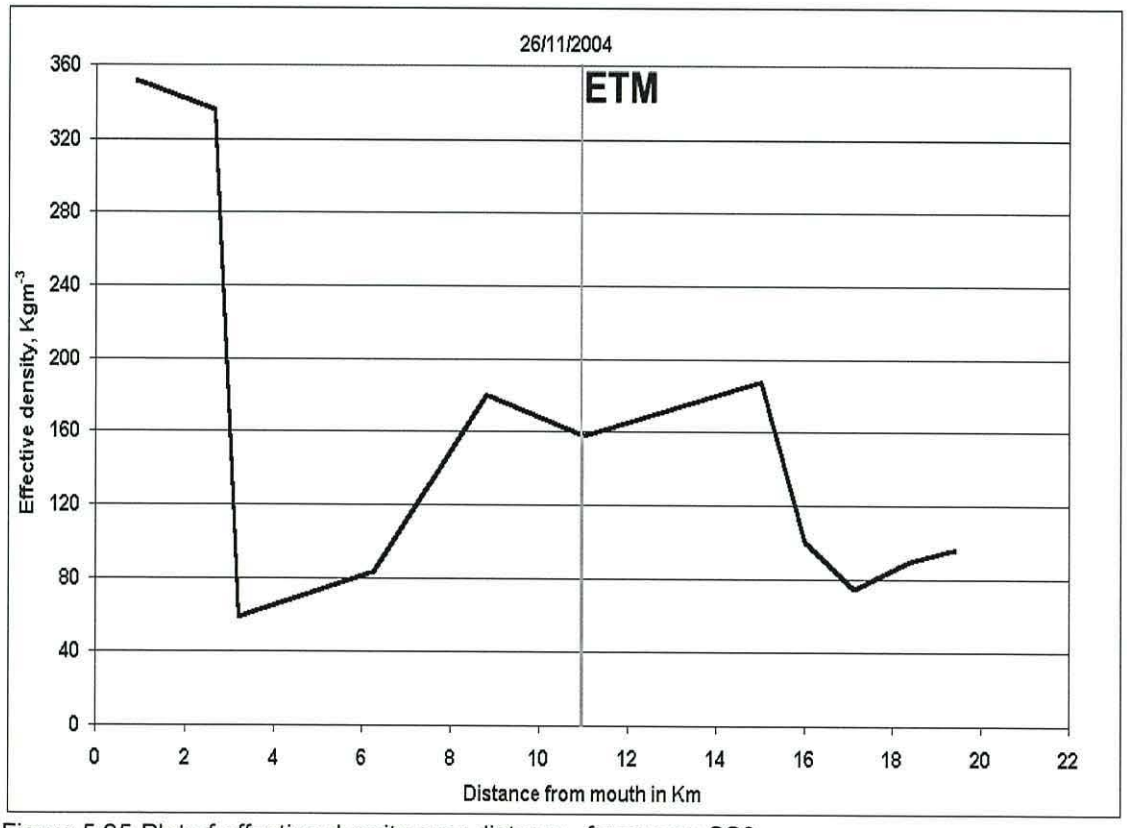

Figure 5.25 Plot of effective density over distance, for survey SS3.

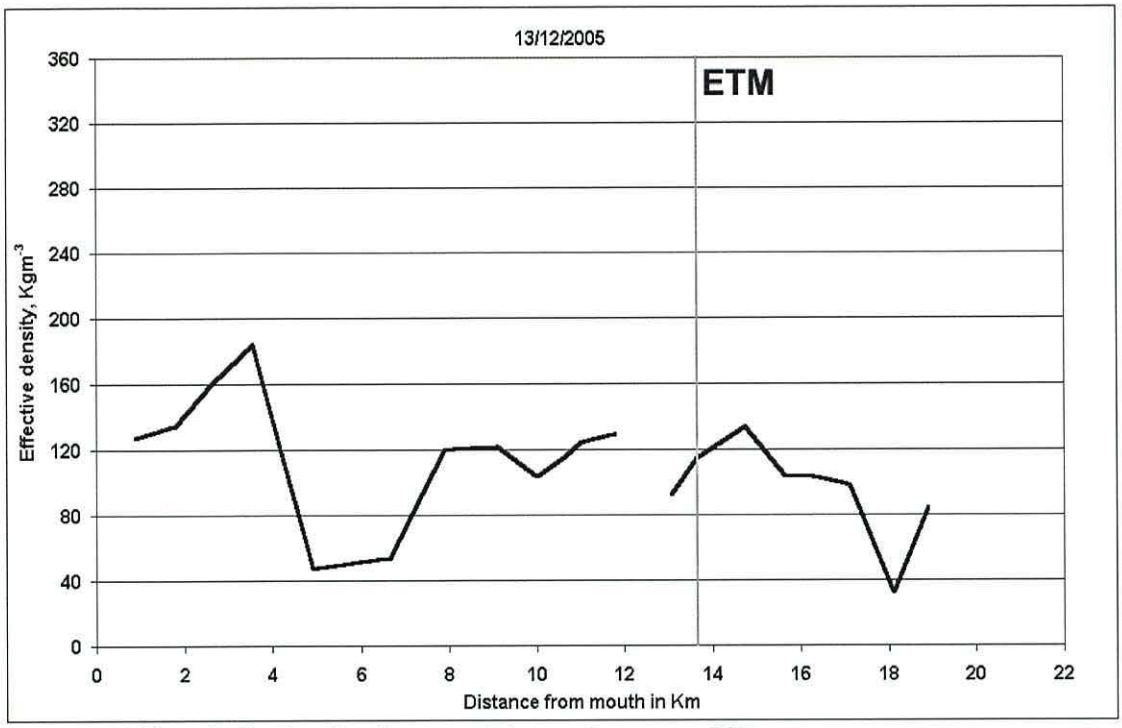

Figure 5.26 Plot of effective density over distance, for survey SS8.

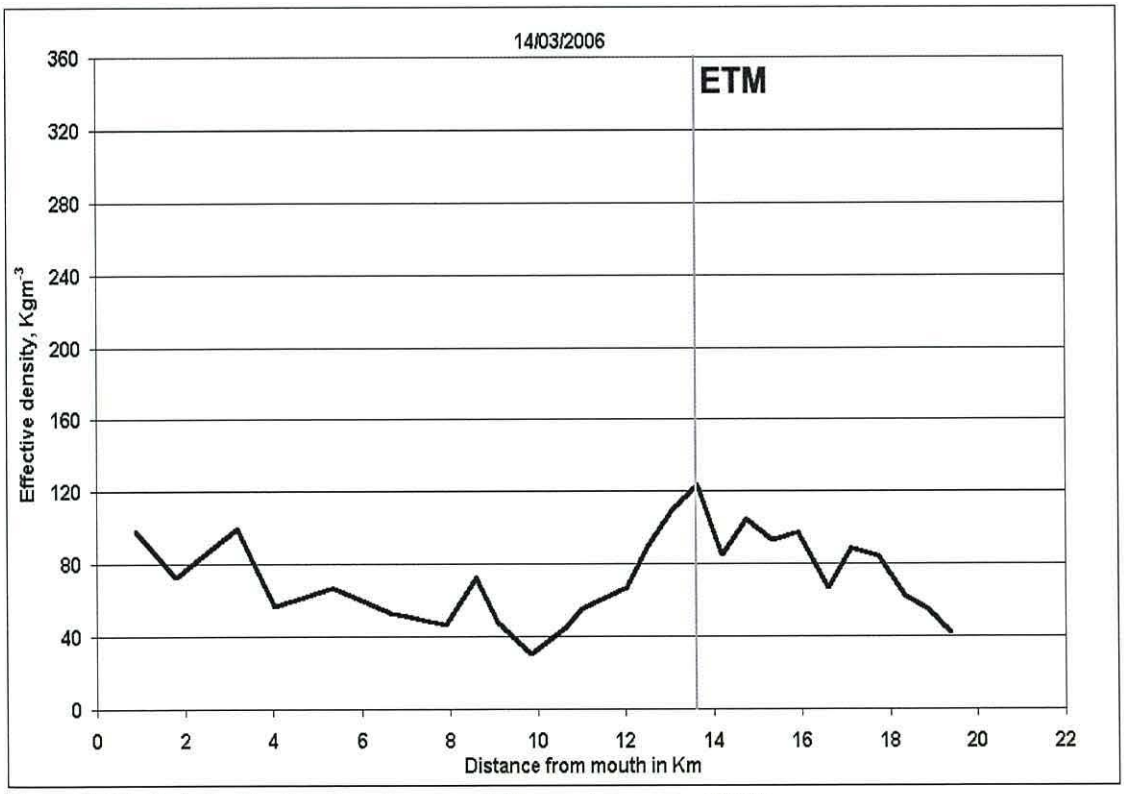

Figure 5.27 Plot of effective density over distance, for survey SS15.

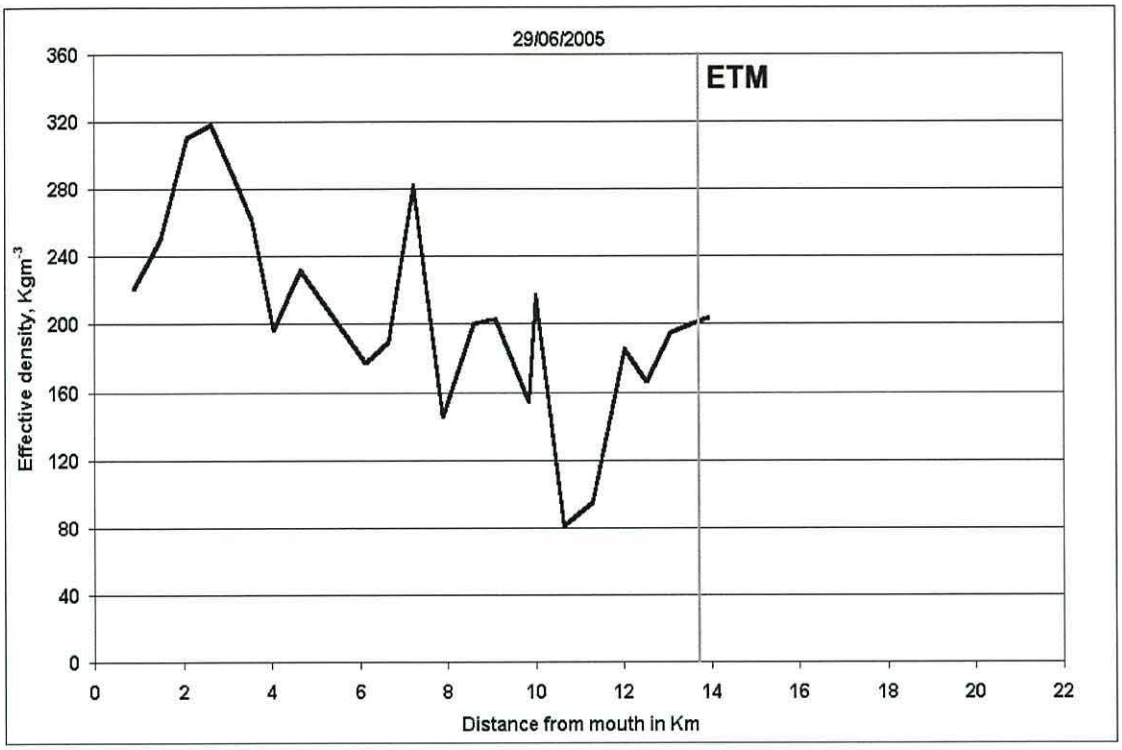

Figure 5.28 Plot of effective density over distance, for survey SS5.

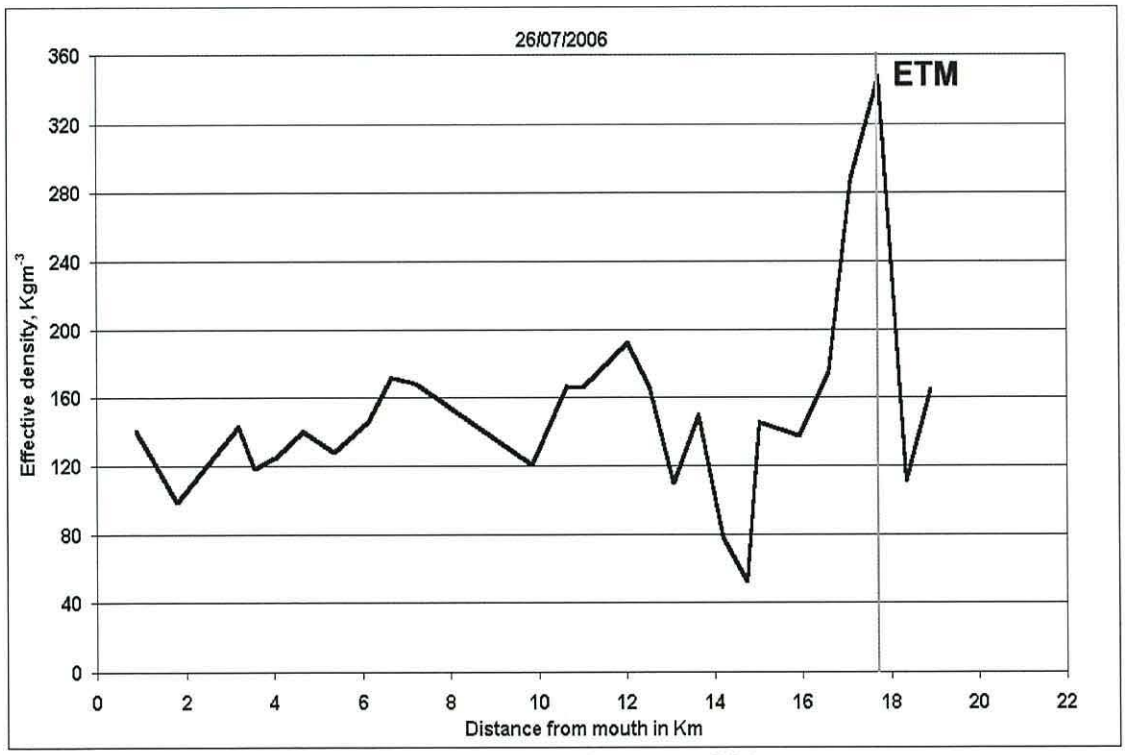

Figure 5.29 Plot of effective density over distance, for survey SS24.

5.3.2 Discussion

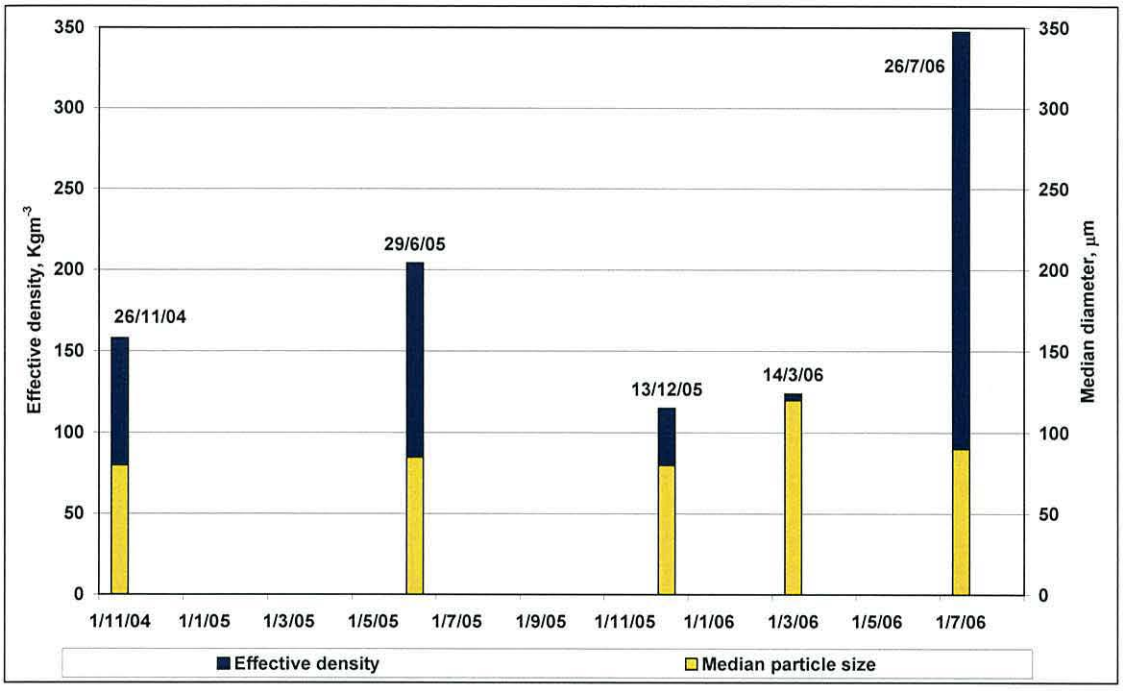

Figure 5.30, showing the effective density and median diameter of surface SPM within the ETM.

Figure 5.30 presents the effective density and median diameter of surface SPM within the ETM for the 5 survey days. With the exception of March 2006, the median diameter of surface SPM is constant at around 80 microns.

From Figures 5.20 through to 5.29 it can be seen that when the percentage of "clay" and "silt" sized fractions increased, the effective density increased also. When these two fractions decreased, so did the effective density.

5.4 The ETM

5.4.1 ETM Properties

The overall properties of the ETM (location, salinity, SSC, VC, floc size, ED, and ρ_f) are shown in Table 5.7. The average depths at the three locations were: Landward Limit (LL) ~ 2.3 m; ETM ~ 2.8 m; and Seaward Limit (SL) ~15 m. The average river discharge for the 16 surveys was 25 m^3s^{-1}, whilst the average tidal range was 5.58 m (Q/T^3 = 0.144).

	Landward limit		ETM		Seaward limit	
	Mean	Median	Mean	Median	Mean	Median
Distance from mouth, km	17.19	18.90	13.90	13.65	0.81	0.90
Water density, kgm^{-3}	999	1000	1001	1000	1023	1024
Salinity	0.14	0.07	2.22	0.80	30.74	31.18
SSC, mgl^{-1}	41.95	29.43	76.31	41.40	23.09	22.44
VC, µl/l	359.22	217.70	526.51	360.20	136.87	134.97
Median diameter, µm	108.25	93.59	88.87	89.23	121.18	126.26
ED, kgm^{-3}	102.85	98.96	142.93	127.44	185.51	160.80
ρ_f, kgm^{-3}	1102	1098	1144	1129	1209	1184

Table 5.7 showing mean and median surface values of the 16 surveys, at 3 the locations: LL; ETM; and SL.

The seasonal properties of the ETM can be found in Table 5.8, below. The values in Table 5.8 are seasonal averages of the surveys within that season: autumn = 3 surveys; winter = 7 surveys; spring = 9 surveys; and summer = 7 surveys.

	Autumn	Winter	Spring	Summer
Distance from mouth, km	11.47	12.28	12.25	16.05
Water density, kgm^{-3}	1005	1001	1002	998
Salinity	6.43	3.17	1.13	0.56
SSC, mgl^{-1}	44.49	22.94	29.08	129.78
VC, µl/l	334.45	275.78	293.79	816.02
Median diameter, µm	103.55	69.10	103.61	84.74
ED, kgm^{-3}	133.02	83.18	98.59	159.04
ρ_f, kgm^{-3}	1138	1084	1101	1157

Table 5.8, showing the seasonal properties of the ETM (values = seasonal averages).

The floc bulk density in the ETM was low throughout the seasons, which indicates that the flocs are composed primarily of low density particulate matter and/or loosely packed particulate matter.

5.4.2 ETM Location

5.4.2.1 Observed ETM Location

In total 26 spatial surveys were carried out between November 2004 and July 2006. Over this period, the location of the ETM was found spread over a range of 10 km, see figure 5.31. From figure 5.31 we have: 3 ETMs out of 26 in the region just before Tal-y-Cafn bridge (10 km); 4/26 in the region after Dolgarrog bridge (~16 km); and 19/26 ETMs in the region between the two bridges.

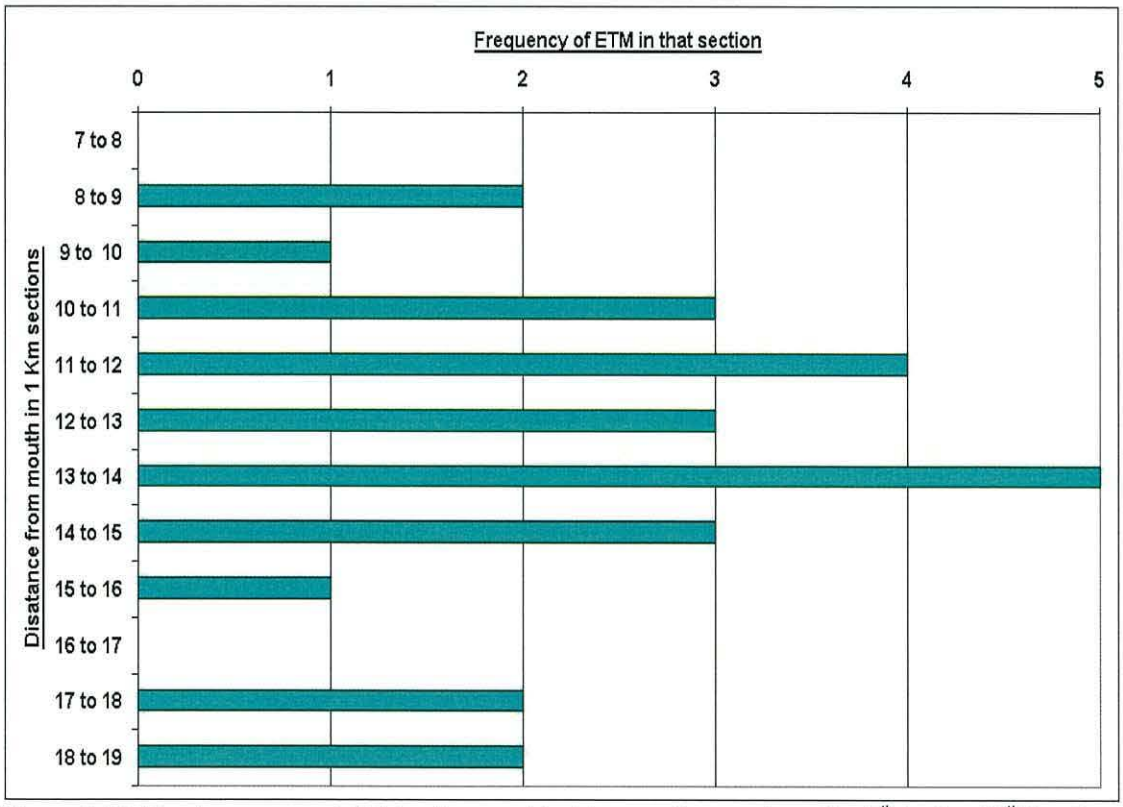

Figure 5.31 The frequency of ETMs observed in 1 km sections – from the 7th to the 19th km from the mouth of the estuary.

After averaging, the mean ETM position was ~13.2 km from the mouth, occurring on a mean tidal range of ~5.6 m and a mean river discharge of ~26 m^3s^{-1}. The most seaward ETM position was observed to be 8.6 km from the mouth, occurring on a below average tidal range (5 m), and an above average river discharge (41 m^3s^{-1}). On the other hand, the most landward ETM position was observed to be 18.9 km from the mouth, occurring on an above average tidal range (6 m), and a well below average river discharge (0.42 m^3s^{-1}).

After splitting and pooling the data of the 26 surveys into seasons, the relationship of the ETM location relevant to the tidal ranges (see Figure 5.32) and river discharges (see Figure 5.33) was found:

- For the autumn surveys, the tidal range and river discharge separately explain 0.84% and 48.08%, respectively, of the ETM location variance.

- For the winter surveys, the tidal range and river discharge separately explain 0.12% and 8.94%, respectively, of the ETM location variance.

- For the spring surveys, the tidal range and river discharge separately explain 53.77% and 2.76%, respectively, of the ETM location variance.

- For the summer surveys, the tidal range and river discharge separately explain 73.56% and 66.94%, respectively, of the ETM location variance.

From the above it can be concluded that the ETM location was not simply related to tidal range in autumn and winter. Also the ETM location was not simply related to river flow in winter and spring.

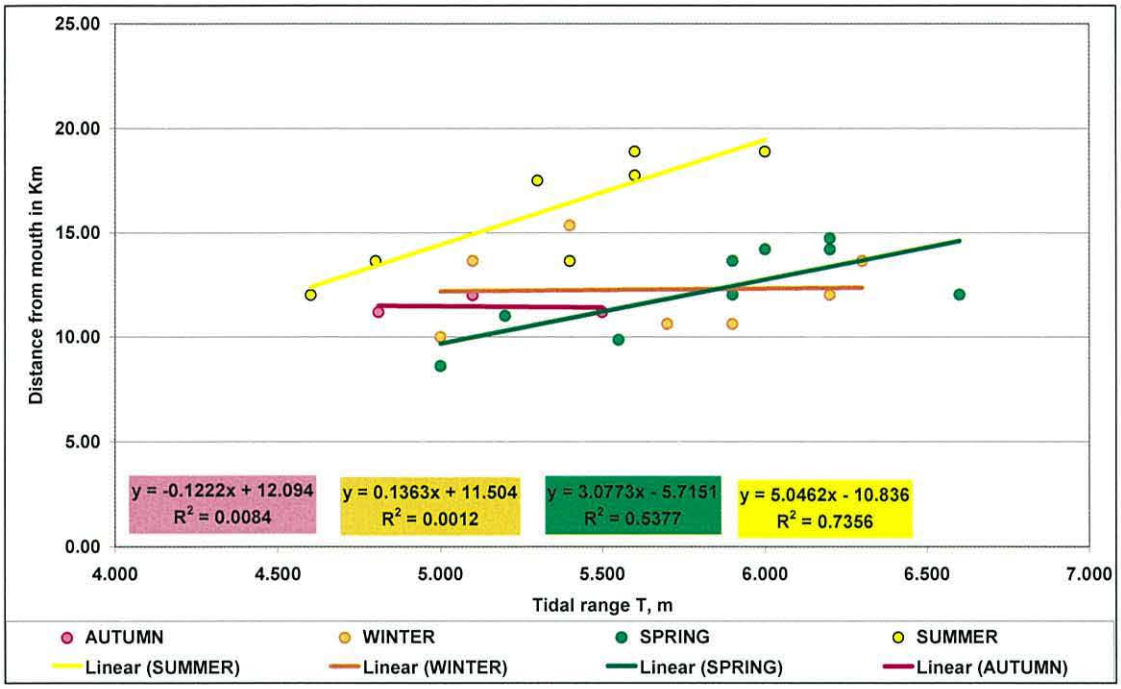

Figure 5.32 Relationship of ETM location (as distance from mouth) and tidal range, T (m).

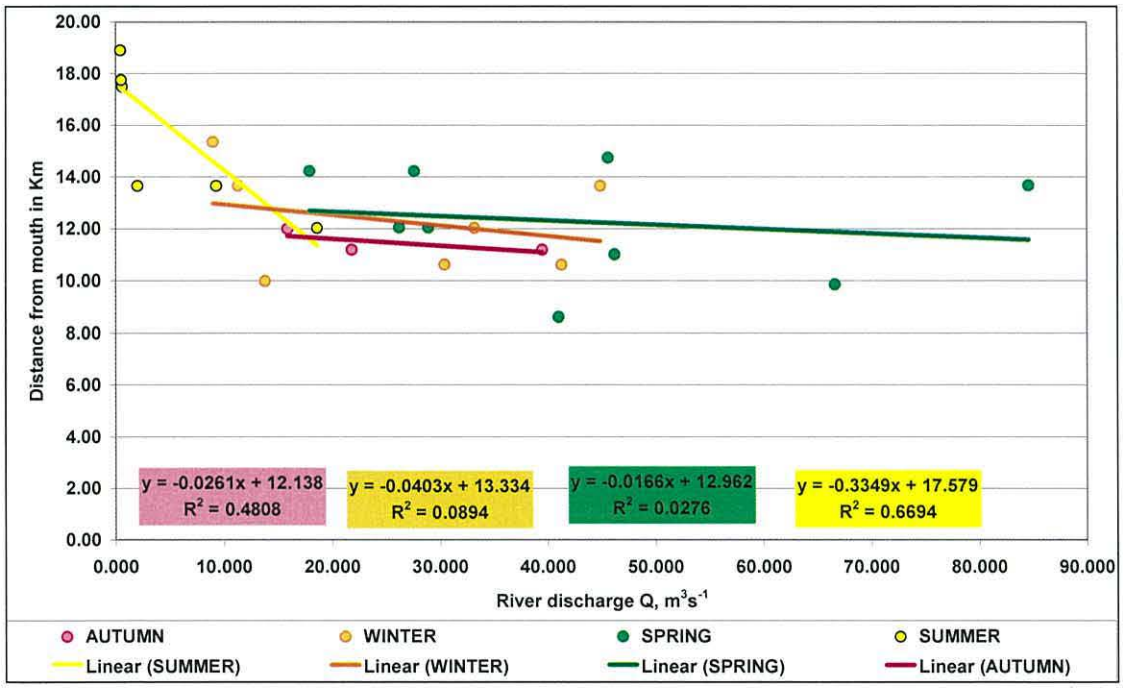

Figure 5.33 Relationship of ETM location (as distance from mouth) and river discharge, Q (m^3s^{-1}).

The ETM in the Conwy estuary was found to occur at, or near, the landward limit of salt water intrusion. Jago et al. (2006), explain that the landward limit of salt intrusion is dependent on the river / tide ratio, Q/T^3, (see section 4.4).

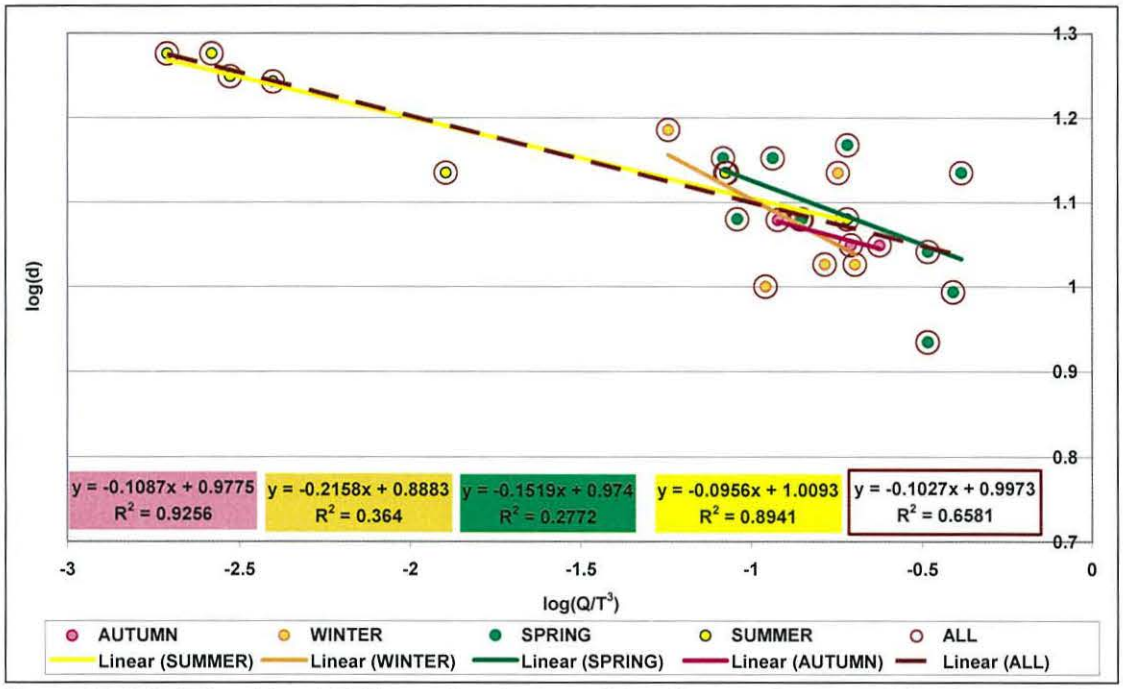

Figure 5.34 Relationship of ETM location (as log of the distance from mouth) to log of the flow ratio Q/T^3.

The dependence of ETM location on the flow ratio varies for each season, see Figure 5.34. When all data is pooled, the overall relationship weakens, but is still significant ($R^2 = 0.6581$).

5.4.2.2 Estimated ETM Location

Using the relationship produced in Figure 5.34, for all data, the distance D of the ETM from the mouth was given by:

$$\log(D) = 0.9973 - 0.1027 * \log(Q/T^3) \qquad [5.2]$$

where D is in km, Q in m^3s^{-1}, and T is in m.

From Equation 5.2, the ETM position could be estimated for any day (assuming that the ETM position is only dependent on the tidal range, the river discharge, and the uniform geometry of the estuary). This was done, on a daily basis, for the three surveying periods. As an example, the positions for the third period (2006) are compared, in Figure 5.35, with the predicted locations derived using Equation 5.2 (which was based on the entire data set).

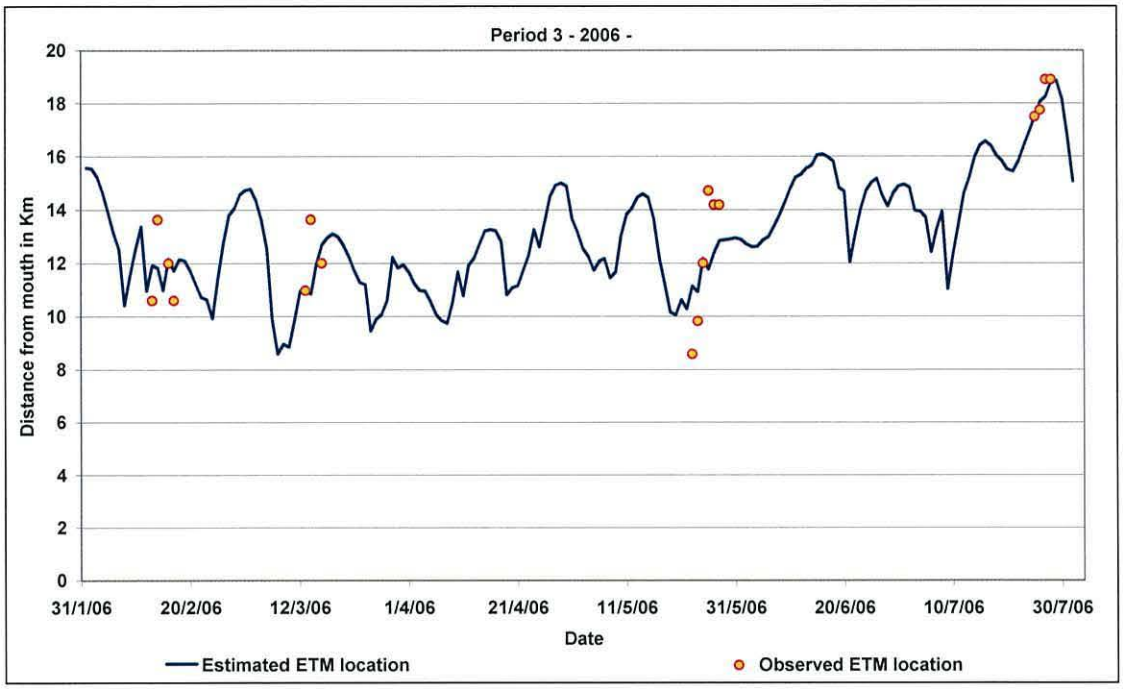

Figure 5.35 Estimated ETM location compared to observed ETM location – period 3.

The fit between estimated and observed ETM locations is good to within ± 2 km (excluding 4 points out of 6 in May). Figure 5.35 indicates that the ETM is positioned between Tal-y-Cafn and Dolgarrog bridges (10 – 16 km form the mouth) in agreement with the observations made.

5.4.3 Estimated SSC at the ETM

The depth average SSC in the ETM can be parameterized in terms of the conceptual flow ratio (Jago et al., 2006). SSC scales on Q/T^3 and 71% of the measured variation in SSC can be explained by Q/T^3, see Figure 5.36, where measured SSC was plotted against Q/T^3.

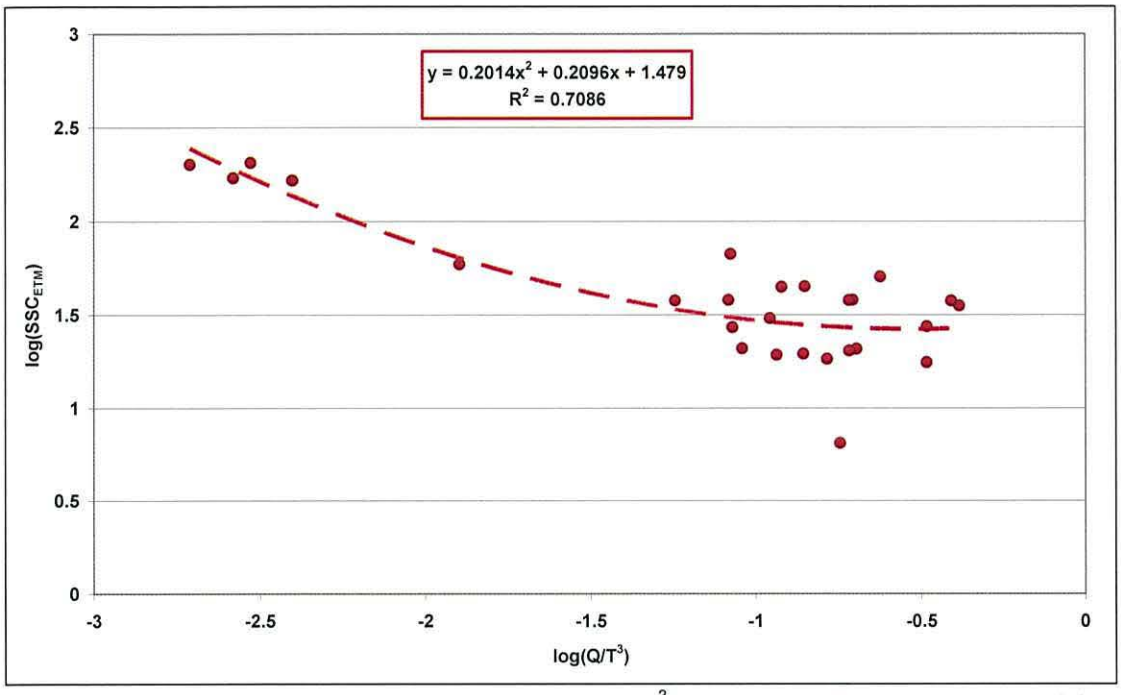

Figure 5.36 Log(SSC) at the ETM plotted against $\log(Q/T^3)$. The regression used is polynomial.

The SSC in the ETM, SSC_{ETM}, was given by:

$$\log(SSC_{ETM}) = 1.479 + 0.2014 * (\log(Q/T^3))^2 + 0.2096 * \log(Q/T^3) \quad [5.3]$$

where SSC_{ETM} is in mgl^{-1}, Q in m^3s^{-1}, and T is in m.

From Equation 5.3, the SSC_{ETM} could be estimated for any day assuming that the SSC_{ETM} is only dependent on the tidal range, the river discharge, and the uniform geometry of the estuary. This was done, on a daily basis, for the three surveying periods. As an example, the SSC_{ETM} for the third period (2006 surveys) are presented in figure 5.37.

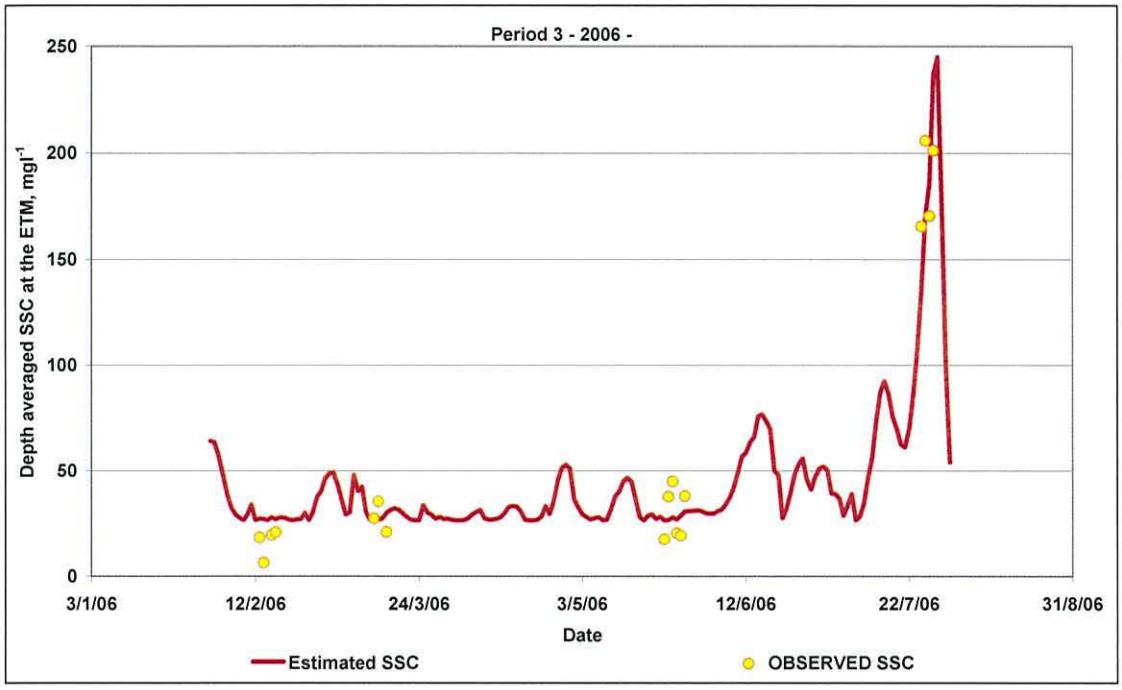

Figure 5.37 Estimated SSC_{ETM} compared with observed SSC_{ETM} – period 3.

Considering the assumptions and the fact that, in reality, the SSC_{ETM} is also dependent on other factors not considered here (such as: biological variability; availability of particulate matter; and actual geometry of estuary at the ETM), the estimated depth average SSC in the ETM is good.

5.4.4 Discussion and Conclusions

5.4.4.1 Longitudinal Variations in SPM Properties

After considering sections 5.1, 5.2, and 5.3 it can be seen that at high water the estuary can be divided into three longitudinal sections. The division is based on the longitudinal variations in the surface salinity. So, each section is characterised by a set of SPM properties, see Figure 5.38.

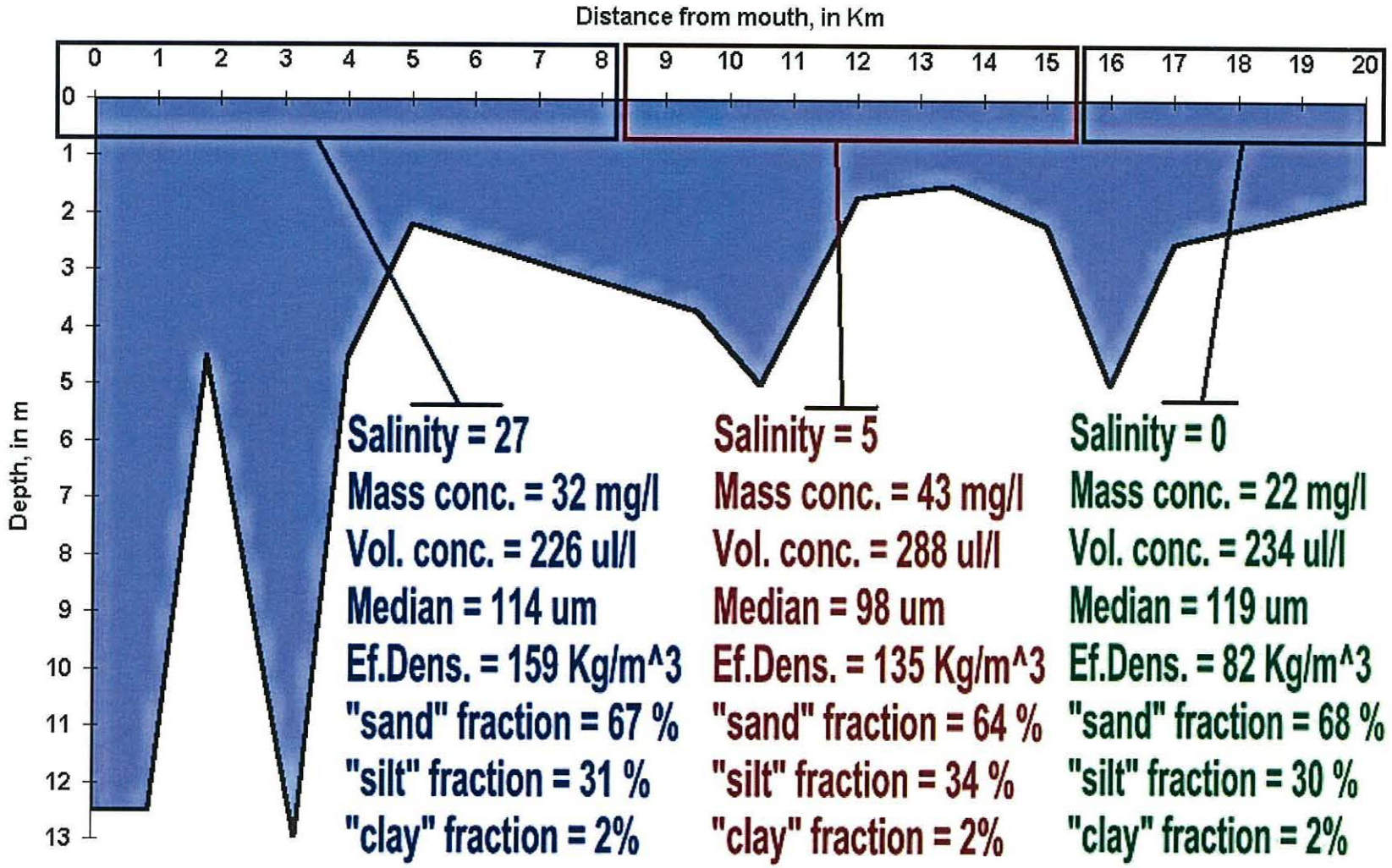

Figure 5.38: longitudinal variations in surface SPM (values are section averages – sections based on average salinity).

- Section one – the upper estuary (section mean salinity of 0). In this section the median diameter (119 μm), the ED (82 kgm^{-3}), the high percentage of the sand-sized fraction (68 %) suggest the presence of flocs and/or the settling of denser smaller particles.

- Section two – the ETM region (section mean salinity of 5). In this section the median particle diameter (98 μm), the ED (135 kgm^{-3}), and the lower percentage of the sand-sized fraction (64 %) suggest that any flocs in existence were being broken down by turbulence or simply the occurring turbulence was restricting the growth of flocs. The average surface SSC was 43 mgl^{-1}.

- Section three – the lower estuary (section mean salinity of 27). In this section, the median floc size (114 μm) was similar to that in the upper estuary, but with twice the floc density (159 kgm^{-3}). The increase in median diameter and sand-sized fraction (67 %) may either be indicating a regional decrease in turbulence (allowing the formation of bigger flocs), or that these larger particles were of different origin – i.e. sourced from offshore.

Overall, when comparing the SPM properties of the lower and upper estuary, their similar floc size and different effective densities suggest that the particulate matter making up the flocs are of different origin. Perhaps the flocs in the lower estuary are made up of marine particulate matter, whilst the flocs in the upper estuary are made up of terrestrial particulate matter.

5.4.4.2 The ETM Location and Strength

The ETM of the Conwy Estuary was observed in the region between 8 and 19 km from the mouth, approximately one hour after high water at Conwy. The main ETM region is narrow (between 50 – 250 m), shallow (average depth of ~3m at local high water), and has sand-banks and small islands narrowing the main channel even more.

Hillier (1985), carried out field work in July, and he observed the location of the ETM to be between Dolgarrog and Trefriw. Those observations are consistent with the observations made in this project, for July.

From section 5.4.2.1, it can be concluded that the factor controlling the ETM location changes with the season. In autumn and winter, the river discharge controlled the location. In spring, the dominant control was the tidal range. Whilst in the summer both tidal range and river discharge controlled the ETM location.

Compositional analysis of the suspended particulate matter in the ETM was not carried out. Hillier (1985), though, found that the ratio of marine-derived sediment to fluvial derived sediment was 7:3.

Jago et al. (2006) carried out spatial surveys within the Taf Estuary, South Wales, during the period between 1994 and 2003. They found that the average effective density of SPM at high water in the ETM was in the range of 120 – 160 kgm^{-3} (for summertime conditions). The average effective density of the SPM in the ETM of the Conwy estuary, for summer conditions, was 159 kgm^{-3}. The average ED (average value off all surveys carried out for this project) of SPM in the Conwy ETM was found to be 118 kgm^{-3}.

From Table 5.7, it can be seen that the SPM properties of the ETM follow a seasonal cyclic pattern:

- In winter, the SSC had the lowest seasonal depth averaged value (mass conc. = 23 mgl^{-1} and volume conc. = 276 μll^{-1}). The ED was found to be 83 kgm^{-3}.

- In spring, the SSC increased slightly (mass conc. = 29 mgl^{-1} and volume conc. = 294 μll^{-1}). The ED was found to be 99 kgm^{-3}.

- In summer, the SSC had the highest seasonal depth averaged value (mass conc. = 130 mgl^{-1} and volume conc. = 816 μll^{-1}). The ED was found to be 159 kgm^{-3}.

- In autumn, the SSC decreased noticeably (mass conc. = 45 mgl^{-1} and volume conc. = 335 μll^{-1}). The ED was found to be 133 kgm^{-3}.

According to Christie and Dyer (1998), the high concentrations in the leading waters' edge were considered to be from the resuspension of (sediment) surface biofilm. This weak layer was considered to be partly the result of deposition during the previous ebb cycle, and the movements of micro-organisms and other biological activity during emersion of the intertidal sediment.

Diatoms secrete biopolymers to move in the surface millimetres of the sediment, to attach to surfaces of grain particles and as a protective layer against changing environmental conditions (Kornman and de Deckere, 1998). The secretions are denoted by the term Extracellular Polymeric Substances (EPS) and consist mainly of polysaccharides.

Micro-organisms living in the surface intertidal sediment migrate vertically in response to tides and light (Perkins, 1974, and Pinckney and Zingmark, 1991). During the summer months the river discharge was at minimum (4.6 m^3s^{-1}) allowing the sand and mud flats to be exposed for longer periods than in winter. This meant that the migrating micro-organisms would stay at the surface for

longer periods, producing greater amounts of EPS and detritus. This low density bio-matter would be suspended during the flood tide, increasing the SPM concentrations.

5.4.4.3 Use of Taf Derived Relationships to Estimate ETM Location and SSC in the Conwy

Both estuaries are similar in their dynamics, with differences in size, geometry and fresh water discharge. The average fresh water discharge for Conwy River is 25 m^3s^{-1}, whilst it is 7 m^3s^{-1} (Jago et al., 2006) for the Taf River.

Jago et al. (2006), when relating the flow ratio to the ETM location and SSC, came up with the following (summer conditions):

$$\log(D) = 0.81 - 0.13 * \log(Q/T^3) \quad [5.4]$$

where D is distance in km, Q in m^3s^{-1}, T is in m and $R^2 = 0.94$.

$$\log(SSC_{ETM}) = 0.22 - 0.95 * \log(Q/T^3) \quad [5.5]$$

where SSC_{ETM} is in mgl^{-1}, Q in m^3s^{-1}, T is in m and $R^2 = 0.98$.

For the summer conditions in the Conwy the relationships were:

$$\log(D) = 1.0095 - 0.0956* \log(Q/T^3) \quad [5.6]$$

where D is distance in km, Q in m^3s^{-1}, T is in m and $R^2 = 0.89$.

$$\log(SSC_{ETM}) = 1.3362 - 0.3517* \log(Q/T^3) \quad [5.7]$$

where SSC_{ETM} is in mgl^{-1}, Q in m^3s^{-1}, T is in m, and $R^2 = 0.86$.

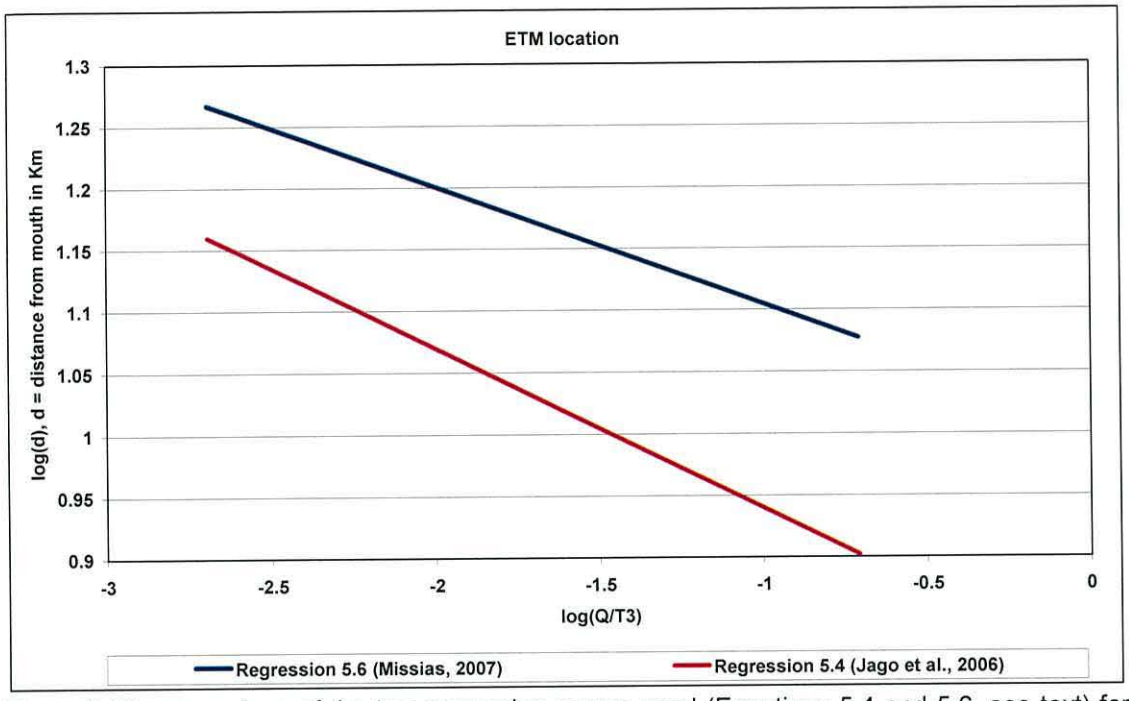

Figure 5.39: comparison of the two regression curves used (Equations 5.4 and 5.6, see text) for predicting the ETM location.

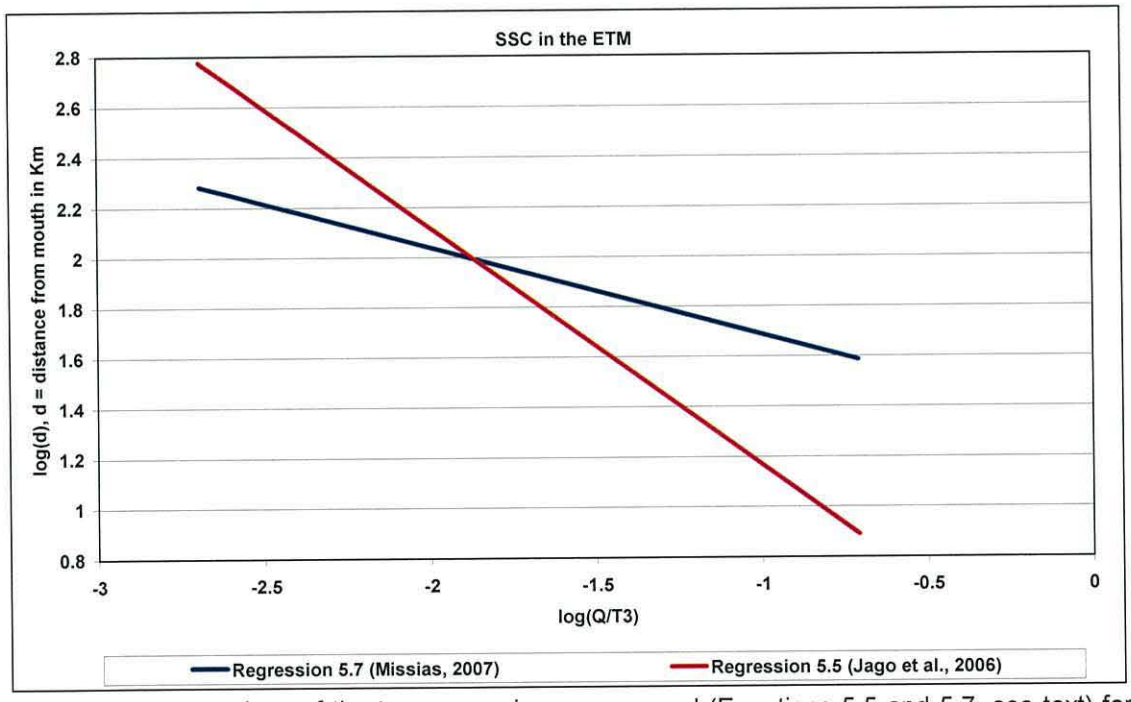

Figure 5.40: comparison of the two regression curves used (Equations 5.5 and 5.7, see text) for predicting the SSC in the ETM.

Figures 5.41 and 5.42 compare the ETM locations predicted by relationships 5.4 and 5.6 (using the Conwy flow ratio). Both relationships follow the same pattern although the Jago et al. (2006) relationship underestimates the ETM location by about 4 km (i.e. places the ETM 4 km closer to the mouth).

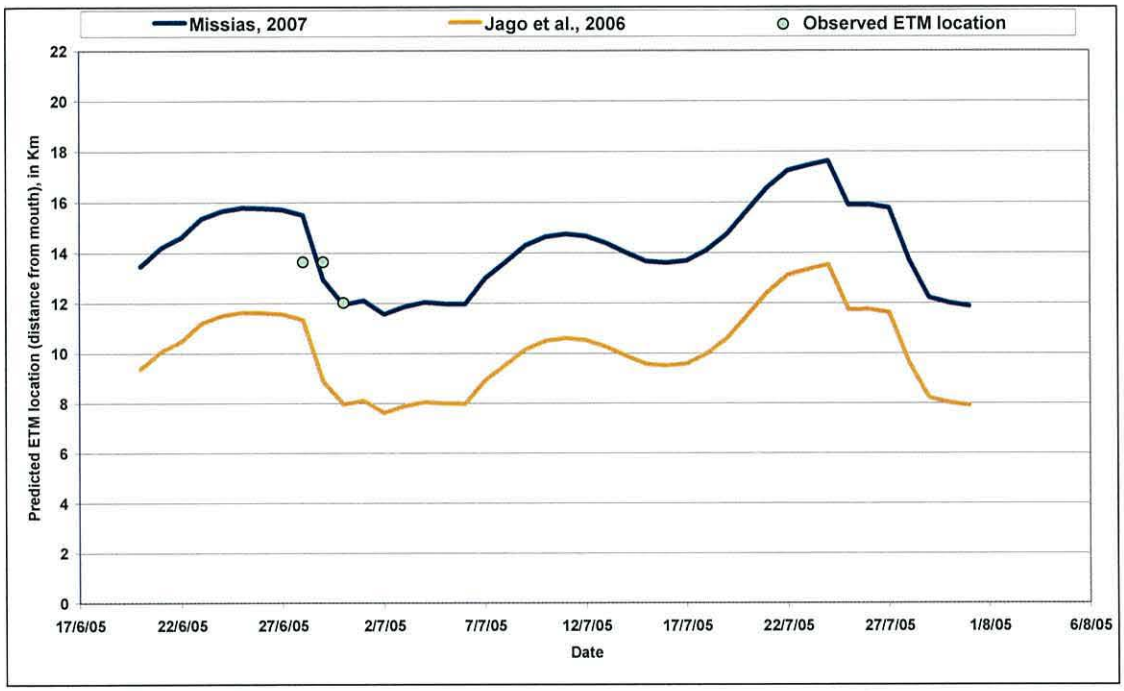

Figure 5.41: comparison between estimated ETM location – period 2 (2005).

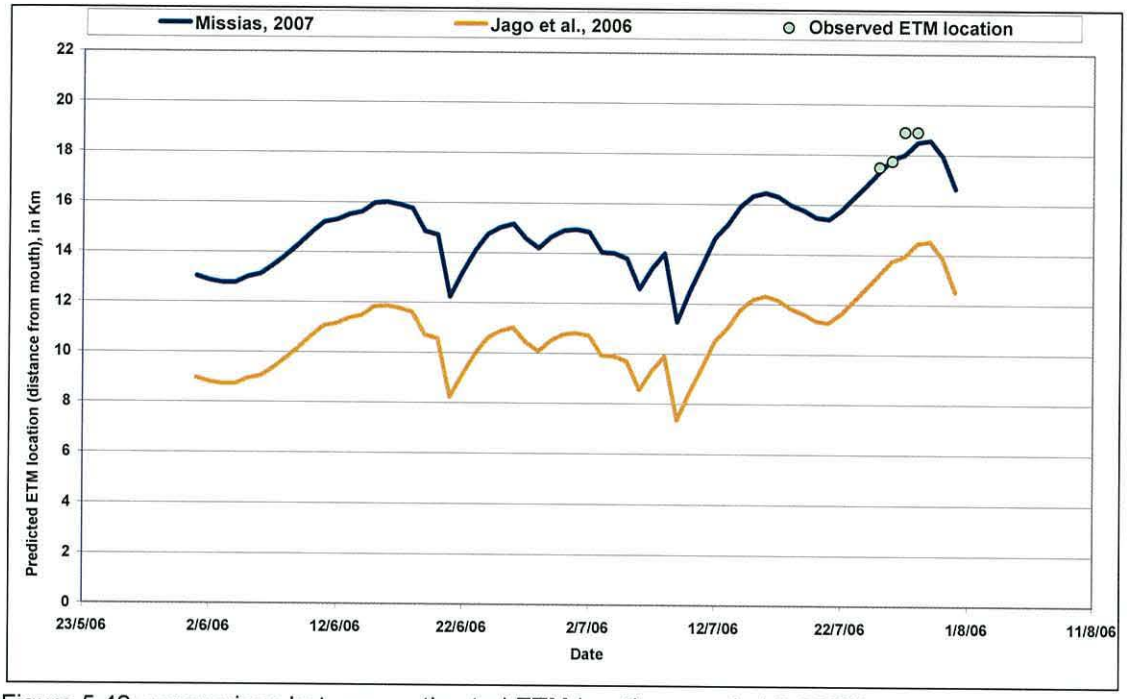

Figure 5.42: comparison between estimated ETM location – period 3 (2006).

Figures 5.43 and 5.44 compare the ETM suspended sediment concentration predicted by relationships 5.5 and 5.7 (using the Conwy flow ratio).

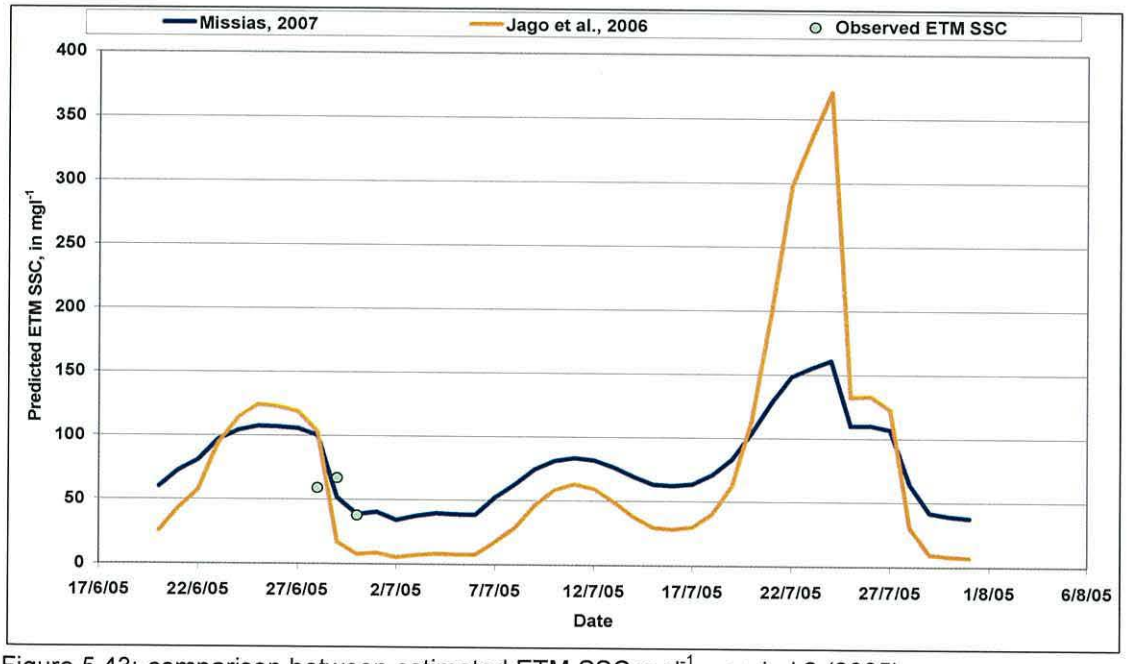

Figure 5.43: comparison between estimated ETM SSC mgl^{-1} – period 2 (2005).

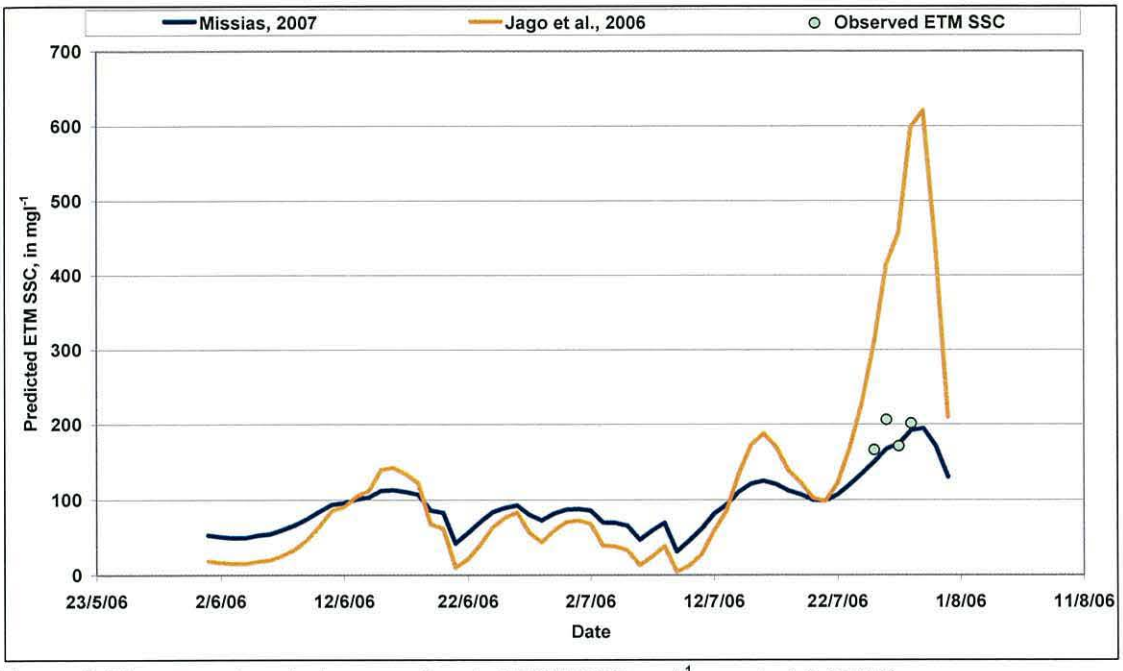

Figure 5.44: comparison between estimated ETM SSC mgl^{-1} – period 3 (2006).

From figures 5.43 and 5.44, it appears that the Taf derived relationship, follows the general pattern, but differs significantly at the end of the summer periods – i.e. the SSC is overestimated, by 200 - 400 mgl^{-1}, at very low flow ratios (~ 0.006 in 2005, and ~ 0.004 in 2006).

The differences in predicting both location and SSC could be down to the difference in the geometry (Taf is shorter with a greater sinuosity of the channel in the section of the ETM, than Conwy), river discharge (Conwy reaches extreme lows), and the timing of low water.

As seen in section 5.4.4.2, the surfaces of the intertidal sediment are covered by a biofilm during low water (exposure). Diatoms produce coloured patches in response to light; similar patches are produced by blue-green algae, dinoflagellates, euglenoids and flatworms. Each of these organisms needs exposure to sunlight either for itself or a symbiont.

Low water (on spring tides) in the Taf is typically during midday, when exposure duration to light is greatest. In comparison, low water (on spring tides) in the Conwy is in the late afternoon-evening, when the exposure duration to light is minimal. This difference in exposure duration could mean that there are more bio-products produced in the Taf, increasing the SPM concentrations during flood.

This is just a hypothesis, no measurements, though, were made to test it. It is clear that more investigation is needed.

6 MOORED SURVEYS (ANCHOR STATIONS)

6.1 Main Results

The main results from the moored surveys are presented in the following two tables (Tables 6.1 and 6.2).

Note: The times of high or low water are that at Conwy on the survey day.

Station No	MS1	MS2	MS3	MS4	MS5
Station location	Conwy	Tal-y-Cafn	Deganwy	Henryd	Glan-Conwy
Time of high water at Conwy, GMT	15:23	05:27	03:47	04:43	06:45
Time of low water at Conwy, GMT	09:48	12:12	10:30	11:18	13:17
Tidal range, m	4.66	3.44	4.18	3.76	3.34
River discharge, m^3s^{-1}	38.7	70.2	2.7	2	4.2
River discharge to Tidal range ratio: Q / T^3	0.382	1.724	0.037	0.038	0.113
Average site depth, in m	9.96	3.06	9.52	1.64	2.13
Wind conditions	Calm	Calm	Calm	Calm	Light wind
Weather	Dry	Light rain	Dry	Dry	Dry
Time of first cast, GMT	06:20	06:10	05:48	05:38	05:25
Time of last cast, GMT	17:09	17:58	17:46	17:32	17:04

Table 6.1, contains the general information for each survey day.

For the velocity negative values indicate motion in the down-estuary direction (i.e. ebb), whilst positive values indicate motion in an up-estuary direction (i.e. flood).

Station No	MS1	MS2	MS3	MS4	MS5
Station location	Conwy	Tal-y-Cafn	Deganwy	Henryd	Glan-Conwy
Time, of maximum SPM concentration, relative to LW – in hours	+3	+1/2	-1	-4	-3
Time, of minimum SPM concentration, relative to LW – in hours	+6	-5	+7	+6	-6
Maximum SPM conc., in mg/l	138	21	27	37	30
Minimum SPM conc., in mg/l	26	11	24	21	24
Salinity at the time of maximum concentration	10.3	0.0	28.6	24.9	21.7
Salinity at the time of minimum concentration	23.0	0.1	32.5	28.1	29.2
Median diameter of SPM at maximum conc., in μm	69	96	99	97	98
Median diameter of SPM at minimum conc., in μm	125	113	127	142	96
Velocity at maximum concentration, in m/s	0.36	-0.73	-0.21	-0.26	-0.61
Velocity at minimum concentration, in m/s	0.03	-0.48	-0.26	0.00	-0.10

Table 6.2, contains information regarding the maximum and minimum SPM concentrations for each survey day.

6.2 The Moored Surveys in Detail

In addition to Tables 6.1 and 6.2, data from the anchor stations are presented in detail using contour plots. For each station, 5 time series are presented in the following order: salinity; velocity; SPM concentration (i.e. SSC); and median diameter of SPM. The order, in which the stations are presented, is chosen on the basis of their Q/T^3 ratio, with the smallest ratio first and the largest last.

6.2.1 Station MS3 (Deganwy)

Station MS3 had a Q/T^3 ratio of 0.037.

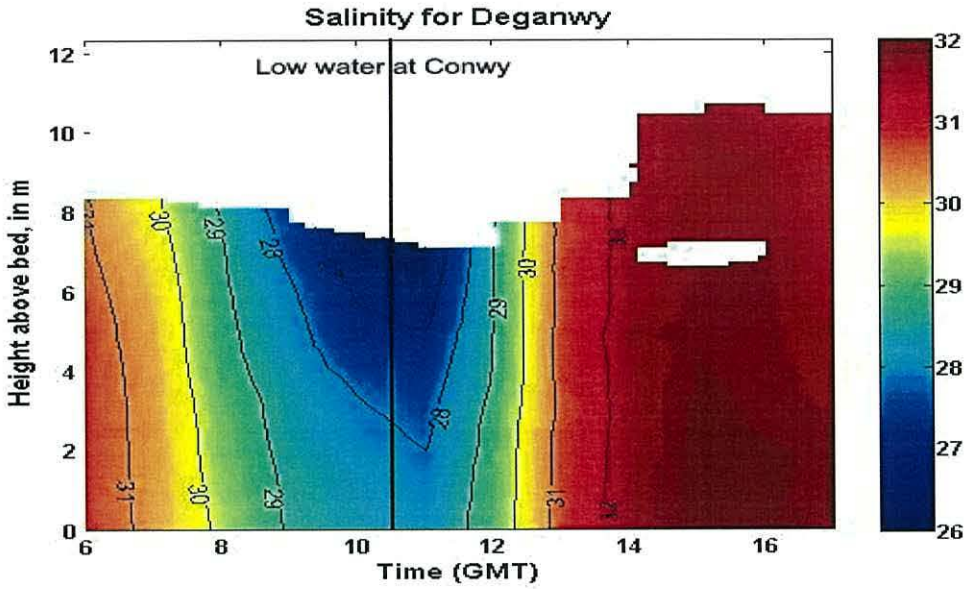

Figure 6.1: salinity at Deganwy.

Figure 6.1 shows salinity, (low water at Conwy: 10:30 am). The salinity reached a maximum around about high water slack, where the water column was well mixed. The salinity reached a minimum in surface water just after low water slack, when it slightly stratified. The flood duration (5 h 30 min) was less than the ebb duration (6 h 45 min).

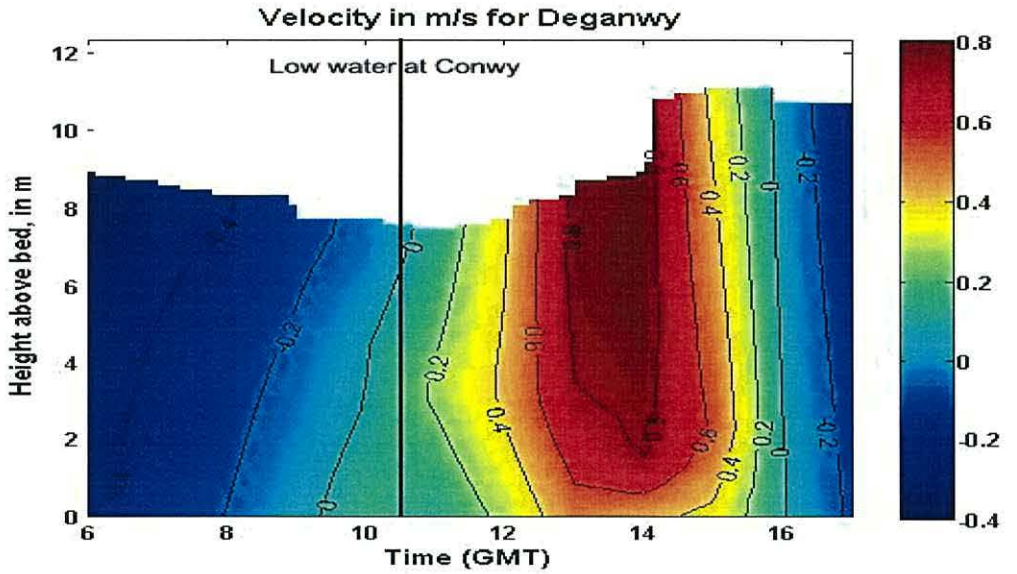

Figure 6.2: velocities at Deganwy.

Figure 6.2 shows velocities; in m/s. Negative values are ebb velocities, whilst positive values are flood velocities. Ebb velocities peaked about 3½ hours before low water, whilst flood velocities peaked about 3 hours after low water. Peak flood velocities were about twice the peak ebb velocities.

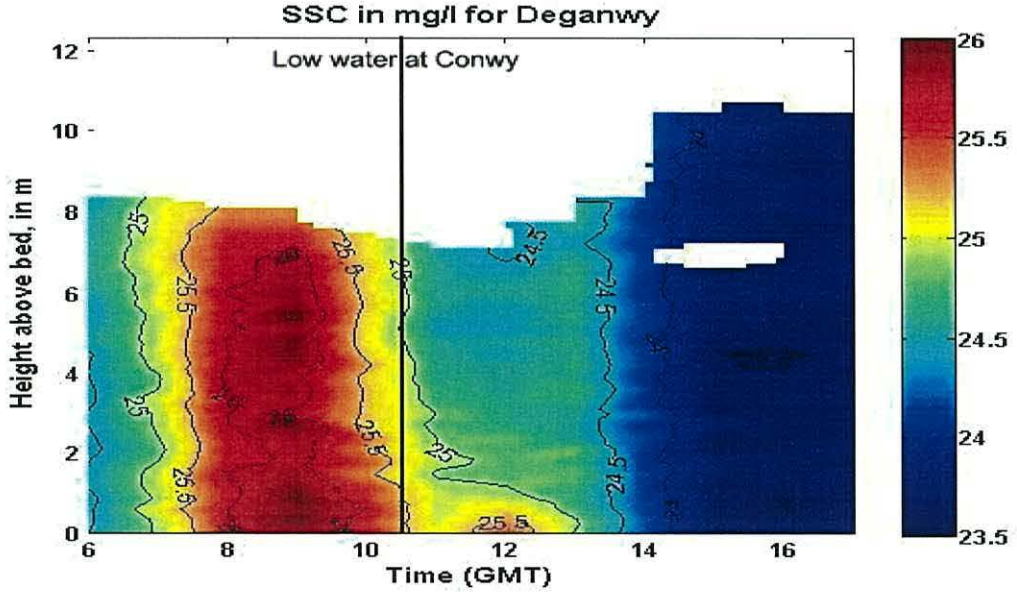

Figure 6.3: SSC at Deganwy.

Figure 6.3 shows total SPM concentration, in mgl^{-1}, derived from the OBS. The SPM concentration reached its maximum about 1 hour and 18 minutes before low water slack (after peak ebb currents), whilst reaching its minimum about an hour after high water slack.

There was no SSC increase at peak flood flow, though there was evidence of resuspension at the bed at the start of the flood. The minimum SSC indicates the lack of resuspended particles, even though the suspension threshold was exceeded (see chapter 7). This suggests that there were, possibly, no particles available for resuspension.

The maximum SSC during the ebb, does not correspond to a velocity maximum, this suggests that it cannot be due to resuspension, but is due to advection of a turbid body of water. This station is located near the narrow mouth of the estuary; the area is usually subject to wind generated waves, increasing turbulence.

Overall, it is clear that SSC was greater on the ebb than on the flood (the converse of the velocity asymmetry), though differences are small.

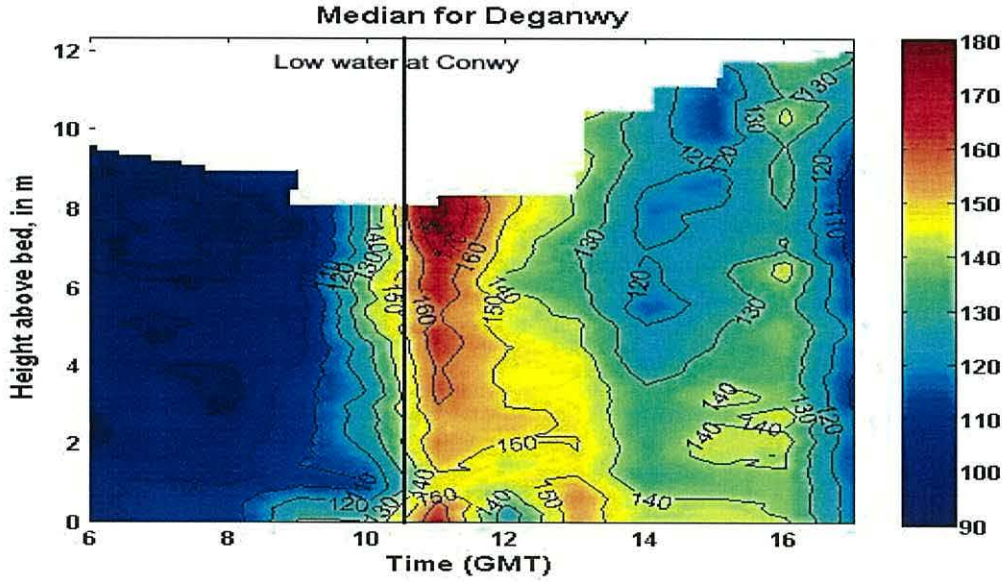

Figure 6.4: median diameter at Deganwy.

Figure 6.4 shows the SPM median diameter, in μm. The median diameter of the suspended matter reached a maximum (>180 μm) in the surface water just after low water slack. This suggests that flocculation was occurring at slack water. The diameter reached a minimum (<90 μm) about 3 hours before low water.

6.2.2 Station MS4 (Henryd)

Station MS4 had a Q/T^3 ratio of 0.038.

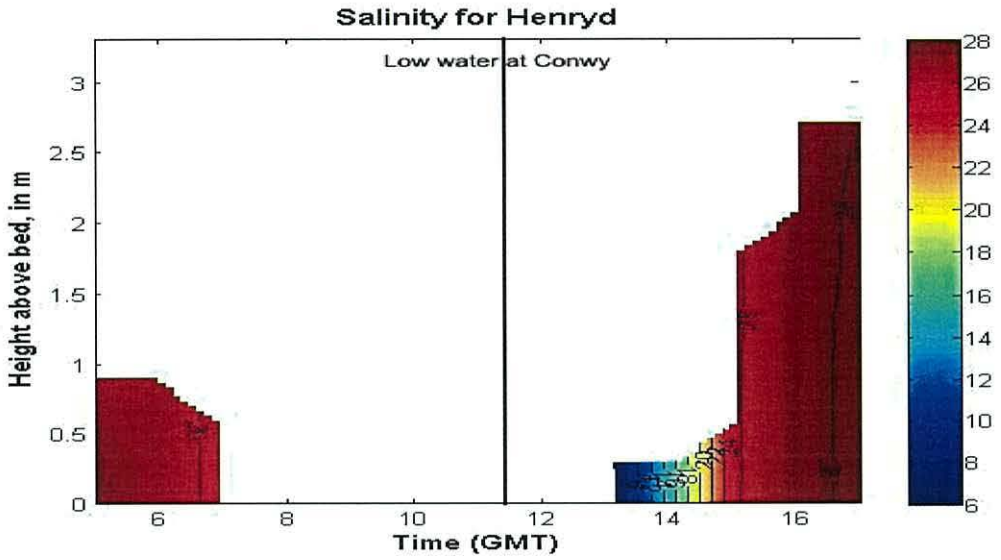

Figure 6.5: salinity at Henryd.

Figure 6.5 shows salinity, (low water at Conwy: 11:18 am). The salinity reached a maximum around about high water slack, where the water column was mixed. The salinity was at a minimum 3 hours after low water slack, when the flood tide entered.

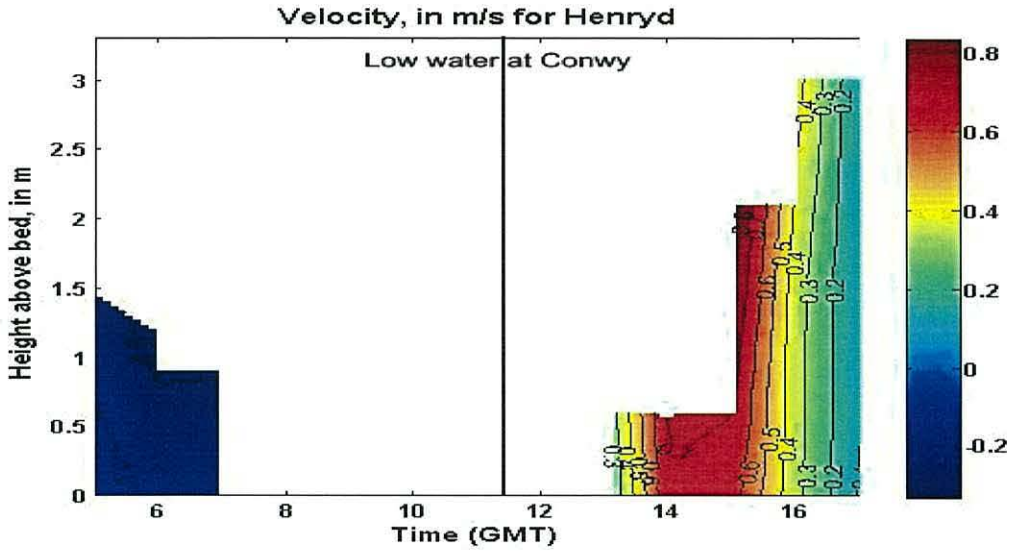

Figure 6.6: velocities at Henryd.

Figure 6.6 shows the velocities; in m/s. Peak flood velocities exceeded peak ebb velocities.

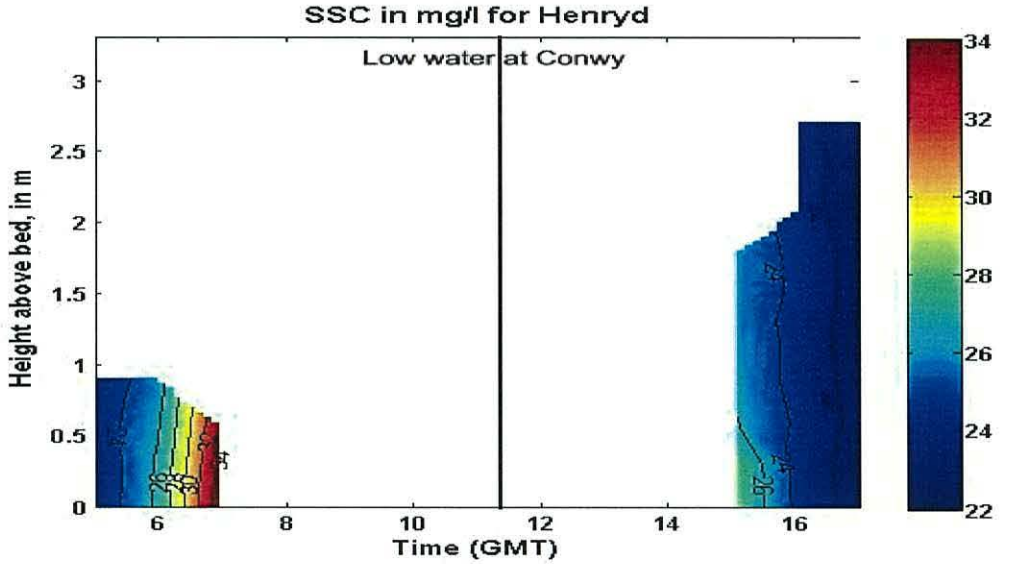

Figure 6.7: SSC at Henryd – there were technical difficulties with the OBS around 14:00.

Figure 6.7 shows total SPM concentration, in mgl^{-1}, derived from the OBS. The SPM concentration reached its maximum about 4 hours before low water slack, whilst reaching its minimum around high water slack.

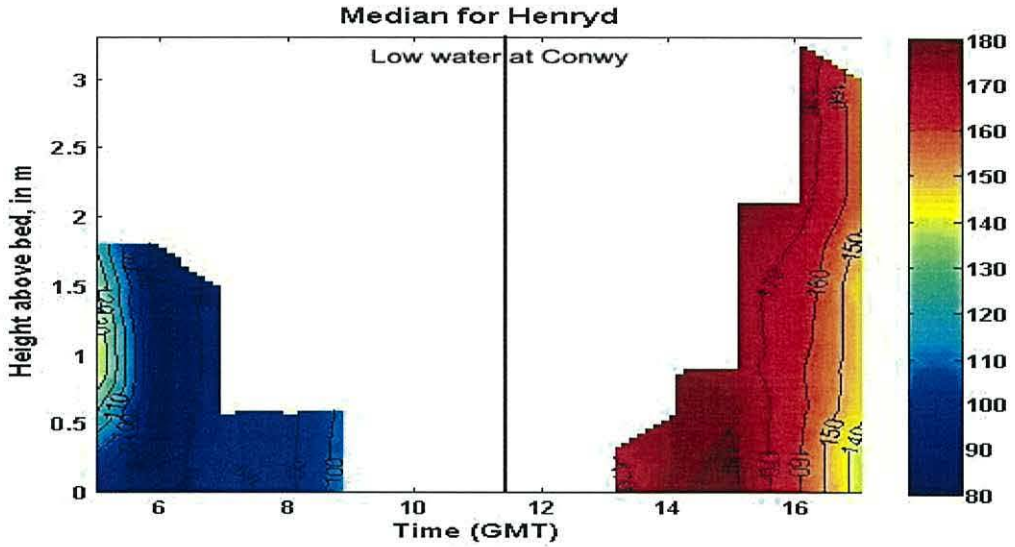

Figure 6.8: median diameter at Henryd.

Figure 6.8 shows the SPM median diameter, in μm. The median diameter of the suspended matter reached a maximum (~180 μm) in the bottom water about 3 hours after low water slack, corresponding to peak flood velocity (so resuspension of larger particles occurred). Median diameter was greater on the flood than on the ebb. The diameter reached a minimum (~80 μm) about 5 hours before low water.

6.2.3 Station MS5 (Glan-Conwy)

Station MS5 had a Q/T^3 ratio of 0.113.

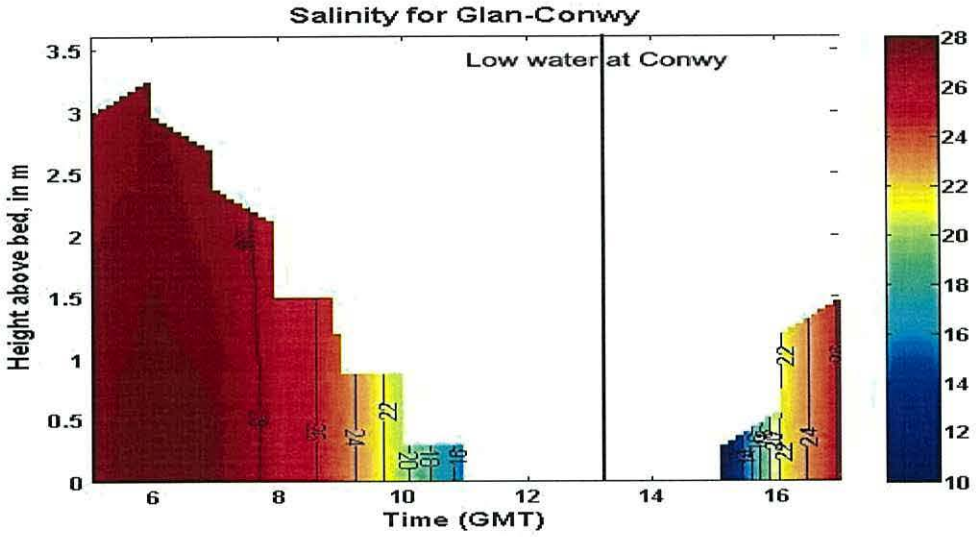

Figure 6.9: salinity at Glan-Conwy.

Figure 6.9 shows salinity, (low water at Conwy: 13:17 pm). The salinity reached a maximum around about high water slack, where the water column was mixed. The salinity reached a minimum about two hours after low water slack. Ebb duration exceeded the flood duration.

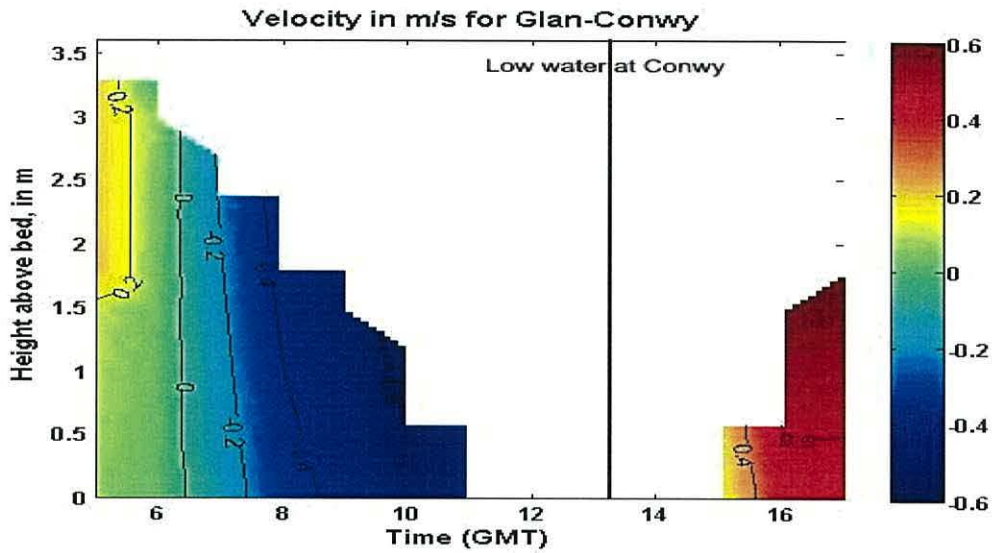

Figure 6.10: velocities at Glan-Conwy.

Figure 6.10 shows the velocities; in m/s. Ebb velocities peaked about 3½ hours before low water, whilst flood velocities mainly peaked about 3 hours after low water. Peak flood and ebb velocities were comparable.

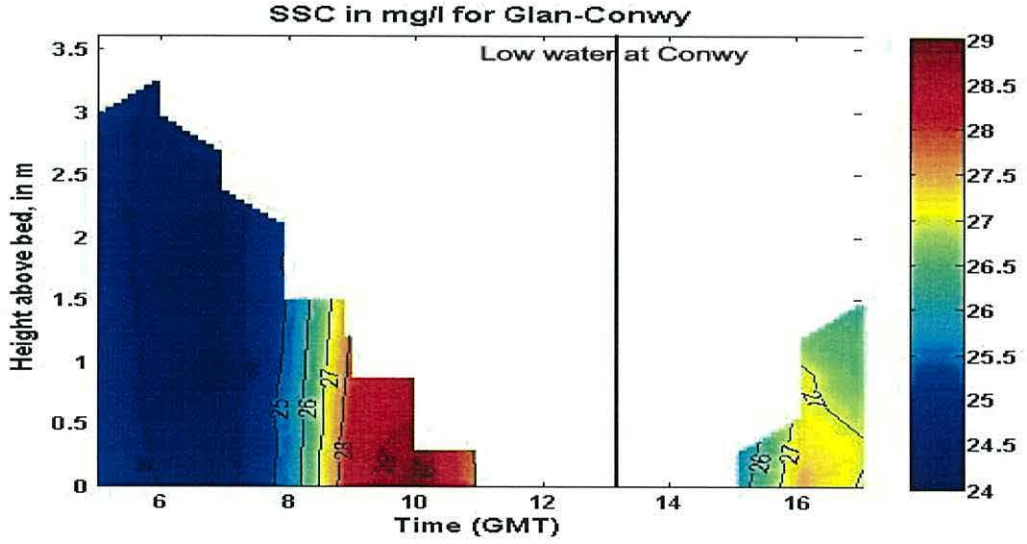

Figure 6.11: SSC at Glan-Conwy.

Figure 6.11 shows total SPM concentration, in mgl^{-1}, derived from the OBS. The SPM concentration reached its maximum about 3 hours and 20 minutes before low water slack (corresponding to peak ebb currents), whilst reaching its

minimum around high water slack. This time series therefore suggests resuspension on flood and ebb tides, with settling and sedimentation of particles around high water slack.

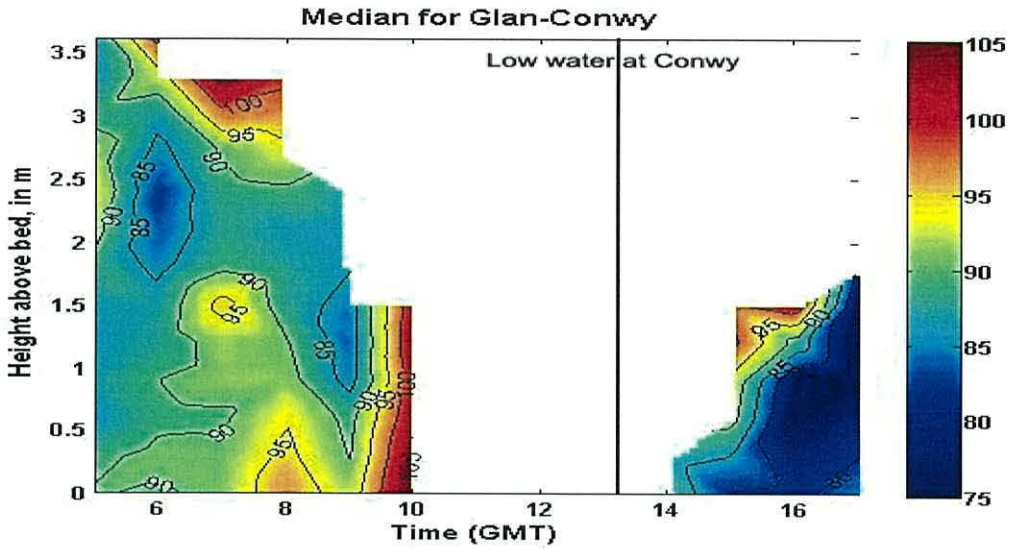

Figure 6.12: median diameter at Glan-Conwy.

Figure 6.12 shows the SPM median diameter, in μm. The median diameter of the suspended matter reached a maximum (~105 μm) in the surface water just after high water slack and about 3 hours before low water slack (corresponding to maximum ebb velocity). The diameter reached a minimum (~75 μm) about 3 hours after low water (at maximum flood velocity).

6.2.4 Station MS1 (Conwy)

Station MS4 had a Q/T^3 ratio of 0.382.

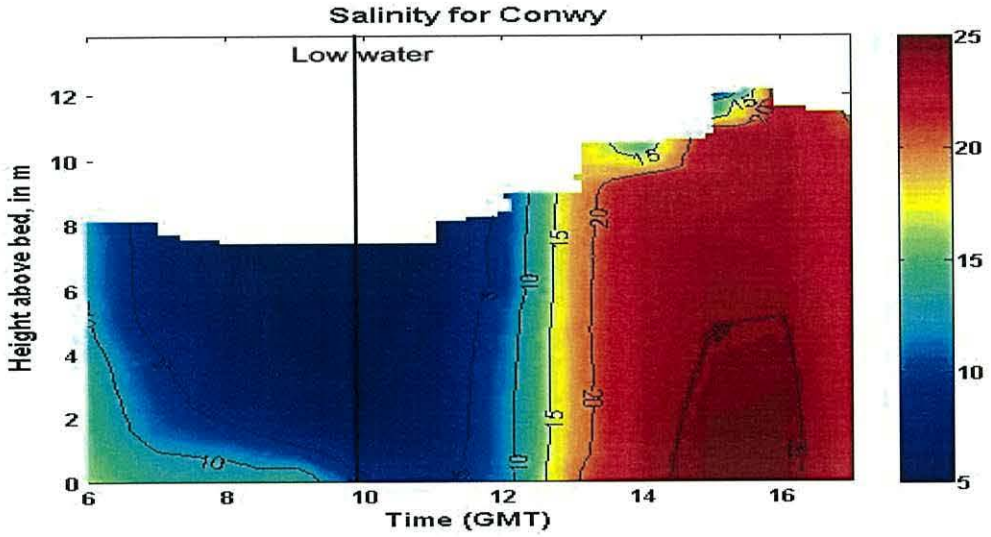

Figure 6.13: salinity at Conwy.

Figure 6.13 shows salinity, (low water at Conwy: 09:48 am). Salinity reached a maximum around about high water slack. The salinity reached a minimum around low water slack. It stratified at high water slack and during the ebb.

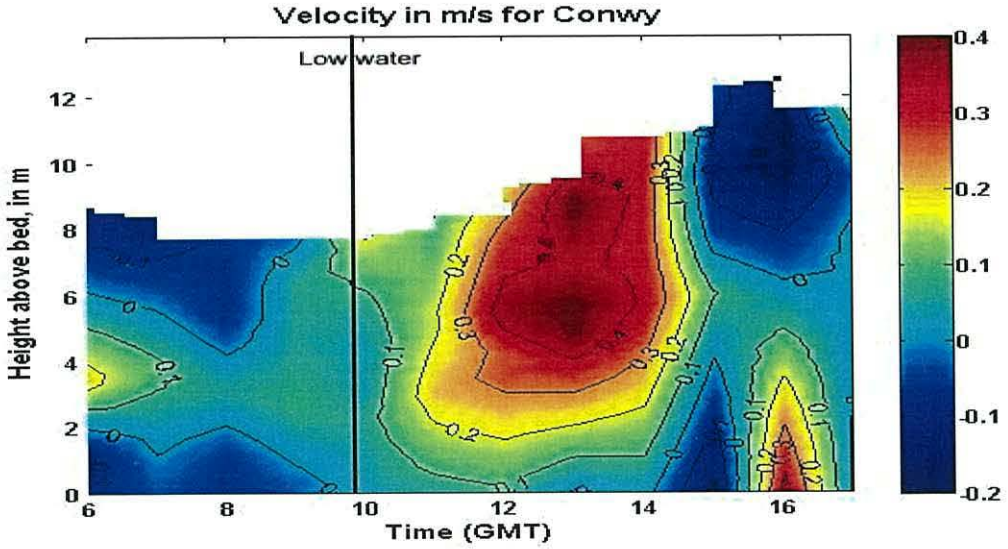

Figure 6.14: velocities at Conwy.

Figure 6.14 shows the velocities; in m/s. Ebb velocities peaked just after high water slack, whilst flood velocities mainly peaked about 3 hours after low water. Flood velocities exceeded ebb velocities.

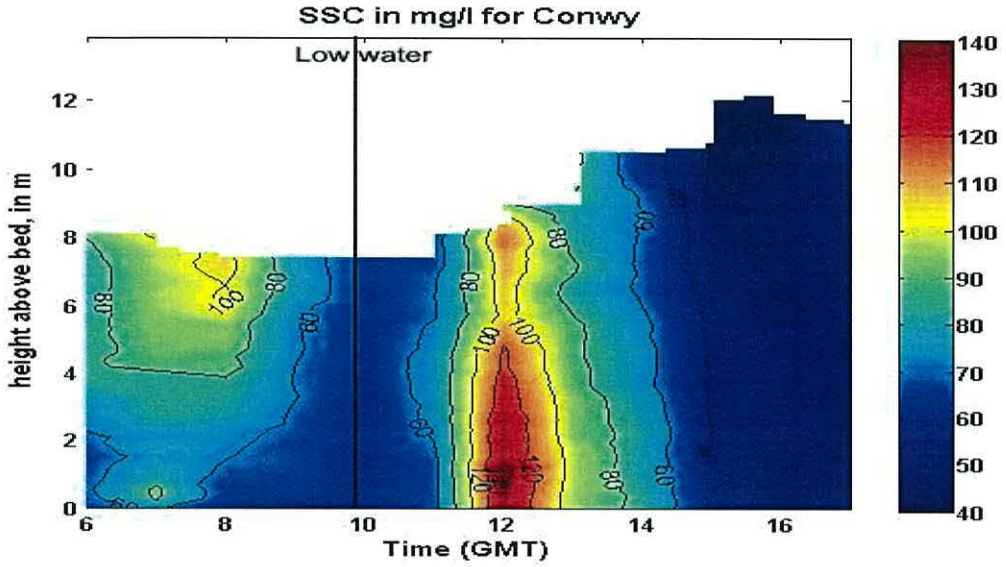

Figure 6.15: SSC at Conwy.

Figure 6.15 shows total SPM concentration, in mgl^{-1}, derived from the OBS. The SPM concentration reached its maximum about 2 hours after low water slack, as flood currents reached their maximum. Whilst reaching its minimum around high water slack, as particles settled to the bed.

Note that the minimum SSC was greater at this station, with a maximum SSC much greater than at other stations.

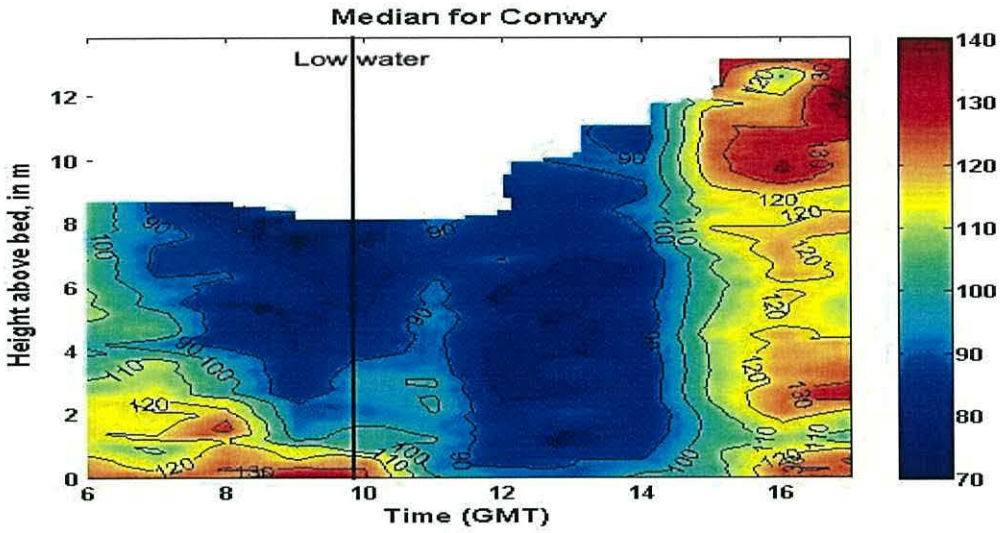

Figure 6.16: median diameter at Conwy.

Figure 6.16 shows the SPM median diameter, in μm. The median diameter of the suspended matter reached a maximum (~ 130 μm) about 6 hours after low water slack (i.e. around HW). This can be due to flocculation at a time of low turbulent shear. From about 08:00 am to 14:00 the grain diameter was predominantly within the range of about 70 to 90 μm, with large median present around high water and in bottom waters during the ebb. The larger particles present throughout the water column at high water persisted in the higher salinity bottom water throughout the ebb. The increased material at peak flood flow was made of smaller particles, suggesting either resuspension of smaller particles, or perhaps disaggregation of larger material.

6.2.5 Station MS2 (Tal-y-Cafn)

Station MS2 had a Q/T^3 ratio of 1.724.

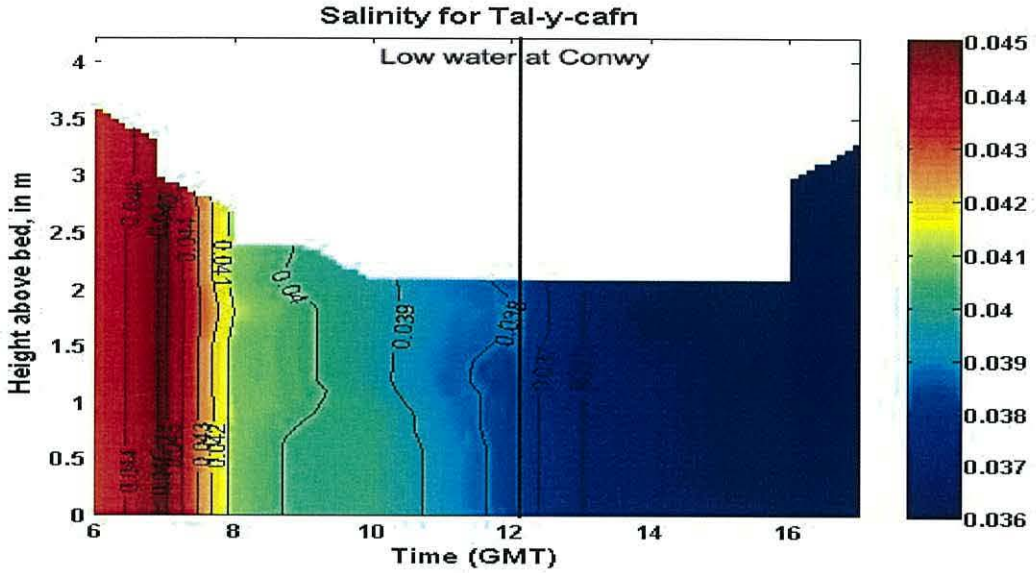

Figure 6.17: salinity at Tal-y-Cafn.

Figure 6.17 shows salinity, (low water at Conwy: 12:12 pm). The salinity reached a maximum around just after high water slack, where the water column was mixed. The salinity reached a minimum 3 hours after low water slack. However, salinities were low at all times since this station was effectively above the up-estuary penetration of salt (on this day, as salinities at Tal-y-Cafn may exceed 25, see section 5.1.2.4 for example).

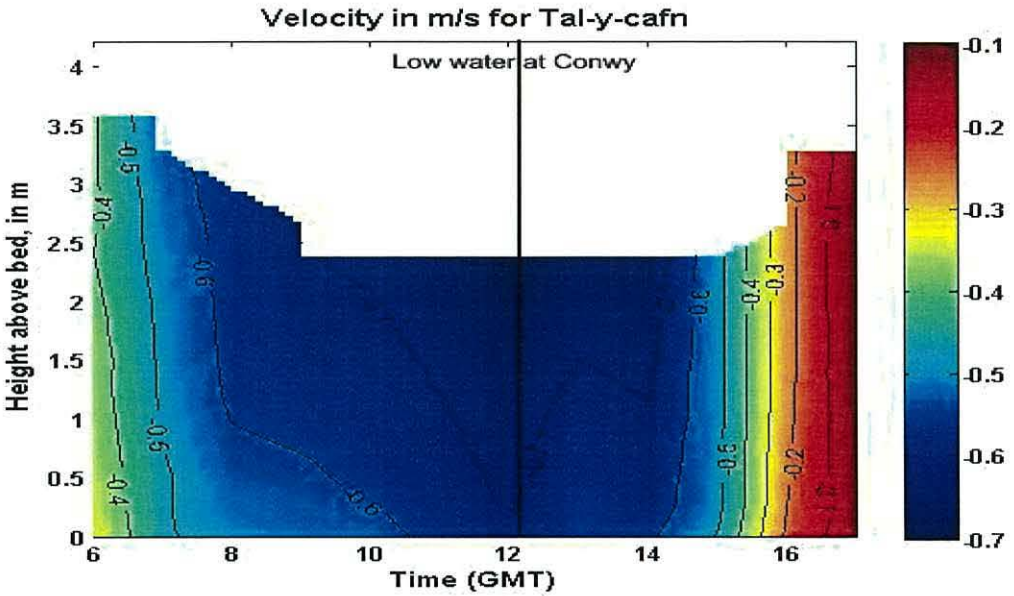

Figure 6.18: velocities at Tal-y-Cafn.

Figure 6.18 shows the velocities; in m/s. On this survey day the river was discharging a large amount of fresh water. This meant that all velocities were in a seaward direction. Velocities peaked at low water, whilst reaching a minimum 5 hours after low water, just before high water. So there was a significant tidal influence even though salinities did not vary much.

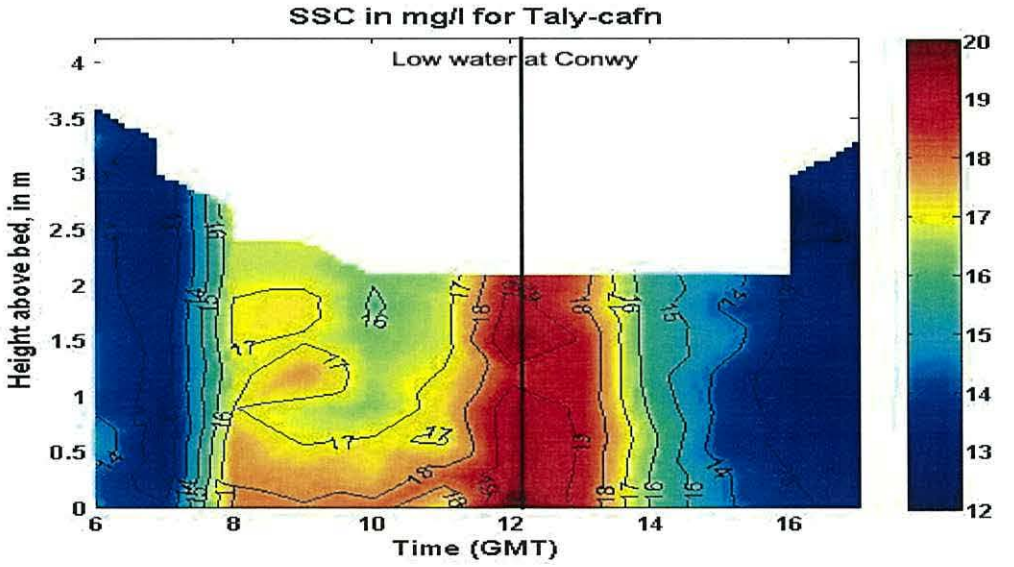

Figure 6.19: SSC at Tal-y-Cafn.

Figure 6.19 shows total SPM concentration, in mgl^{-1}, derived from the OBS. The SPM concentration reached its maximum around low water slack, whilst reaching its minimum about 5 hours before and after low water. Hence, SSC related directly to flow velocities (dominated by river flow).

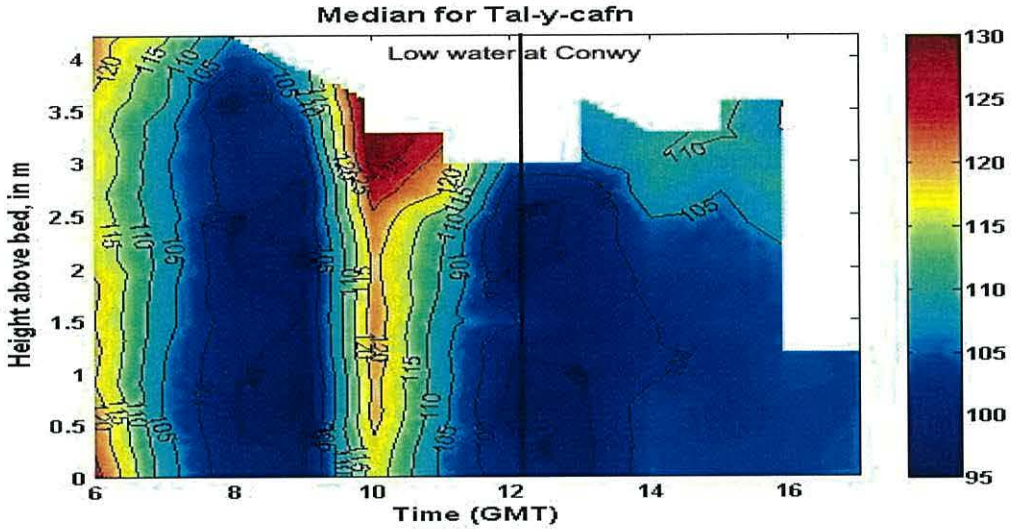

Figure 6.20: median diameter at Tal-y-Cafn.

Figure 6.20 shows the SPM median diameter, in μm. The median diameter of the suspended matter reaches a maximum (~130 μm) in the surface water about 1½ hours before low water slack. The diameter reaches a minimum (<95 μm) about 3 hours before and about 1 hour after low water. Median size appeared to be inversely related to SSC: higher SSC to relation to smaller size.

6.3 SPM Particle Analysis

6.3.1 SPM Particle Size Analysis

The suspended particulate matter within the water column throughout the duration of the moored surveys was comprised of three grain size ranges: "clays" < 3.9 μm; "silts" 3.9 – 62.5 μm; and "fine sands" 62.5 – 250 μm.

Each size range was present at different volume concentrations. By acquiring the volume concentration of each size range, and dividing it with the total volume concentration, the percentage of the total volume representing the size range was found (e.g. total volume concentration is made up of 3% clays, 37% silts and 60% sands).

This was done for all surface water readings, collected during the five moored surveys. Surface values were chosen, so that a comparison of the results and the effective density could be made. Figures 6.21, 6.22, 6.23, 6.24, and 6.25 present the calculated percentages of each size range.

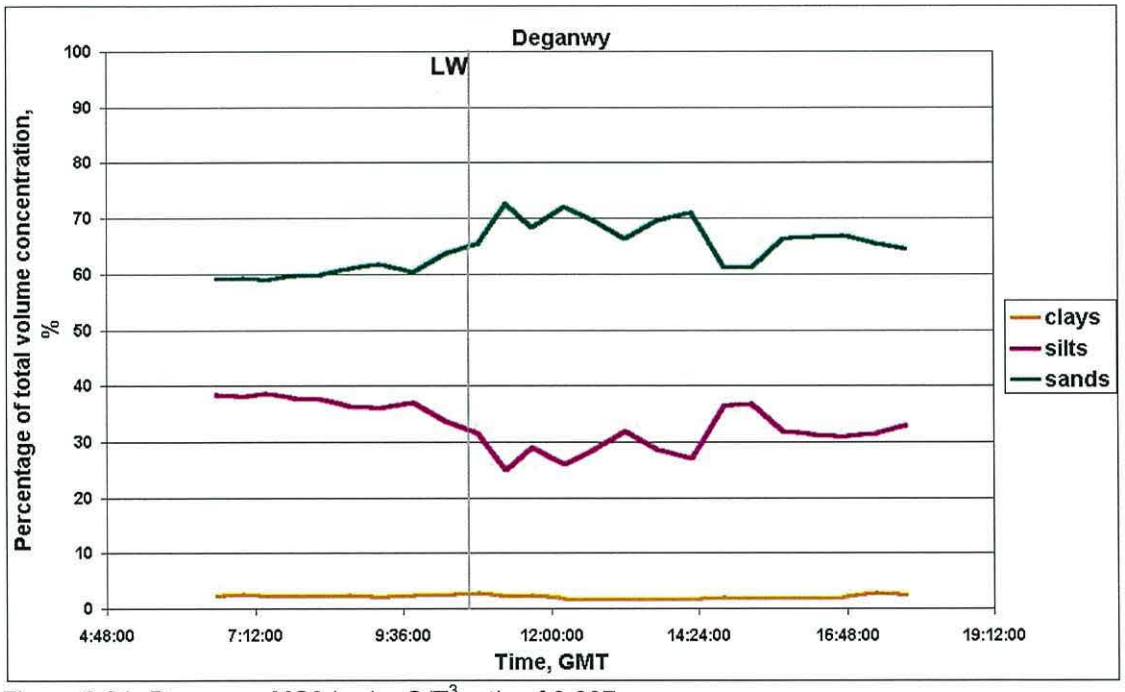

Figure 6.21: Deganwy, MS3 had a Q/T^3 ratio of 0.037.

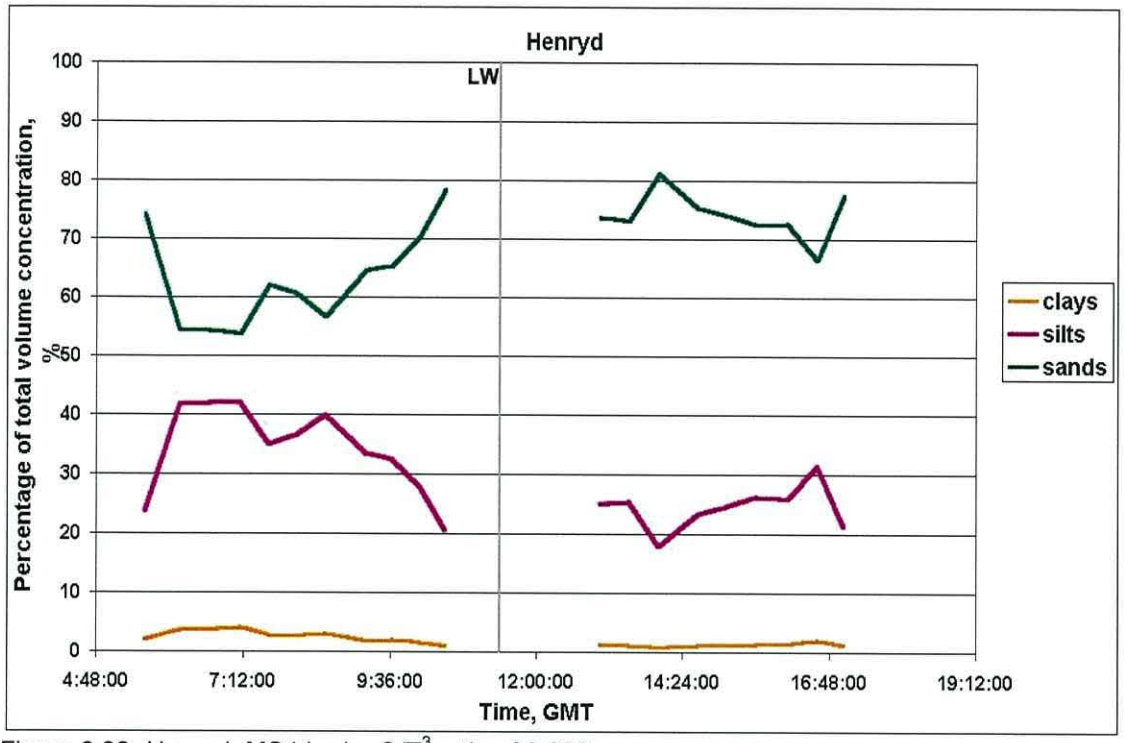

Figure 6.22: Henryd, MS4 had a Q/T^3 ratio of 0.038.

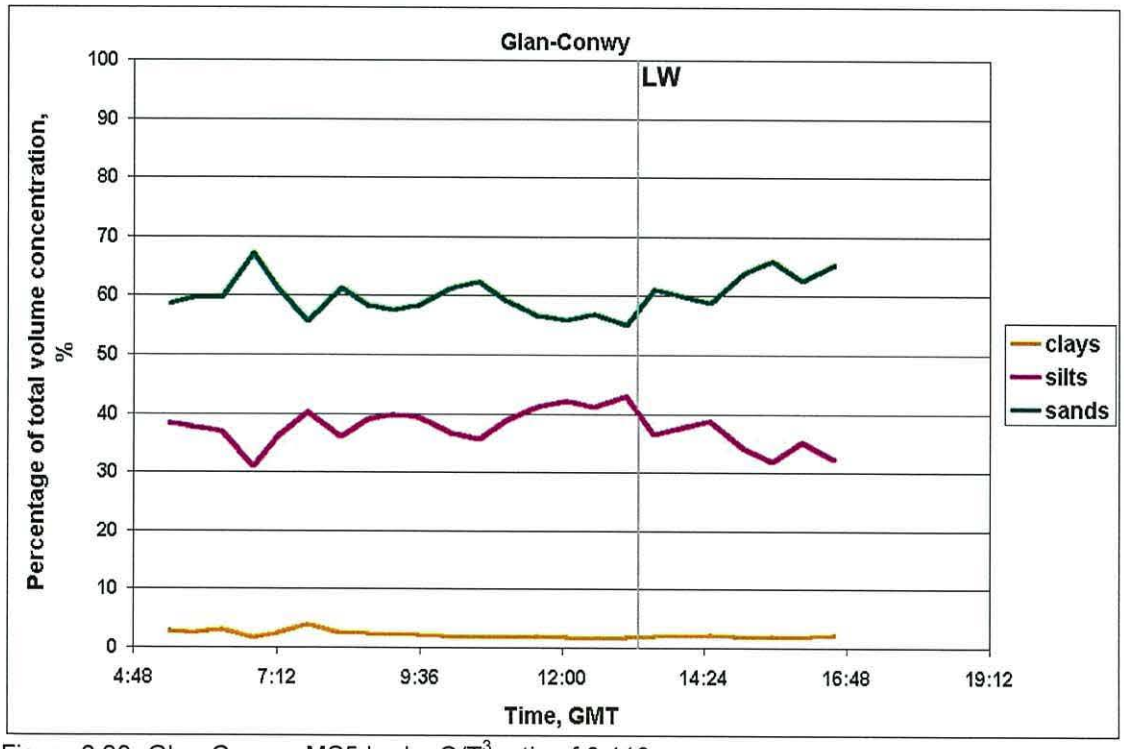

Figure 6.23: Glan-Conwy, MS5 had a Q/T^3 ratio of 0.113.

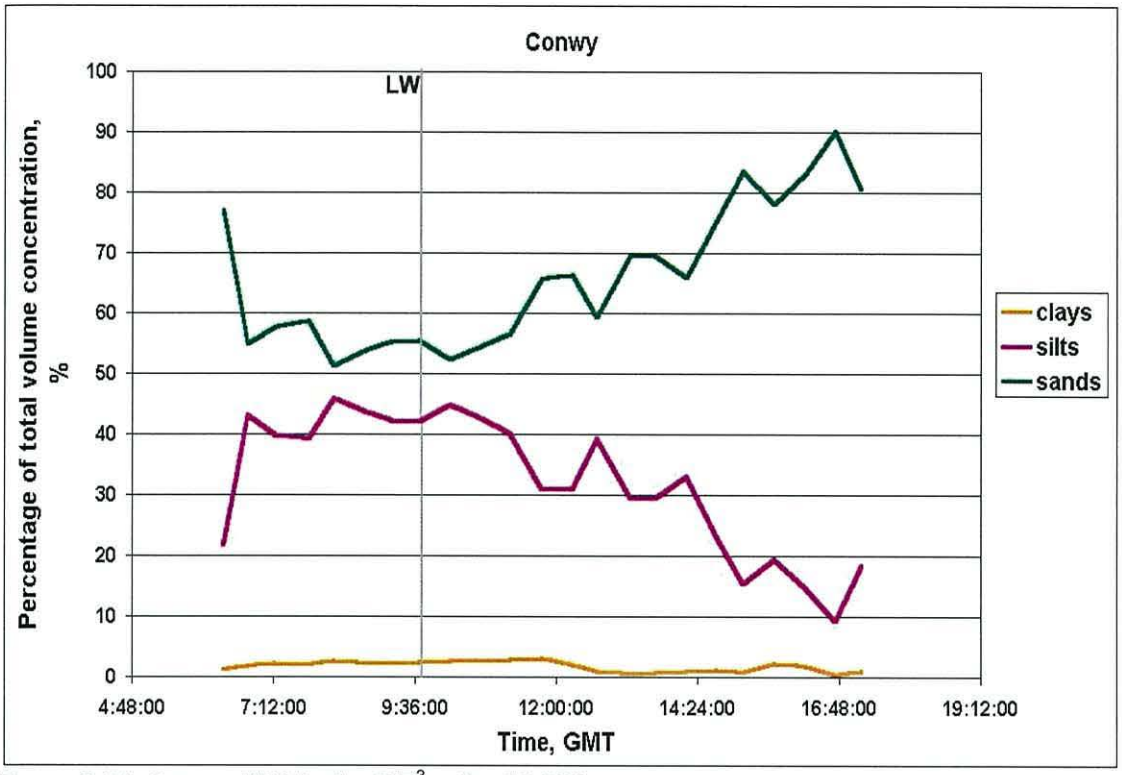

Figure 6.24: Conwy, MS1 had a Q/T^3 ratio of 0.382.

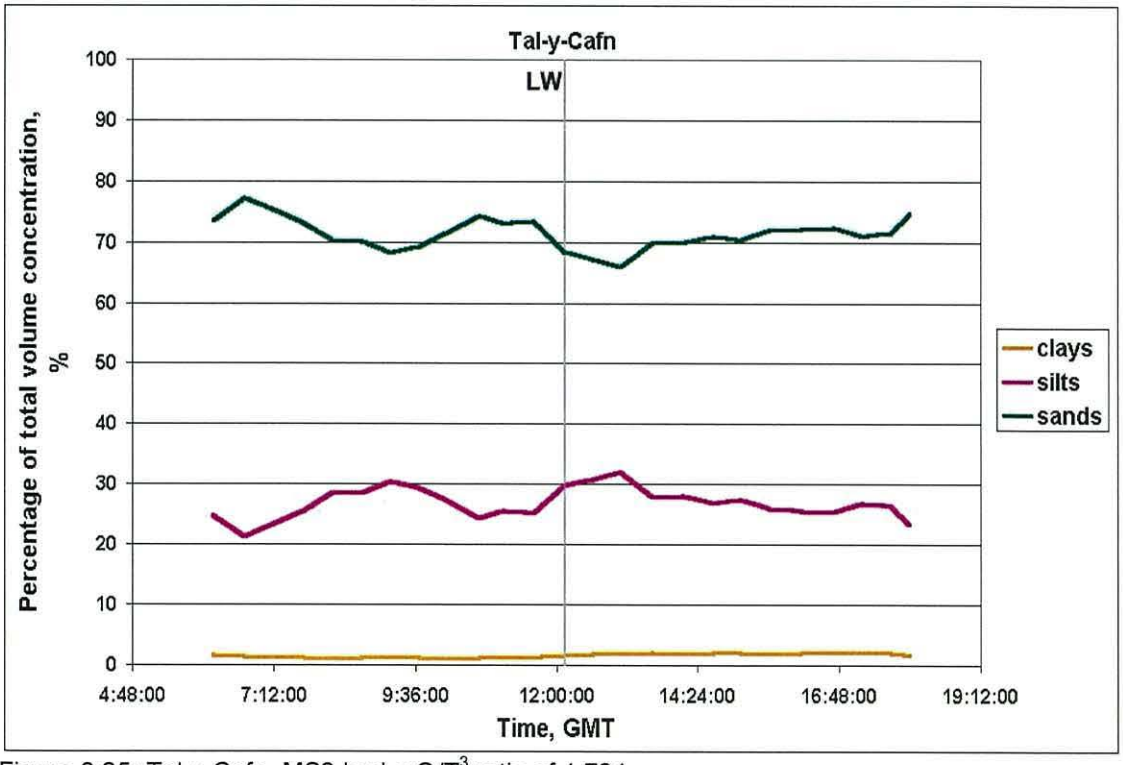

Figure 6.25: Tal-y-Cafn, MS2 had a Q/T^3 ratio of 1.724.

Figures 6.21 through to 6.25 indicate variations in the comparison between the three size fractions, see Table 6.3.

	Clay-sized	Silt-sized	Sand-sized
Deganwy, MS3	3%	32%	65%
Henryd, MS4	---	---	---
Glan-Conwy, MS5	2%	40%	58%
Conwy, MS5	2%	42%	56%
Tal-y-Cafn, MS2	2%	30%	68%

Table 6.3 presents the percentage of total volume concentration in each size fraction during the low water slack.

The percentage, of clay-sized particles remained constantly below 4%, with an average percentage of 2%. The percentage, of silt-sized particles was in the range between 9 – 46 %, with an average percentage of 31%. Finally, the percentage, of sand-sized particles was in the range between 51 – 91 %, with an average percentage of 67%.

6.3.2 Discussion and Conclusions

The suspended sediment, as seen in sections 5.2 and 6.3.1, is made up of three grain size ranges. Assuming that the spatial surveys were carried out at, or around, high water slack; the data could be compared to that from the moored surveys at high water.

By comparing the surface data from the five moored and thirteen spatial surveys, the following average percentages were found:

Distance from mouth	Clay-sized	Silt-sized	Sand-sized
0.90 km	1.88%	35.29%	62.83%
3.20 km	1.42%	24.93%	73.65%
5.35 km	1.57%	26.00%	72.43%
6.65 km	2.09%	26.17%	71.74%
10.00 km	2.59%	33.91%	63.56%

Considering the above, one would come to the conclusion that about two thirds of the SPM is fine sand-size. When comparing this to the effective densities an apparent contradiction occurs. The mean value (derived from all surveys) of effective density is 180 kgm^{-3}, which gives a particulate matter density (using ρ = 1013 kgm^{-3}) of 1193 kgm^{-3}, considerably less than the density of quartz. After careful re-examination of the data processing done in this project, the author concluded that there are two possible explanations for the contradiction: suspended organic matter influencing instrument readings; and the presence of flocs.

All water samples collected from the field were taken back to the lab for gravimetric analysis. After carrying out the procedure described in section 3.1.3.1.1, one more processing stage was conducted on the filters belonging to November 2004, June 2005, December 2005, and February 2006 surveys. This

additional stage, involved placing the filters into a furnace, at 500° C, for three hours. This was done to remove the organic component. Once the filters were removed from the furnace, they were re-weighed, to determine the amount of inorganic material. A mistake in the actual procedure made these readings inaccurate to use for calibrating the instruments. These readings, though, were accurate enough to produce an estimate of inorganic and organic component percentage of the total sample. The mean percentages were found to be: 98% of the total sample was inorganic, whilst the remaining 2% was organic.

With organic matter making up only 2% of the total sample on the filter, the effect of organics influencing the instrument readings is disregarded. This means that the most likely explanation for the low effective densities is that the sediment is forming flocs.

6.4 SPM density

6.4.1 Effective density

The effective densities (ED) of the surface suspended particulate matter were calculated for all moored surveys, by using Equation 5.1. In the following table (table 6.4) the values of SSC, VC and ED are presented for five different phases: HW_1 = first high water; LW_{-3h} = LW minus three hours; LW = low water; LW_{+3h} = low water plus three hours; and HW_2 = second high water. These phases were chosen in order to be able to make a comparison between stations. Please see Figures 6.26, 6.27, 6.28, 6.29, and 6.30 for plots of ED against time.

Station No	Phase	Time, GMT	SSC, mgl^{-1}	VC, µl/l	Median, µm	ED, kgm^{-3}	Velocity, ms^{-1}
MS1	HW_1	---	---	---	---	---	---
	LW_{-3h}	06:45	87.92	295.68	119	297.35	-0.5
	LW	09:39	51.64	350.07	142	147.51	-0.1
	LW_{+3h}	12:41	143.92	1277.61	73	112.65	0.3
	HW_2	15:41	12.88	123.92	120	103.94	0.1
MS2	HW_1	---	---	---	---	---	---
	LW_{-3h}	09:10	16.33	95.24	98	171.42	-0.6
	LW	12:07	17.07	95.08	142	179.49	-0.9
	LW_{+3h}	15:06	15.45	88.23	73	175.11	-0.7
	HW_2	17:58	12.22	80.21	106	152.33	-0.1
MS3	HW_1	---	---	---	---	---	---
	LW_{-3h}	07:22	26.40	98.96	105	266.78	-0.5
	LW	10:49	44.27	148.61	132	297.86	-0.1
	LW_{+3h}	13:12	23.10	179.64	142	128.59	0.7
	HW_2	17:16	18.63	77.23	154	241.27	0
MS4	HW_1	---	---	---	---	---	---
	LW_{-3h}	08:36	42.43	248.06	84	171.06	---
	LW	11:30	---	---	---	---	---
	LW_{+3h}	14:39	30.00	488.65	195	61.39	0.9
	HW_2	17:04	24.07	169.09	145	142.33	0.3
MS5	HW_1	06:50	22.10	130.75	95	169.03	-0.1
	LW_{-3h}	10:38	30.07	298.66	120	100.67	-0.6
	LW	13:33	22.50	208.30	80	108.02	---
	LW_{+3h}	16:36	24.00	223.64	80	107.32	0.8
	HW_2	---	---	---	---	---	---

Table 6.4: effective densities (ED) of all five anchor stations, at the five different phases.

Note: Times of high or low water correspond to that at Conwy on the day.

The average water density (kgm^{-3}) for each station was: MS1 = 1010; MS2 = 999; MS3 = 1022; MS4 = 1017; and MS5 = 1018. From the ED and the water density the floc bulk density (ρ_f) can be calculated. The ρ_f values were found to be in the range of 1078 to 1319 kgm^{-3}, which are too low to be individual quartz sand grains (density of 2650 kgm^{-3}).

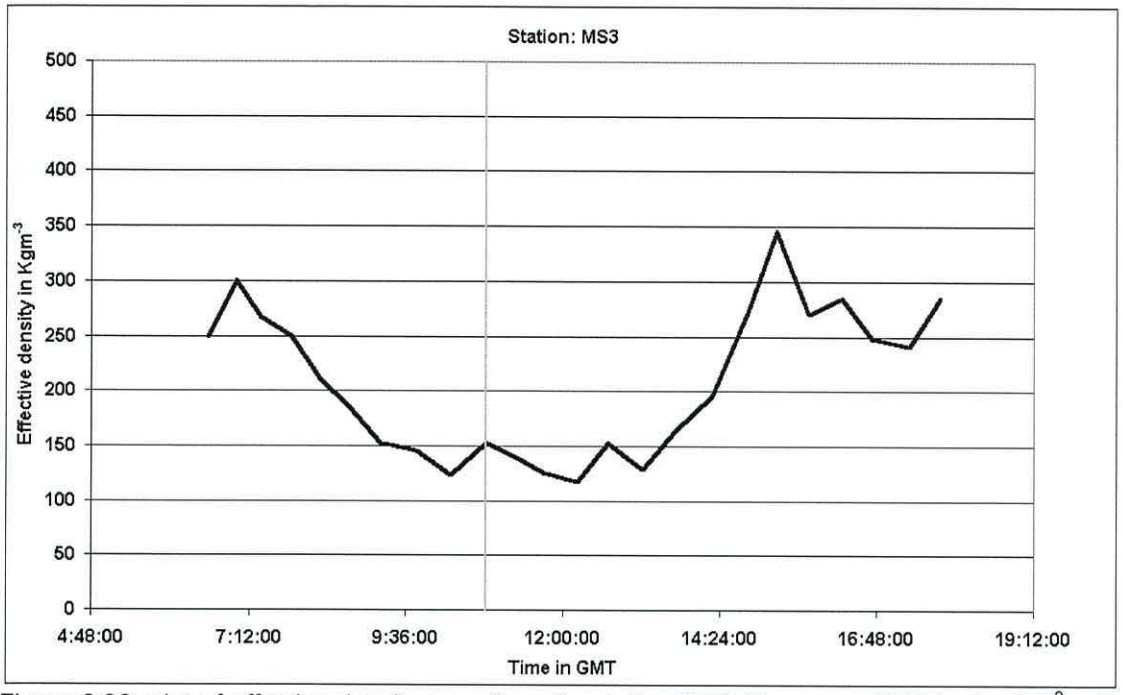

Figure 6.26: plot of effective density over time, for station MS3. Deganwy, MS3 had a Q/T^3 ratio of 0.037.

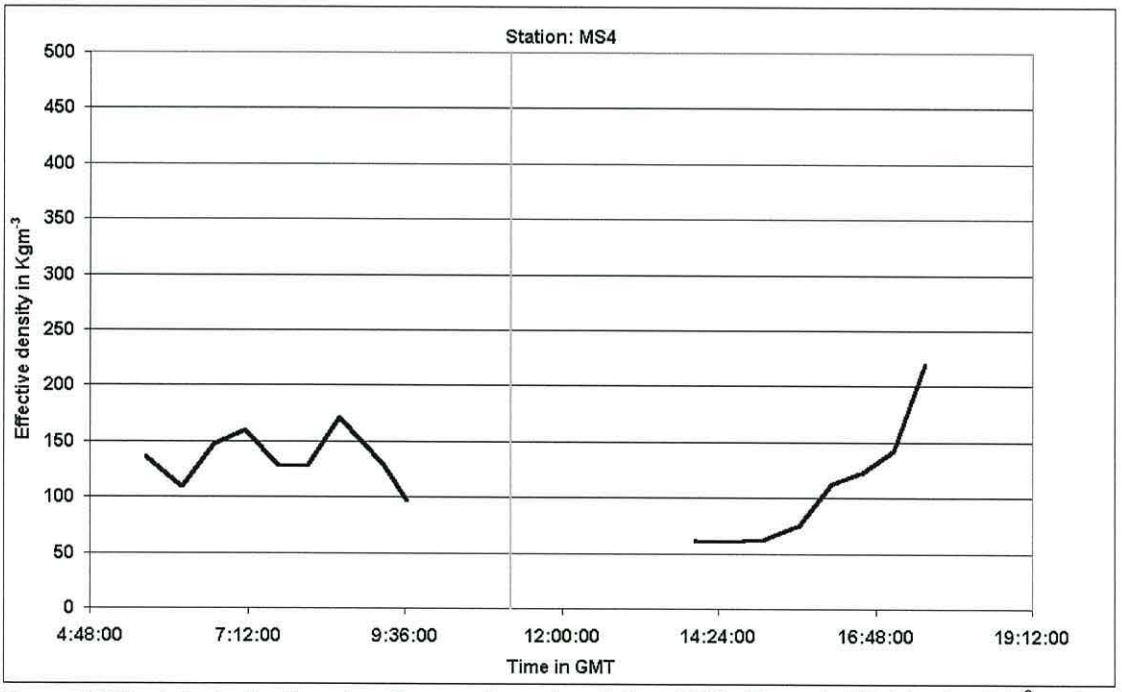

Figure 6.27: plot of effective density over time, for station MS4, Henryd. MS4 had a Q/T^3 ratio of 0.038.

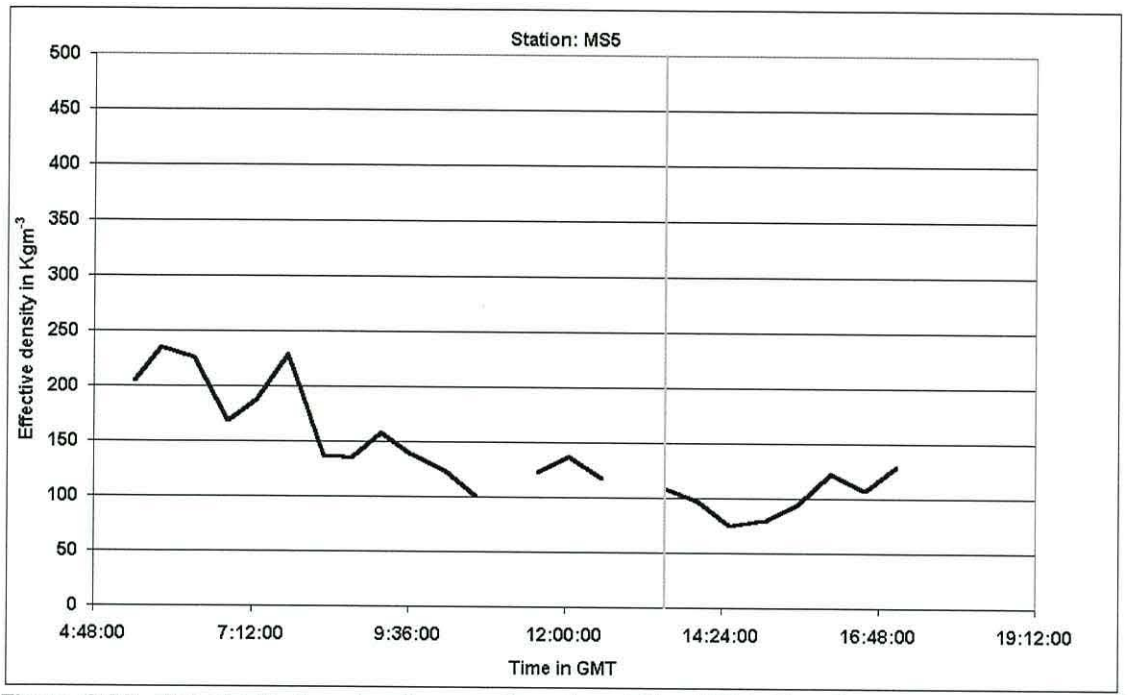

Figure 6.28: plot of effective density over time, for station MS5. Glan-Conwy, MS5 had a Q/T^3 ratio of 0.113.

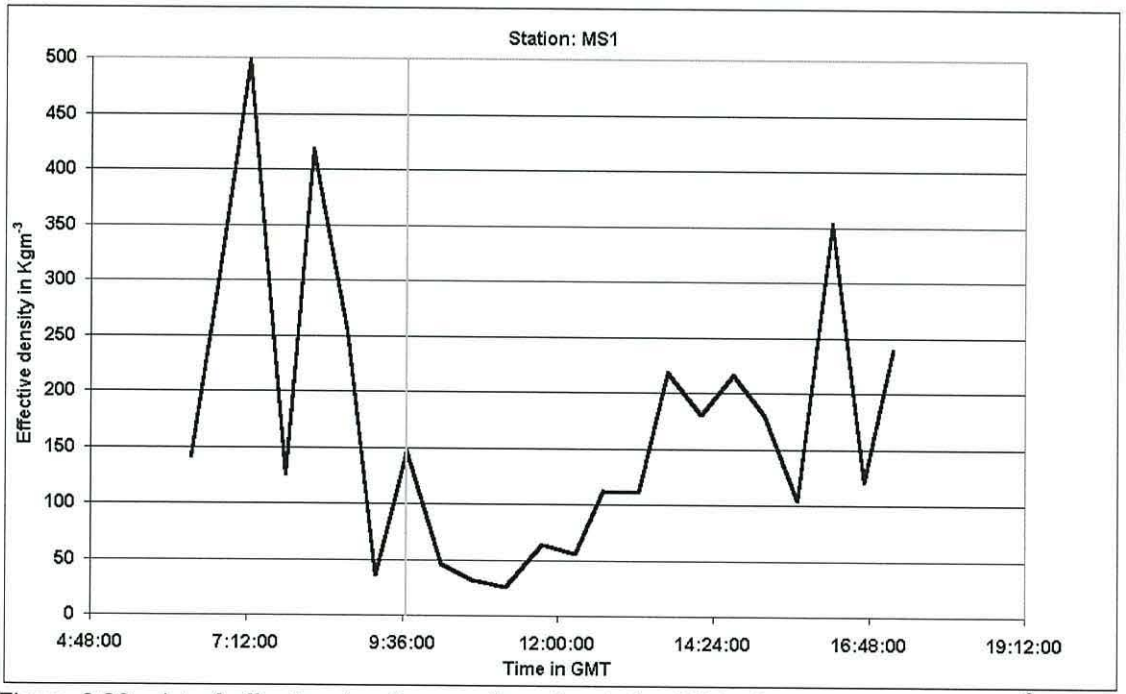

Figure 6.29: plot of effective density over time, for station MS1. Conwy, MS1 had a Q/T^3 ratio of 0.382.

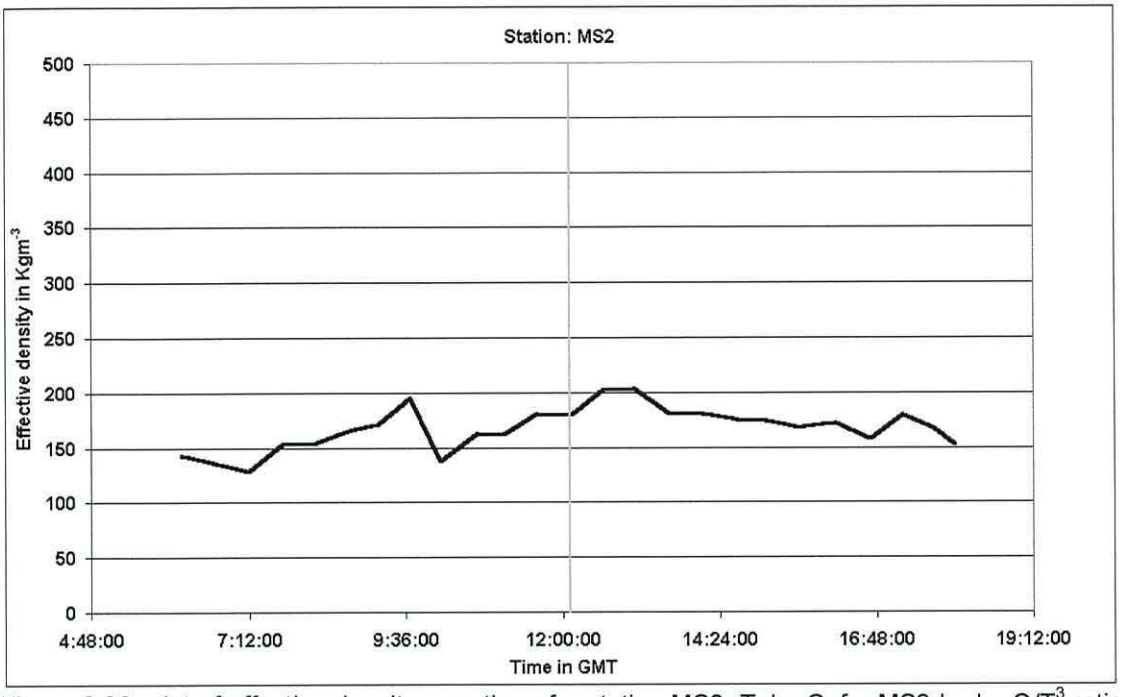

Figure 6.30: plot of effective density over time, for station MS2. Tal-y-Cafn, MS2 had a Q/T^3 ratio of 1.724.

6.4.2 Discussion and Conclusions

Figures 6.26 through to 6.30 indicate an overall trend of ED reaching a minimum around low water. At low water slack, the higher density particles have settled out of suspension. ED increases on the flood and the ebb due to resuspension.

From section 6.2 an overall trend in surface median SPM particle diameter can be seen. The median diameter decreases at or around low water, and increases during flood and ebb.

The two observed general trends complement each other. At low water slack the smaller denser particles settle out of suspension, but when the currents increase during the flood and ebb, the particles tend to increase in size and decrease in density. This could be due to resuspension.

Ishak (1997) showed that flocs have a size limit above which they cannot grow further, but instead they start falling apart. The LISST-100b is limited to a particle size of 250 microns, so if there was anything bigger than this, it has gone unrecorded.

6.4.2.1 Tidal Cycle

In this section an attempt is made to describe a typical tidal cycle. In order to do this, the values for each of the 5 phases (Table 6.7) were averaged over the five stations, so to produce an average value for each property at each phase, for the first 10km of the estuary (see Table 6.5 below).

PHASE	Salinity	SSC, mgl^{-1}	VC, µl/l	ED, kgm^{-3}	Median, µm
LW-3h	15	40	207	200	105
LW	9	34	201	184	114
LW+3h	14	47	452	118	117
HW	18	19	119	170	124

PHASE	Velocity, ms^{-1}	% sand-sized fraction	% silt-sized fraction	% clay-sized fraction
LW-3h	-0.6	60.4	37.4	2.2
LW	-0.4	63.7	34.4	2.0
LW+3h	0.4	71.1	27.0	1.9
HW	0.0	72.8	25.4	1.8

Table 6.5: section averaged surface values.

With the exception of MS5, no measurements were made on the first high water, so our tidal cycle (on a neap tide) starts on the ebb tide 3 hours before low water.

Three hours before low water the combined ebb and river flow is in a down-estuary direction with a surface mean of 0.6 ms^{-1}. The salinity and the SSC is decreasing as a result of the combined flow. During this phase (LW_{-3h}), the percentage of clay-sized fraction is at its maximum (2.2 % indicative of riverine load), whilst the SPM median diameter is at its minimum (105 µm), possibly because of increased turbulence.

At low water the salinity reaches its minimum (9), the SSC has decreased to 34 mgl^{-1}. The tide flow is at a slack, but the water is still flowing down-estuary at about 0.4 ms^{-1}(at the surface), as a result of the river flow. The decreased velocities allow the formation of flocs and partial sedimentation of suspended mater. As a result there is an increase in SPM median diameter, and in the percentage of sand-sized fraction.

Three hours after low water (flood tide) the surface flow is now in the up-estuary direction (0.4 ms^{-1}). The SSC has now reached its maximum (section average surface value of 47mgl^{-1}). The effective density has reached its minimum, whilst the median particle diameter has slightly increased. The percentage of sand-sized fraction has also increased. The increase in particle size and decreased ED could be due to flocculation.

As seen in section 5.4.4.2, the influence of benthic organisms is great when it comes to increased concentration and flocculation. According to Lawrence et al. (2005), EPS represents a major structural component of flocs. Specifically, organic material on the particles, such as mucal films caused by bacterial activity and organics absorbed from suspension, have positive charges and significantly enhance flocculation (Dyer, 1986).

Being a neap tide (low water occurring in morning to mid-day) the intertidal sediments are exposed to higher light levels. During this exposure biological activity is taking place. When the flood tide covers the previously exposed sediments, loose biological matter will be entrained into suspension.

At high water slack the section mean surface velocity approaches zero. The salinity (18), median diameter (124 μm) and percentage of sand-sized fraction (72.8 %) have all reached their maximum. On the other hand, the SSC (19 mgl^{-1}),

and the percentages of silt and clay sized particles (25.4 % and 1.8 % respectively) have reached their minimum.

At slack water the turbulence reaches a minimum (if wind activity in not significant) allowing the formation of bigger flocs.

6.4.2.2 High Water Values Compared to Spatial Survey Values

Assuming that the spatial surveys were carried out at, or around, high water slack; the data could be compared to that from the moored surveys at high water.

	Spatial surveys, lower estuary	Moored surveys, excluding MS2	Moored surveys, including MS2
Salinity	26	23	18
Mass conc., mgl^{-1}	24	21	20
Vol. conc. μll^{-1}	179	128	122
Median, μm	124	129	124
Effective. Dens., kgm^{-3}	154	175	169
% of sand-sized fraction	72	72	73
% of silt-sized fraction	26	26	25
% of clay-sized fraction	2	2	2

Table 6.6: comparing results from the spatial survey to those from the moored surveys.

On previous days and on the day of survey MS2 (which was 10 km from the mouth), the river discharge was at an extreme high. For this reason Table 6.6, has two columns for the moored surveys. Overall there is good agreement between the surveys, even though the spatial surveys were carried out on spring tides and the moored ones on neap tides. This suggests that at high water there is little difference between neap and spring tides (considering average values).

6.5 SPM Flux

The water column on each cast was split into depth bins of 30 cm. The SPM flux ($kgm^{-2}s^{-1}$) for each bin was calculated by multiplying the SSC (mgl^{-1}) of that bin with the corresponding current velocity (ms^{-1}). By assuming unit width, the units of flux can be written as $kgm^{-1}s^{-1}$.

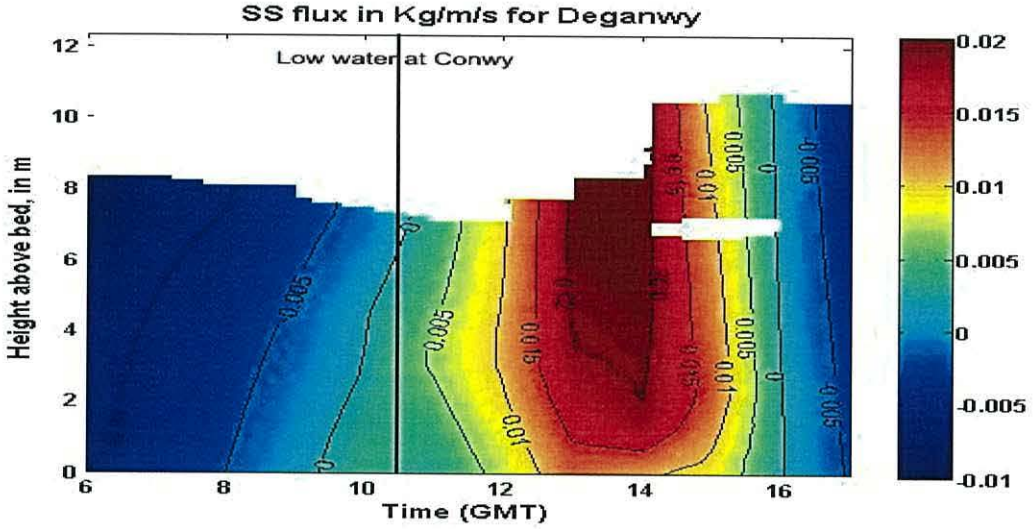

Figure 6.31: SPM flux at Deganwy

Figure 6.31 shows the SPM fluxes per unit width; in $kgm^{-1}s^{-1}$. Negative values are seaward fluxes, whilst positive values are landward fluxes. Ebb SPM fluxes peaked about 3½ hours before low water, whilst flood fluxes mainly peaked about 3 hours after low water, i.e. at peak flows. Flood flux exceeded ebb flux.

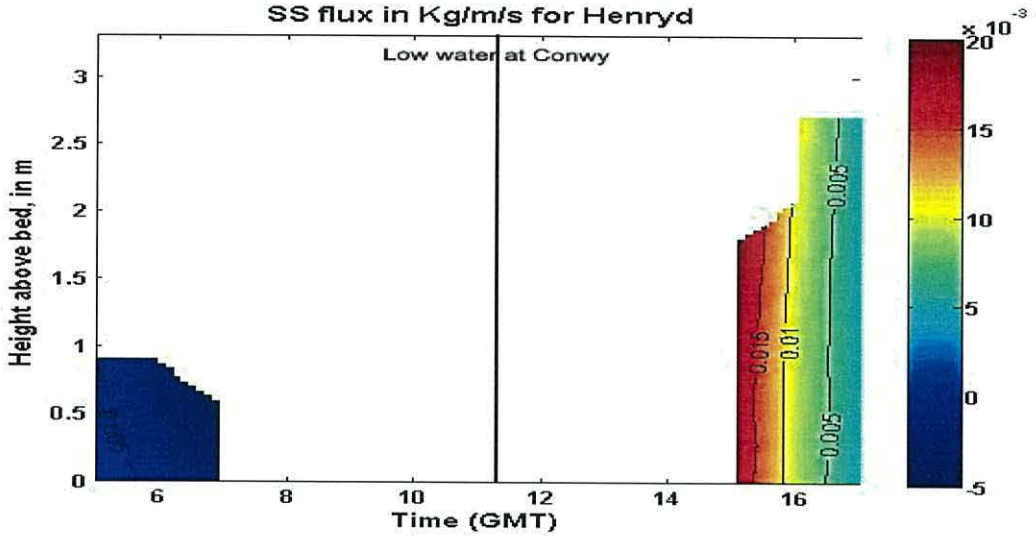

Figure 6.32: SPM flux at Henryd

Figure 6.32 shows the SPM fluxes per unit width; in $kgm^{-1}s^{-1}$. Ebb SPM fluxes peaked about 5 hours before low water, whilst flood fluxes mainly peaked about 4 hours after low water; presumably at peak flows.

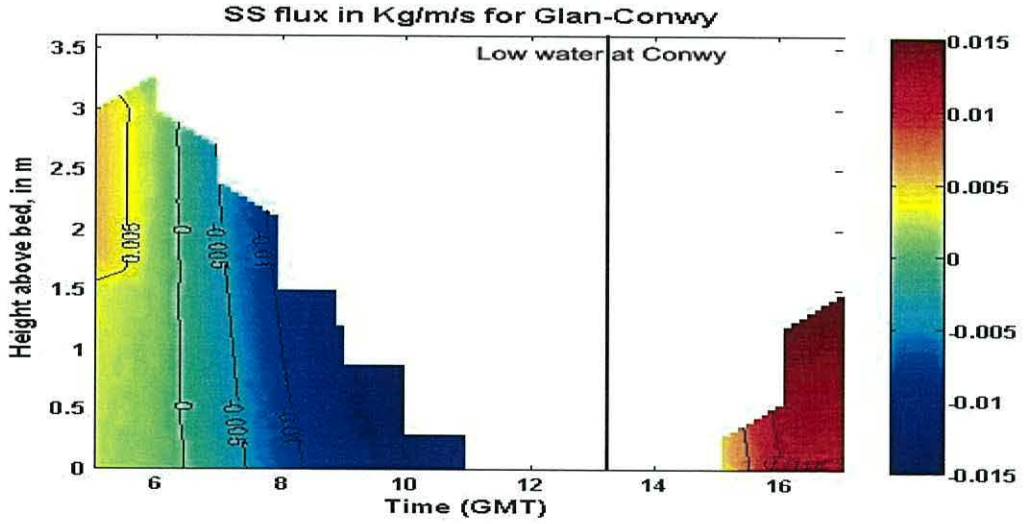

Figure 6.33: SPM flux at Glan-Conwy

Figure 6.33 shows the SPM fluxes per unit width; in $kgm^{-1}s^{-1}$. Ebb SPM fluxes peaked about 3½ hours before low water, whilst flood fluxes mainly peaked about 3 hours after low water, i.e. at peak flows.

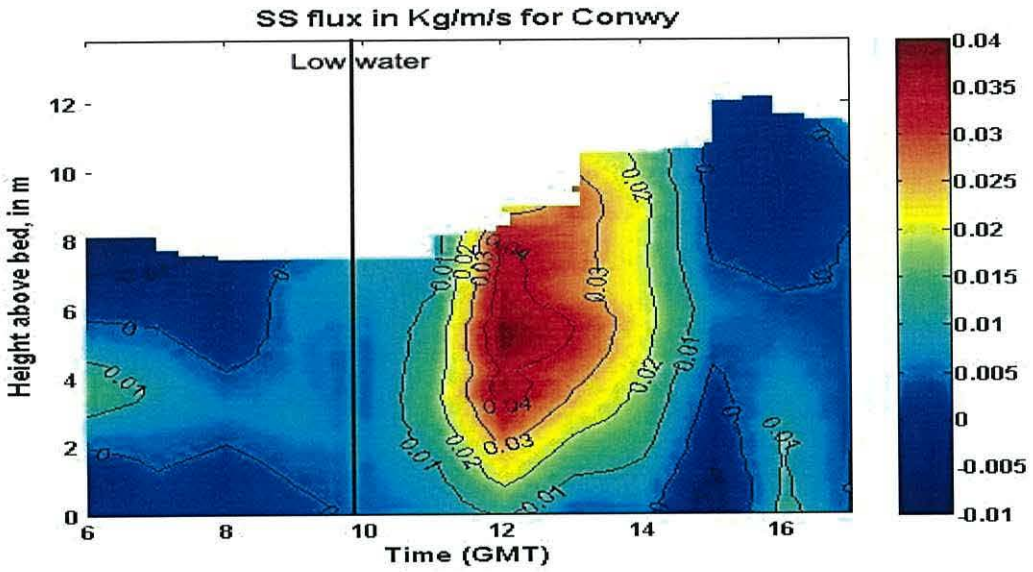

Figure 6.34: SPM flux at Conwy

Figure 6.34 shows the SPM fluxes per unit width; in $kgm^{-1}s^{-1}$. Ebb SPM fluxes peaked in the surface about 4 hours before low water, and near the bed about 5 hours after low water. Flood fluxes mainly peaked about 2 hours after low water, at about peak flow.

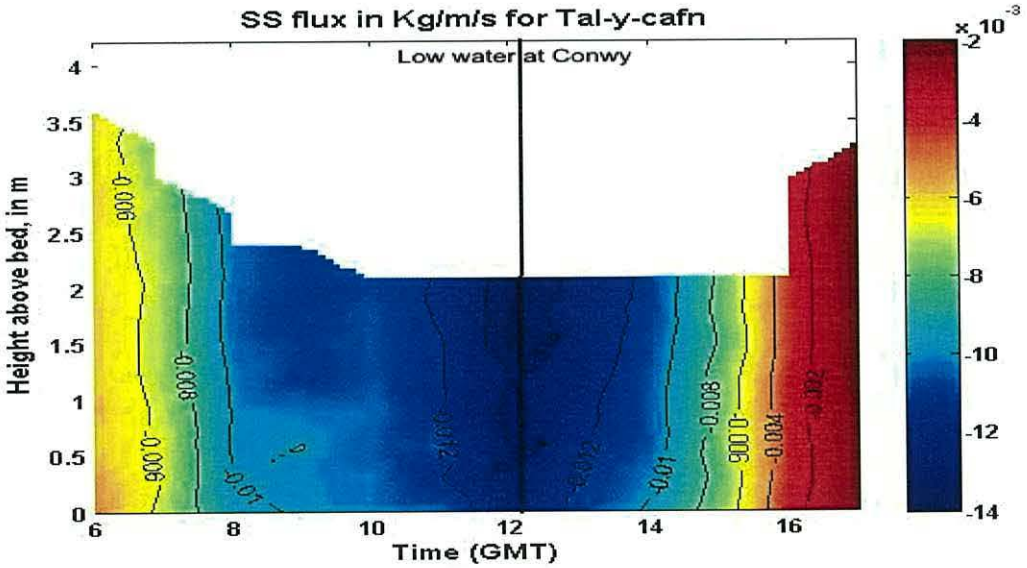

Figure 6.35: SPM flux at Tal-y-Cafn

Figure 6.35 shows the SPM fluxes; in $kgm^{-1}s^{-1}$. As with the velocities, all fluxes have negative values indicating an overall down-estuary flux. SPM fluxes peak around low water, whilst reaching a minimum around high water.

6.5.1 Comparison of Total Flood Flux to Total Ebb Flux

From the data presented in Figures 6.31 through to 6.35, the total flood and ebb fluxes were found. The fluxes are presented in Table 6.10, with ebb fluxes being in a down-estuary direction and the flood fluxes in an up-estuary direction.

	$kgm^{-1}Flood^{-1}$	$kgm^{-1}Ebb^{-1}$
Deganwy, MS3	4.23	-2.76
Henryd, MS4	0.55	-0.26
Glan-Conwy, MS5	0.54	-0.65
Conwy, MS1	6.13	-0.15
Tal-y-Cafn, MS2	-0.69	-1.23
Total flux	10.76	-5.05

Table 6.7: comparing results from the spatial survey to those from the moored surveys.

The total flux was produced by first depth integrating the flux values over the tidal cycle for each station. Once that was done, the flux values were integrated over the flood and ebb tides, producing two values for each station. The total (cumulative) flood flux and total (cumulative) ebb flux are simply the sum of all flood values and the sum of all ebb values, respectively.

The total cumulative flood flux, at all 5 anchor stations, (10.76 $kgm^{-1}Flood^{-1}$, up-estuary) was twice the total cumulative ebb flux (5.05 $kgm^{-1}Ebb^{-1}$, down-estuary). This meant that the net suspended sediment flux (5.71 kgm^{-1} per tidal cycle) measured at the 5 stations, was in the up-estuary direction.

7 SEDIMENT TRANSPORT RATES

7.1 Introduction

In chapter one (section 1.4.1) the objectives, of the project, were stated. The purpose of this chapter is:

- To identify the thresholds of motion and suspension for the estuarine sands.

- To determine the net bedload and suspended load transport directions and rates, over a tidal cycle at specified locations.

In order to do so, the sediment transport rates at the five anchor stations were investigated. The sediment transport rate, $kgm^{-1}s^{-1}$ (or $m^3m^{-1}s^{-1}$), is defined as the mass (or volume) of sediment per unit time, passing through a vertical plane of unit width perpendicular to the flow direction (Soulsby, 1997).

In a shallow estuary, like the Conwy, there are four basic sedimentary agents: flood and ebb tides; river flow; waves; and wind during low water. Due to logistics, no wave or wind data were collected. Waves from offshore cannot progress very far into the estuary because of its restricted mouth; local waves have limited fetch. Much of the intertidal sand flats remain wet for most of the tidal cycle, thus limiting the potential for wind-driven sand transport. For this reason, it was assumed that transport due to wave or wind action, was not significant in comparison with transport due to tides.

Also, for simplicity it was assumed that:

I. The bed sediment was made up of quartz and/or feldspar sand (density of 2650 kgm^{-3}).

II. The only friction exerted on the bed was that due to water currents.

III. The kinematic viscosity, ν, and the density of water were the same for all five stations (using average values of $\nu = 1.15*10^{-6}$ m^2s^{-1}, and $\rho = 1013$ kgm^{-3}).

7.2 Thresholds of Motion and Suspension

This section is divided into three main parts: threshold of motion; threshold of suspension; and discussion/conclusions. The first part is further divided into two: threshold current speed; and threshold bed shear-stress.

7.2.1 Threshold of Motion

7.2.1.1 Threshold Current Speed

Sand grains are set in motion, when the depth-averaged current speed, $\overline{U}$, exceeds the threshold (or critical) depth-averaged current speed, $\overline{U_{cr}}$. So the first step in calculating the bedload transport rate was to determine if the sand grains on the bed were set in motion. To do this, the threshold depth-averaged current speed was calculated and compared to the measured depth-averaged current speed.

For a steady current, the $\overline{U_{cr}}$ required to move a grain of diameter *d* on a flat bed horizontal, un-rippled bed in water of depth h can be predicted by using Soulsby's, (1997), equation:

$$\overline{U_{cr}} = 7(h/d_{50})^{1/7}[g(s-1)d_{50}f(D_*)^{1/2}] \qquad [7.1]$$

with

$f(D_*) = [0.30/(1+1.2D_*)]+0.055[1-\exp(-0.020\ D_*)]$

$D_* = [g(s-1)/\nu^2]^{1/3}\ d_{50}$

where:

h is the total water depth, metres; d_{50} is the median grain diameter, in metres; g is the acceleration due to gravity, 9.81 ms^{-2}; s is the ratio of densities of grain and water (ρ_s/ρ); and D_* is the dimensionless grain size.

Equation 7.1 is valid for any non-cohesive sediment and water conditions for which $D_* > 0.1$, and valid in any units.

Figure 7.1, shows the threshold depth-averaged speed of a range of grain sizes for four different water depths: h = 10 m; h = 5 m; h = 3 m; and h = 1m.

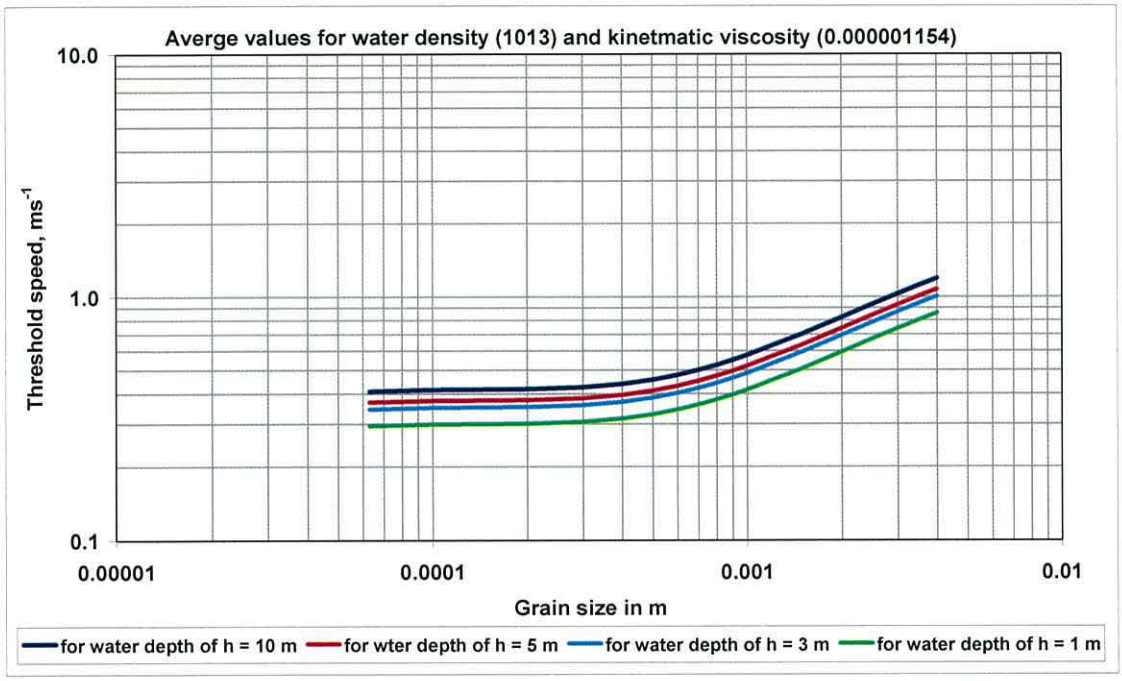

Figure 7.1: the threshold depth-averaged speed of a range of grain sizes for four different water depths: h = 10 m; h = 5 m; h = 3 m; and h = 1m.

Figure 7.2, shows the threshold depth-averaged speed of a range of water depths for the two predominant grain sizes: d = 0.23 mm; and d = 1.5 mm.

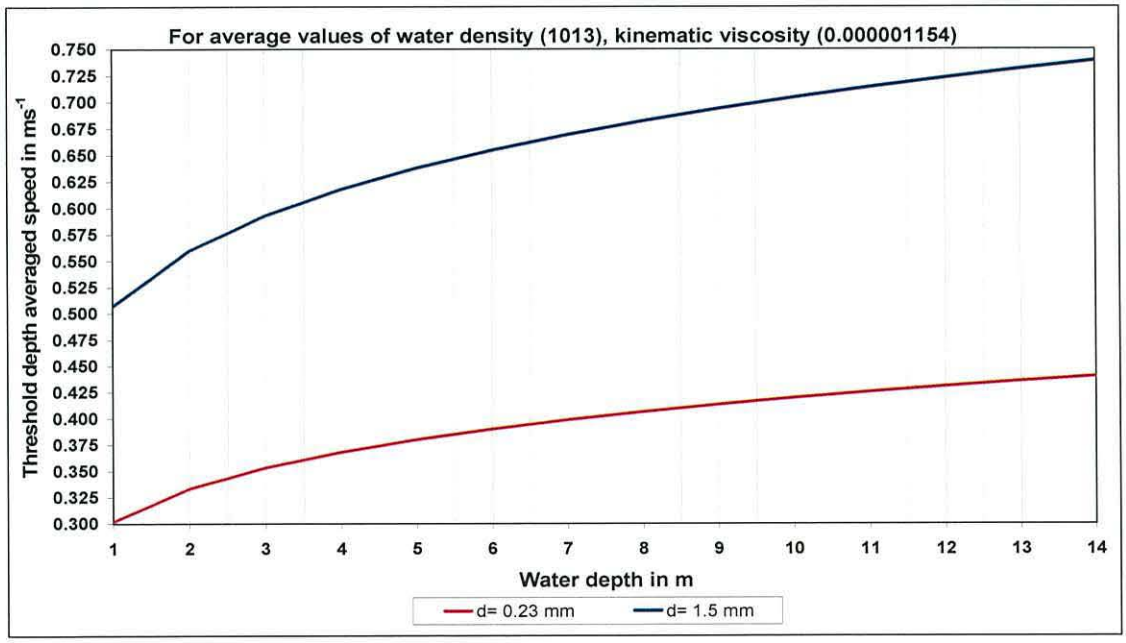

Figure 7.2: the threshold depth-averaged speed of a range of water depths for the two predominant grain sizes: d = 0.23 mm; and d = 1.5 mm.

In Figures 7.3 (lowest flow ratio), 7.4, 7.5, 7.6, and 7.7 (highest flow ratio), the threshold depth-averaged current speeds are compared with the measured depth-averaged current speeds for each station over the survey times. It appears that there was no bedload transport occurring at station MS1 (Conwy). For all other stations bedload transport took place. The Conwy station was an exception, because the station was not in the main channel.

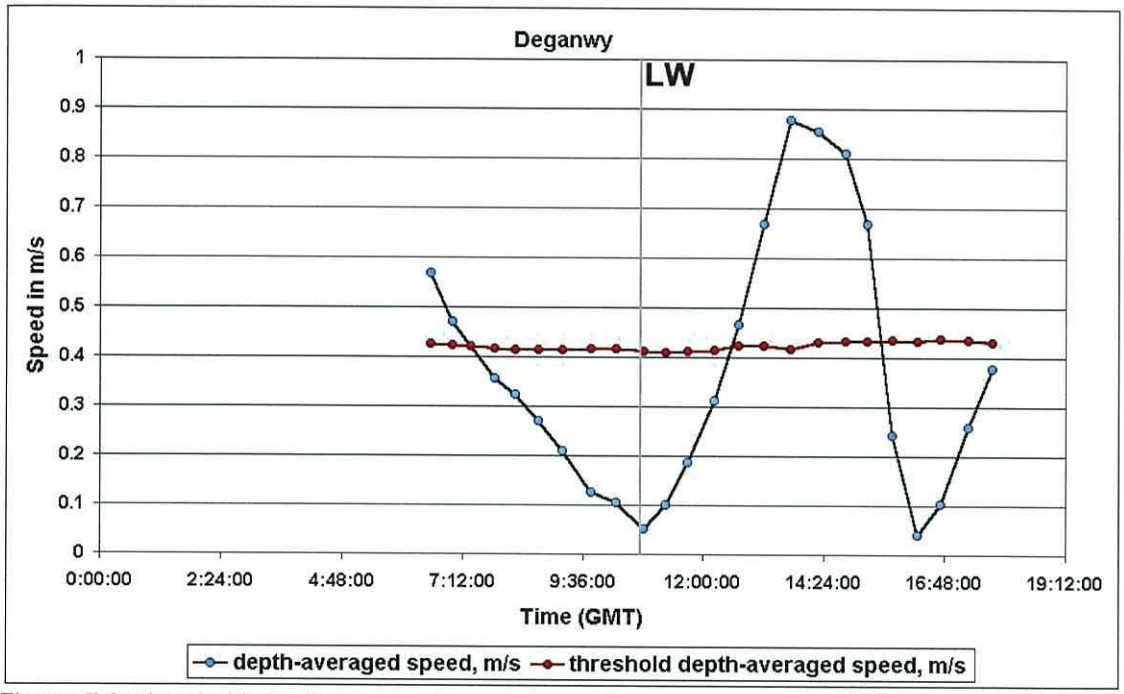

Figure 7.3: threshold depth-averaged current speeds are compared with the measured depth-averaged current speeds for station MS3 (Deganwy) over the survey time.

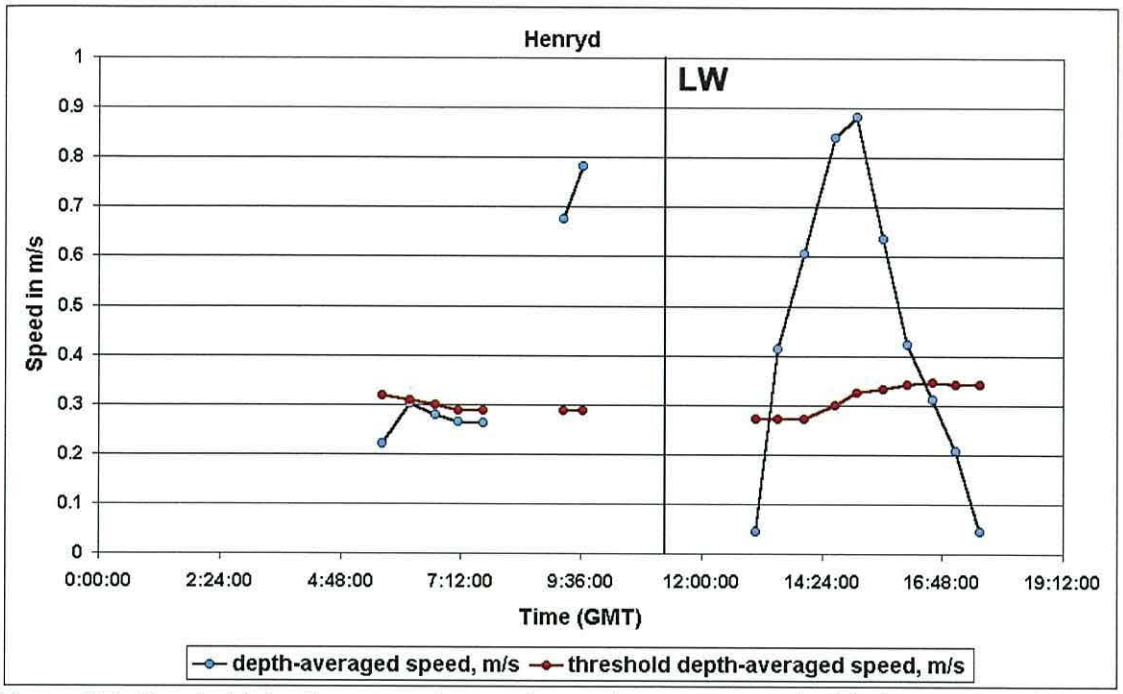

Figure 7.4: threshold depth-averaged current speeds are compared with the measured depth-averaged current speeds for station MS4 (Henryd) over the survey time.

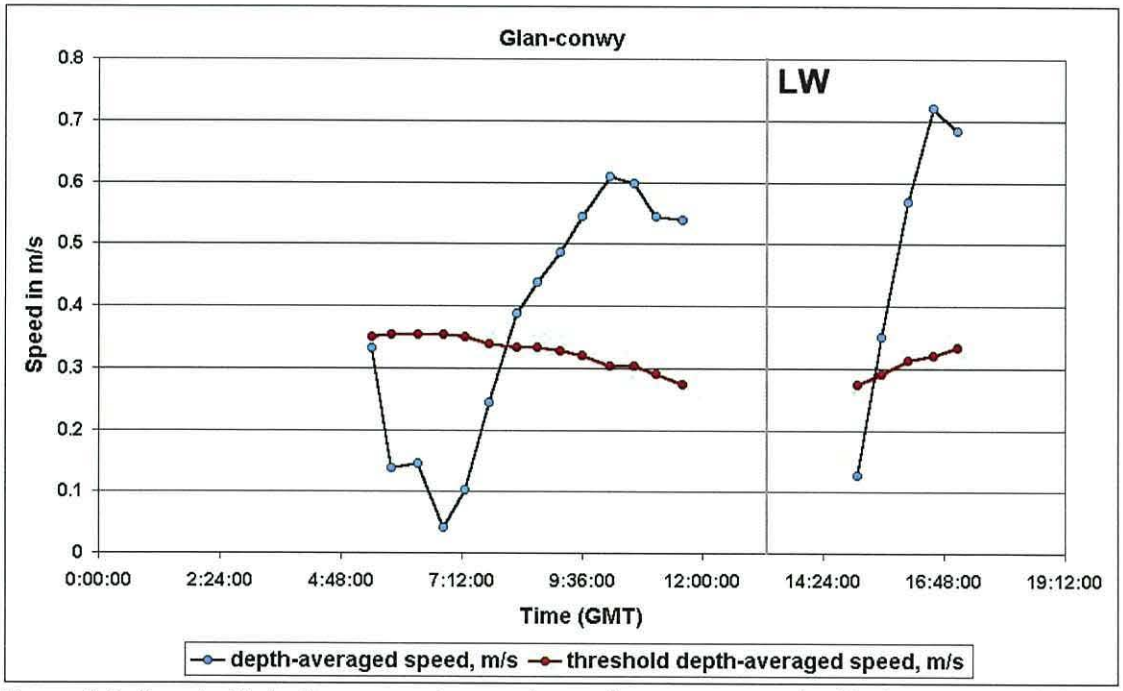

Figure 7.5: threshold depth-averaged current speeds are compared with the measured depth-averaged current speeds for station MS5 (Glan-Conwy) over the survey time.

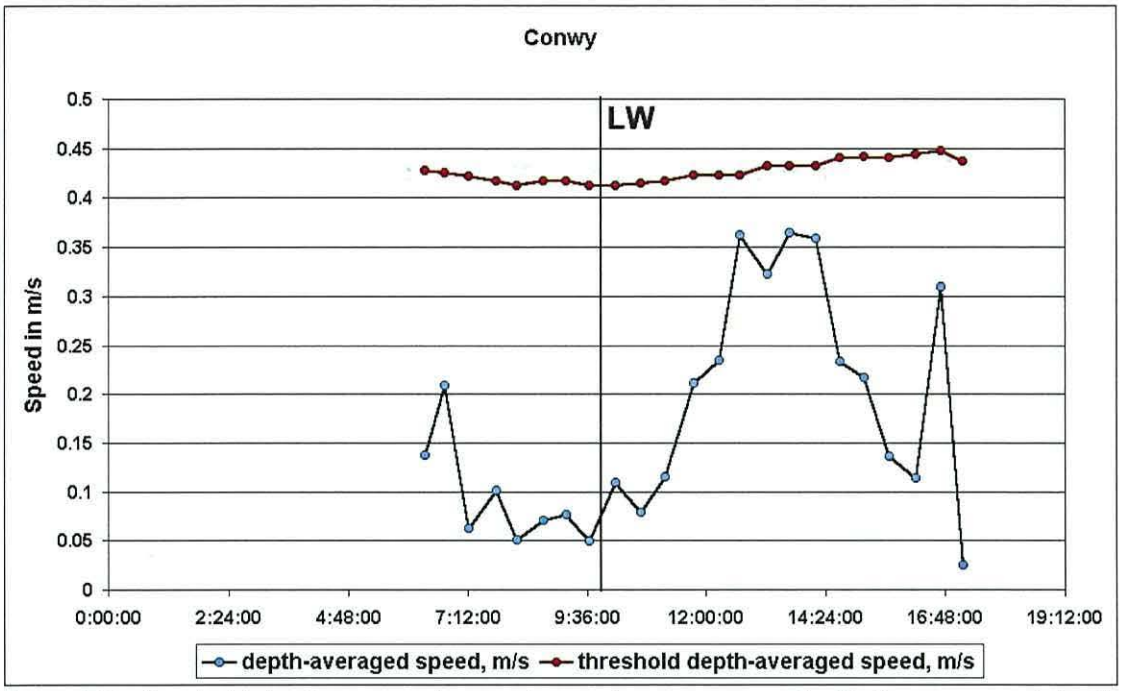

Figure 7.6: threshold depth-averaged current speeds are compared with the measured depth-averaged current speeds for station MS1 (Conwy) over the survey time.

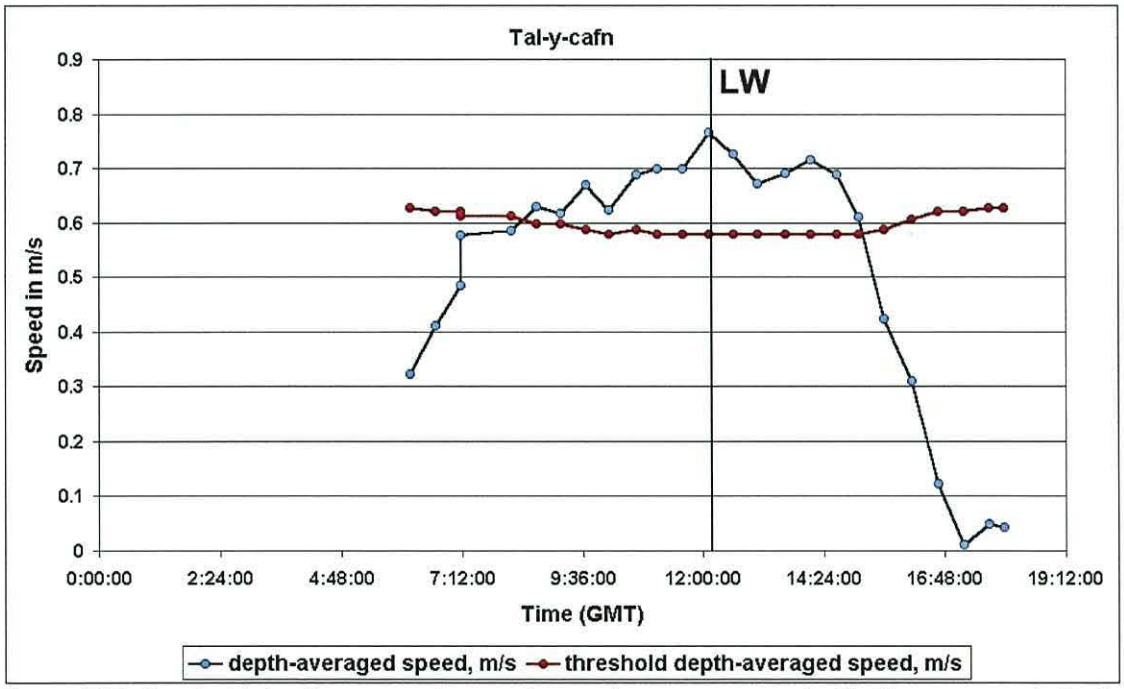

Figure 7.7: threshold depth-averaged current speeds are compared with the measured depth-averaged current speeds for station MS2 (Tal-y-Cafn) over the survey time.

7.2.1.2 Threshold Bed Shear-Stress

A more precise measure of the threshold of motion can be given in terms of the bed shear-stress. In 1936 Shields introduced the threshold Shields parameter, θ_{cr}, which is the ratio of the force exerted by the bed shear-stress acting to move a grain on the bed, to the submerged weight of the grain counteracting this (Dyer, 1986; and Soulsby, 1997).

$$\theta_{cr} = \tau_{cr} / [g (\rho_s - \rho) d] \qquad [7.2]$$

where: θ_{cr} is the threshold Shields parameter; τ_{cr} is the threshold bed shear-stress in Nm^{-2}; g is the acceleration due to gravity; ρ_s is the grain density; ρ is the water density; and d is the grain diameter.

In 1936 Shields produced the threshold curve, which was a plot of θ_{cr} versus the Reynolds number ($Re_* = u_{*cr}d/\nu$, where $u_{*cr} = (\tau_{cr} / \rho)^{1/2}$). Note that by doing this, the u_{*cr} appears on both axes. Soulsby (1997), suggested plotting θ_{cr} against the dimensionless grain size D_*, which is easier to use in practical applications (see Figure 7.8).

The dimensionless grain size, D_*, is given by

$$D_* = [g(s-1)/ \nu^2]^{1/3} d_{50} \qquad [7.3]$$

By using the average kinematic viscosity and density of water a plot relating median grain size to D_* was produced. Figure 7.8 shows this relationship.

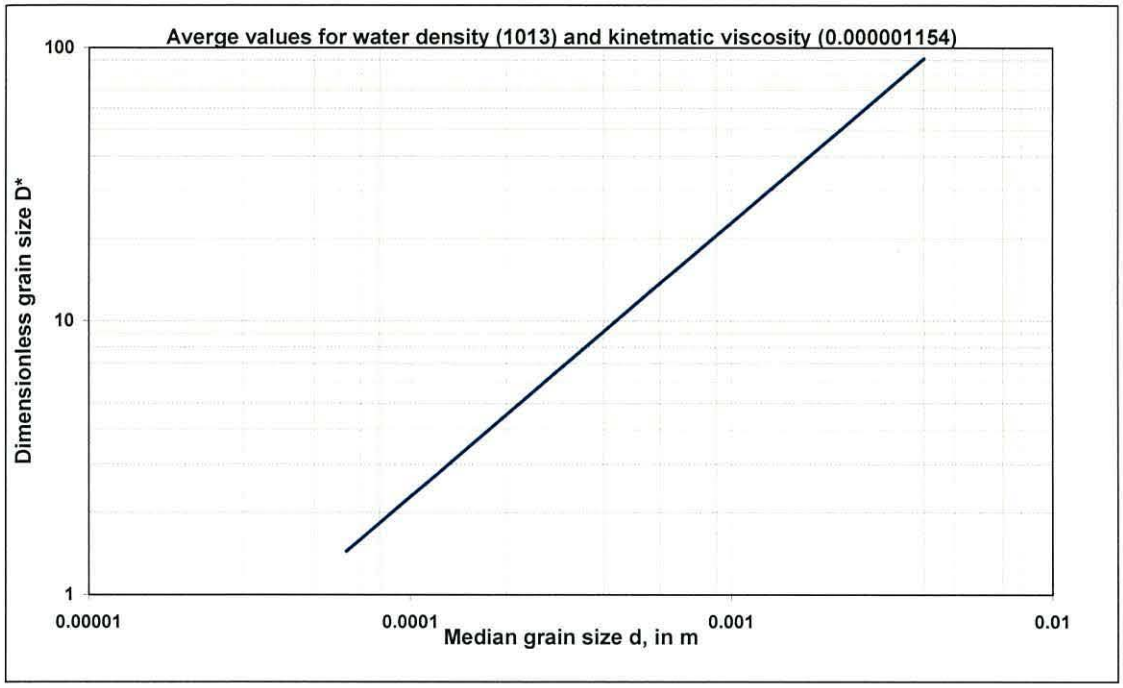

Figure 7.8: relationship between median grain size and D_*.

In 1997, Soulsby and Whitehouse proposed an algebraic expression that fits Shields curve closely, see Equation 7.4.

$$\theta_{cr} = [0.30/(1+1.2D_*)]+0.055[1-\exp(-0.020\ D_*)] \qquad [7.4]$$

Using the bed median grain size data from this project and Equation 7.4, θ_{cr} was calculated and then plotted against D_* (see figure 7.9).

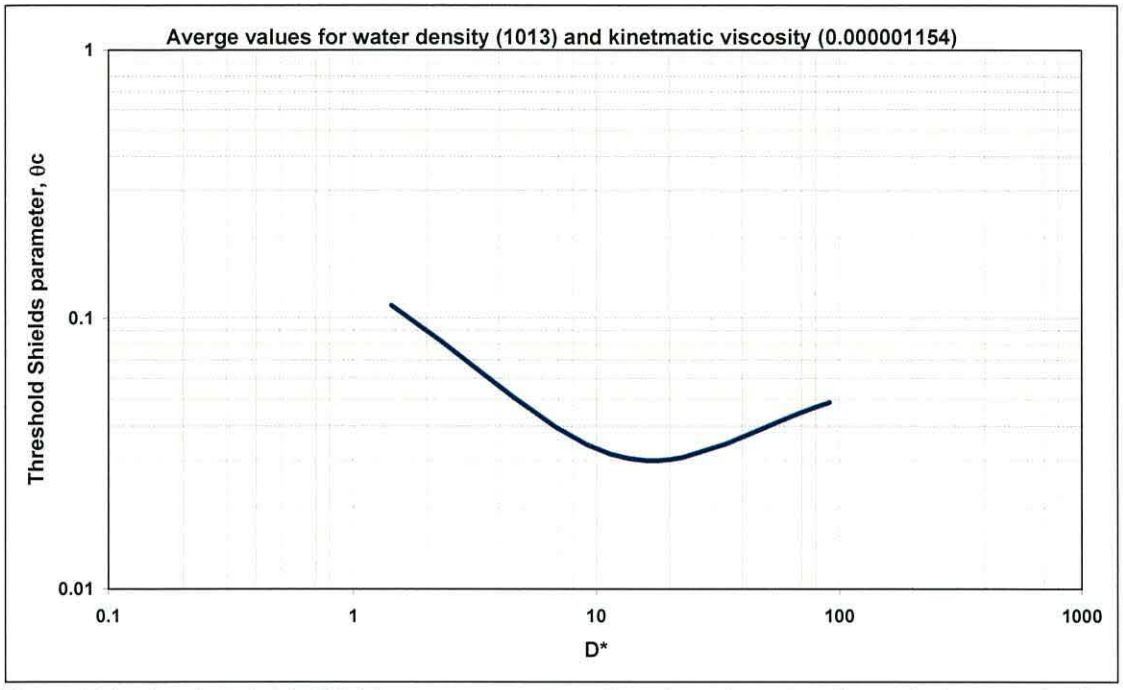

Figure 7.9: the threshold Shields parameter was plotted against the dimensionless grain size, using data from this project.

The threshold bed shear-stress, for a range of grain diameters, was calculated by rearranging Equation 7.2 and using θ_{cr} values derived from Equation 7.4.

$$\tau_{cr} = \theta_{cr} g (\rho_s - \rho) d \qquad [7.5]$$

The calculated threshold bed shear-stress, Nm^{-2}, for individual grain sizes is shown in figure 7.10.

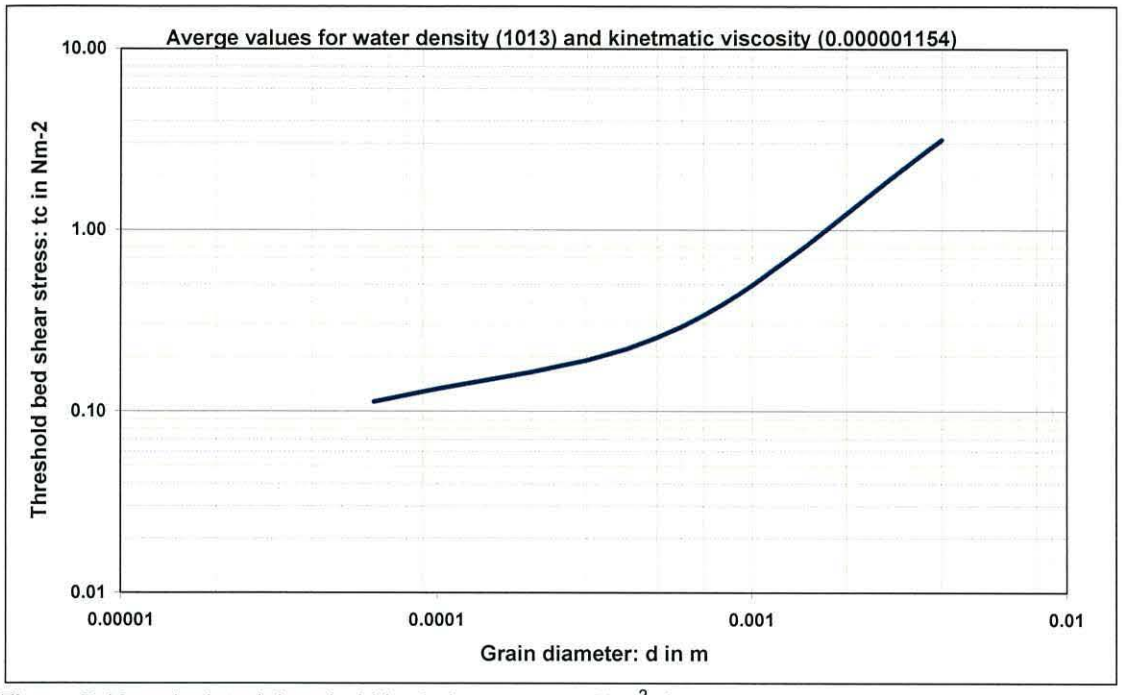

Figure 7.10: calculated threshold bed shear-stress, Nm^{-2}, for individual grain sizes.

Sand grains are set in motion when the bed shear-stress (see section 2.4.1), τ_0, is equal or greater than the threshold bed shear-stress, τ_{cr}. In figures 7.11 (lowest flow ratio), 7.12, 7.13, 5.14, and 7.15 (highest flow ratio), the calculated τ_0, for each cast is compared to the calculated τ_{cr}, for that specific site and time. The τ_0, is calculated using Equation 2.1. u_* can be found using the following relationship (Soulsby, 1997):

$$u_* = \rho [(\overline{U} / 7) (d / h)^{1/7}]^2 \qquad [7.6]$$

where: u_* is the shear velocity in ms^{-1}, $\overline{U}$ is the depth averaged velocity in ms^{-1}; d is the median grain diameter in m; h is the water depth in m; and ρ is the water density in kgm^{-3}.

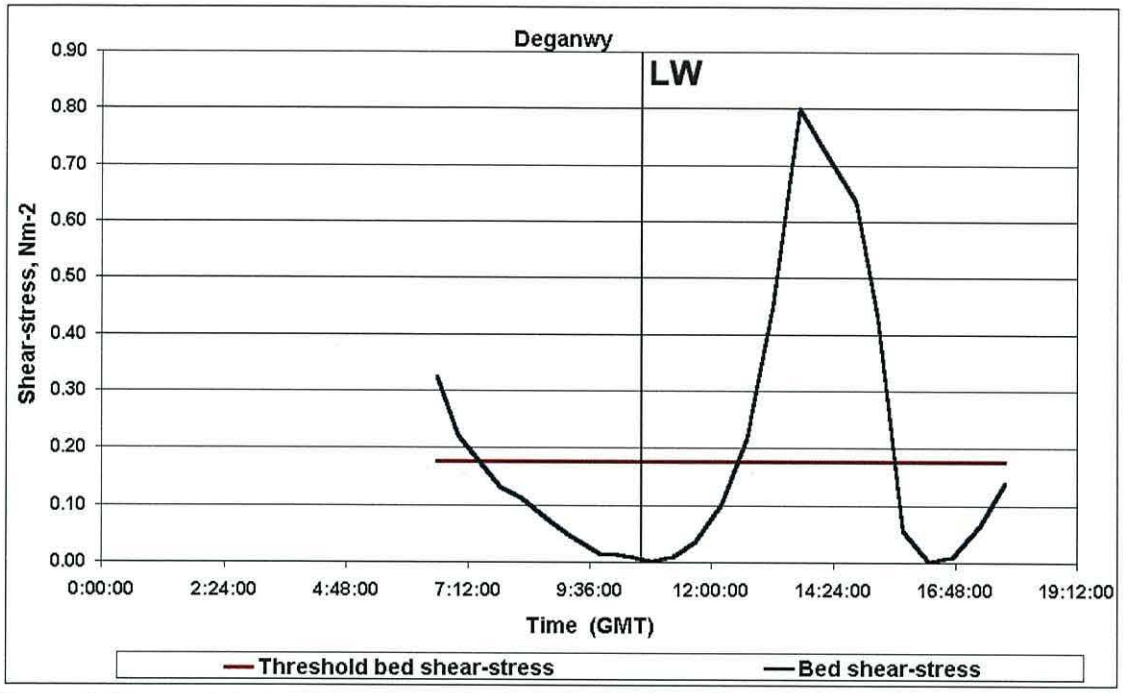

Figure 7.11: calculated τ_0 is compared to the calculated τ_{cr}, for each cast of the survey. Station MS3, Deganwy.

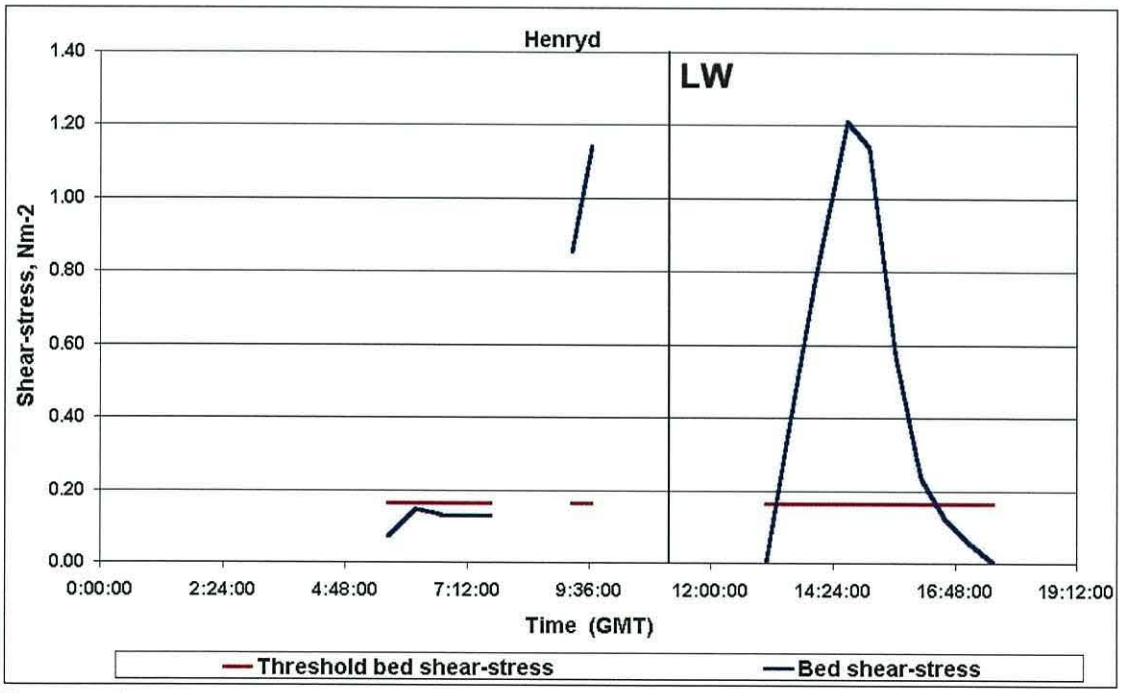

Figure 7.12: calculated τ_0 is compared to the calculated τ_{cr}, for each cast of the survey. Station MS4, Henryd.

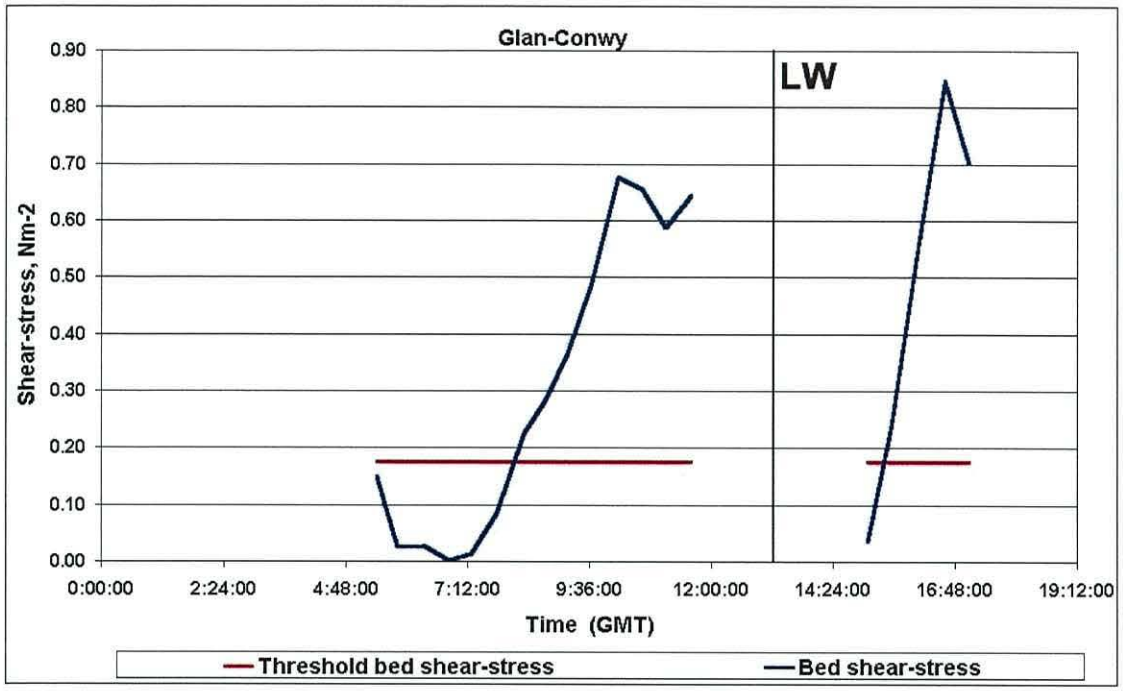

Figure 7.13: calculated τ_0 is compared to the calculated τ_{cr}, for each cast of the survey. Station MS5, Glan-Conwy.

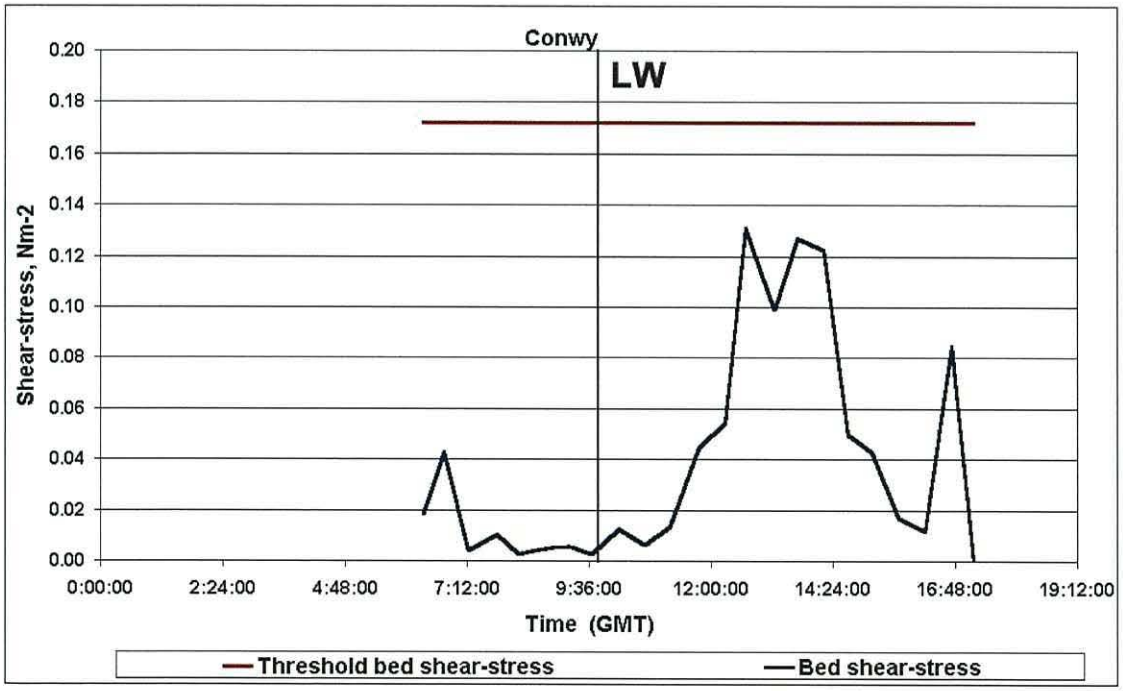

Figure 7.14: calculated τ_0 is compared to the calculated τ_{cr}, for each cast of the survey. Station MS1, Conwy.

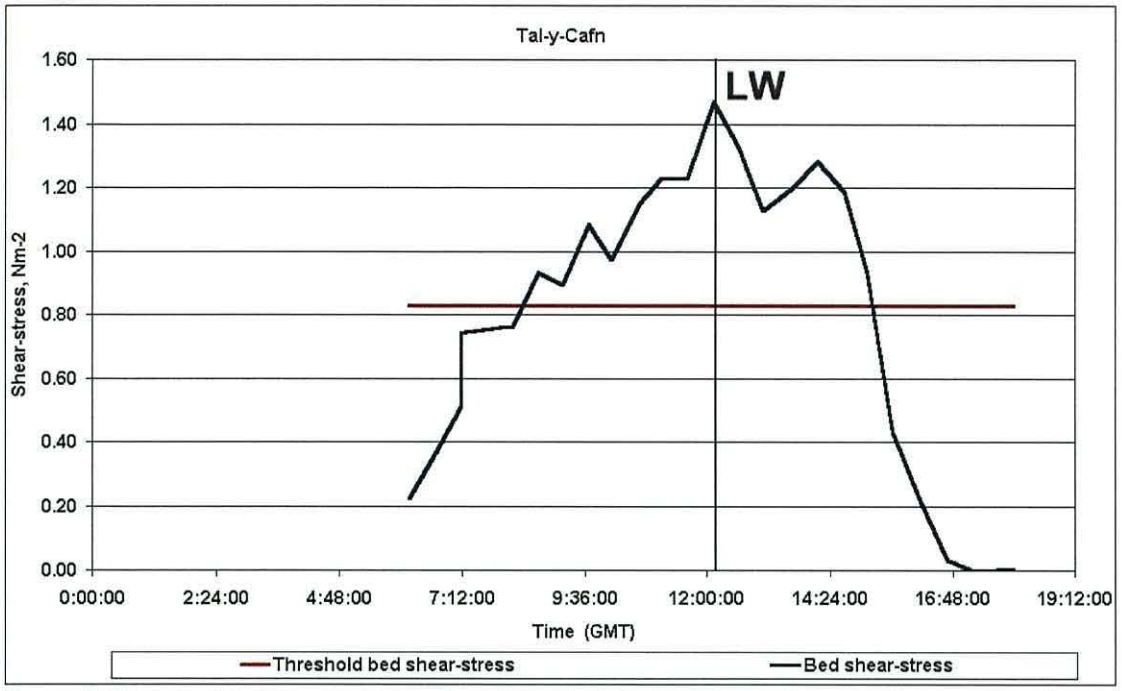

Figure 7.15: calculated τ_0 is compared to the calculated τ_{cr}, for each cast of the survey. Station MS2, Tal-y-Cafn.

From figures 7.11, through to 7.15, it appears that there was no bedload transport occurring at station MS1 (Conwy), as it was not situated in the main flow. For all other stations bedload transport took place at some time during the survey.

7.2.2 Threshold of Suspension

In section 7.2.1.2, it was shown that in order for a quartz grain, of a certain diameter, to start moving as bedload, a threshold bed shear-stress had to be achieved. When the shear-stress is increased further, a new threshold is reached, at which the quartz grains start moving as suspended load.

Bagnold (1956), and McCave (1971), proposed a threshold suspension Shields parameter, θ_s, (see Dyer, 1986, for explanation):

- Threshold of suspension according to Bagnold (1956): $\theta_s = 0.4\ (w_s^2/gd)$ [7.7]

- Threshold of suspension according to McCave (1971): $\theta_s = 0.19 (w_s^2/gd)$ [7.8]

where: θ_s is the threshold of suspension, w_s is the settling velocity, g is the acceleration due to gravity, and d is the grain diameter.

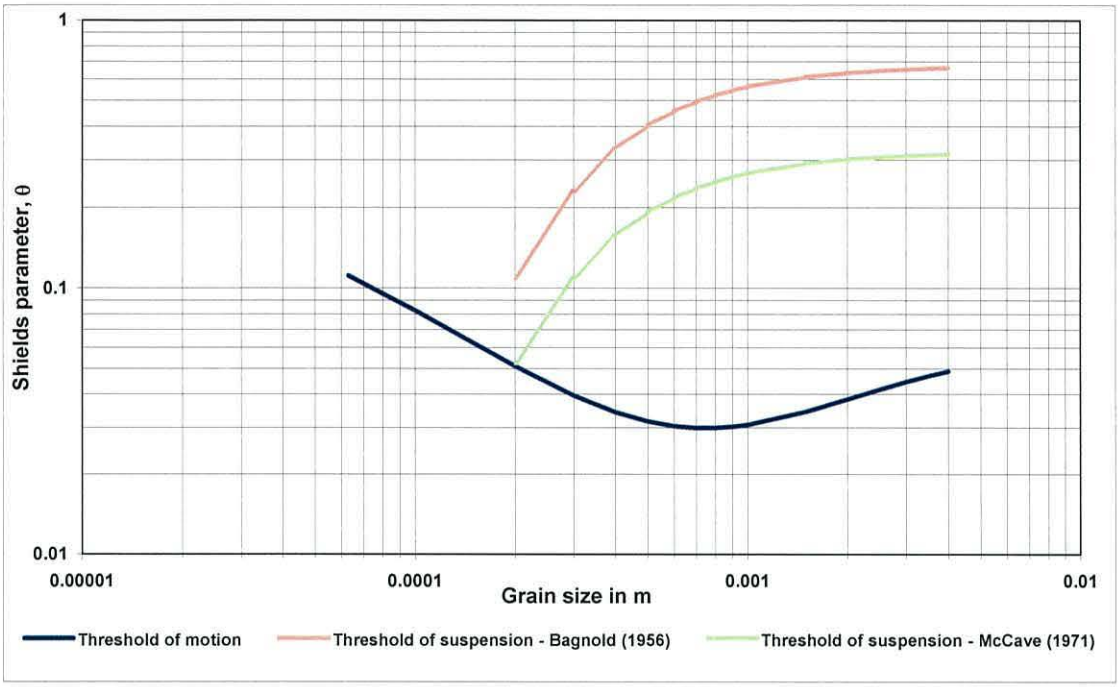

Figure 7.16: threshold of suspension: red line for Bagnold (1956); green line for McCave (1971).

In section 7.2.1, the θ was calculated for each cast of the five moored surveys. Using the θ and the Bagnold and McCave θ_s, the following five diagrams were produced. These diagrams illustrate that suspension of quartz sand did not occur continuously throughout the survey period. In fact, there was no sand suspended during the MS1 (Conwy) and MS2 (Tal-y-Cafn) surveys (see Figures 7.17 (lowest flow ratio), 7.18, 7.19, 7.20, and 7.21 (highest flow ratio)). Note that a grain diameter of 1.5 mm was used for station MS2, whilst a diameter of 0.25 mm was used for all other stations – these diameters represent the bed mean diameter at the specified location.

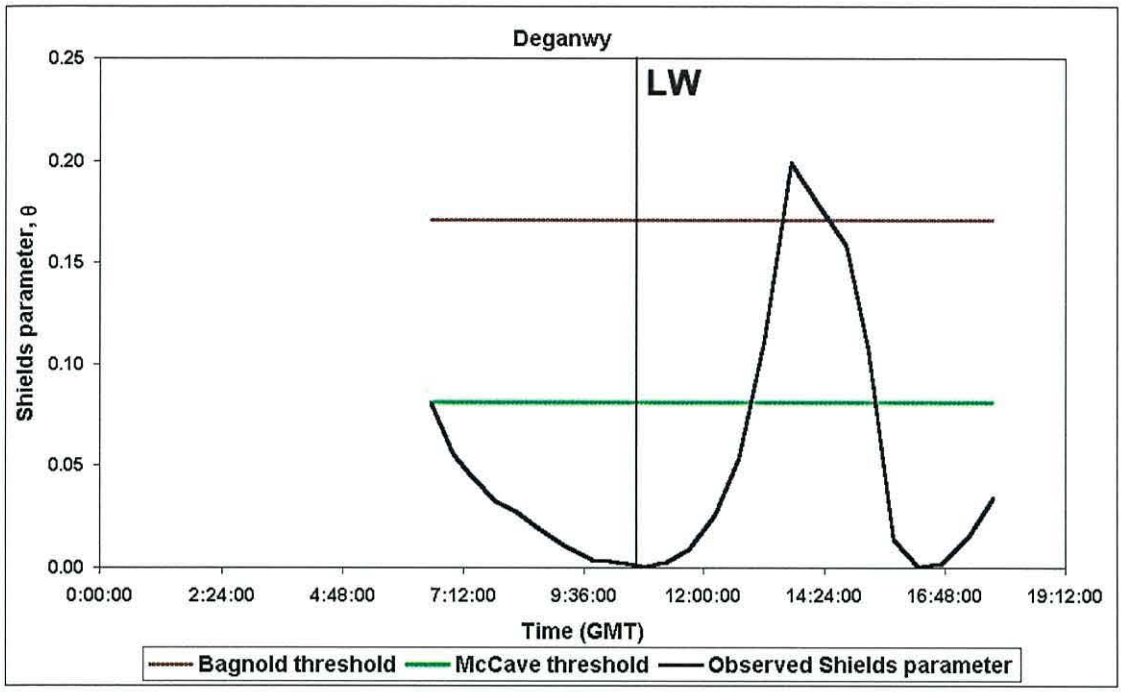

Figure 7.17: threshold suspension of quartz sand compared to Bagnold and McCave suspension thresholds. Station MS3, Deganwy.

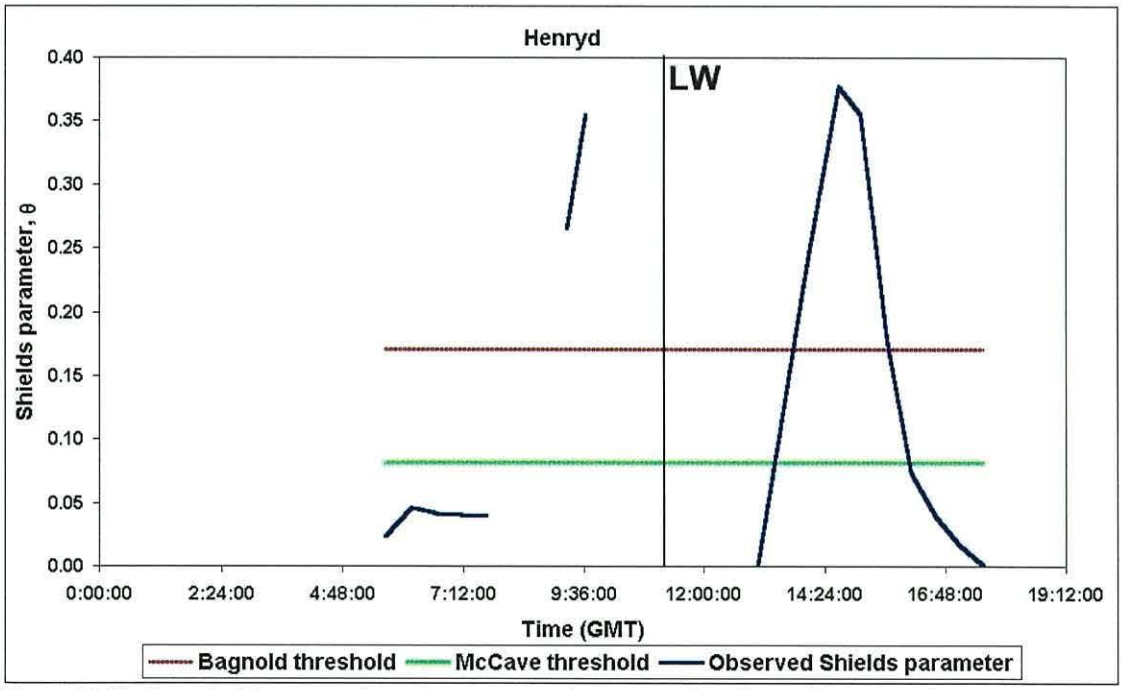

Figure 7.18: threshold suspension of quartz sand compared to Bagnold and McCave suspension thresholds. Station MS4, Henryd.

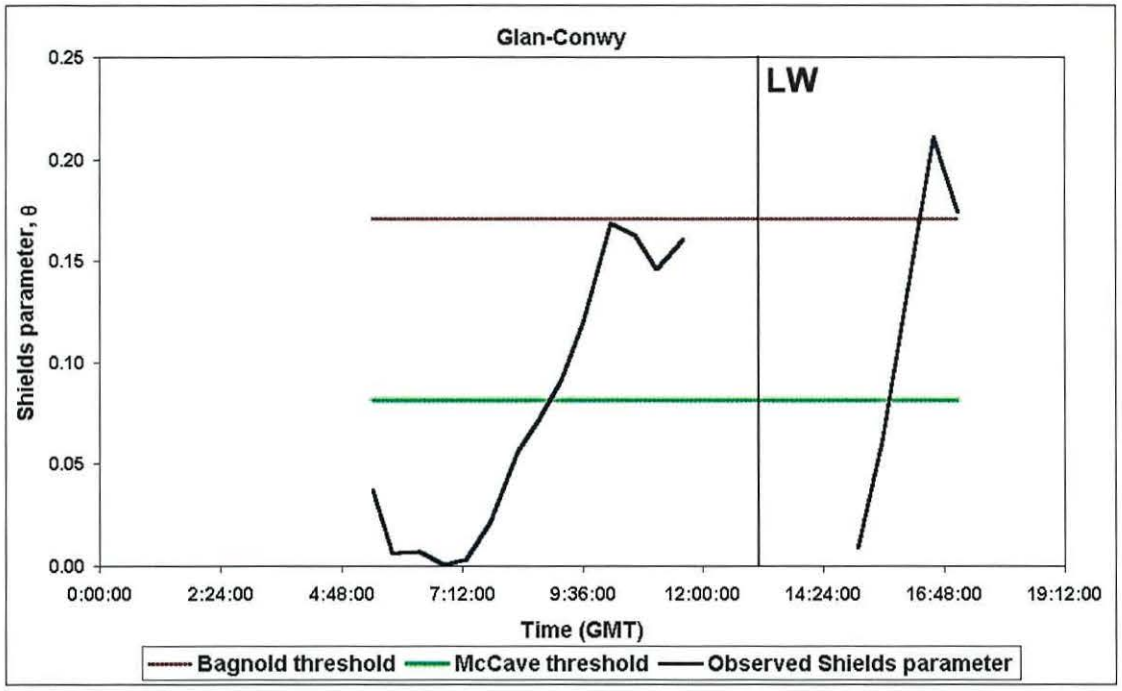

Figure 7.19: threshold suspension of quartz sand compared to Bagnold and McCave suspension thresholds. Station MS5, Glan-Conwy.

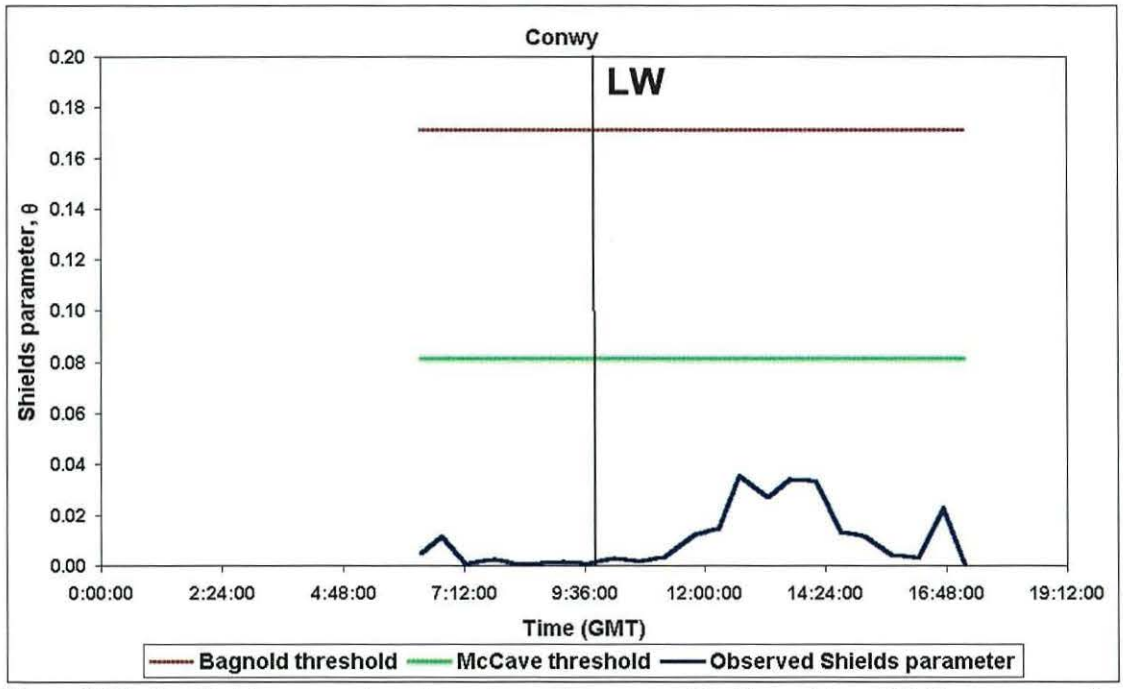

Figure 7.20: threshold suspension of quartz sand compared to Bagnold and McCave suspension thresholds. Station MS1, Conwy.

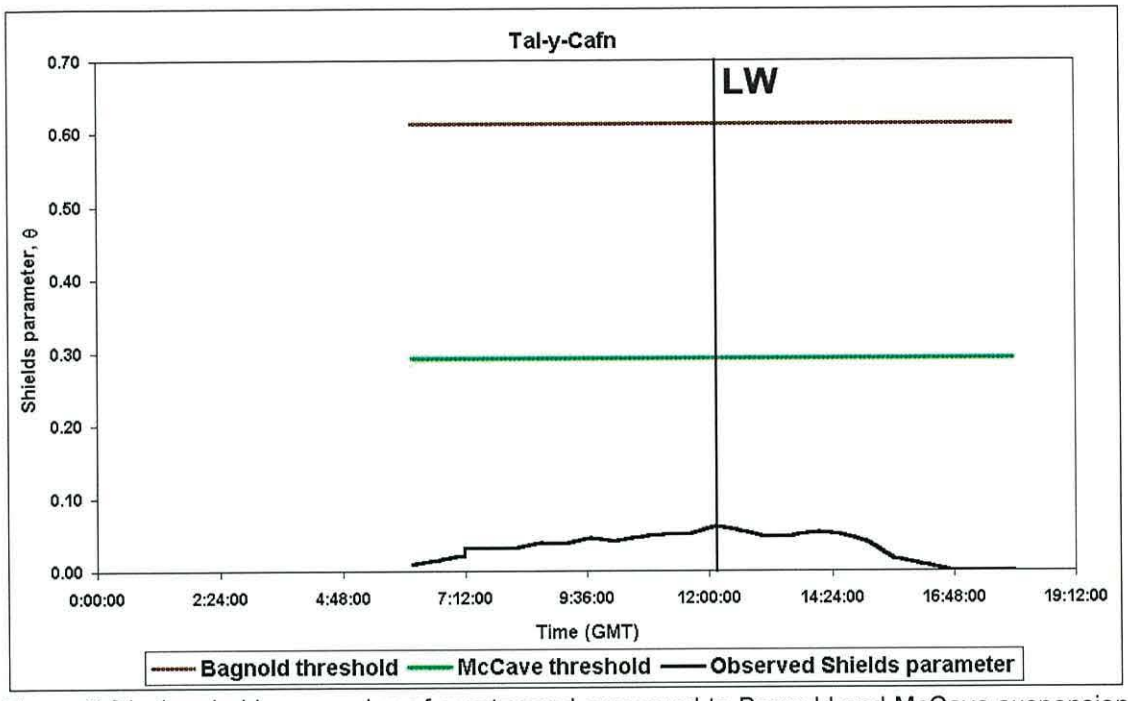

Figure 7.21: threshold suspension of quartz sand compared to Bagnold and McCave suspension thresholds. Station MS2, Tal-y-Cafn.

7.2.3 Discussion and Conclusions

After investigating the threshold of motion by determining the threshold depth-averaged current speed and the threshold bed shear-stress, it was established that sand of median diameter was not transported as bedload at station MS1 (Conwy) on the day of the survey. This could be due to the fact that this station was not situated within the main flow.

Similarly, after investigating the threshold of suspension, it was established that sand of median grain diameter did not enter suspension during the tidal cycle at MS1 and MS2. For all other anchor stations, sand suspension occurred. After sand was resuspended, for how long did it stay in suspension? To answer this, the settling velocities of quartz grains were investigated.

7.2.3.1 Settling Velocity for Quartz Grains

Soulsby (1997), derived Equation 7.9 for natural sands, based on optimising two coefficients in a combined viscous plus bluff-body drag law against data for irregular grains:

$$w_s = (\nu/d)[(10.36^2 + 1.049D_*^3)^{1/2} - 10.36] \text{ for all } D_* \qquad [7.9]$$

were ν is the kinematic viscosity of water, d the grain diameter, and D_* is the dimensionless grain diameter (see section 7.2.1.2, Figure 7.8).

The settling or fall velocity for a range of sand diameters can be seen in the following diagram, Figure 7.22.

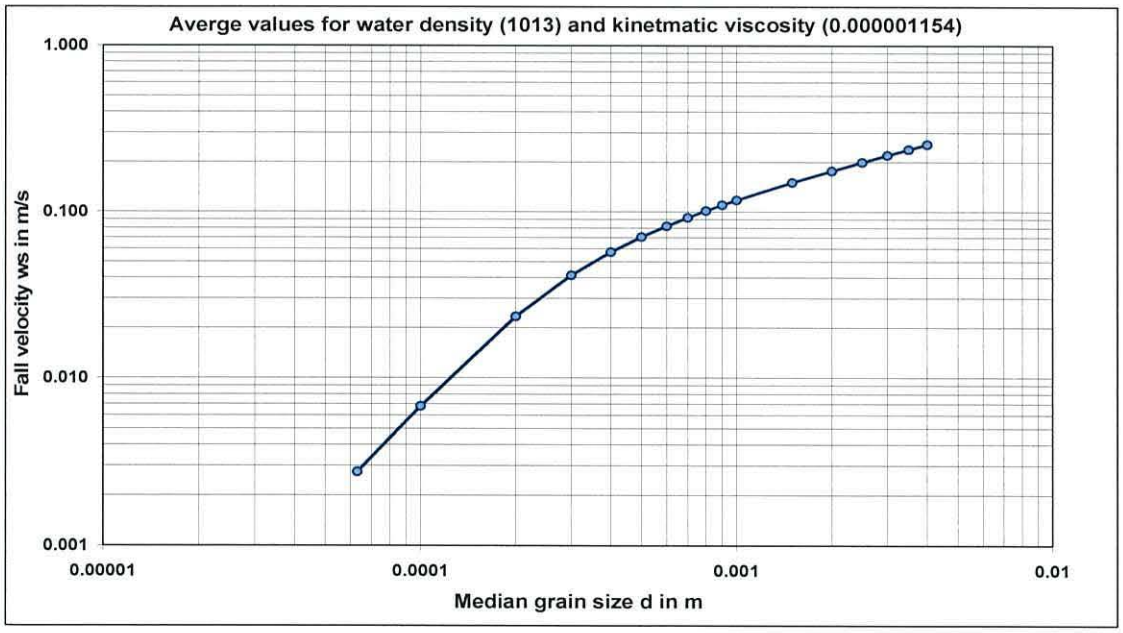

Figure 7.22: diagram shows the fall velocity for a range of grain diameters.

The time taken for a quartz grain to settle through one metre of the water column is shown in figure 7.23. The settling times are produced for the conditions met during this project, and assuming that the water is still, or at least moving at a

velocity lower than the threshold of suspension. So according to Figure 7.23 the quartz grains cannot stay in suspension at slack water for very long..

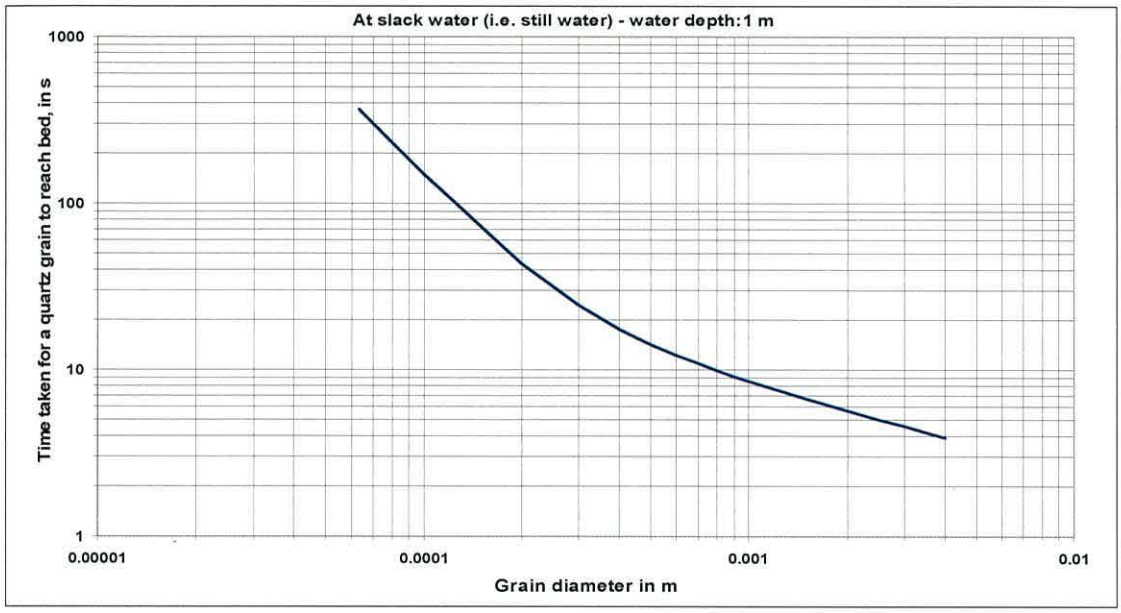

Figure 7.23: the diagram shows the time taken for a quartz grain to settle through 1m of water.

The results from Figure 7.23 show that during the spatial surveys at high water, bed sands were not in suspension. In actual fact, though, the spatial surveys – because of their extent and the duration of HW slack in the upper reaches of the estuary – were not carried out exactly on high water slack. So an amount of quartz sand may have been in suspension, though, it is concluded that the SPM at high water was made up mostly of non-quartz particles.

7.3 Sediment Transport Rates

This section is divided into four main parts: bedload transport rates; suspended load transport rates; total load transport rates; and discussion/conclusions. The first part is further divided into two: threshold current speed; and threshold bed shear-stress.

7.3.1 Bedload Transport Rates

Following the example of Soulsby (1997), the bedload transport rate was expressed as a volumetric transport rate, q_b, ($m^3m^{-1}s^{-1}$ = m^2s^{-1}) during calculations. Once the rate was calculated, it was converted into a mass transport rate, Q_b, ($kgm^{-1}s^{-1}$) by multiplying q_b with the grain density.

According to Soulsby (1997), a number of bedload transport formulae have been proposed. Many of which can be expressed in the form:

$$\Phi = f(\theta, \theta_{cr}) \qquad [7.10]$$

where:

Φ is the dimensionless bedload transport rate = $q_b / [g\ (s\text{-}1)\ d^3]^{1/2}$ [7.11]

θ is the Shields parameter = $\tau_0 / [g\ \rho\ (s\text{-}1)\ d]$ [7.12]

θ_{cr} is the threshold Shields parameter

Soulsby (1997), presents eight bedload transport formulae, proposed by various authors: Meyer-Peter and Muller (1948); Bagnold (1963); Yalin (1963); Wilson (1966); Ashida and Michiue (1972); Van Rijn (1984); Madsen (1991); and Nielsen (1992).

In this project the formula proposed by Nielsen (1992) was used, as it was the simplest and gave a reliable result (Soulsby, 1997):

$$\Phi = 12\ \theta^{1/2}\ (\theta - \theta_{cr}) \qquad [7.13]$$

The dimensionless bedload transport rate, Φ, was calculated for stations MS2, MS3, MS4, and MS5. After rearranging Equation 7.11, the volumetric transport rate was calculated:

$$q_b = \Phi [g (s-1) d^3]^{1/2} \quad [7.14]$$

Finally the volumetric transport rate was converted into mass transport rate:

$$Q_b = \rho_s q_b \ (kgm^{-1}s^{-1}) \quad [7.15]$$

The resulting mass bedload transport rates are seen in Figures 7.24 (lowest flow ratio), 7.25, 7.26, and 7.27 (highest flow ratio). Negative values indicate transport in the down-estuary direction, whilst positive values indicate transport in the up-estuary direction.

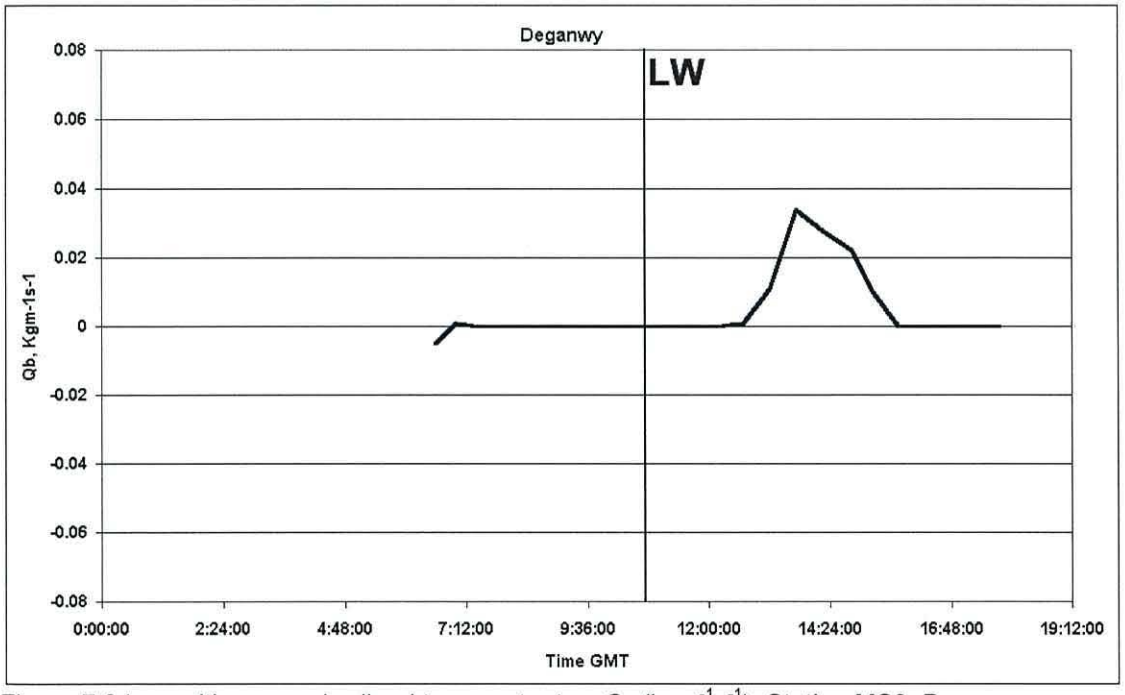

Figure 7.24: resulting mass bedload transport rates, Q_b ($kgm^{-1}s^{-1}$). Station MS3, Deganwy.

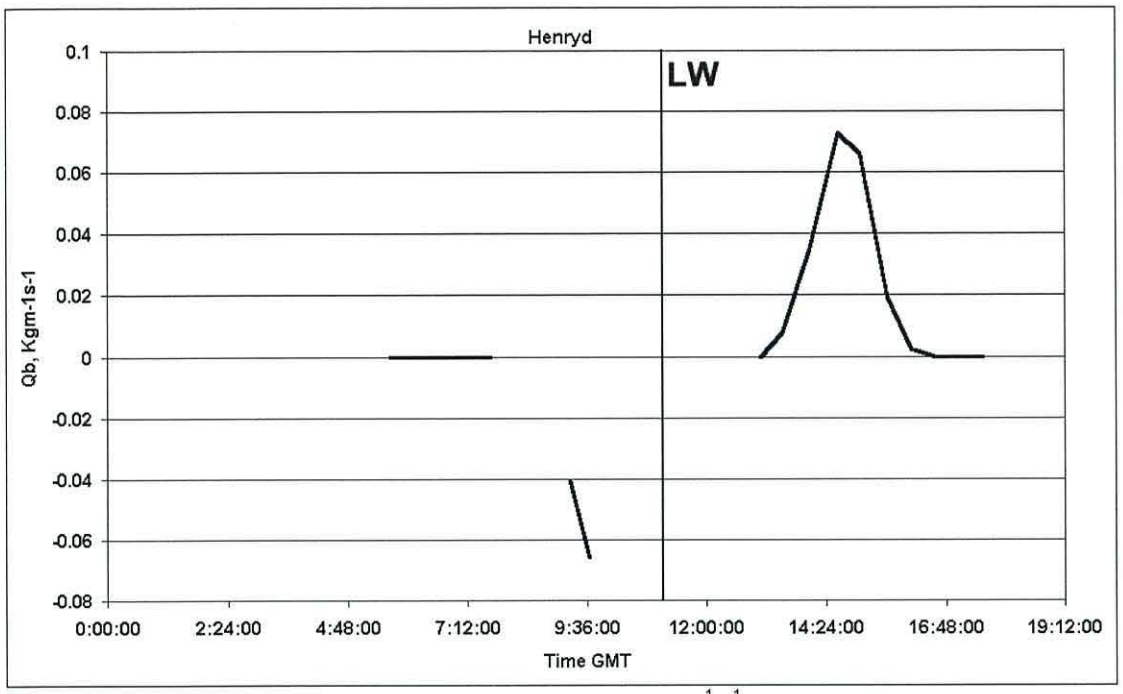

Figure 7.25: resulting mass bedload transport rates, Q_b ($kgm^{-1}s^{-1}$). Station MS4, Henryd.

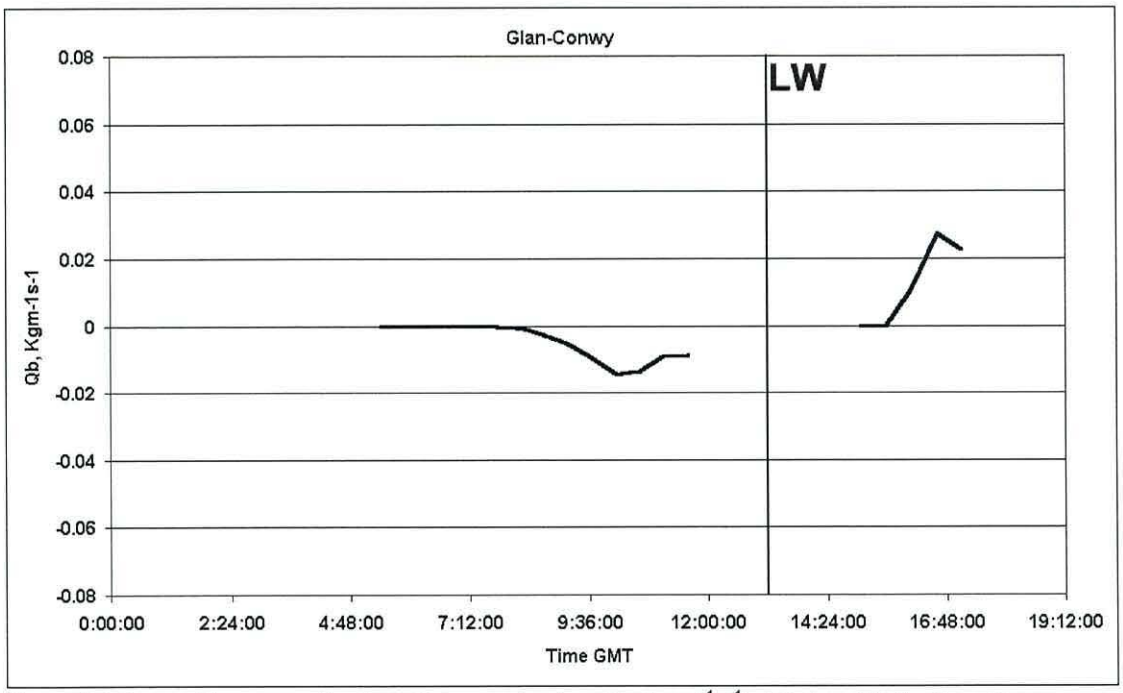

Figure 7.26: resulting mass bedload transport rates, Q_b ($kgm^{-1}s^{-1}$). Station MS5, Glan-Conwy.

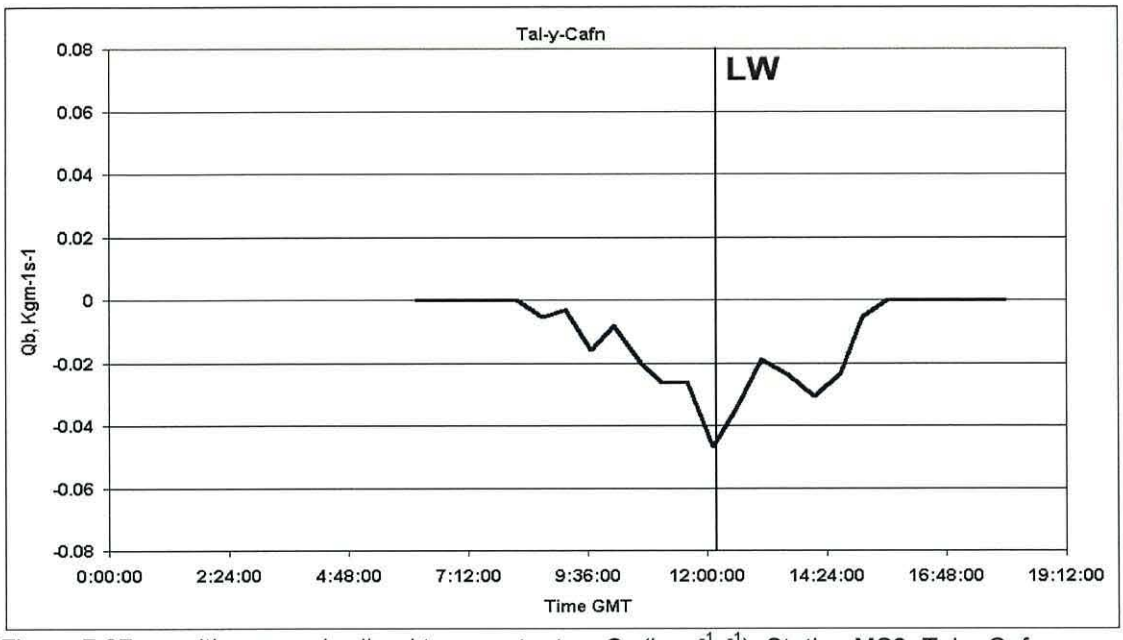

Figure 7.27: resulting mass bedload transport rates, Q_b ($kgm^{-1}s^{-1}$). Station MS2, Tal-y-Cafn.

The next step in the process was to calculate the net bedload transport. To do this all Q_b were summed for each individual station:

Q_{bN} = net bedload transport load = $\sum Q_b$

The results can be seen in Table 7.1, below. Note that the transport rate is per survey, as the surveys did not start on high or low water, so using the term per tide would not be correct.

Station	Q_{bN}	Direction of net bedload transport	Comments
MS1	n/a	n/a	No transport as the station was situated outside the main flow.
MS2	-0.303	down-estuary	High river discharge
MS3	0.102	up-estuary	
MS4	0.094	up-estuary	
MS5	-0.033	down-estuary	Situated within ebb/river channel

Table 7.1: Q_{bN} is in kgm^{-1}/survey.

7.3.2 Suspended Load Transport Rates

The water column on each cast was split into bins of 30 cm. The SPM flux for each bin was calculated by multiplying the SSC of that bin with the corresponding current velocity (see section 6.5). A total flux for each cast was produced by integrating the flux values throughout the water column.

The total SPM flux, $kgm^{-2}s^{-1}$, is defined as the mass of sediment per unit time, passing through a vertical plane perpendicular to the flow direction. By assuming unit width for the plane, the flux is transformed into transport rate, $kgm^{-1}s^{-1}$.

Figures 7.28 (low flow ratio), 7.29, 7.30, 7.31, and 7.32 (highest flow ratio), show the total suspended load transport rate, Q_s, for each cast. Negative values indicate transport in the down-estuary direction, whilst positive values indicate transport in the up-estuary direction.

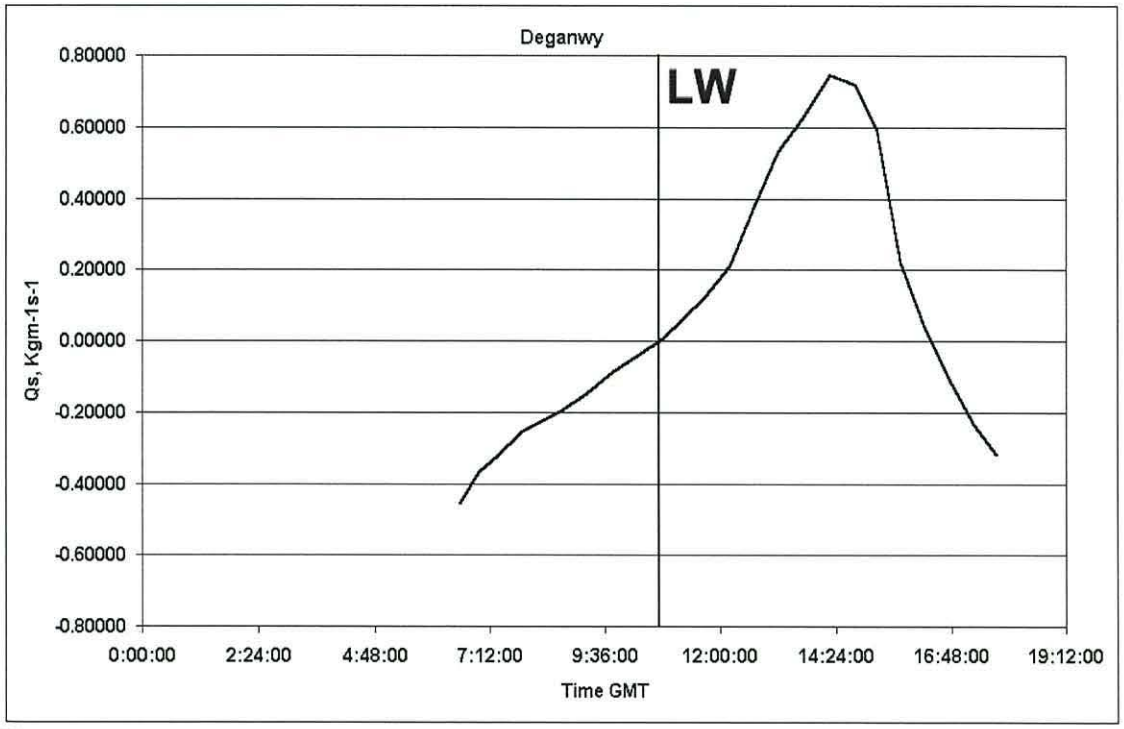

Figure 7.28: total suspended load transport rate, Q_s, for each cast at station MS3, Deganwy.

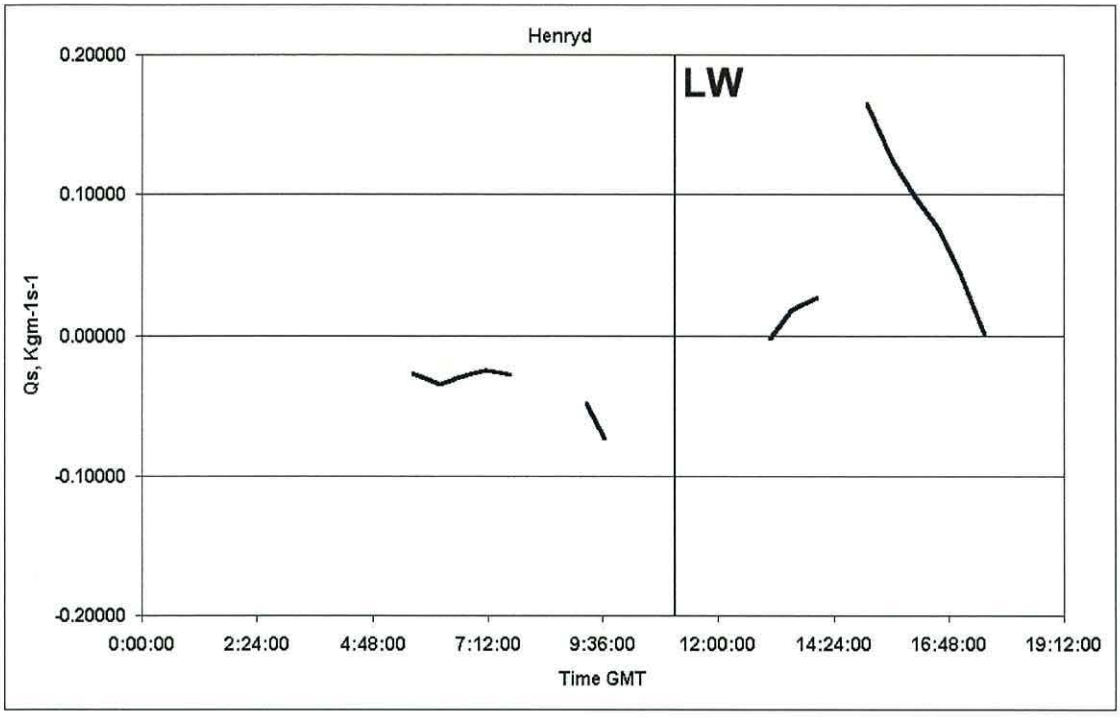

Figure 7.29: total suspended load transport rate, Q_s, for each cast at station MS4, Henryd.

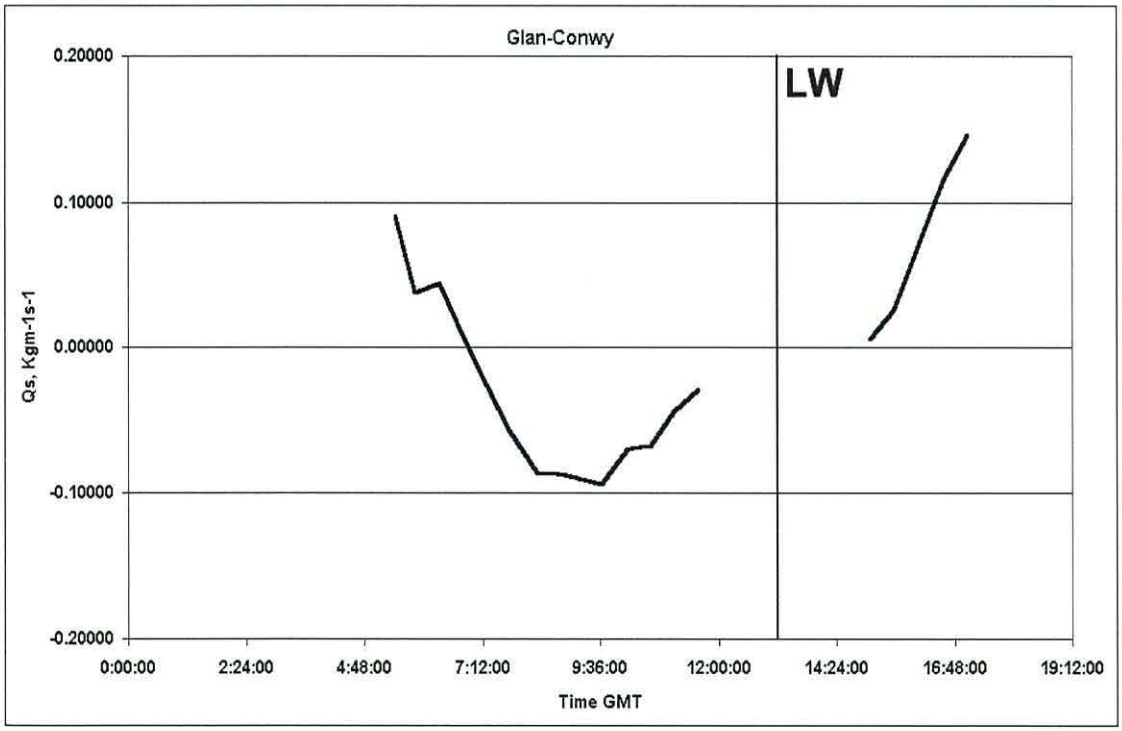

Figure 7.30: total suspended load transport rate, Q_s, for each cast at station MS5, Glan-Conwy.

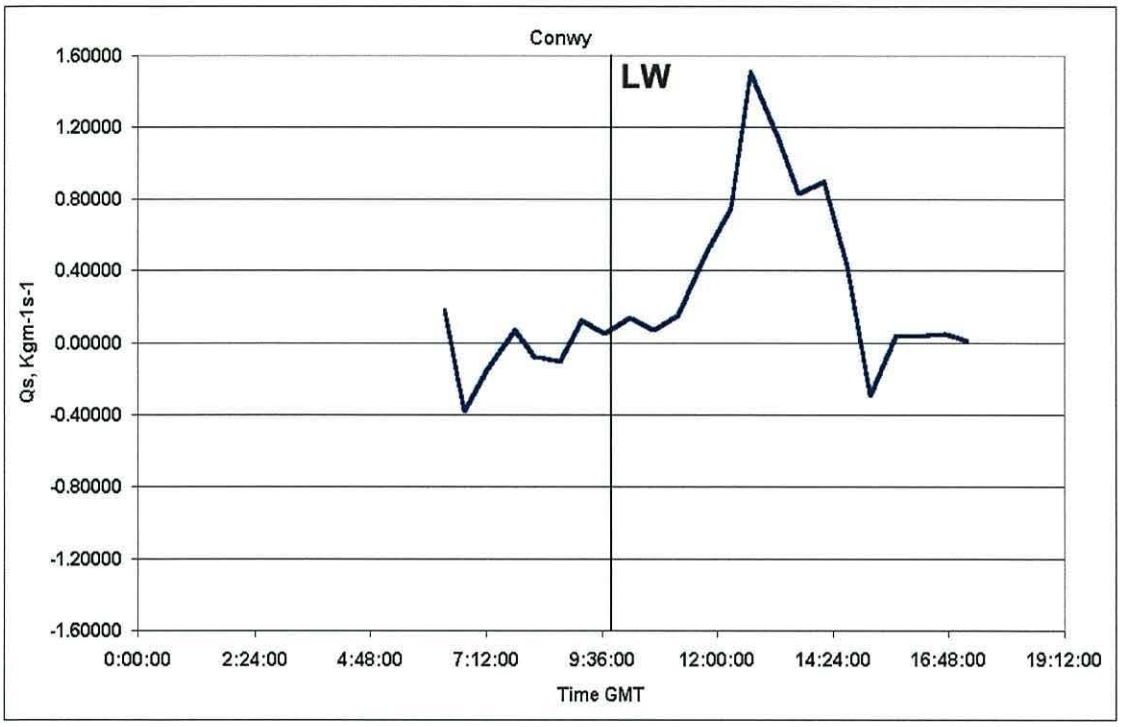

Figure 7.31: total suspended load transport rate, Q_s, for each cast at station MS1, Conwy.

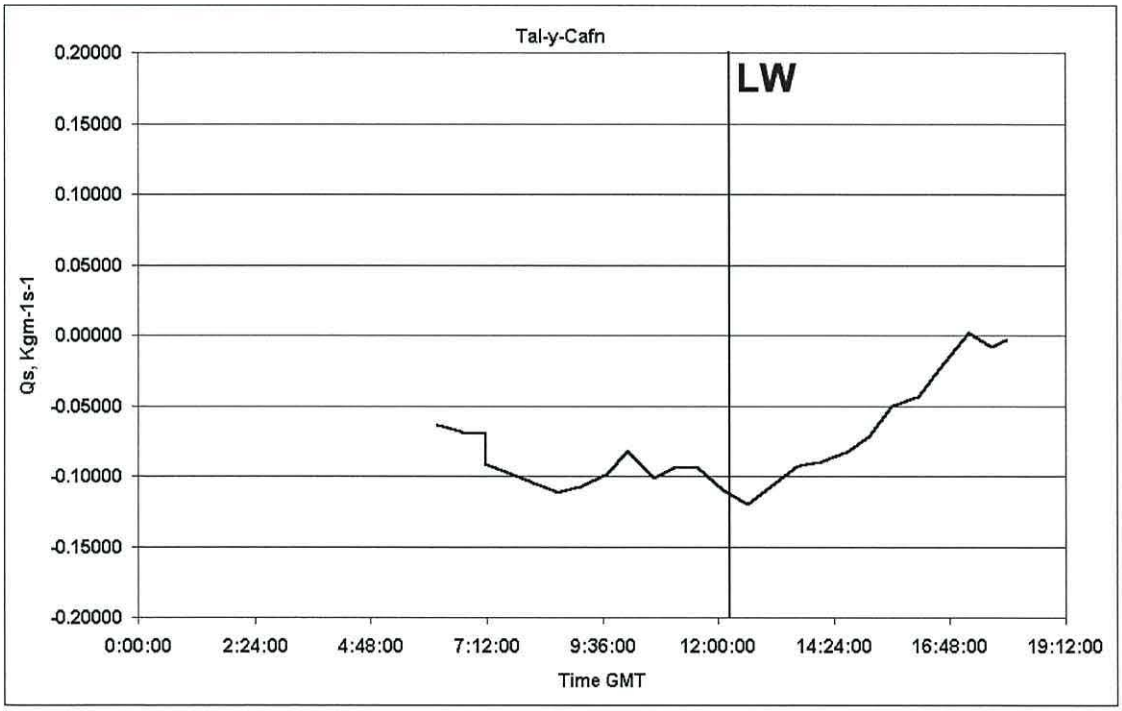

Figure 7.32: total suspended load transport rate, Q_s, for each cast at station MS2, Tal-y-Cafn.

As with the bedload transport, the next step in the process was to calculate the net suspended load transport. To do this all Q_s were summed for each individual station:

Q_{sN} = net suspended load transport load = $\sum Q_s$

The results can be seen in table 7.2, below. Note that the transport rate is per survey.

Station	Q_{sN}	Direction of net suspended load transport
MS1	5.987	up-estuary
MS2	-1.891	down-estuary
MS3	1.469	up-estuary
MS4	0.285	up-estuary
MS5	-0.108	down-estuary

Table 7.2: the Q_{sN} is in kgm^{-1}/survey.

7.3.3 Total Load Net Transport Rates

In order to obtain the total net transport rate, Q_{TN}, the net bedload transport rate and the suspended load transport rate, were summed.

$$Q_{TN} = Q_{bN} + Q_{sN} \qquad [7.16]$$

Station	Q_{sN}	Direction of net total transport
MS1	5.987	up-estuary
MS2	-2.194	down-estuary
MS3	1.571	up-estuary
MS4	0.380	up-estuary
MS5	-0.141	down-estuary

Table 7.3: the Q_{TN} is in kgm^{-1}/survey.

Figure 7.33 shows the total load net transport rate, Q_{TN}, for each station – the stations are presented according to their distance from the mouth, with Deganwy being at the mouth and Tal-y-Cafn 10 km from it. Negative values indicate transport in the down-estuary direction, whilst positive values indicate transport in the up-estuary direction.

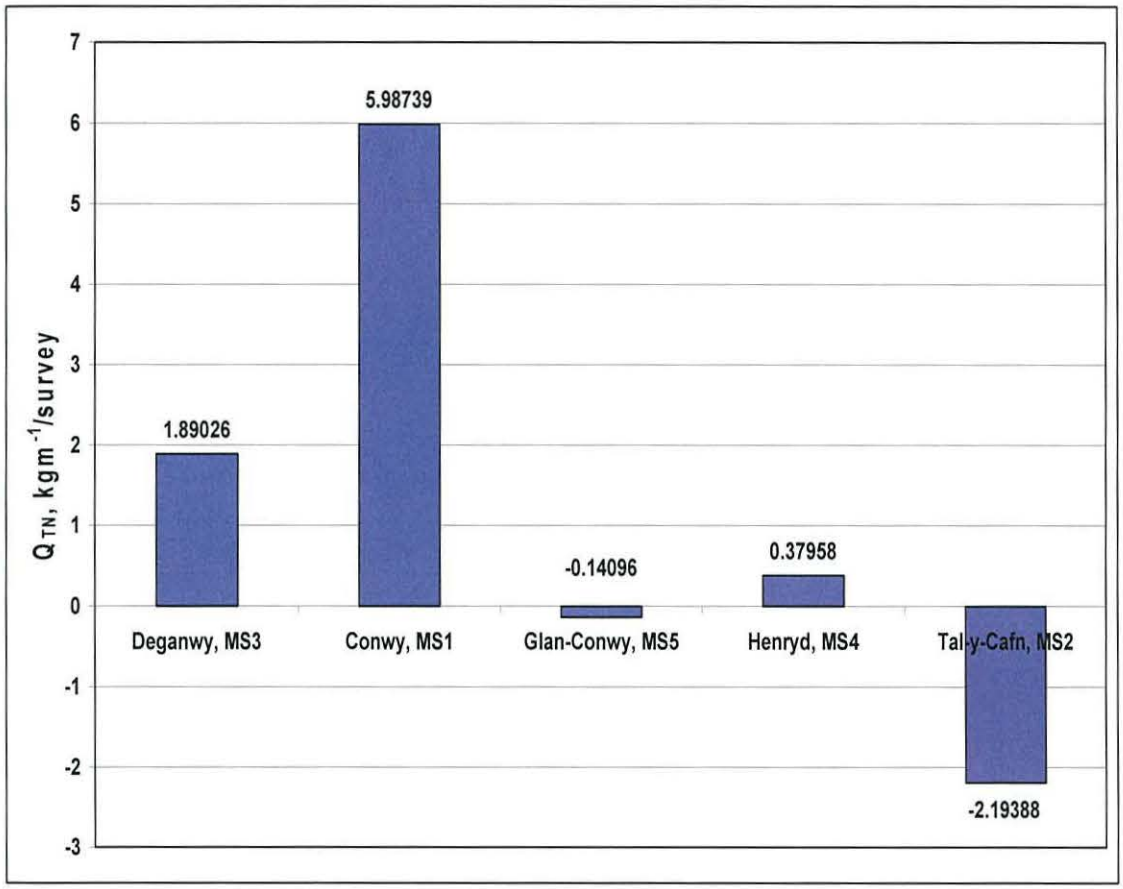

Figure 7.33: total net transport rates during the five moored surveys. Here, the stations are presented according to their distance from the mouth, with Deganwy being at the mouth and Tal-y-Cafn 10 km from it.

Figure 7.34 presents the total load net transport rate and directions in relation to their location within the Conwy estuary.

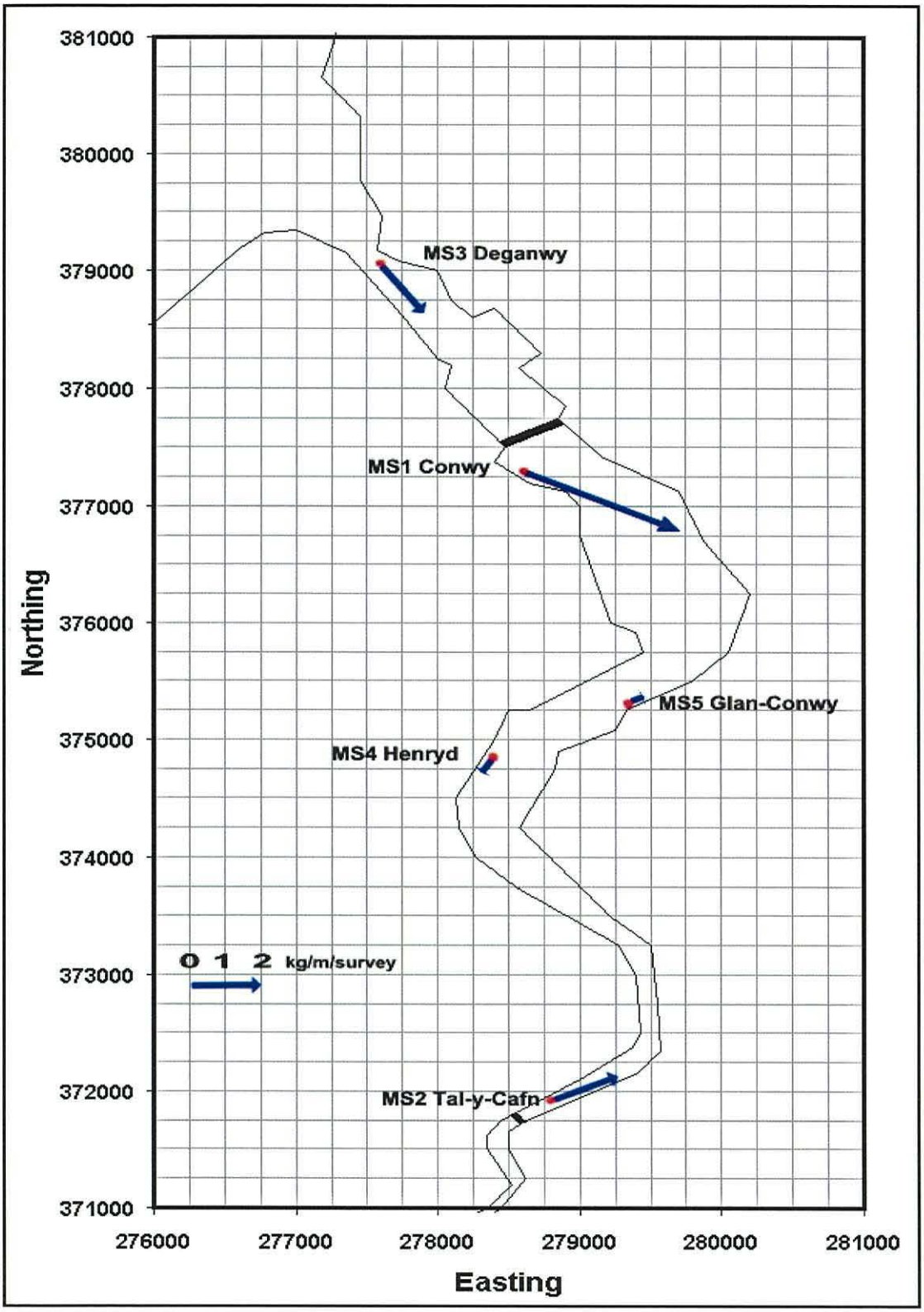

Figure 7.34: total load net sediment transport rates and directions.

7.3.4 Discussion and Conclusion

From section 7.3, there are three main points that need mentioning:

- Section 7.3, concentrates on quartz sand transport. This neglects all of the non-quartz particles that are carried in suspension, some of which settle out of suspension during low velocities, i.e. at slack water. These particles will have the tendency to be resuspended when velocities increase. Further information is needed to establish the exact nature of the SPM, but from the data collected, it appears that although there may be some fine quartz sand in suspension, the majority of the SPM is made up of a mixture of less dense particles, such as flocs or organic material.

- It was established (section 7.3.1) that there was no bedload transport at station MS1 (Conwy), yet the suspended sediment transport rate for that station was 2 to 5 times greater than the transport rates at the other stations. Since there was no suspension of quartz sand at this station, the SPM most be made up off flocs, finer sediments, or organic matter. Figure 7.31 shows that the suspended load transport rate was at its maximum about 3 hours after low water slack – i.e. on the flood. The area surrounding station MS1, excluding the main channel, is exposed at low water. The exposed sand flats at the mouth and lower estuary play hosts to benthic diatoms that thrive in such an environment. These diatoms can be observed as iridescent surface films especially in areas where the sands retain high water content (Jago et al., 2006). On the onset of the flood, diatoms and their products enter suspension. The geometry of the area (narrow channel under Conwy Bridge) meant that the suspended organic material was concentrated increasing the overall SSC. Also, down estuary of the station, a tributary joins the Conwy. This tributary may have supplied material that formed flocs, once the tide forced the flow up-estuary; the flocs headed pass the survey station, increasing the concentration of low density SPM.

- The direction of the total sediment transport at each station was determined by the location of that station, and the fresh water discharge. Stations MS1, MS3, and MS4 (see Figure 3.4), showed total sediment transport in the up-estuary direction. This suggests that a part of the SPM could be of marine origin. Stations MS2 and MS5 (see Figure 7.34) showed total sediment transport in the down estuary direction. This was expected for MS2, as the river discharge was at a high. It was unexpected for MS5, as the river flow was at a low. The fact that sediment was carried down estuary at this station suggests that the station was situated within an ebb channel, which is not necessarily used by the flood tide.

8 ESTUARINE SANDS AND NET TRANSPORT PATHS

The purpose of this chapter is:

1. To establish the provenance of the estuarine sands

2. To determine the transport paths of estuarine sands, from their textural characteristics.

8.1 Analysis of Sand Samples

Note: The grain size analysis was carried out using ϕ (phi units) as a unit for the grain diameter (Folk, 1968).

8.1.1 Median and Graphic Mean Diameters

Two measurements of 'average' grain size have been used: the median diameter; and the graphic mean diameter.

Median diameter (M_d): "Half of the particles by weight are coarser than the median, and half are finer. It is the diameter corresponding to the 50% mark on the cumulative curve." (Folk, 1968)

Graphic mean diameter (M_z): According to Folk (1968), the graphic mean is the best graphic measure for determining overall size and is given by

$$M_z = (\phi_{16} + \phi_{50} + \phi_{84}) / 3 \qquad [8.1]$$

where ϕ_{16},ϕ_{50}, and ϕ_{84} are the phi diameter equal to the 16^{th}, 50^{th} and 84^{th} percentiles from the cumulative curve, see example in Appendix A.

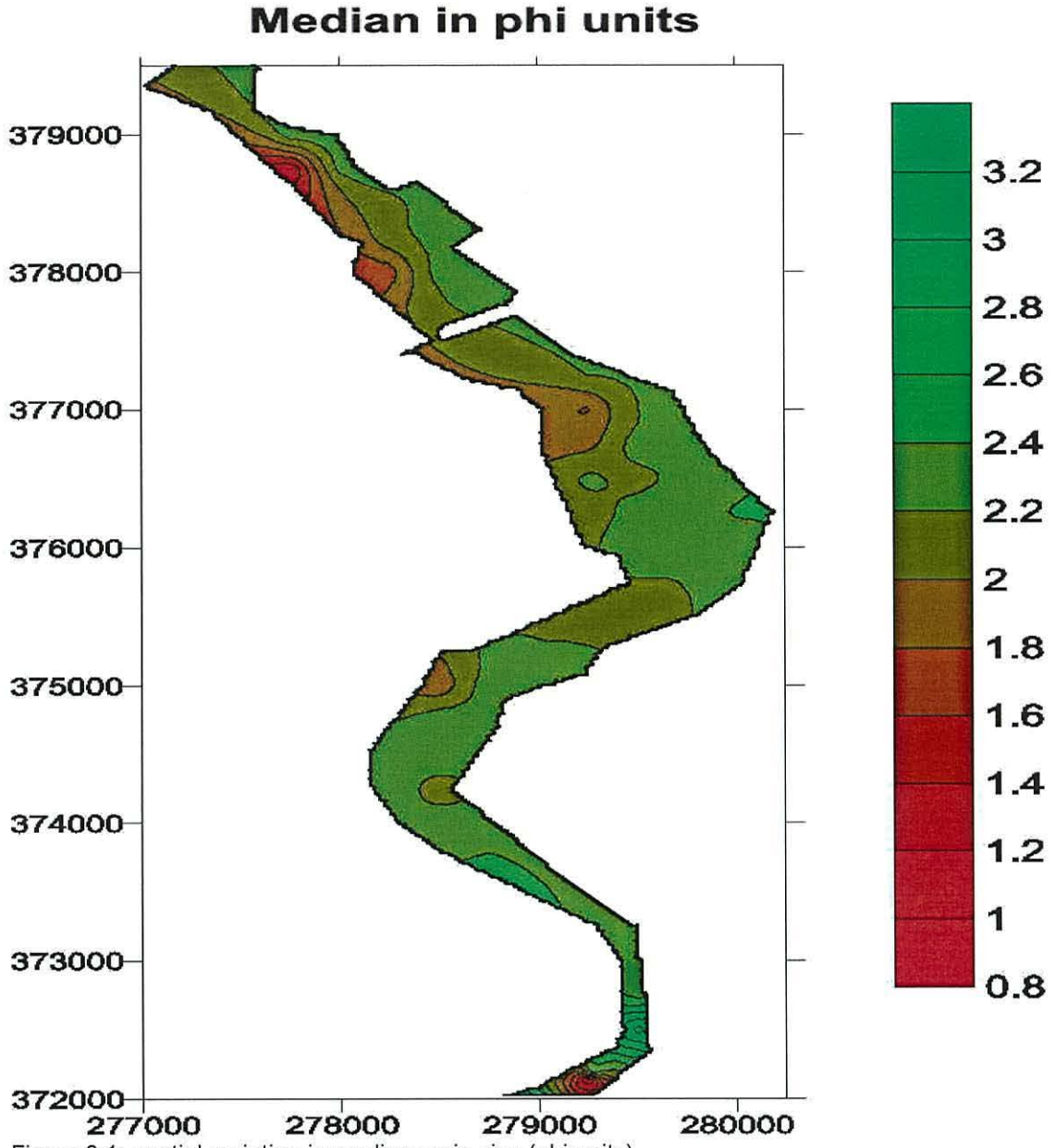

Figure 8.1: spatial variation in median grain size (phi units).

Figure 8.1 shows the range of median grain size (0.8 to 3.3 ϕ) within the main body of the estuary. Both the median and the graphic mean diameter, of all samples collected, spanned from -2.1 ϕ to 3.33 ϕ, a range of 5.4 ϕ. The range was divided into ten subgroups of 0.54 ϕ. The percentages of total sand sample in each subgroup were calculated. Figure 8.2 shows the frequency distribution of median and mean diameter of all the sand samples. Most of the sand samples fell into a narrow range of median/mean grain size.

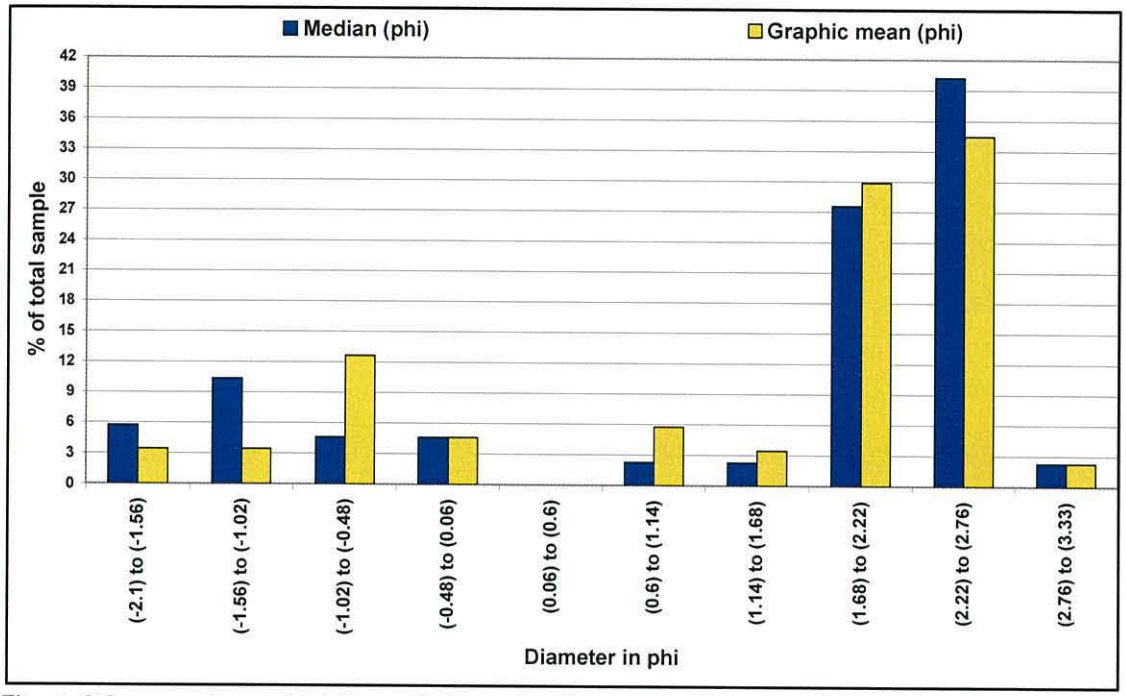

Figure 8.2: percentage of total sample in each subgroup – subgroups of diameter in phi, with blue representing the median, and orange the graphic mean.

8.1.2 Inclusive Standard Deviation (sorting)

Inman (1952) proposed the phi standard deviation (σ_ϕ) as a measure of sorting:

$$\sigma_\phi = (\phi_{84} - \phi_{16}) / 2 \qquad [8.2]$$

where ϕ_{16}, and ϕ_{84} are the phi diameters equal to the16th and 84th percentiles from the cumulative curve.

In 1957, Folk and Ward proposed a more efficient measure for sorting, the inclusive standard deviation (σ_I) defined as:

$$\sigma_I = [(\phi_{84} - \phi_{16}) / 4\} + \{(\phi_{95} - \phi_5) / 6.6] \qquad [8.3]$$

where ϕ_5, ϕ_{16}, ϕ_{84}, and ϕ_{95} are the phi diameters equal to the 5th, 16th, 84th and 95th percentiles from the cumulative curve.

Figure 8.3 shows the spatial variation of the inclusive standard deviation.

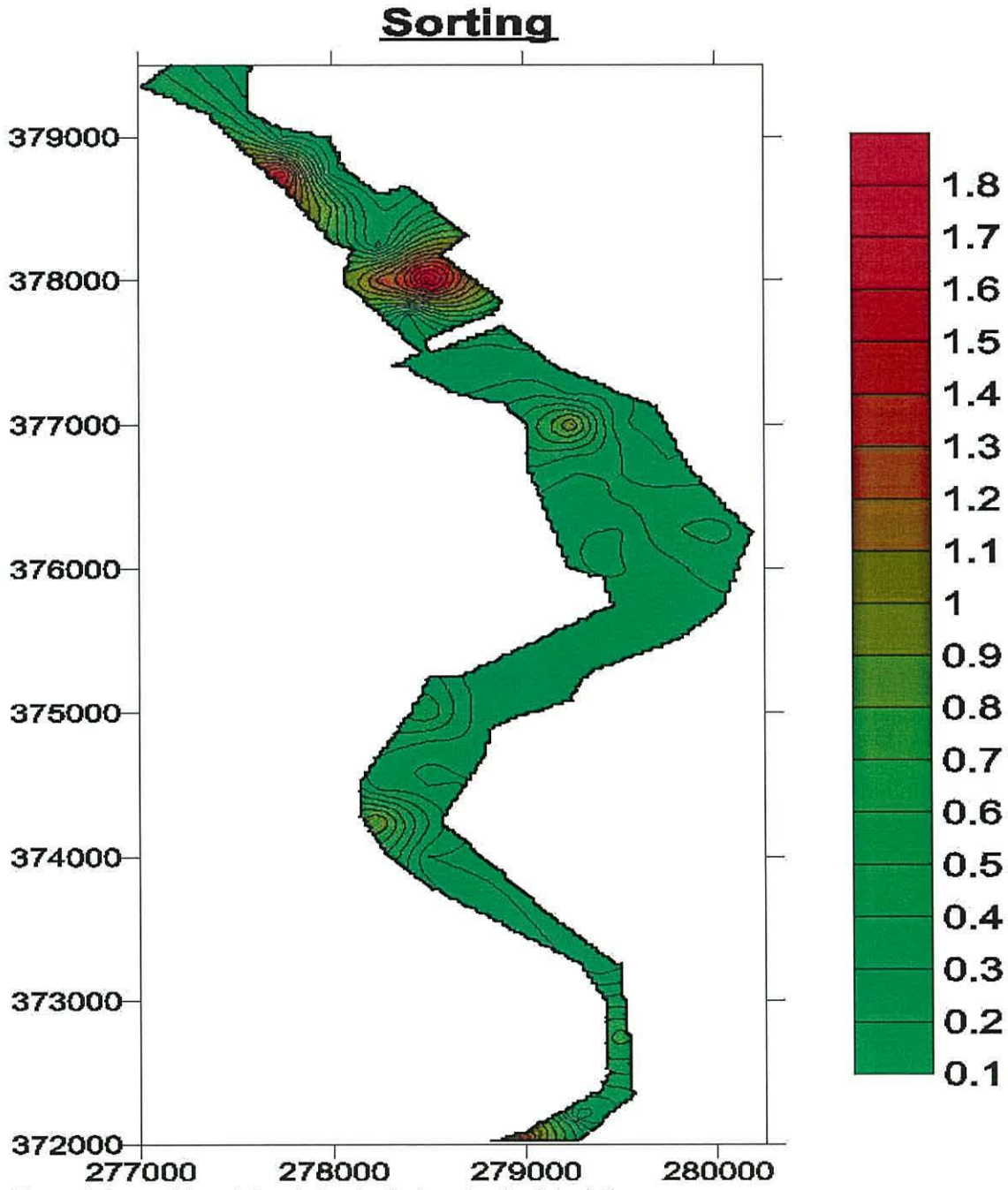

Figure 8.3: spatial variation in the inclusive standard deviation.

Figure 8.4 shows the frequency distribution of σ_I. The most common value of σ_I was < 0.35. Using Folk and Ward's (1957) definition, 53% of the sand samples where very well sorted.

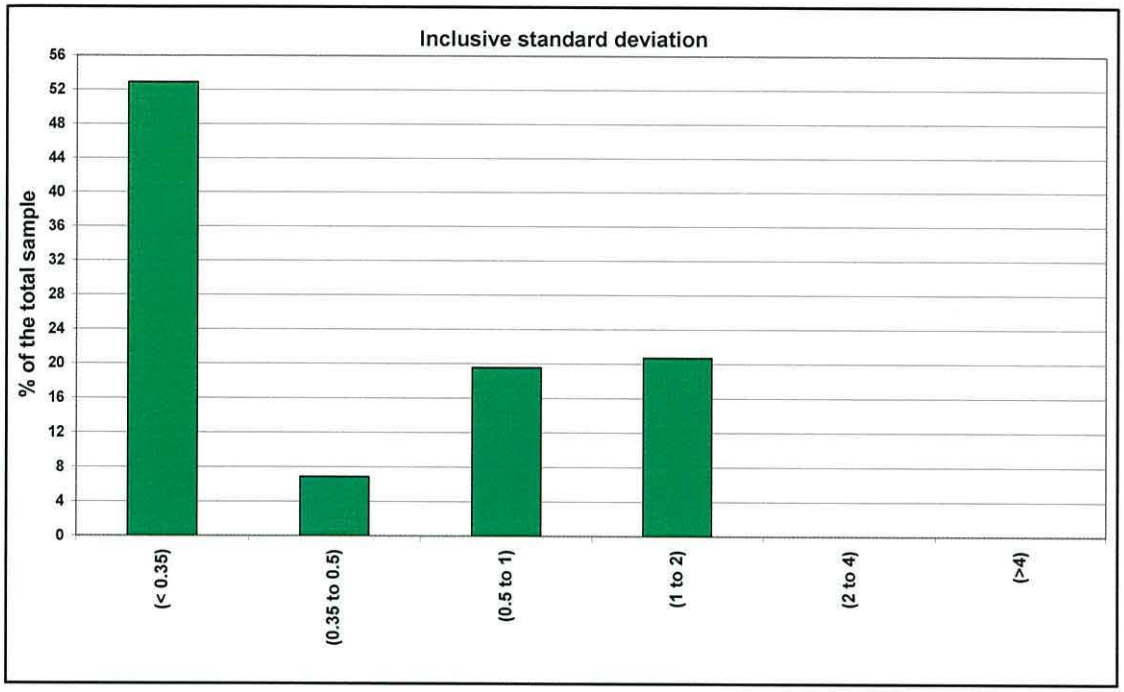

Figure 8.4: percentage of total sample in each subgroup – subgroups according to Folk and Ward, 1957: (<0.35) = very well sorted; (0.35 to 0.5) = well sorted; (0.5 to 1) = moderately sorted; (1 to 2) = poorly sorted; (2 to 4) = very poorly sorted; and (>4) = extremely poorly sorted.

8.1.3 Inclusive Graphic Skewness

Inman (1952) proposed two measures for skewness (α_ϕ and $\alpha_{2\phi}$):

$$\alpha_\phi = (\phi_{84} + \phi_{16} - 2*\phi_{50}) / (\phi_{84} - \phi_{16}) \quad [8.5]$$

and

$$\alpha_{2\phi} = (\phi_{95} + \phi_5 - 2*\phi_{50}) / (\phi_{84} - \phi_{16}) \quad [8.6]$$

In 1957, Folk and Ward combined equations 4.4 and 4.5 to obtain a more efficient measure of skewness, the inclusive graphic skewness (S_{KI}) defined as:

$$S_{KI} = [(\phi_{84} + \phi_{16} - 2*\phi_{50}) / 2*(\phi_{84} - \phi_{16})] + [(\phi_{95} + \phi_{5} - 2*\phi_{50}) / 2*(\phi_{95} - \phi_{5})] \quad [8.7]$$

Figure 8.5 shows the spatial variation of the inclusive graphic skewness.

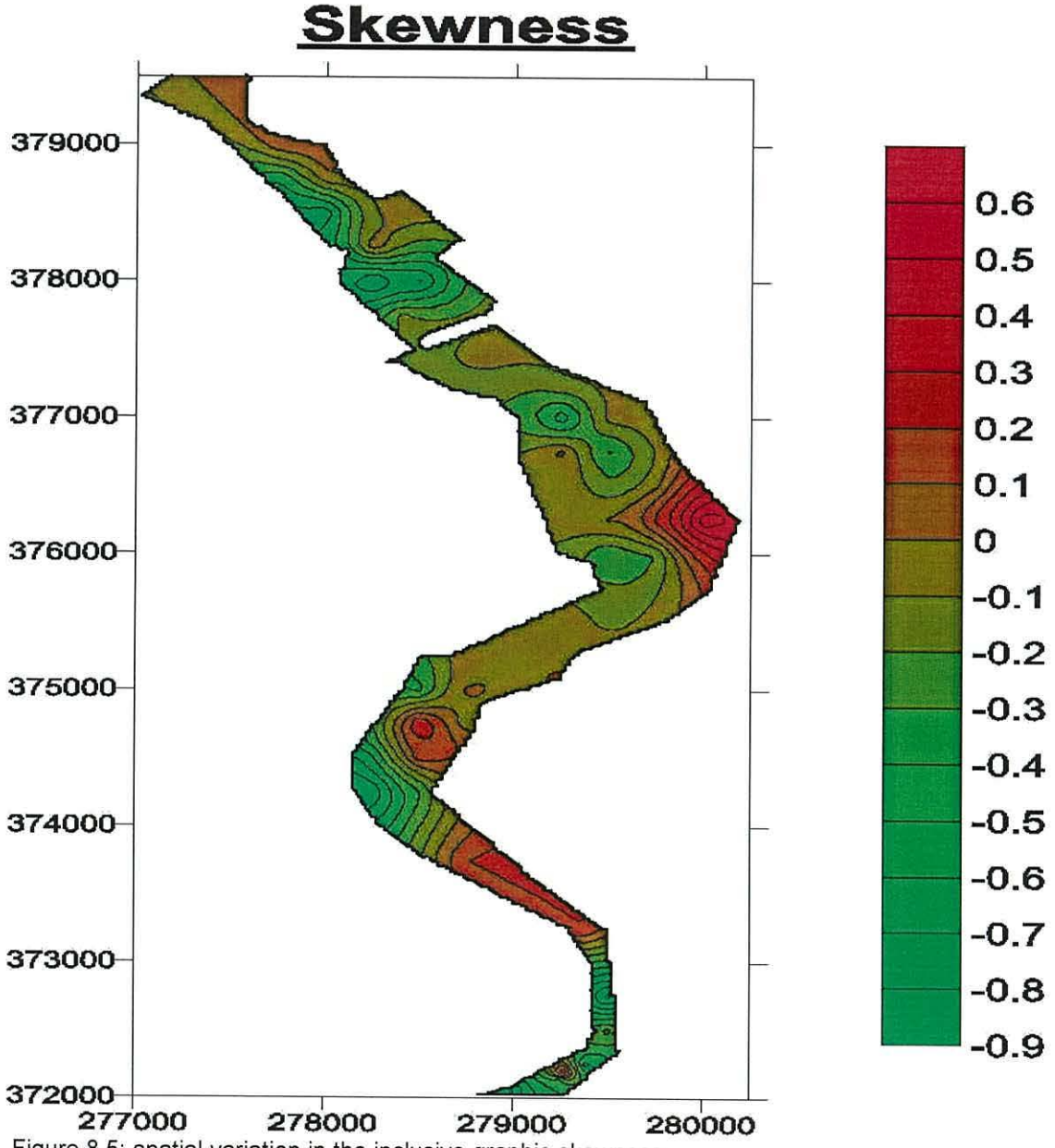

Figure 8.5: spatial variation in the inclusive graphic skewness.

The inclusive graphic skewness has absolute limits of -1 and +1. Figure 8.6 shows the frequency distribution of S_{KI}. The largest percentage of the sample was found to have an inclusive graphic skewness of -0.1 to 0.1. According to Folk and Ward's (1957) definition, this means that 30% of the sand samples were nearly symmetrically skewed.

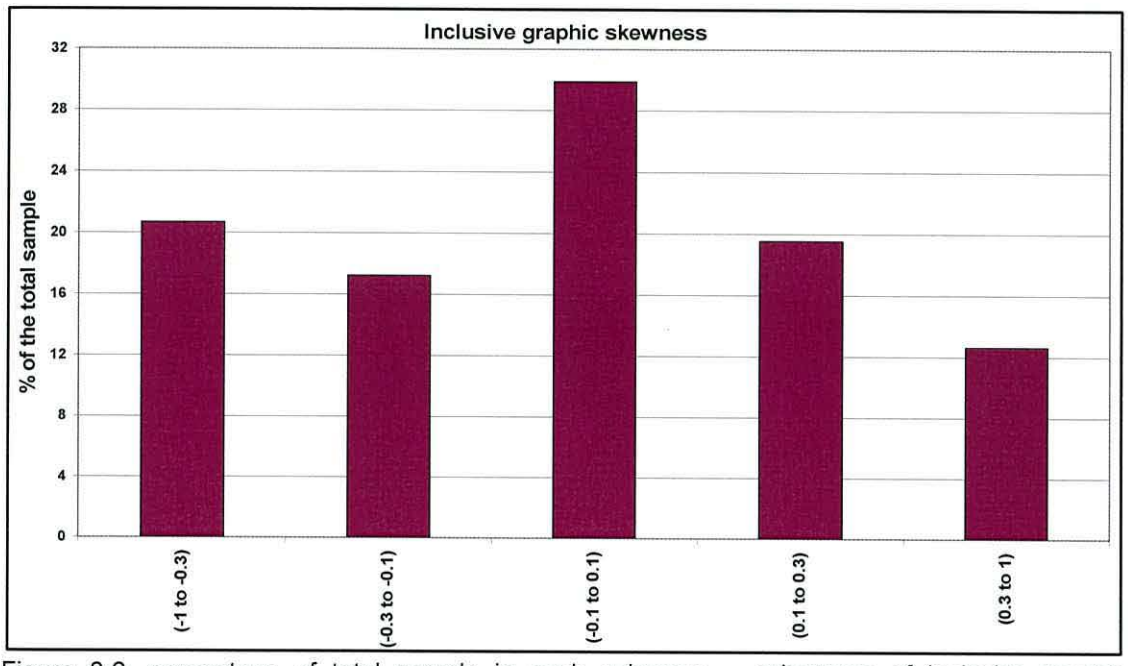

Figure 8.6: percentage of total sample in each subgroup – subgroups of inclusive graphic skewness. According to Fold and Ward (1957): (-1 to -0.3) = very negative; (-0.3 to -0.1) = negative; (-0.1 to 0.1) nearly symmetrical; (0.1 to 0.3) = positive; and (0.3 to 1) very positive.

8.1.4 Inclusive Graphic Kurtosis

Inman (1952) proposed a measure for kurtosis (β_ϕ):

$$\beta_\phi = [(\phi_{95} - \phi_5) - (\phi_{84} - \phi_{16})] / (\phi_{84} - \phi_{16}) \qquad [8.8]$$

In 1957, Folk and Ward produced another measure of kurtosis, the inclusive graphic kurtosis (K_G) defined as:

$$K_G = (\phi_{95} - \phi_5) / [2.44 * (\phi_{75} - \phi_{25})] \quad [8.9]$$

The inclusive graphic kurtosis has a mathematical minimum of 0.41 and a maximum (seemingly) of 8 (Dyer, 1986). Figure 8.7 shows the frequency distribution of K_G, highlighting two subgroups as dominant. The first subgroup was from 0.9 to 1.11 (30%) and the second subgroup was from 1.11 to 1.5 (29%). According to Folk and Ward's (1957) definition, this means that 32% of the total sand sample is mesokurtic, while 29% is leptokurtic.

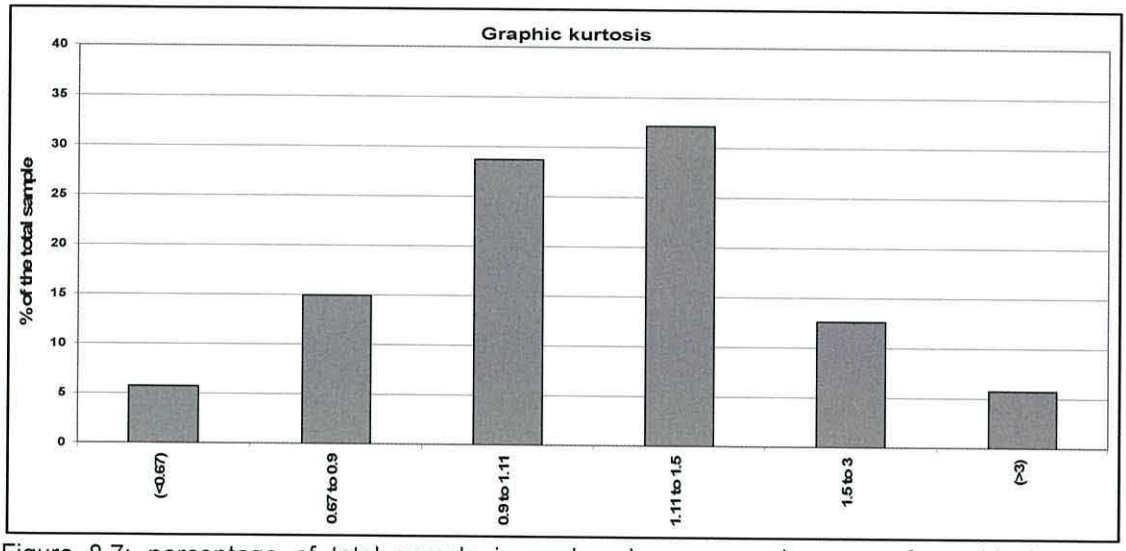

Figure 8.7: percentage of total sample in each subgroup – subgroups of graphic kurtosis. According to Fold and Ward (1957): (<0.67)) = very platykurtic; (0.67 to 0.9) = platykurtic; (0.9 to 1.11) mesokurtic; (1.11 to 1.5) = leptokurtic; (1.5 to 3) very leptokurtic; and (>3) = extremely leptokurtic.

8.1.5 Results After Microscopy

After obtaining the 0.18 mm fraction from each of the 42 sand samples, the samples were divided into three groups, according to their origin: bay; estuary and river. From each sand sample 126 grains from the 0.18 mm fraction were classified into 7 subgroups. The subgroups were based on the characterisation of

the grains and were: clear quartz/feldspar; milky quartz/feldspar; iron stained quartz/feldspar; lithic; dark coloured; shell fragments; and others.

The results presented here are split into two parts. The first part presents the overall results of the analysis, whilst the second part presents a representative sample from each location group (bay, estuary, and river).

8.1.5.1 Overall Results

Figure 8.8 shows the overall frequencies of the seven mineralogical subgroups in the bay, estuary and river samples.

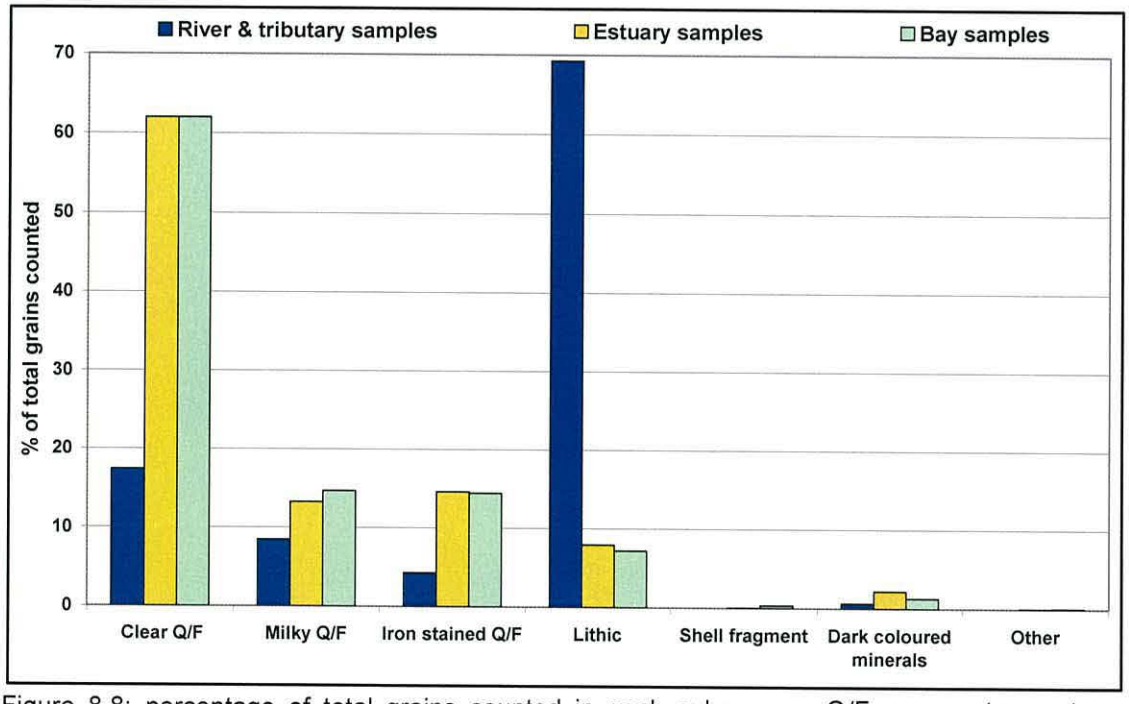

Figure 8.8: percentage of total grains counted in each subgroup – Q/F represents quartz or feldspar grains.

The dominant subgroup for the river samples is that characterised by lithic grains, whilst the dominant subgroups for both estuary and bay samples are those characterised by clear quartz/feldspar grains.

8.1.5.2 River, Estuary and bay Samples

River

Sand sample No 5 is representative of the samples taken from the river and the tributaries see Figure 8.9. The largest percentage (88%) of the total grains counted were characterised as lithic.

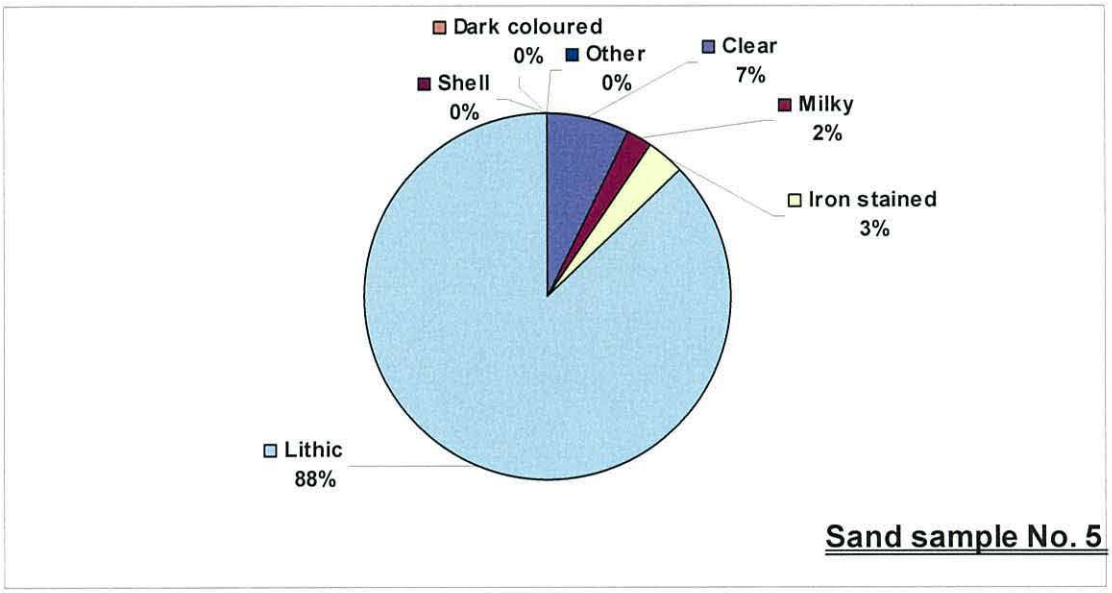

Figure 8.9: pie chart of the percentages making up the 126 grains of sand sample No 5. Clear, milky and iron stained refer to quartz and/or feldspar grains.

Estuary

Sand sample No 39 is representative of the samples taken from the estuary, see Figure 8.10. The largest percentage (71%) of the total grains counted were characterised as clear quartz/feldspar. Notice that this sample is only 5% lithic.

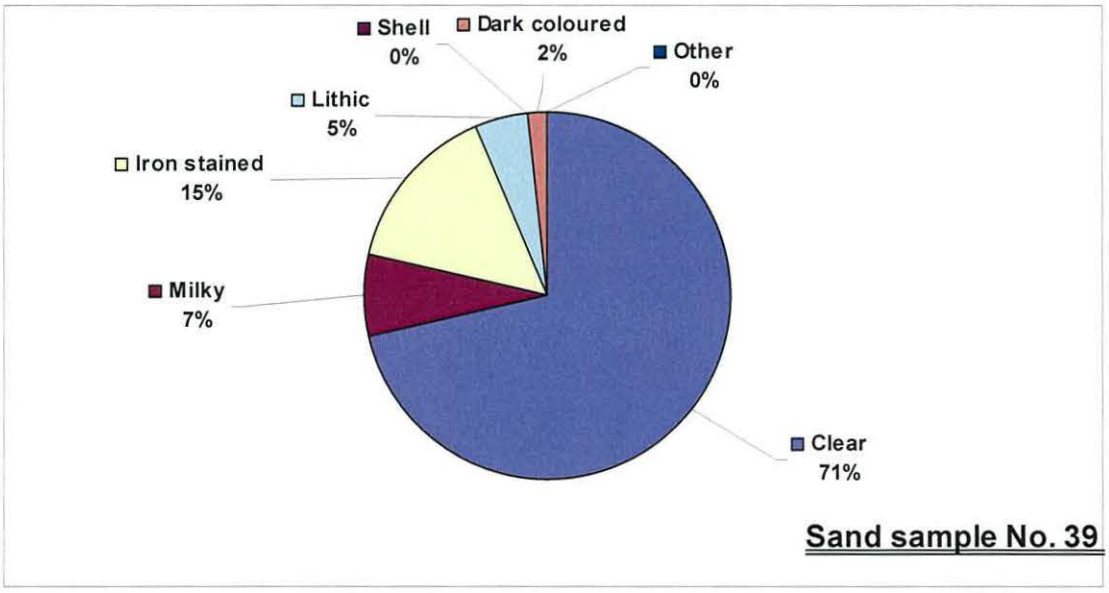

Figure 8.10: pie chart of the percentages making up the 126 grains of sand sample No 39. Clear, milky and iron stained refer to quartz and/or feldspar grains.

Bay

Sand sample No 91 is representative of the samples taken from the bay, see Figure 8.11. The largest percentage (75%) of the total grains counted were characterised as clear quartz/feldspar. Notice that this sample is only 3% lithic.

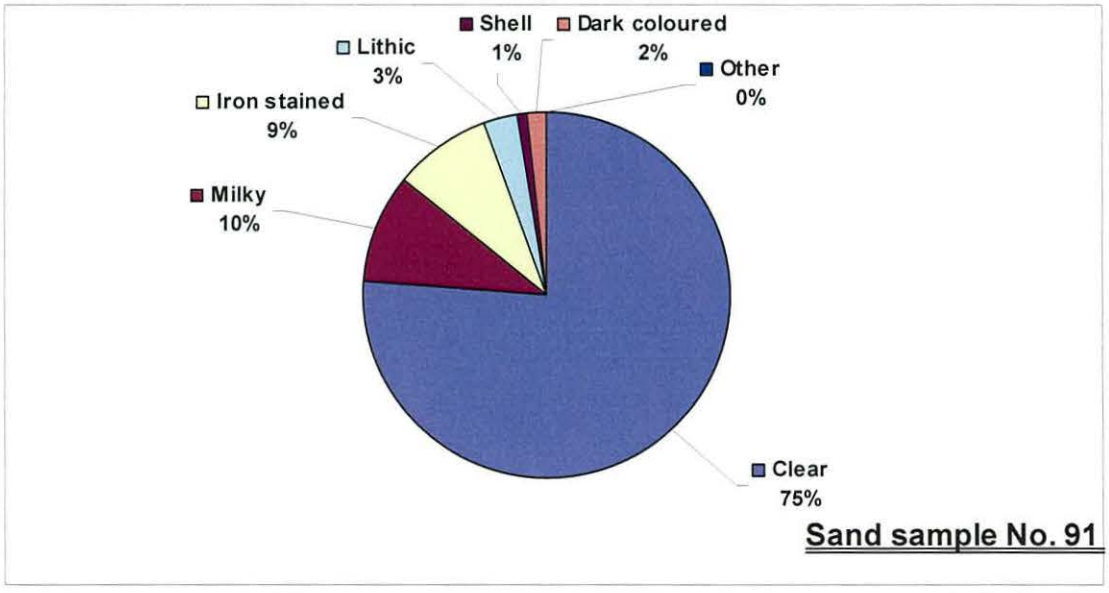

Figure 8.11: pie chart of the percentages making up the 126 grains of sand sample No 5. Clear, milky and iron stained refer to quartz and/or feldspar grains.

8.2 Sediment Provenance – Statistical Analysis

The estuarine sand has two possible provenances: Conwy bay and the Conwy River. The bay sands are characterised by quartz/feldspar (clear, milky, and iron stained), whilst the fluvial sands are characterised by lithic fragments.

Statistical analysis (one- way ANOVA in MINITAB) of the data set was carried out to determine the provenance. This was done by using the mean values of the frequency of quartz/feldspar or lithic fragments found in each provenance group.

8.2.1 Lithic Fragment Component

The frequency of lithic fragments found in each provenance group was compared with the other two groups. The null hypothesis is that the two groups chosen for comparison have the same mean frequency of lithic fragments.

8.2.1.1 River and Bay Samples

One-way ANOVA: Lithic versus Location (location 1 = river, location 3 = bay).

```
Analysis of Variance for Lithic
Source      DF        SS        MS        F        P
Location     1     36433     36433    54,42    0,000
Error       22     14727       669
Total       23     51160

                                  Individual 95% CIs For Mean
                                  Based on Pooled StDev
Level        N      Mean     StDev  --+---------+---------+---------+----
1           11     87,27     34,30                              (----*----)
3           13      9,08     15,72  (----*----)
                                  --+---------+---------+---------+----
Pooled StDev =     25,87              0        30        60        90
```

Where: DF = degrees of freedom, SS = sum of squares, MS = mean square, F = probability distribution, P = p-value, and N = non-missing values (number of values in each group).

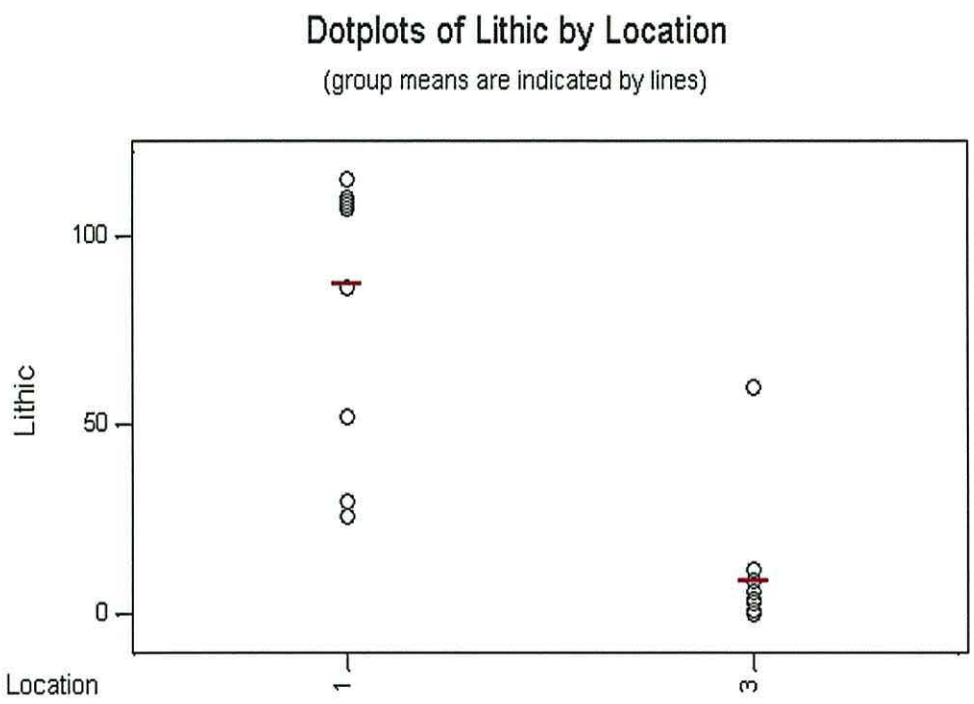

Figure 8.12: showing the mean (red line) amount of lithic component in each location group: location 1 = river, location 3 = bay.

The P-value is 0.000 dismissing the null hypothesis. The difference in the mean values is great; mean value of ~ 87 for the river samples and ~ 9 for the bay samples.

8.2.1.2 Estuary and River Samples

One-way ANOVA: Lithic versus Location (location 1 = river, location 2 = estuary).

```
Analysis of Variance for Lithic
Source      DF        SS        MS         F         P
Location     1     37959     37959    63,75     0,000
Error       24     14291       595
Total       25     52250

                                    Individual 95% CIs For Mean
                                    Based on Pooled StDev
Level        N      Mean     StDev  --+---------+---------+---------+----
1           11     87,27     34,30                              (----*----)
2           15      9,93     13,44   (---*----)
                                    --+---------+---------+---------+----
Pooled StDev =     24,40               0         30        60        90
```

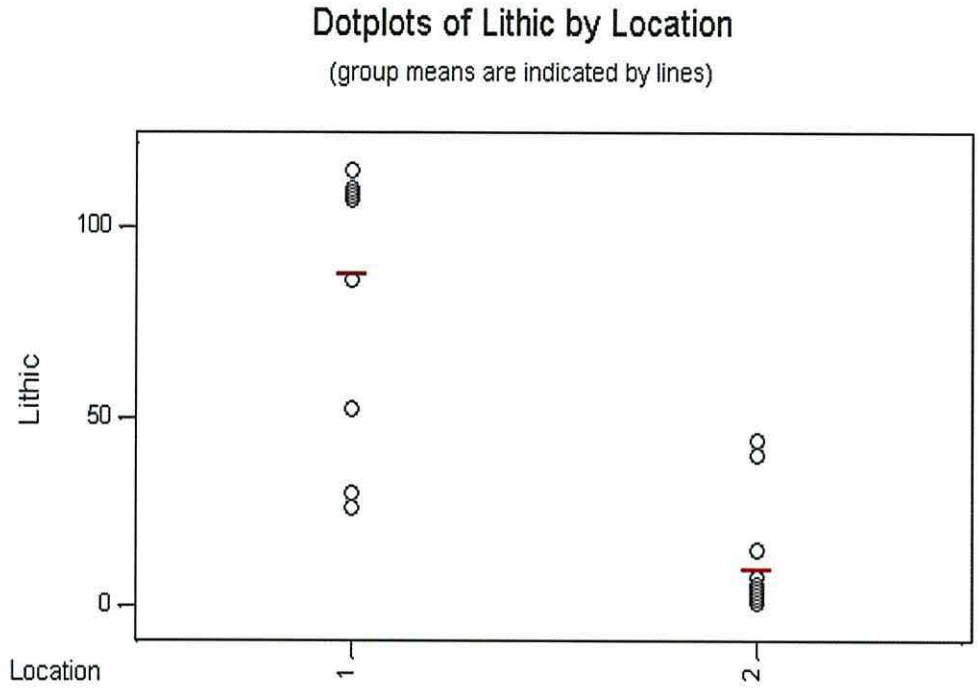

Figure 8.13: showing the mean amount of lithic component in each location group: location 1 = river, location 2 = estuary.

The P-value is 0.000 dismissing the null hypothesis. The difference in the mean values is great; mean value of ~ 87 for the river samples and ~ 10 for the estuary samples.

8.2.1.3 Estuary and Bay Samples

One-way ANOVA: Lithic versus Location (location 2 = estuary, location 3 = bay).

```
Analysis of Variance for Lithic
Source      DF        SS        MS         F         P
Location     1         5         5      0,02     0,878
Error       26      5494       211
Total       27      5499

                                      Individual 95% CIs For Mean
                                      Based on Pooled StDev
Level        N      Mean     StDev  ---------+---------+---------+-------
2           15      9,93     13,44     (---------------*--------------)
3           13      9,08     15,72   (----------------*----------------)
                                      ---------+---------+---------+-------
Pooled StDev =     14,54                    5,0      10,0      15,0
```

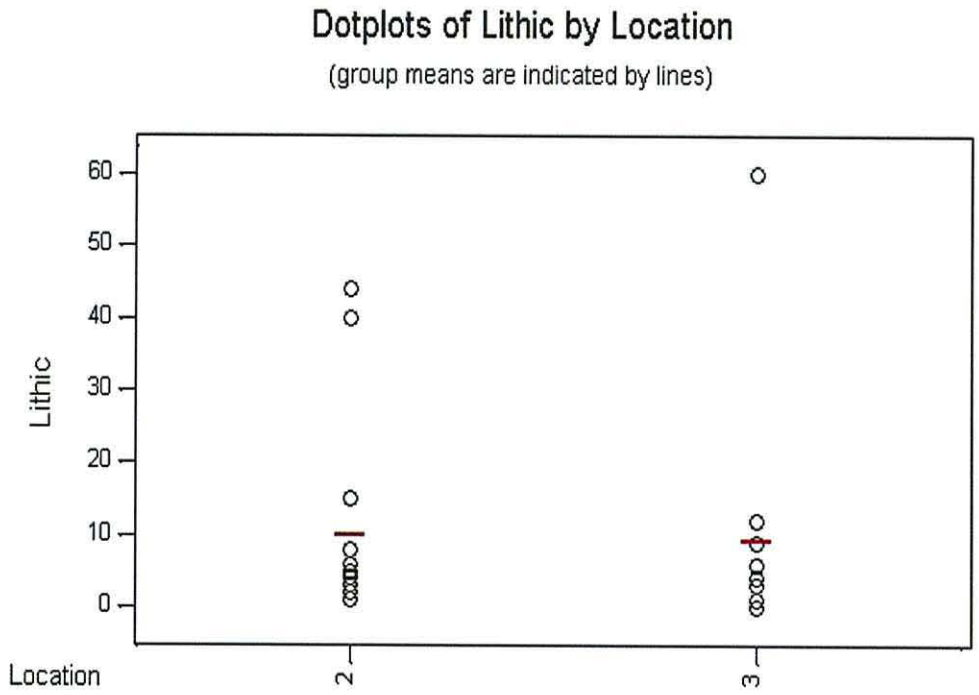

Figure 8.14: showing the mean amount of lithic component in each location group: location 2 = estuary, location 3 = bay.

The null hypothesis is accepted as the P-value is 0.878 (>0.05). The mean values are almost the same; mean value of ~ 10 for the estuary samples and ~ 9 for the bay samples.

8.2.2 Quartz/feldspar Component

The amount of quartz/feldspar found in each provenance group was compared with the other two groups. The null hypothesis is that the two groups chosen for comparison have the same mean amount of quartz/feldspar (Q/F).

8.2.2.1 River and Bay Samples

One-way ANOVA: Q/F versus Location (location 1 = river, location 3 = bay).

```
Analysis of Variance for Q/F
Source      DF        SS        MS         F        P
Location     1     35199     35199     52,74    0,000
Error       22     14683       667
Total       23     49882

                                    Individual 95% CIs For Mean
                                    Based on Pooled StDev
Level        N      Mean     StDev  ---+---------+---------+---------+---
1           11     37,91     34,15  (-----*----)
3           13    114,77     15,87                        (----*----)
                                    ---+---------+---------+---------+---
Pooled StDev =     25,83              30        60        90       120
```

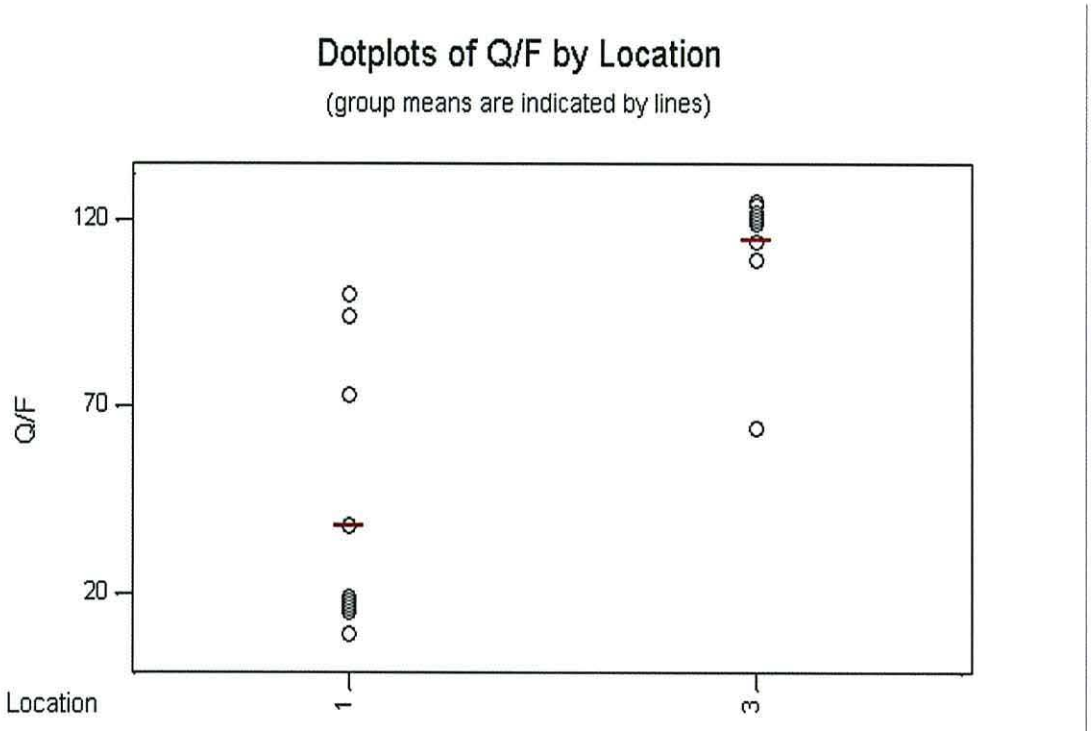

Figure 8.15: showing the mean amount of quartz/feldspar component in each location group: location 1 = river, location 3 = bay.

The P-value is 0.000 dismissing the null hypothesis. The difference in the mean values is great; mean value of ~ 38 for the river samples and ~ 115 for the bay samples.

8.2.2.2 Estuary and River Samples

One-way ANOVA: Q/F versus Location (location 1 = river, location 2 = estuary).

```
Analysis of Variance for Q/F
Source      DF        SS        MS         F         P
Location     1     35975     35975     59,89     0,000
Error       24     14417       601
Total       25     50392

                                    Individual 95% CIs For Mean
                                    Based on Pooled StDev
Level        N      Mean     StDev  ---+---------+---------+---------+---
1           11     37,91     34,15    (----*----)
2           15    113,20     14,03                        (----*---)
                                    ---+---------+---------+---------+---
Pooled StDev =     24,51              30        60        90       120
```

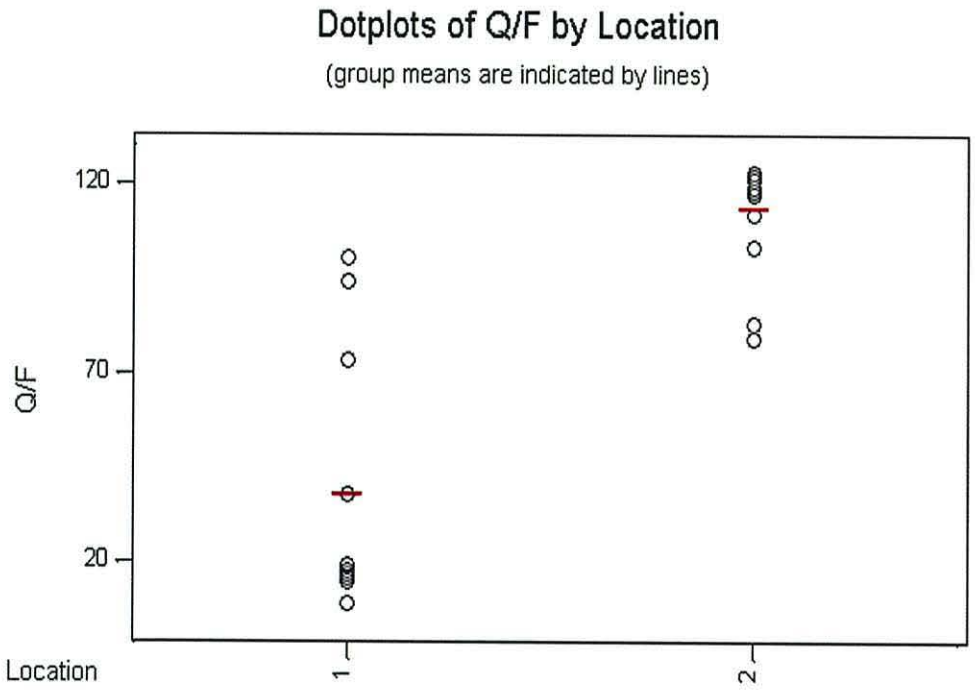

Figure 8.16: showing the mean amount of quartz/feldspar component in each location group: location 1 = river, location 2 = estuary.

The P-value is 0.000 dismissing the null hypothesis. The difference in the mean values is great; mean value of ~ 38 for the river samples and ~ 113 for the estuary samples.

8.2.2.3 Estuary and Bay Samples

One-way ANOVA: Q/F versus Location (location 2 = estuary, location 3 = bay).

```
Analysis of Variance for Q/F
Source      DF        SS        MS         F         P
Location     1        17        17      0,08     0,783
Error       26      5779       222
Total       27      5796

                                    Individual 95% CIs For Mean
                                    Based on Pooled StDev
Level        N      Mean     StDev  ----------+---------+---------+------
2           15    113,20     14,03    (--------------*--------------)
3           13    114,77     15,87      (----------------*----------------)
                                    ----------+---------+---------+------
Pooled StDev =    14,91                 110,0     115,0     120,0
```

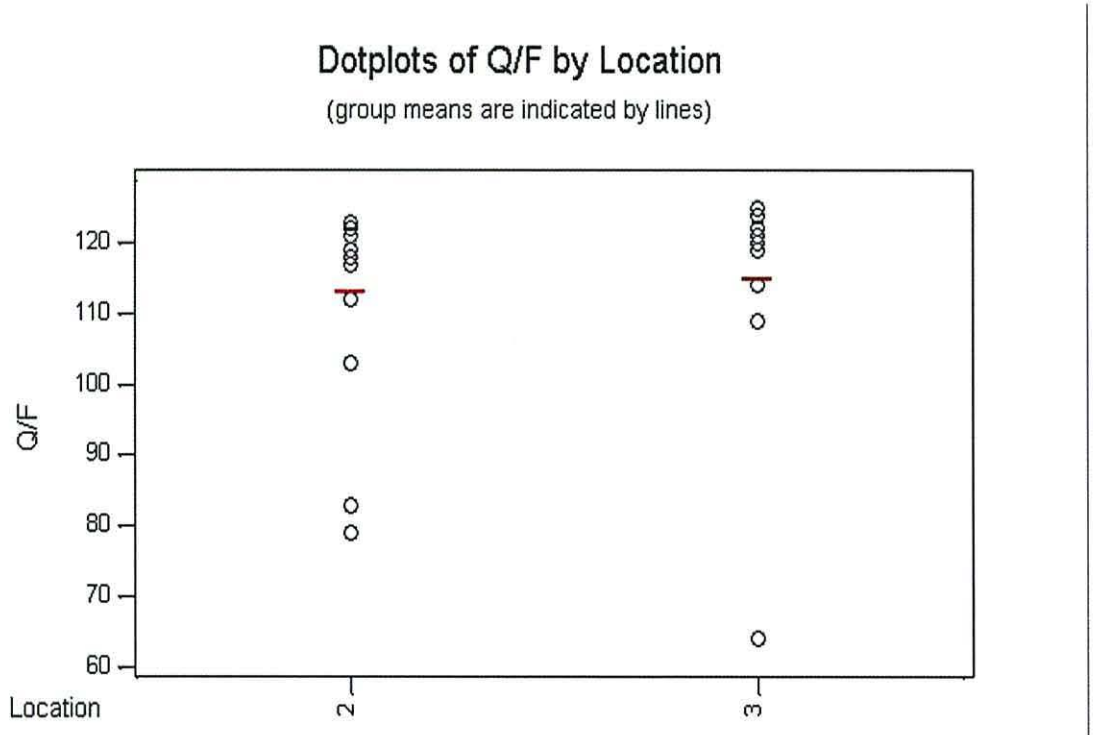

Figure 8.17: showing the mean amount of quartz/feldspar component in each location group: location 2 = estuary, location 3 = bay.

The null hypothesis is accepted as the P-value is 0.783 (>0.05). The mean values are almost the same; mean value of ~ 113 for the estuary samples and ~ 115 for the bay samples.

8.2.3 Sediment Provenance: Conclusion

The modal grain diameter, for the estuarine sands, was 180 μm (see Figure 3.10). From Figure 8.10, it can be seen that the estuarine sands (at the modal grain size) are made-up of 70 – 90% quartz/feldspar particles. The Conwy Bay samples are statistically identical to the estuarine samples, whilst the Conwy River samples are radically different. The comparison of sand samples – by means of pie charts – and the statistical analysis suggest that the lithic component of the estuarine sands is mostly derived from the river, whilst the quartz/feldspar component is derived from the bay. Since the majority, of the sands, are made up of quartz grains, it can be concluded that the provenance of these sands is Conwy Bay.

8.3 Net Sediment Transport Paths

8.3.1 Background Theory

The identification of sediment transport paths is of major importance in many sedimentological studies (le Roux, 1994). Within any sedimentary environment, grain-size trends may be present. These trends are in response to a variety of processes, such as abrasion, selective transport, and the addition of locally produced sediment particles (Gao and Collins, 1992). Many attempts have been made to relate grain-size trends to sediment transport paths, using a single grain-size parameter (for examples see Gao and Collins, 1992; le Roux, 1994).

McLaren (1981) considered a combination of parameters and concluded that the mean grain size, sorting and skewness of a sedimentary deposit are dependent on the sediment grain size distribution of its source and the sedimentary processes of erosion, selective deposition and total deposition.

In 1985, McLaren and Bowels (McLaren and Bowels, 1985) proposed a hypothesis that related two cases of grain-size trends to net transport paths. These two trends were:

- Case I. Sediments become finer, better sorted and more negatively skewed in the direction of transport.
- Case II. Sediments become coarser, better sorted and more positively skewed in the direction of transport.

McLaren and Bowles (1985)	Case I: $\sigma_2^2 < \sigma_1^2$, $\mu_2 > \mu_1$ and $Sk_2 < Sk_1$
	Case II: $\sigma_2^2 < \sigma_1^2$, $\mu_2 < \mu_1$ and $Sk_2 > Sk_1$
Gao and Collins (1992)	Case I: $\sigma_2^2 \leq \sigma_1^2$, $\mu_2 \geq \mu_1$ and $Sk_2 \leq Sk_1$
	Case II: $\sigma_2^2 \leq \sigma_1^2$, $\mu_2 \leq \mu_1$ and $Sk_2 \geq Sk_1$

Table 8.1: showing the slight differences in the definitions of the two trends; where σ^2 is the sorting, μ is the mean grain-size, and Sk is the skewness, all in phi units.

The above table defines the two grain-size trends related to net transport. Note that in this project the definitions by Gao and Collins (1992) are used.

Gao and Collins (1992), argue that the method proposed by McLaren and Bowels, is one-dimensional in character. This argument led Gao and Collins to suggest a two-dimensional treatment of data, which could produce, more meaningful results. This implied using their slightly modified Case I and II, to define a grid of trend vectors.

8.3.2 Defining the Trend Vectors

The Gao and Collins (1990) method was used to define the trend vectors. First, each sand sample was compared, in terms of its grain-size parameters, with its immediate neighbouring sample.

Vectors of unit length were drawn in for each Case I situation, with the direction of the vector lying from a higher to a lower sorting coefficient. Such vectors were then summed, so that only a single vector was left for each sampling site.

Following that, an average was taken for each site. This was done by averaging the vectors of a specific site and its immediate neighbouring sites (see Figure 8.18).

The whole procedure was repeated for the Case II patterns between samples, see Figure 8.19.

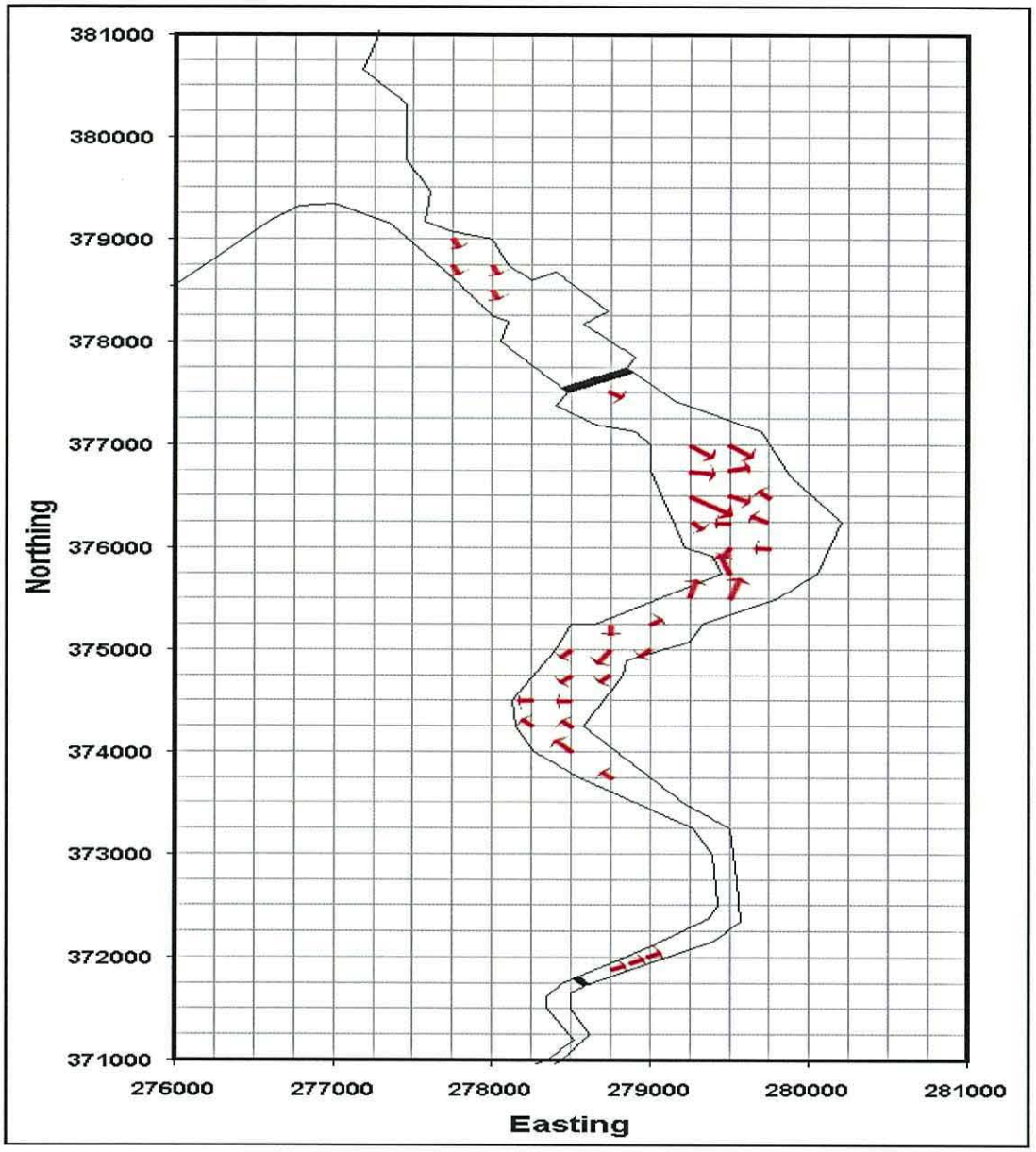

Figure 8.18: defined trend vectors for Case I – see text for explanation.

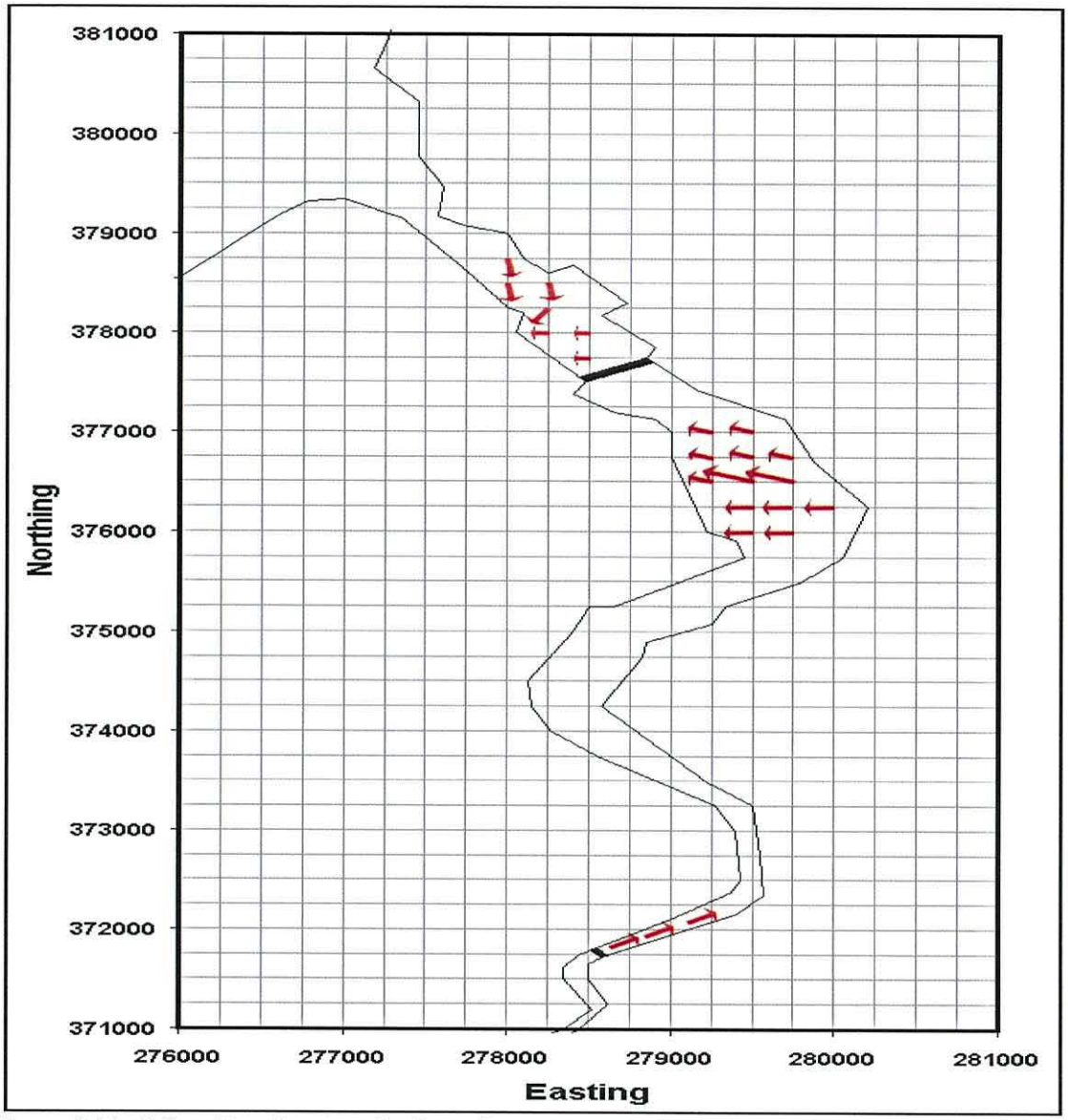

Figure 8.19: defined trend vectors for Case II – see text for explanation.

8.3.3 Defining the net transport paths

Figures 8.18 and 8.19 above, present the trend vectors associated with the transport paths. In order to obtain the net transport paths, more vector summation was done. This time ten points were selected (for both Case I and II) and all vectors within a set perimeter were summed to produce one vector for each of the ten points. Hence, defining the net transport paths, see Figures 8.20 and 8.21.

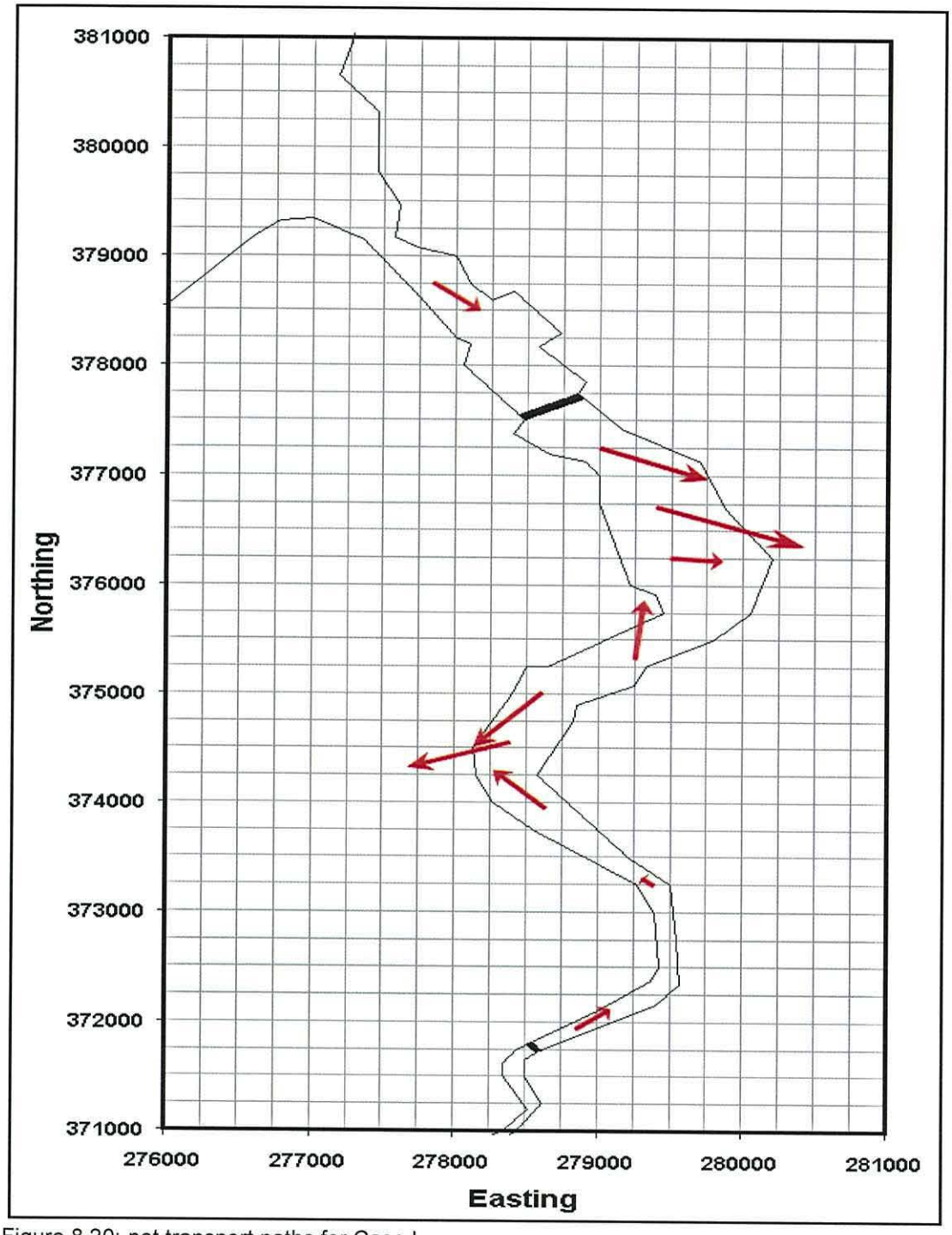

Figure 8.20: net transport paths for Case I.

Note that for figure 8.20, the length of the vectors is the result of vector summation, and is arbitrary.

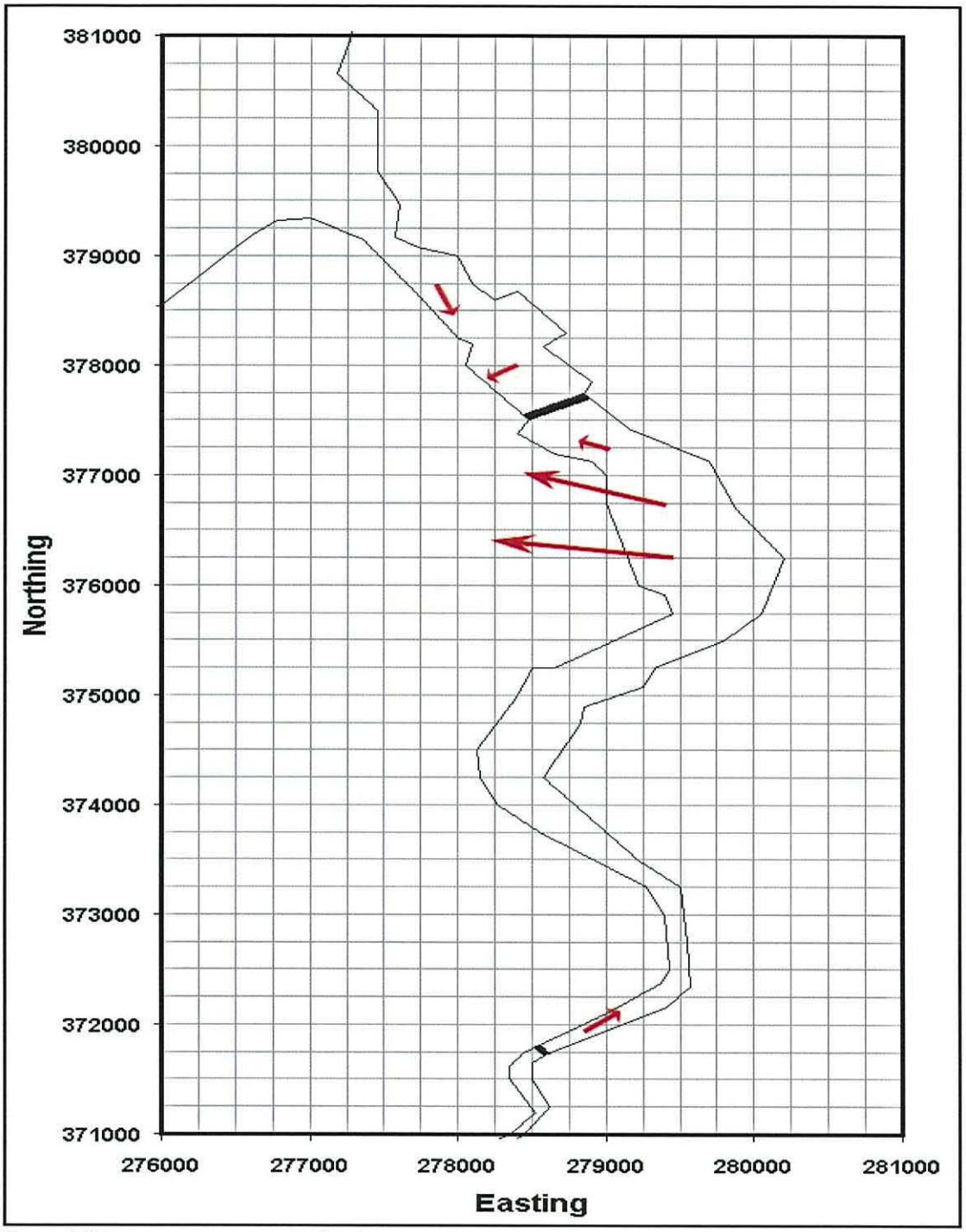

Figure 8.21: net transport paths for Case II.

Note that for figure 8.21, the length of the vectors is the result of vector summation, and is arbitrary.

8.3.4 Discussion and Conclusions

Section 8.3, investigated the net sand transport paths by comparing grain size characteristics. From figure 8.20, the transport direction at each anchor station was:

Station No	Easting	Northing	Transport direction
MS1	278700	377250	up-estuary, at an azimuth of ~110°
MS2	278750	371835	down-estuary, at an azimuth of ~55°
MS3	277600	379000	up-estuary, at an azimuth of ~120°
MS4	278329	374736	up-estuary, at an azimuth of ~230°
MS5	279271	375347	down-estuary, at an azimuth of ~15°

These transport directions agree with the total net sediment transport directions (see Figure 7.34), suggesting that the method used in section 8.3 is valid to an extent.

The velocity readings during the moored surveys had the following net flow directions:

Station No	Down-estuary direction	Up-estuary direction
MS1	~295°	~115°
MS2	~65°	~245°
MS3	~330°	~150°
MS4	~25°	~205°
MS5	~80°	~260°

Although, the azimuths of the sand transport are not exactly the same as the azimuths of the flow, they are very similar (note that the difference in azimuths could be a result of error produced by the method in 8.3). From this similarity of azimuths, it can be concluded that the method used in this section produced meaningful results.

9 Summary and Conclusions

In respect to the specific objectives (stated in chapter one), this chapter attempts to summarise the main points of the thesis.

9.1 Study Site and Methods

- The Conwy Estuary is the largest and most westerly of the major estuaries of the North Wales coast, lying on a north-south axis. It is considered to be well-mixed and macrotidal in nature, with a tidal range varying between 3 and 7 m, and a daily average river discharge of about 25 m^3s^{-1}.

- During this project, the temporal and spatial variations of suspended particulate matter (SPM) properties were investigated. Also investigated, was the provenance and the transport of estuarine sands. The survey area occupied the entire Conwy estuary extending from the Deganwy beacon at the mouth to Llanrwst in the upper reaches.

- In order to obtain the SPM properties, a CTD profiler, an OBS, a Transmissometer, and a LISST profiler were deployed in both moored and spatial surveys. During the moored surveys, a current meter was also used for obtaining flow velocities.

- Moored surveys were carried out at five different locations within the main body of the estuary. In total there were about 25 deployments at each location, taking place every 30 minutes over a period of about 12.5 hours.

- In total, 26 spatial surveys were carried out. They started as far up estuary as it was physically possible on each day, and finished down estuary at approximately 0.9 km from the mouth (following the main channel). Each axial

survey consisted of about 25 profiling stations spread out over a typical range of about 14 to 20 km.

- Sand samples from the mouth, body, and head of the estuary were collected using a grab sampler, deployed from a Zodiac inflatable. Sampling was done on a 0.25 x 0.25 km grid.

- Sand samples from the tributaries, the river and the bay were also collected in order to establish the provenance of the estuarine sand.

9.2 Temporal Variations in SPM Properties over a Tidal Cycle

- The percentage of clay-sized particles remained constant at about 2%. The percentage of silt-sized particles was on average about 31%, whilst the percentage of sand-sized particles was on average about 67%.

- The SPM particle density (ρ_f) values in surface waters were found to be in the range of 1078 to 1319 kgm^{-3}, which was too low to be individual quartz sand grains (density of 2650 kgm^{-3}) and were therefore flocs.

- Three hours before low water the combined ebb and river flow was in a down-estuary direction with a surface mean velocity of 0.6 ms^{-1}; salinity and the SSC were decreasing. During this phase (LW_{-3h}), the percentage of clay-sized fraction was at a maximum (2.2%), whilst the SPM median diameter was at a minimum (105 μm), possibly due to increased turbulence rupturing flocs.

- At low water the salinity reached a minimum (9), SSC decreased to about 34 mgl^{-1}. Although the tide flow was at a slack the surface water was still flowing down-estuary at about 0.4 ms^{-1}, as a result of river flow. The decreased velocities allowed the formation of flocs and partial sedimentation of suspended

mater. As a result there was an increase in SPM median diameter, and in the percentage of sand-sized fraction.

- Three hours after low water (flood tide) the surface flow was in the up-estuary direction (0.4 ms^{-1}). SSC reached a maximum (average surface value of 47 mgl^{-1}). Particle effective density (ED) reached a minimum, whilst median particle diameter slightly increased. The percentage of sand-sized fraction also increased. The increase in particle size and decreased ED could be due to resuspension of low density larger particles.

- At high water slack the mean surface velocity approached zero. The salinity (18), median diameter (124 μm), and percentage of sand-sized fraction (73%) all reached their maximum. On the other hand, the SSC (19 mgl^{-1}), and the percentages of silt and clay sized particles (25% and 1.8% respectively) reached their minimum. From the above, it was concluded that at slack water turbulence reached a minimum allowing the formation of bigger flocs, while at the same time there was sedimentation so that SSC reduced.

- The total cumulative flood flux, at all 5 anchor stations, (10.76 $kgm^{-1}Flood^{-1}$, up-estuary) was twice the total cumulative ebb flux (5.05 $kgm^{-1}Ebb^{-1}$, down-estuary). This meant that the net suspended sediment flux (5.71 kgm^{-1} per tidal cycle) measured at the 5 stations, was in the up-estuary direction.

9.3 Longitudinal (Spatial) Variations in SPM Properties

The estuary was divided into 3 longitudinal sections based on the longitudinal variations in surface salinity (surface values from 16 surveys). Each section was characterised by a set of SPM properties (see Figure 5.38):

- Section one – the upper estuary (section mean salinity of 0). In this section the median diameter (119 μm), the ED (82 kgm^{-3}), the high percentage of the

sand-sized fraction (68%) characterise SPM supplied from river transport (since this section was landward of the salt intrusion).

- Section two – the ETM region (section mean salinity of 5). In this section the median particle diameter (98 μm), the ED (135 kgm^{-3}), and the lower percentage of the sand-sized fraction (64%) suggest that any flocs in existence were being broken down by residual turbulence or the source of particles to the ETM supplied smaller flocs. The average surface SSC was 43 mgl^{-1}.

- Section three – the lower estuary (section mean salinity of 27). In this section, the median floc size (114 μm) was similar to that in the upper estuary, but with twice the floc density (159 kgm^{-3}). The increase in median diameter and sand-sized fraction (67%) may either be indicating a regional decrease in turbulence at high slack water – allowing the formation of bigger flocs, or that these larger particles were of different origin – i.e. sourced from offshore.

9.4 Location and Strength of the ETM

- The ETM of the Conwy Estuary was observed to be in the region between 8 and 19 km from the mouth, approximately one hour after high water at Conwy. The main ETM region is narrow (between 50 and 250 m), shallow (average depth of around 3 m at local high water), and has sand-banks and small islands narrowing the main channel even more.

- Formation of the ETM: Since the ETM forms in the low salinity water near the top of the estuary, and this water is flushed out during the ebb, a new ETM must form on the next flood. The rising flood tide, advancing rapidly across intertidal shoals, entrains particulate matter. The turbid front, pushed up the estuary, becomes the ETM.

- From section 5.4.2.1, it was concluded that the factor controlling the ETM location changes with the season. In autumn and winter, the river discharge controlled the location, because of higher discharge. In spring, the dominant control was the tidal range, suggesting input of biological material due to tidal resuspension and/or advection. Whilst in the summer both tidal range and river discharge controlled the ETM location.

It was found that the SPM properties of the ETM followed a seasonal cyclic pattern:

- In winter, the SSC had the lowest seasonal depth averaged value (mass conc. = 23 mgl^{-1} and volume conc. = 276 μll^{-1}). The ED was found to be 83 kgm^{-3}.

- In spring, the SSC increased slightly (mass conc. = 29 mgl^{-1} and volume conc. = 294 μll^{-1}). The ED was found to be 99 kgm^{-3}.

- In summer, the SSC had the highest seasonal depth averaged value (mass conc. = 130 mgl^{-1} and volume conc. = 816 μll^{-1}). The ED was found to be 159 kgm^{-3}. This is the optimum season for ETM formation.

- In autumn, the SSC decreased noticeably (mass conc. = 45 mgl^{-1} and volume conc. = 335 μll^{-1}). The ED was found to be 133 kgm^{-3}.

This shows that SSC in the ETM was related, more, to biological and tidal processes in summer than to storm or other related processes in the water column.

9.5 Predicting the ETM Location and Strength

After relating the ETM location and strength to the flow ratio (see sections 5.4.2.2 and 5.4.3) the following relationships were found:

- The location of the ETM was given by
  $\log(D) = 0.9973 - 0.1027 * \log(Q/T^3)$, where D is the distance from the mouth in km, Q is the river discharge in m^3s^{-1}, and T is the tidal range in m.

- The SSC_{ETM}, was given by
  $\log(SSC_{ETM}) = 1.479 + 0.2014 * (\log(Q/T^3))^2 + 0.2096 * \log(Q/T^3)$
- Considering the assumptions, the fit between estimated and observed ETM locations was good. Figure 5.35 indicates that the ETM is positioned between Tal-y-Cafn and Dolgarrog bridges (10 – 16 km) in agreement with the observations made.

- Considering the assumptions and the fact that, in reality, the SSC_{ETM} is also dependent on other factors not considered (such as: biological variability; availability of particulate matter; and actual geometry of estuary at the ETM), the estimated SSC_{ETM} was in good agreement with observations.

After refining the relationships for summer conditions only, they were compared with the Jago et al. (2006) relationships (see section 5.4.4.3); by using the Conwy flow ratios.

- Both relationships followed the same pattern (see figures 5.41 and 5.42) although the Jago et al. (2006) relationship underestimated the ETM location by about 4 km (i.e. places the ETM 4 km closer to the mouth).

- When it came to predicting the SSC_{ETM}, both relationships followed the general pattern (see figures 5.43 and 5.44), but the Jago et al. (2006) relationship differed significantly at the end of the summer periods – i.e. the SSC was overestimated, by 200 - 400 mgl^{-1}, at very low flow ratios (~ 0.006 in 2005, and ~ 0.004 in 2006).

- The differences in predicting both location and SSC could be down to the difference in the geometry (Taf is shorter with a greater sinuosity of the channel in the section of the ETM, than Conwy), river discharge (Conwy discharge has greater extremes), and the timing of low water relative to day light. Low water (on spring tides) in the Taf is typically during midday, when exposure duration to light is greatest. In comparison, low water (on spring tides) in the Conwy is in the late afternoon-evening, when the exposure duration to light is minimal. This difference in exposure duration could mean that there are more bio-products produced in the Taf, increasing the SPM concentrations during flood. This is just a hypothesis, no measurements, were made to test it.

- If such relationships can be successfully applied to a number of estuaries then the ETM position and strength can be obtained just by monitoring the river discharge and tidal range of that estuary. This would mean that the ETM dynamics could be established for a number of estuaries on a nearly daily basis. This would further assist the study and monitoring of ETM dynamics and its influence (e.g. on biology, or on transportation of pollutants).

9.6 Estuarine Sands: the Threshold of Motion and Suspension

- The thresholds of motion of the estuarine sands were established by determining the threshold depth-averaged current speed and the threshold bed shear-stress at each anchor station (see section 7.2).

- Similarly, the thresholds of suspension of the estuarine sands were established. Sand of median grain diameter (2.3 mm) did not enter suspension during the tidal cycle at MS1. For all other anchor stations, sand suspension occurred. After sand was resuspended, the time it stayed in suspension was investigated.

The settling velocities of quartz grains were investigated, in order to determine the amount of time the resuspended sand could stay in suspension (see section 7.2.3.1, and Figure 7.23 for details and results). These show that quartz sand cannot remain in the water column at slack water.

- The results from Figure 7.23 show that during the spatial surveys at high water, bed sands were not in suspension. So it was concluded that the SPM at high water was made up mostly of non-quartz particles (i.e. flocs).

9.7 Transport Rates and Directions

- It was established that local sand of median diameter (2.3 mm) was not transported neither as bedload, nor as suspended load, at station MS1 (Conwy) on the day of the survey, as the station was not situated within the main flow.

The transport rates, at the 5 anchor stations, were found to be (in kgm^{-1} per survey):

Distance from mouth	Bedload	Suspended load	Total load
0.90 km	0	5.99	5.99
3.20 km	-0.30	-1.89	-2.19
5.35 km	0.1	1.47	1.57
6.65 km	0.09	0.29	0.38
10.00 km	-0.03	-0.11	-0.14

Negative values indicate a down-estuary direction, whilst positive values indicate an up-estuary direction.

- The direction of the total sediment transport at each station was determined. Stations MS1, MS3, and MS4 (see Figure 7.34), showed total sediment transport in the up-estuary direction. This suggests that a part of the SPM could be marine in origin. Stations MS2 and MS5 (see Figure 7.34) showed

total sediment transport in the down estuary direction. This was expected for MS2, as the river discharge was at a high. It was unexpected for MS5, as the river flow was at a low. The fact that sediment was carried down estuary at this station suggests that the station was situated within an ebb channel, which is in agreement with the bathymetry (see Figure 3.11).

9.8 The Provenance of the Estuarine Sands

- It was established that the estuarine sands (at the modal grain size, 180 μm) are made-up of 70 – 90% quartz/feldspar particles.

- The Conwy Bay samples were statistically identical to the estuarine samples, whilst the Conwy River samples were radically different. The comparison of sand samples and the statistical analysis suggest that the lithic component of the estuarine sands is mostly derived from the river, whilst the quartz/feldspar component is derived from the bay.

- From the above, it was concluded that the provenance of most of the estuarine sands is Conwy Bay.

9.9 The Net Transport Paths of Estuarine Sands

- In order to establish the net sand transport paths from the grain size characteristics, the following two trends were used:

  Case I. Sediments become finer, better sorted and more negatively skewed in the direction of transport.

  Case II. Sediments become coarser, better sorted and more positively skewed in the direction of transport.

- The net transport paths were defined (see Figures 8.20 and 8.21), by comparing grain size characteristics. The overall sand transport was in the up-estuary direction (for case I).

- Case II did not produce many significant outcomes.

- The sand transport direction (for case I) at each anchor station was established and then compared with the total load net transport direction for that station. The transport directions were in agreement (see Figures 7.34 and 8.20), suggesting that the method used in section 8.3 was valid.

9.10 Future Field Work

During this project it was understood that in order to have a more complete picture of the estuarine sediment dynamics, more data are needed. Some suggestions for further field work are presented below:

- Moored and longitudinal surveys. As seen in this thesis, the SPM properties of the estuary follow a seasonal pattern. The author suggests 4 longitudinal survey sets (5 survey days in each set), with a moored survey taking place simultaneously on day 3. In order to test the seasonal variations, the surveys should be undertaken in July, October, January and April. The instruments deployed should be the same as those used in this project, with the addition of a fluorometer (for observing chlorophyll levels). The 4 survey sets should be repeated annually as many times as logistically possible.

- Use of ADCP (Acoustic Doppler Current Profiler). The ADCP has been used to observe SPM properties within shelf seas, an example can be found in Missias (2003). There are 3 suggested ways of deployment of the instrument. The first way is to have it attached to the side of the survey

boat (during moored surveys) looking downwards. This will produce a more complete picture of part of the water column over a tidal cycle. The second way of deployment is to have the ADCP mounted to a frame, place on the estuary bed (at selected location) looking upwards. A set of these frames could be deployed. The ADCP only covers a part of the water column, but the SPM properties within that part could be measured continuously over a neap-spring cycle. Finally the third way the ADCP can be deployed is in formation. Three ADCPs mounted on an inverted "pi" arrangement. One instrument on each side of the channel, looking towards the centre of the channel and the other on the bed looking upwards. This formation will give a high resolution data set for the covered area, over a long time frame.

In general the field techniques one could use will vary as our understanding and technologies advance. One thing that is absolutely clear is the need of more complete data sets.

Finally, it is necessary to underline the importance of investigating the biogeochemical controls of floc formation within the estuary over seasonal cycles.

REFERENCES

Agrawal, Y.C. and Pottsmith, H.C., 2000. Instruments for particle size and settling velocity observations in sediment transport. *Mar. Geol.*, **166**, 89-114.

Allen, G.P., Sauzay, G., Castaing, P., and Jouanneau, J.M., 1976. Transport and deposition of sediment in the Gironde Estuary, France. In: Wiley, M. (Ed.), *Estuarine Processes. Vol. II: Circulation, Sediments, and Transfer of Material in the Estuary.* Academic Press, New York, 1-18

Aston, S.R., and Chester, R., 1976. Estuarine sediment processes. In: Burton, J.D., and Liss, P.S. (Eds.), *Estuarine Chemistry.* Academic Press, UK, 37-53.

Bagnold, R.A., 1956. Flow of cohesionless grains in fluids. *Phil. Trans. R. Soc. London,* **A249**, 235-297.

Bale, A.J., 1996. In situ laser optical sizing. *J. Sea Res.,* **36**, 31-36.

Bowden, K.F., 1976. Circulation and diffusion. In: Lauff, G.H. (Ed.), *Estuaries.* American Association for the Advancement of Science, USA, Publ. **83**,15-36.

Brenon, I., and Le Hir, P., 1998. Modelling fine sediment dynamics in the Seine estuary: Interaction between turbidity patterns and sediment balance. In: Dronkers, J., and Scheffers, M. (Eds.), *Physics of Estuaries and Coastal Seas.* Balkema A.A., Rotterdam, 103-114.

Bunt, J.A.C., Larcombe, P., and Jago, C.F., 1999. Quantifying the response of optical backscatter devices and transmissometers to variations in suspended particulate matter. *Cont. Shelf Res.*, **19**, 1199-1220.

Campbell, A.R., 1996. *Effects of turbulence on suspended sediment concentrations in a tidal flow.* PhD Thesis, University of Wales Bangor.

Cambell, D.E., and Spinrad, R.W., 1987. The relationship between light attenuation and particle characteristics in a turbid estuary. *Estuarine, Coastal and Shelf Sci.*, **25**, 53-65.

Christie, M.C., and Dyer, K.R., 1998.Measurements of the turbid tidal edge over the Skeffling mudflats. In: Black, K.S., Paterson, D.M., and Cramp, A. (Eds.), *Sedimentary Processes in the Intertidal Zone.* Geol. Soc., Special Publications, London, **139**, 45-55.

Clement, S., 1999. *Investigations into the salt balance in the Conwy Estuary.* MSc Thesis, University of Wales Bangor.

Connor, C.S., and De Visser, A.M., 1992. A laboratory investigation of particle size effects on an optical backscatterance sensor. *Mar. Geol.*, **108**, 151-189.

Davidson, N.C., et al., 1991. *Nature conservation and estuaries in Great Britain.* Nature Conservancy Council, UK.

Davies, J.L., 1973. *Geographical Variation in Coastal Development.* Hafner, New York.

Downing, J.P., Sternberg, R.W. , and Lister, C.R.B., 1980. New instrumentation for the investigation of sediment suspension processes in the shallow marine environment. *Mar. Geol.*, **42**, 19-34.

Dunning, F.W., et al., 1978. *Britain's offshore oil and gas.* Geological Museum: United Kingdom Offshore Operators Association, UK.

Dyer, K.R., 1972. Sedimentation in estuaries. In: Barnes, R.S.K. and Green, J. (Eds.), *The estuarine environment.* Applied Science Publishers Ltd, UK, 10-32.

Dyer, K.R., 1973. *Estuaries: A physical introduction.* John Wiley, London.

Dyer, K.R., 1986. *Coastal and Estuarine Sediment Dynamics*, John Wiley and Sons Ltd, UK.

Dyer, K.R., 1997. *Estuaries: A physical introduction, 2nd edn.* John Wiley and Sons Ltd, UK.

Fairbridge, R.W. 1980. The estuary: its definition and geodynamic cycle. In: Olausson, E. and Cato, I. (Eds.), *Chemistry and Biogeochemistry of Estuaries.* John Wiley and Sons Ltd, UK.

Festa, J.F., and Hansen, D.V. 1978. Turbidity maxima in partially mixed estuaries: a two dimensional numeric model. Estuarine, Coastal and Marine Sci., **7**, 347-359.

Folk, R.L., 1968. *Petrology of sedimentary rocks.* The University of Texas, USA.

Folk, R.L., and Ward, W.C., 1957. Brazes river bar: a study in the significance of grain size parameters. *J. Sed. Petrol.*, **27**, 3-26.

Fugate, D.C., and Friedrichs, C.T., 2002. Determining concentration and fall velocity of estuarine particle populations using ADV, OBS and LISST. *Cont. Shelf Res.*, **22**, 1867-1886.

Gao, S., and Collins, M., 1992. Net sediment transport patterns inferred from grain-size trends, based upon definition of "transport vectors". *Sed. Geol.*, **40**, 47-60.

Garrison, T., 1998. *Oceanography: An invitation to marine science, 3rd edn.* Wadsworth Publishing Company, USA.

Gibbs, R.J., 1977. Suspended sediment transport and the turbidity maximum. In: *Studies in Geophysics: Estuaries, geophysics and the environment.* National Academy of Science, USA, 104-109.

Grabemann, I., Uncles, R.J., Krause, G. and Stephens, J.A., 1997. Behaviour of turbidity maxima in the Tamar (UK) and Weser (FRG) estuaries. *Estuarine, Coastal and Shelf Sci.*, **45**, 235-246.

Green, M.O. and Boon III, J.D., 1993. The measurement of constituent concentrations in non-homogenous sediment suspensions using optical backscatter sensors. *Mar. Geol.*, **110**, 73-81.

Guilcher, A., 1967. Origin of sediment in estuaries. In: Lauff, G.H. (Ed.), *Estuaries*. American Association for the Advancement of Science, USA, Publ. **83**, 149-157.

Hansen, D.V., and Rattray M.Jr., 1966. New dimensions in estuary classification. *Limnology and Oceanography.* Vol. XI, **3**, 319-326.

Hatcher, A., Hill, P., Grant, J., and McPherson, P., 2000. Spectral optical backscatter of sand in suspension: effects of particle size, composition and colour. *Mar. Geol.*, **168**, 115-128.

Hayes, M.O., 1975. Morphology of sand accumulation in estuaries: an introduction to the symposium. In: Cronin, L.E. (Ed.), *Estuarine Research*, Vol. II. Academic Press, New York, 3-22.

Hillier, G.J., 1985. *The Conwy River estuary turbidity maximum.* MSc thesis, University of Wales Bangor.

Humphreys, H.J., 1998. *Modelling the salinity intrusion in the Conwy Estuary.* MSc Thesis, University of Wales Bangor.

Inman, D.L., 1952. Measures for describing the size distribution of sediments. *J. Sed. Petrol.*, **22**, 125-145.

Ishak, A.K., 1997. Suspended sediment dynamics and flux in the macrotidal Taf estuary, South Wales. PhD thesis, University of Wales Bangor.

Jago, C.F., and Mahamod, Y., 1999.A tidal load algorithm for sand transport by fast steady currents. *Estuarine, Coastal and Shelf Sci.*, **48**, 93-99.

Jago, C.F., and Jones, S.E., 2002. Turbulence control of the properties and flux of suspended matter in tide-stirred shelf seas. *Research Proposal*, School of Ocean Sciences, University of Wales Bangor.

Jago, C.F., Ishak, A.K., Jones S.E., and Goff, M.R.G., 2006. An ephemeral turbidity maximum generated by resuspension of organic-rich matter in a macrotidal estuary, S.W. Wales. *Estuaries and Coasts Vol. 29.* **No 2**, 197-208.

Ketchum, B.H., 1983. Estuarine characteristics. In: Ketchum, B.H. (Ed.), *Ecosystems of the World, 26: Estuaries and Enclosed Seas*. Elsevier Scientific Publishing Company, Amsterdam, 1-14.

Kineke, G.C., and Sternberg, R.W., 1992. Measurements of high concentration suspended sediments using the optical backscatter sensor. *Mar. Geol.*, **108**, 253-258.

Knight, D.W., 1981. Some field measurements concerned with the behaviour of the resistance coefficient in a tidal channel. *Estuarine, Coastal and Shelf Sci.*, **12**, 303-322.

Kornman, B.A., and de Deckerem E.M.G.T., 1998. Temporal variations in sediment and suspended sediment dynamics in the Dollard Estuary. In: Black, K.S., Paterson, D.M., and Cramp, A. (Eds.), *Sedimentary Processes in the Intertidal Zone.* Geol. Soc., Special Publications, London, **139**, 231-242.

Le Roux, J.P., 1994. An alternative approach to the identification of net sediment transport paths based on grain-size trends. *Sed. Geol.*, **94**, 97-107.

Maynard, K.C., 1985. Geophysical survey and sediment dynamics of estuarine sediments. MSc thesis, University of Wales, Bangor, UK.

McCave, I.N., 1971. Sand waves in the North Sea off the coast of Holland. *Mar. Geol.*, **10**, 199-225.

McDowell, D.M., and O'Connor, B.A., 1977. *Hydraulic Behaviour of Estuaries.* The Macmillan Press Ltd, UK,

McLaren, P., 1981. An interpretation of trends in grain-size measurements. *J. Sed. Petrol.*, **51**, 611-624.

McLaren, P., and Bowles, D., 1985. The effects of sediment transport on grain-size distributions. *J. Sed. Petrol.*, **55**, 457-470.

Mehta, A.J., and Dyer, K.R. 1990. Cohesive sediment transport in estuarine and coastal waters. In: (Eds.), *Ocean Engineering Science, the Sea – 3rd edn, Vol. 9*. John Wiley and Sons Inc., USA, 815-839.

Mikkelsen, O.A., and Perjup, M., 2000. In situ particle size spectra and density of particle aggregates in a dredging plume. *Mar. Geol.*, **170**, 443-459.

Missias, S., 2003. *Investigation of suspended particle dynamics using optical and acoustical techniques*. MSc thesis, University of Wales Bangor.

Mitchell, S.B., 2003. Use of continuous turbidity sensor in the prediction of fine sediment transport in the turbidity maximum of the Trent Estuary, UK. *Estuarine, Coastal and Shelf Sci.*, **58**, 645-652.

National River Authority, 1995. River Conwy catchment plan: Action plan 1995. National River Authority, Wales, UK.

Nielsen, P., 1992. *Coastal bottom boundary layers and sediment transport*. World scientific Publishing, Singapore, Advancement Series on Ocean Engineering, Vol. 4.

Normant, et al., 1998. Three dimensional modelling of cohesive sediment transport in estuaries. In: Dronkers, J., and Scheffers, M. (Eds.), *Physics of Estuaries and Coastal Seas*. Balkema A.A., Rotterdam, 65-72.

Nunes, R.A., and Simpson, J.H., 1985. Axial convergence in a well-mixed estuary. *Estuarine, Coastal and Shelf Sci.*, **20**, 637-649.

Officer, C.B., 1983. Physics of the estuarine circulation. In: Ketchum, B.H. (Ed.), *Ecosystems of the World, 26: Estuaries and Enclosed Seas*. Elsevier Scientific Publishing Company, Amsterdam, 15-41.

Orton, P.M. and Kineke, G.C., 2001. Comparing calculated and observed vertical suspended sediment distributions from a Hudson River estuary turbidity maximum. *Estuarine, Coastal and Shelf Sci.*, **52**, 401-410.

Perkins, E.J., 1974. *The biology of estuaries and coastal waters*. Academic Press Ltd. UK.

Pinckney, J.L., and Zingmark, R., 1991. Effects of tidal stage and sun angles on intertidal benthic microalgal productivity. *Mar. Ecol. Prog. Series*, **76**, 81-89.

Postma, K.F., 1980. Sediment transport and sedimentation. In: Olauson, E. and Cato, I. (Eds.), *Chemistry and biogeochemistry of estuaries.* John Wiley and Sons Ltd, UK.

Press, F., and Siever, R., 1998. *Understanding Earth – 2nd edn.* W.H. Freeman and Company, USA.

Pritchard, D.W., 1967. What is an estuary: Physical viewpoint. In: Lauff, G.H. (Ed.), *Estuaries.* American Association for the Advancement of Science, USA, Publ. **83**, 3-5.

Pritchard, D.W., 1967. Observation of circulation in coastal plain estuaries. In: Lauff, G.H. (Ed.), *Estuaries.* American Association for the Advancement of Science, USA, Publ. **83**, 37-44.

Schoelhamer, D.H., 1993. Biological interference of optical backscatterance sensors in Tampa Bay, Florida. *Mar. Geol.*, **110**, 303-313.

Schubel, J.R., 1969. Size distribution of the suspended particles of the Chesapeake Bay turbidity maximum. *Netherlands Journal of Sea res.*, **4**(3), 283-309.

Senior, M., 1984. *The Conwy Valley and its long history.* Gwasg Carreg Gwalch, Wales, UK.

Simpson, J.H., Vennell, R., and Souza, A.J., 2001. The salt fluxes in a tidally-energetic estuary. *Estuarine, Coastal and Shelf Sci.*, **52**, 131-142.

Soulsby, R., 1997. *Dynamics of marine sands.* Thomas Telford Publications, Thomas Telford Services Ltd, UK.

Turrell, W.R., Brown, J., and Simpson, J.H., 1996. Salt intrusion and secondary flow in a shallow, well-mixed estuary. *Estuarine, Coastal and Shelf Sci.*, **42**, 153-169.

Uncles, R.J., and Stephens, J.A., 1993. Nature of the turbidity maximum in the Tamar Estuary, UK. *Estuarine, Coastal and Shelf Sci.*, **36**, 413-431.

Uncles, R.J., Barton, M.L., and Stephens, J.A., 1994. Seasonal variability of fine-sediment concentrations in the turbidity maximum region of the Tamar Estuary. *Estuarine, Coastal and Shelf Sci.*, **38**, 19-39.

Uncles, R.J., Stephens, J.A., and Smith, R.E., 2002. The dependence of estuarine turbidity on tidal intrusion length, tidal range and residence time. *Cont. Shelf Res.*, **22**, 1835-1856.

Wallis, S.G., and Knight, D.W., 1984. Calibration studies concerning a one-dimensional numerical tidal model with particular reference to resistance coefficients. *Estuarine, Coastal and Shelf Sci.*, **19**, 541-562.

Zhou, J.L., Liu, Y.P., and Abrahams, P.W., 2003. Trace metal behaviour in the Conwy Estuary, North Wales. *Chemosphere*, **51**, 429-440.

APPENDICES

APPENDIX: A

Four random examples of cumulative coarser than, values, plotted on a probability graph, against phi diameter.

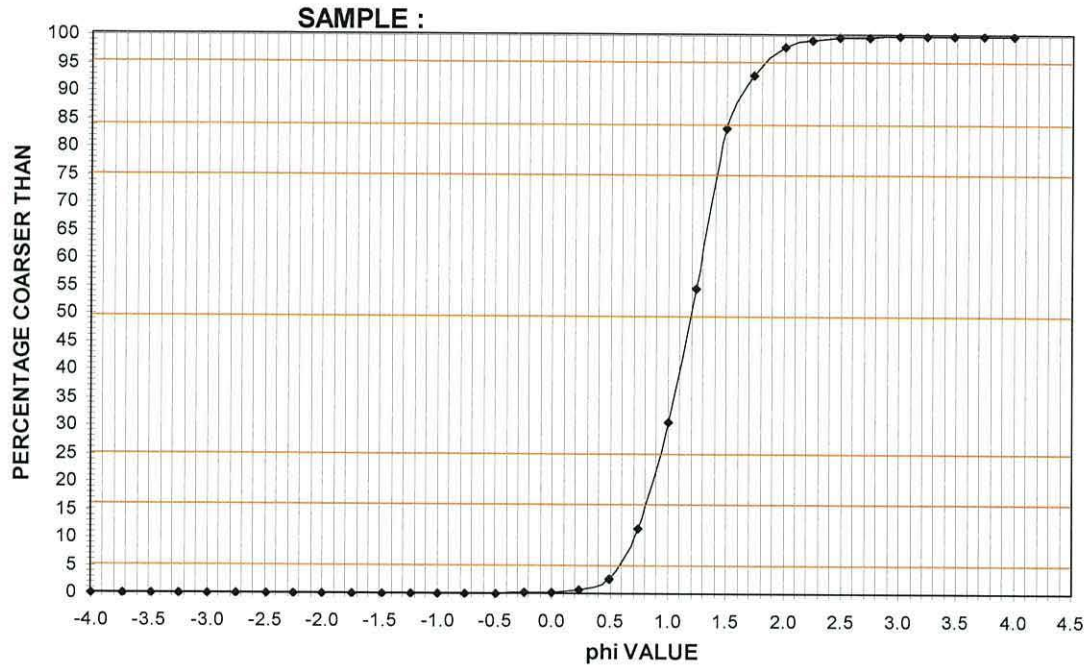

Sample G44-5 (upper estuary)

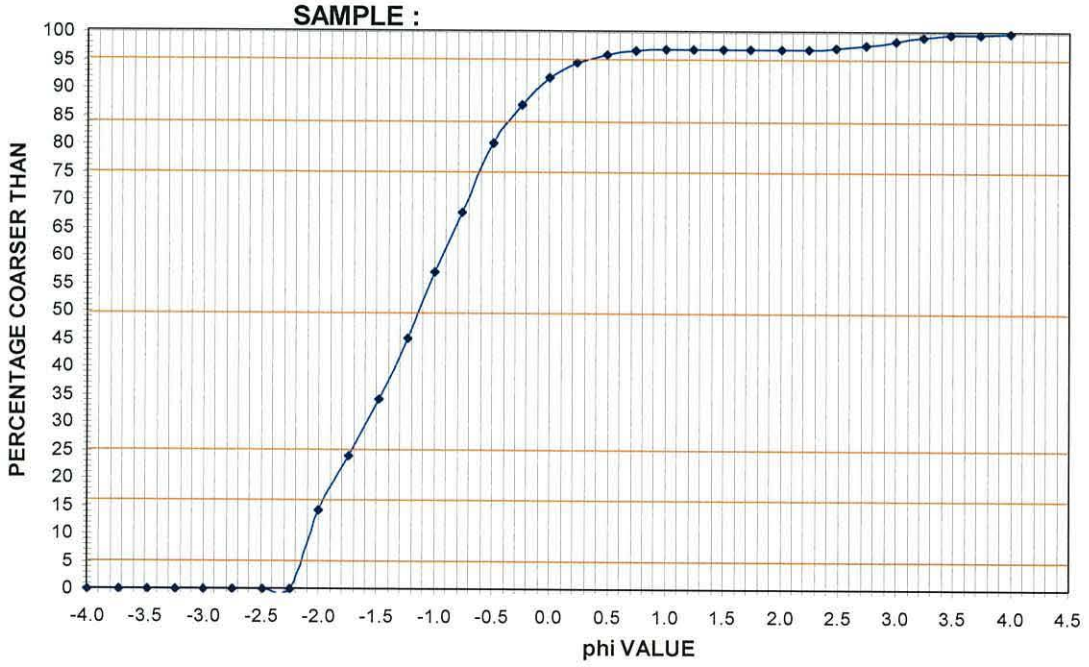

Sample G16-S58 (mid-upper estuary)

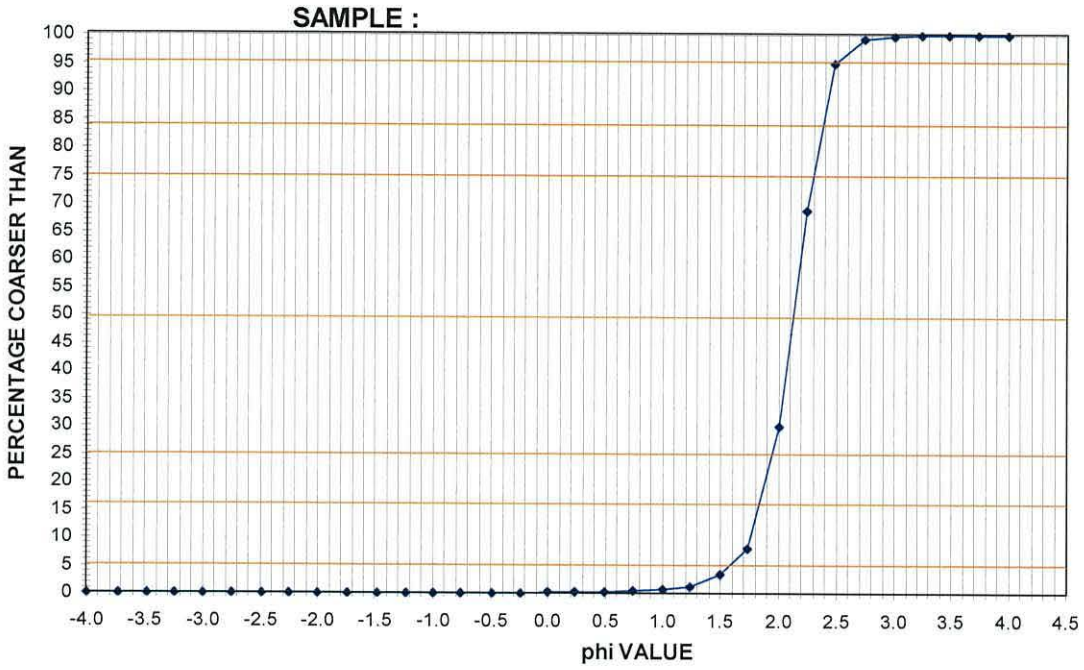

Sample G68-S40 (mid-lower estuary)

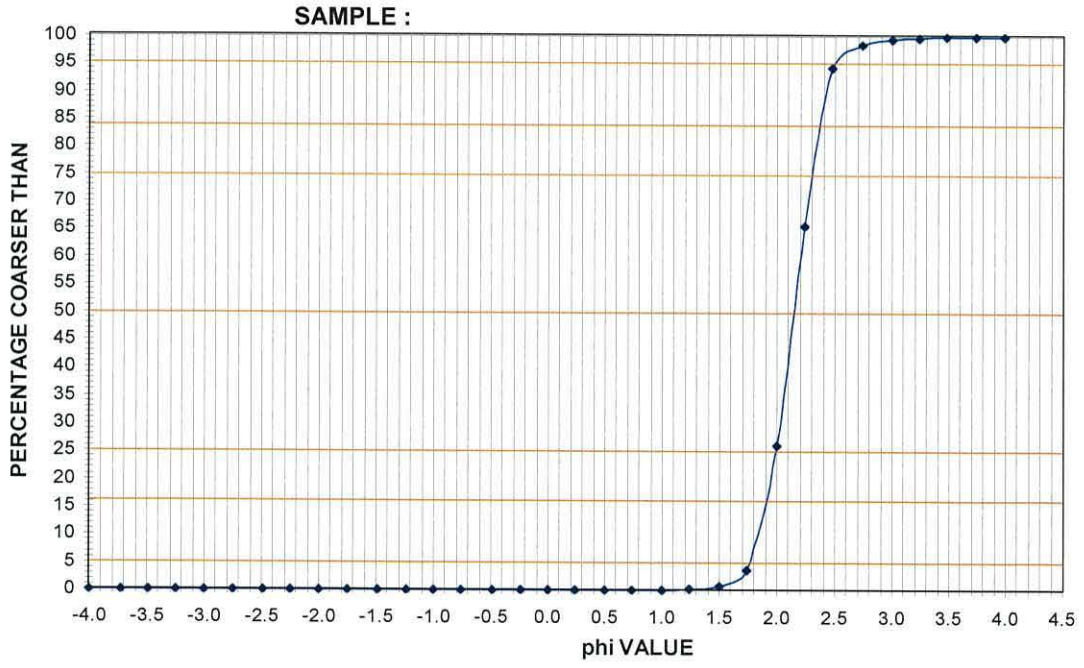

Sample G43-S57 (lower estuary)

APPENDICES: B, C, D and E

Please find appendices B, C, and D on the compact disk attached to the end of this thesis.

- Appendix B: This appendix is a folder containing all the result derived from the dry sieving of the sand samples. (Inman parameters & cumulative curves).

- Appendix C: This appendix is an Excel spread sheet containing all pie-charts, showing the results of the microscopy analysis, of sand samples.

- Appendix D: In the main thesis, the longitudinal SPM variations plots (contour plots), were of selected days (7 out of 26). This appendix presents the longitudinal SPM variations for the remaining 19 survey days.

- Appendix E: Comparison between the OBS and the transmissometer.

- Appendix F: Correlation between blank derived concentrations and salinity.